Interlocked Host Structures for Anion Recognition and Sensing in Aqueous Solutions

Matthew J. Langton

Lincoln College, University of Oxford

A thesis submitted for the degree of Doctor of Philosophy

Inorganic Chemistry Laboratory

University of Oxford

Trinity Term 2014

Interlocked Host Structures for Anion Recognition and Sensing in Aqueous Solutions

Matthew J. Langton, Lincoln College, University of Oxford

Abstract of thesis submitted for the degree of Doctor of Philosophy, Trinity Term 2014

This thesis describes the synthesis of interlocked anion host systems which exploit hydrogen bonding, halogen bonding, and lanthanide-coordination for anion recognition and sensing in aqueous solution.

Chapter 1 introduces the field of anion supramolecular chemistry, with particular focus on areas of particular relevance to this thesis, namely anion recognition and sensing, anion templation and the synthesis of interlocked structures.

Chapter 2 describes the synthesis of hydrogen bonding rotaxane and catenane hosts for recognising and sensing oxoanions in aqueous solvent media. The novel use of nitrate anion templation for the synthesis of interlocked molecules is reported, and the unprecedented selective recognition of nitrate in aqueous solvent media is demonstrated.

Chapter 3 details the preparation of water soluble permethylated β-cyclodextrin-stoppered rotaxane hosts that utilise halogen bonding and hydrogen bonding interactions to bind anions in pure water. The first thermodynamic investigation into halogen bonding in water is reported, and the relative capabilities of halogen and hydrogen bonding for anion recognition in water are compared.

Chapter 4 investigates the incorporation of lanthanide cations into rotaxane hosts for optical anion sensing. The seminal use of lanthanide cation templation for interlocked molecule synthesis is described, before anion templation approaches towards the synthesis of lanthanide-based rotaxanes are discussed. The luminescence anion sensing capabilities of these interlocked hosts are investigated.

Chapter 5 describes the experimental procedures used in this work, and details the characterisation of compounds presented in Chapters 2–4.

Chapter 6 summarises the conclusions of this thesis.

Acknowledgements

I would like to thank Professor Paul Beer for the opportunity to carry out this work, his guidance, encouragement and many ideas along the way. I have been incredibly fortunate to have worked with such a trusting, supportive and friendly supervisor.

The three years I have spent in Beer group have been hugely enjoyable, and I thank the group members, past and present, who have made that possible. Asha Brown has been an endless source of guidance and discussion throughout my whole DPhil, for which I am very grateful. Thanks to Jim Mercurio, Rich Knighton, Graeme Spence, Nick White and Lydia Gilday for help and advice, and to current group members Stuart Cornes, Tim Barendt, Sean Robinson, Alex Hess, Jason Lim, Tom Mole and Ben Mullaney who have made my last year so entertaining. I would like to thank those with whom I have collaborated: Lucy, of course, for being such an amazing Part II student, Sean, Fabiola Zapata, Octavia Blackburn, Vitor Félix and Igor Marques. I was fortunate to learn the art of X-ray crystallography from Amber Thompson and Nick White, who were also great company on many an overnight shift at Diamond. I am extremely appreciative to Lydia, Sean, Asha, Tim, Alex, Tom and Mel who diligently proof-read my thesis.

Outside of the lab I would like to thank all of my great friends and team mates from archery, particularly Angie and Timmins, for all the fun, successes and adventures. I am grateful to my other friends from home and Oxford: Mel, Gus, James, Felix, Laura, Diana, Kat, Greg, Maz, Alex and many others, for their continued friendship and encouragement, and for putting up with my long periods of absence when archery took over.

And finally, thank you to Lucy, my family and especially my parents, Robert and Anne, for their continued love and support. None of this would have been possible without them.

M.J.L August 2014

Previously published work

Some of the work described in this thesis has already been published:

Peer-reviewed journal articles

"Halogen bonding in water: enhanced anion recognition in acyclic and rotaxane hosts"
M. J. Langton, S. W. Robinson, I. Marques, V. Félix and P. D. Beer, ***Nat. Chem.,*** in press, 2014, DOI: 10.1038/NCHEM.2111

"Nitrite-Templated Synthesis of Lanthanide-Containing [2]Rotaxanes for Anion Sensing"
M. J. Langton, O. A. Blackburn, T. Lang, S. Faulkner and P. D. Beer,
Angew. Chem. Int. Ed., 2014, **53**, 11463–11466

"Nitrate anion templated synthesis of a [2]catenane for nitrate recognition in organic–aqueous solvent media"
M. J. Langton and P. D .Beer, ***Chem. Commun***., 2014, **50**, 8124–8127

"Nitrate anion templated assembly of a [2]rotaxane for selective nitrate recognition in aqueous solvent mixtures"
M. J. Langton, L. C. Duckworth and P. D. Beer, ***Chem Commun.,*** 2013, **49**, 8608–8610

"Lanthanide-cation templated synthesis of rotaxanes"
F. Zapata, O. Blackburn, M. J. Langton, S. Faulkner and P. D. Beer, ***Chem Commun***., 2013, **49**, 8157–8159

"Sulfate-Selective Binding and Sensing of a Fluorescent [3]Rotaxane Host System"
M. J. Langton and P. D. Beer, ***Chem. Eur. J.,*** 2012, **18**, 14406–14412

Further work conducted during the course of this thesis has also been published:
Rotaxane and catenane host structures for sensing charged guest species
M. J. Langton and P.D. Beer, ***Acc. Chem. Res.,*** 2014, 47, 1935–1949

Oral presentations

"Interlocked host molecules for anion recognition and sensing"
Macrocyclic and Supramolecular Chemistry Meeting, December 2012, Queen Mary's College, University of London.

"Enhancing anion recognition by rotaxane hosts in competitive aqueous solvent media"
Inorganic Chemistry Laboratory Graduate Symposium, April 2014.

Poster presentations

Halogen bonding in water: enhanced anion recognition in acyclic and rotaxane hosts"
M. J. Langton, S. W. Robinson and P. D. Beer. 1st International Symposium on Halogen Bonding, June 2014, Porto Cesareo, Italy.

Glossary of abbreviations

δ	chemical shift
Δ	change, heat
λ	wavelength
μ	micro
+ve	positive
−ve	negative
Å	Angstrom
AcO^-	acetate anion
AIBN	azobisisobutyronitrile
app.	apparent
aq	aqueous
ATP	adenosine triphosphate
a.u.	arbitrary units
bipy	2,2'-bipyridine, 2,2'-bipyridyl
Boc	*tert*-butoxycarbonyl
Bn	benzyl
br.	broad
Bu	butyl
BzO^-	benzoate anion
ºC	degrees Celsius
cat.	catalytic
CD	cyclodextrin
Celite	diatomaceous silica
conc.	concentrated
COSY	homonuclear correlation spectroscopy
CuAAC	copper(I)-catalyzed azide–alkyne cycloaddition
d	deuterated
d	doublet
dd	double doublet
DFT	density functional theory
DIBAL	diisobutylaluminium hydride
DIPEA	*N*,*N'*-diisopropylethylamine
DMF	*N*,*N'*-dimethylformamide
DMSO	dimethylsulfoxide
DNA	deoxyribonucleic acid
E	potential
$E_{1/2}$	half-wave potential
e.g.	*exempli gratia*
EDC·HCl	*N*-(3-dimethylaminopropyl)-*N*'-ethylcarbodiimide hydrochloride
en	ethylenediamine
equiv. eq	equivalent

ES	electrospray
Et	ethyl
eT	energy transfer
ET	electron transfer
Fc	ferrocene
Fc^+	ferrocenium
g	gram, gas
G	Gibbs free energy
GAFF	General Amber Force Field
Grubbs' II	Grubbs' second generation catalyst
H	enthalpy
HB	hydrogen bond
hr	hour
HRMS	high resolution mass spectrometry
Hz	Hertz
IUPAC	International Union of Pure and Applied Chemistry
J	joule
J	coupling constant
^3J	three bond coupling constant
^4J	four bond coupling constant
K	Kelvin
K_a	association constant
L	litre
Ln	lanthanide
m	milli, multiplet
M	moles per litre
MD	molecular dynamics
Me	methyl
min	minute
MLCT	metal-to-ligand charge transfer
MM	molecular mechanics
mol	mole
MS	mass spectrometry
Ms	mesyl
m/z	mass/charge ratio
n	nano
NDI	naphthalene diimide
NMR	nuclear magnetic resonance
Oxone	potassium peroxymonosulfate
p	*para*
PBP	phosphate binding protein
PET	photo-induced electron transfer
Ph	phenyl
pH	$-\log_{10}[H^+]$

pK_a	$-\log_{10}K_a$
ppm	parts per million
Pr	propyl
q	quartet
R	alkyl or aryl substituent
RCM	ring closing metathesis
R_f	Retention factor
ROESY	rotating-frame nuclear Overhauser effect correlation spectroscopy
rt	room temperature
s	singlet
S	entropy
sat.	saturated
SBP	sulfate binding protein
t	triplet
t, tert	*tertiary*
TBA^+	tetrabutylammonium cation
TBTA	tris[(1-benzyl-1,2,3-triazol-4-yl)methyl]amine
TFA	trifluoroactetic acid
TfO^-	triflate anion
THF	tetrahydrofuran
TLC	thin layer chromatography
TMS	trimethylsilyl
Ts	4-toluenesulfonyl
UV	ultraviolet
vdW	van der Waals
wt.	weight
X	halogen atom
XB	halogen bond

Table of contents

CHAPTER 1

Chapter 1 Introduction

1.1 Anion supramolecular chemistry

Supramolecular chemistry, meaning literally "*chemistry beyond the molecule,"* is concerned with non-covalent intermolecular interactions and their pertinence to the assembly of complex molecular architectures and functional systems.[1] The field can be considered to encompass two main areas: host–guest chemistry and self-assembly. The former concerns the design and synthesis of receptor molecules that employ intermolecular interactions to bind a smaller guest substrate, whilst the latter involves the spontaneous assembly of small substrate molecules into higher-order architectures of greater complexity. The origins of supramolecular chemistry, in particular host–guest chemistry, are found in the pioneering work of Lehn,[2] Cram[3] and Pedersen,[4] who were jointly awarded the Nobel prize for chemistry in 1987 for "*their development and use of molecules with structure-specific interactions of high selectivity*". Their investigations into cation binding by cryptands, spherands and crown ethers, respectively, stimulated the rapid expansion of this field (Figure 1.1a–c). Less than a year after Pedersen's crown-ether cation receptors were reported, Park and Simmons prepared the seminal example of an anion receptor, in the form of a protonated cage structure capable of halide anion recognition in aqueous TFA solution (Figure 1.1d).[5]

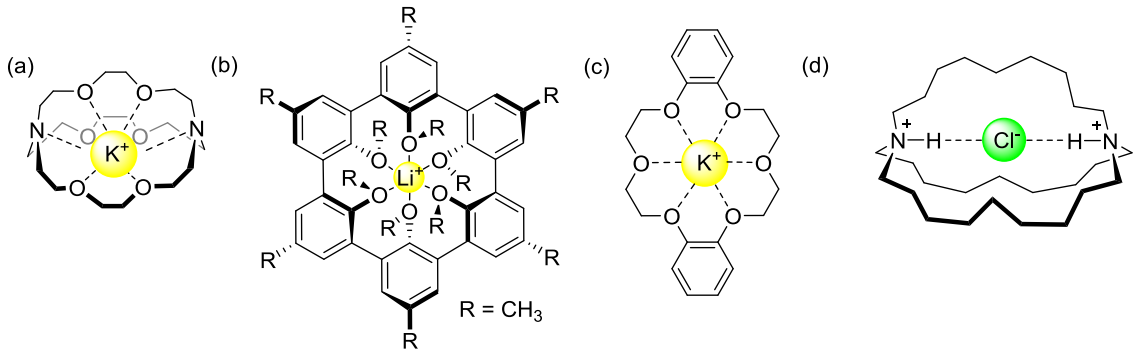

Figure 1.1 Cation receptors: (a) Lehn's [2,2,2]cryptand,[2] (b) Cram's spherands[3] and (c) Pedersen's dibenzo-18-crown-6.[4] (d) Park and Simmon's "katapinate" chloride anion receptor.[5]

Surprisingly, in contrast to the field of cation coordination chemistry which developed rapidly in the subsequent years, anion supramolecular chemistry remained largely overlooked until the early 1980s. Over the past few decades, however, there has been an explosion of interest in the field, with significant research effort being focused on both anion recognition and template-directed self-assembly mediated by anionic species.

This introductory chapter focuses initially on anion host–guest chemistry, with particular emphasis on anion recognition in competitive aqueous solvents, followed by an introduction to the template-directed assembly of interlocked molecular architectures and their applications.

1.1.1 The case for anion recognition

Anions play important roles in numerous biological, medical, environmental and industrial processes. In biology, the genetic information required for the development and function of all known organisms is encoded within the DNA poly-anion, whilst the phosphate-derived co-enzyme ATP acts as the molecular energy currency for intercellular energy transfer.[6] Indeed, the majority of biological substrates are negatively charged under physiological conditions. Inorganic anions also play fundamental roles *in vivo*: the iodide anion is necessary for hormone biosynthesis by the thyroid gland,[7] whilst mis-regulation of chloride channels has been implicated in cystic fibrosis, a genetic disorder.[8] In the environment phosphates and nitrates are used extensively in agricultural fertilisers, yet their over-use has led to the eutrophication (excessive plant growth) of natural water courses and disruption of the ecosystem.[9] Furthermore, over-exposure to nitrate can result in health problems, such as *in vivo* formation of carcinogenic nitrosamines, and has been implicated as a cause of methemoglobinemia (blue baby syndrome) in infants.[10] Sulfate and nitrate are present in acid rain,[11] whilst the radioactive pertechnetate anion is a waste by-product of nuclear fuel

reprocessing and poses a significant risk to human health.[12] Accordingly, the case for the design and synthesis of artificial anion receptors, sensors and sequestering agents is a compelling one and is an area of intense current research.

1.1.2 The challenge of anion binding in aqueous media

Anion recognition is widely considered to be a more challenging prospect than that of cation binding,[13] owing to a number of fundamental properties:

Size: Anions are larger than their isoelectronic cations and as a consequence exhibit a lower charge-to-radius ratio (eg. Cl^- compared to K^+; ionic radii 1.81 and 1.37 Å respectively). This significantly weakens the favourable electrostatic interactions between an anion host and guest species.

pH dependence: Many anions exist under multiple protonation equilibria and may lose their charge upon protonation at low pH. Furthermore, certain classes of anion receptors, for example those containing poly-ammonium and guanidinium motifs, are contingent on protonation to gain both the positive charge and hydrogen bond donors that are prerequisite for anion binding. As a result, recognition can only occur within a limited "pH window" in which, simultaneously, the anion is deprotonated and the receptor is protonated (Figure 1.2). Moreover, highly basic anions, such as fluoride and acetate, may also deprotonate acidic sites on the receptor species.

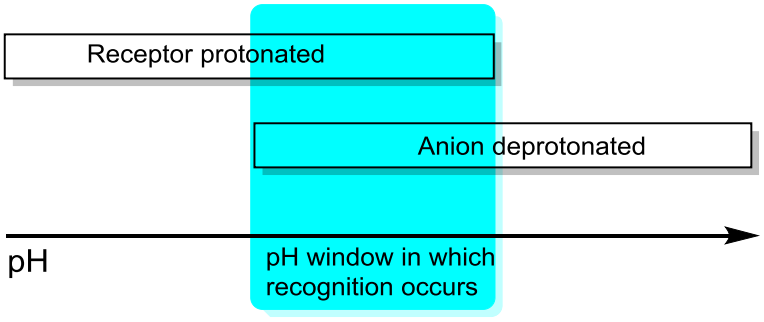

Figure 1.2 Schematic illustration of the pH window in which anion recognition by a pH-dependent receptor may occur.

Geometry: In contrast to cations, which are in general spherical, anions can adopt a wide range of geometries, including spherical (halides), linear (azide), bent (nitrite), trigonal-planar (nitrate), tetrahedral (phosphate, sulfate) and octahedral (hexafluorophosphate). This property can be used to the chemist's advantage, however, and exploited to achieve selectivity on the basis of designing anion receptors of complementary shape and size.

Solvation: The solvent plays a critical role in the recognition of negatively charged species. Anions exhibit large free energies of solvation, the extent of which is related to the Hofmeister series of anion hydrophobicity,[13,14] and which are typically greater than for cations of comparable charge and size.[1,15] The extent of solvation of both the host and guest strongly depends on the choice of solvent. Hydroxylic solvents such as methanol and water strongly solvate charged species, forming hydrogen bonds with both the anion and the host molecule. Thus receptors employing strong electrostatic interactions are usually required to compete effectively with protic solvents for the negatively charged guest species. In contrast, in lower polarity aprotic solvents such as acetone or chloroform the anion is more weakly solvated, and in such solvent media neutral receptors are able to function. Binding anions in water is particularly challenging, and approaches to designing receptors capable of anion recognition in both water and competitive aqueous–organic solvent media are discussed below.

1.2 Anion receptors

1.2.1 Naturally occurring anion receptors

The strong and highly selective binding achieved by naturally occurring anion receptors provides inspiration to supramolecular chemists seeking to reproduce such exquisite recognition with synthetic host molecules. The sulfate-binding protein (SBP)[16] and phosphate-binding protein (PBP)[17] are responsible for anion transport in bacteria and are noteworthy examples of highly selective anion recognition. SBP binds a de-solvated sulfate anion within a deep cleft in the protein, *via* a network of seven hydrogen bonds from neutral donors ($K_a = 8.3 \times 10^6$ M^{-1}, Figure 1.3a).

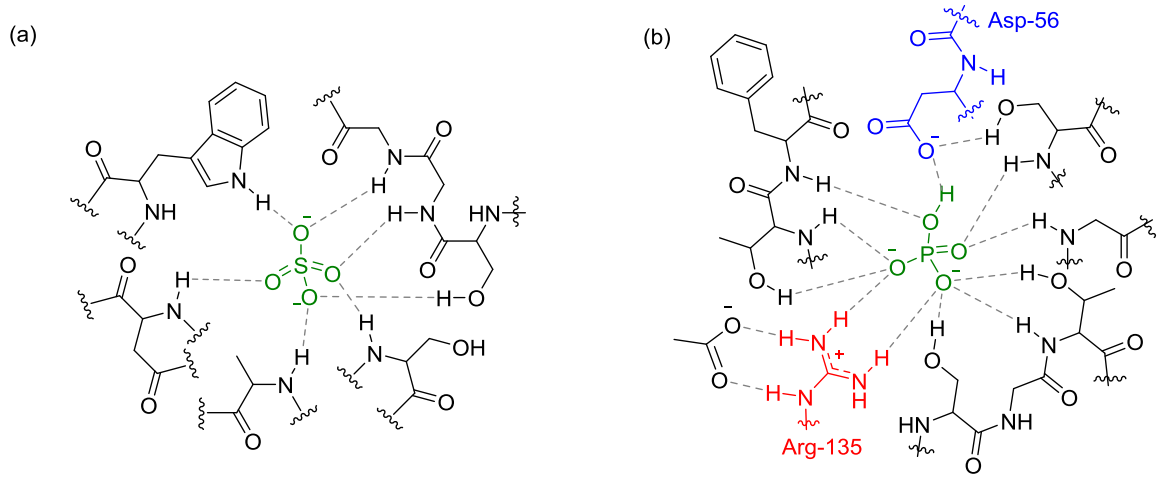

Figure 1.3 Schematic representation of the array of hydrogen bonds which bind the anion in (a) sulfate-[16] and (b) phosphate-binding proteins.[17]

In contrast, the PBP binds hydrogen phosphate strongly ($K_a = 3.2 \times 10^6$ M^{-1}), *via* twelve hydrogen bonds: nine originate from neutral donors and two from the positively charged guanidinium motif of the Arg-135 residue, whilst the twelfth is donated from the anion to the carboxylate hydrogen bond acceptor of Asp-56 (Figure 1.3b). It is this negatively charged residue that is crucial for the selectivity of the binding site: a fully deprotonated tetrahedral anion such as sulfate, which lacks a hydrogen bond donor, experiences unfavourable electrostatic repulsion and accordingly binds with lower affinity.

1.2.2 The design of synthetic anion receptors

Synthetic anion receptors strive to mimic the impressive recognition found in nature by using a range of intermolecular interactions and employing many fundamental supramolecular design principles, such as pre-organisation and the macrocyclic effect,[1] to bind the target guest species with high affinity and selectivity. These intermolecular interactions are discussed in more detail below, before specific examples of their use in charged and neutral receptors for anion binding in competitive aqueous solvents are presented.

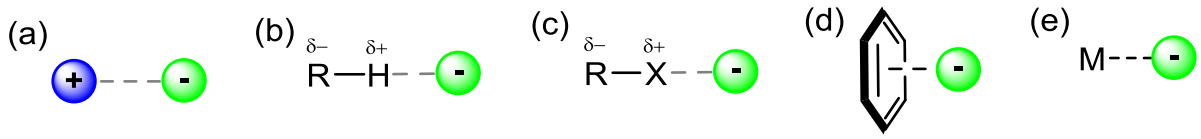

Figure 1.4 Intermolecular interactions for anion recognition: (a) electrostatics, (b) hydrogen bonding, (c) halogen bonding, (d) anion–π interactions, (e) coordinate bonds. R = electronegative atom or electron withdrawing group, M = Lewis acidic metal cation or main-group element.

***Electrostatics*:** Due to the very nature of anions, positively charged receptors are used extensively for recognition in polar solvents, for example in quaternary ammonium- or pyridinium-based anion receptors. Ion-ion interactions (Figure 1.4a) are strong but non-directional and thus are often used in concert with ion-dipole interactions such as hydrogen and halogen bonds. These interactions are much weaker but their directionality, arising from the dipole orientation, can be advantageous when designing selective anion receptors.

Hydrogen bonds are a common example of ion-dipole interaction, in which a hydrogen atom that is covalently attached to a more electronegative atom (e.g. O, C, N) or electron-withdrawing group, is polarised and can interact with an anion (Figure 1.4b) or dipole. Hydrogen bonds are ubiquitous in nature and play a crucial role in, for example, defining the secondary and tertiary structure of proteins, in DNA base pair recognition,[18] and in anion recognition and membrane transport (Figure 1.3). The interaction is used extensively in supramolecular chemistry for anion recognition (*vide infra*).[1]

Halogen bonds are closely related to the analogous hydrogen bond, but with the hydrogen atom replaced by a halogen (Figure 1.4c). The halogen bond (XB) interaction is more stringently linear, but is of comparable strength to a hydrogen bond.[19,20] A recently published IUPAC definition states: *"A halogen bond occurs when there is evidence of a net attractive interaction between an electrophilic region associated with a halogen atom in a molecular entity and a nucleophilic region in another, or the same, molecular entity."*[21] Theoretical calculations have indicated that the electron density of a halogen atom covalently attached to an electron-withdrawing group is anisotropically distributed, such that an area of partial positive charge forms at the halogen end of the R–X bond, which is termed the "sigma hole." The size of the sigma hole is greatest for the larger, more polarisable halogens, and can be further enhanced by increasing the electron withdrawing nature of the substituent.

Whilst halogen bonding has been exploited extensively in solid state crystal engineering (Figure 1.5a),[22–28] its utilisation in the solution phase remains underdeveloped. Seminal applications of halogen bonding in self-assembly[29–34] medicinal chemistry,[35–39] anion transport,[40–42] catalysis,[43,44] structural biology[45,46] and solution phase anion recognition (*vide infra*) [29,32,34,47–49] have only recently been reported. For example, Li has demonstrated that a triazole foldamer can bind a tridentate organo-iodine guest species in $CDCl_3$ solution, by means of three XB interactions (Figure 1.5b).[31] Furthermore, recent analysis of the Protein Data Bank (PDB) has revealed that many of the deposited crystal structures of protein-small molecule complexes exhibit one or more halogen bonds between the bound substrate and the protein, most commonly to the backbone carbonyl oxygen.[35] Halogen atoms are typically incorporated into potential drug molecules to improve hydrophobicity, as well as absorption, distribution, metabolism and excretion (ADME) properties. They are also increasingly being included to enhance drug binding affinity *via* halogen bonding interactions to the protein

binding cleft, for example in the integrin-α4β1 inhibitor shown in Figure 1.5c which forms a XB to a protein backbone carbonyl oxygen atom.[37]

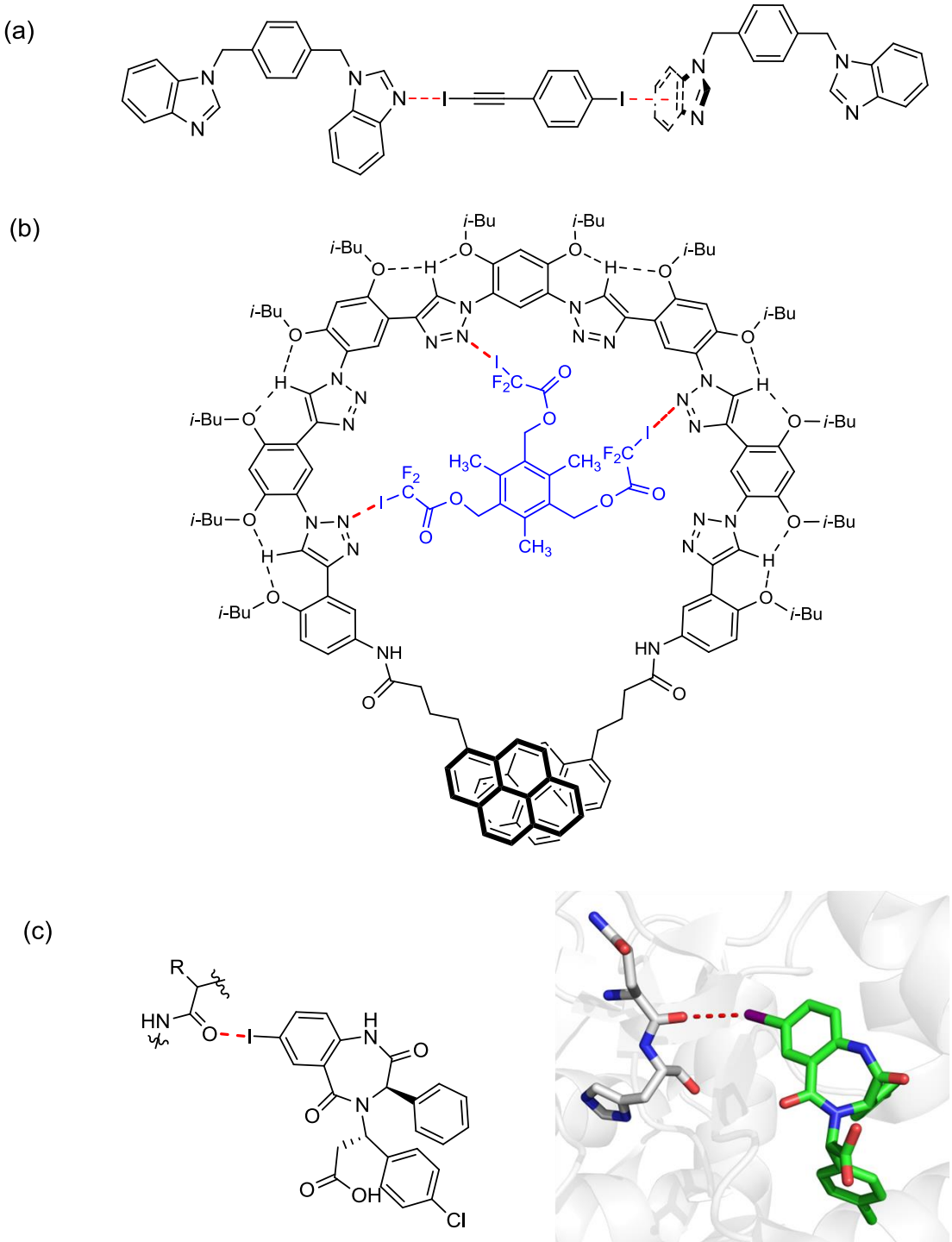

Figure 1.5 Halogen bonding in supramolecular chemistry (XB interaction depicted by red dashed line): (a) XB in the solid state,[28] (b) Li's XB-directed foldamer[31] and (c) an integrin-α4β1 inhibitor which forms a XB to a protein backbone carbonyl oxygen atom.[37]

Anion–π interactions are a relatively new and underexploited interaction for anion recognition and are dominated by electrostatics and anion-induced polarisation of the π-delocalised electron density (Figure 1.4d).[50,51] For example, Matile and co-workers have reported anion–π interactions between halides and a series of naphthalenediimides, such as the cyano-functionalised derivative shown in Figure 1.6a, and demonstrated the ability of such compounds to transport anions across bilayer membranes.[52] Due to their weak nature, however, anion–π interactions are often augmented by additional non-covalent interactions and utilised in aprotic, weakly competitive solvents.

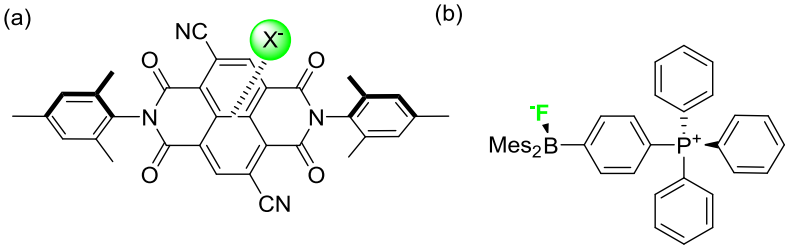

Figure 1.6 Examples of anion receptors employing (a) anion–π interactions[52] and (b) coordinate bonds.[53]

Coordinate bonds are not strictly considered non-covalent interactions due to the high degree of orbital overlap between the donor and acceptor species (Figure 1.4e).[6] Nevertheless, they are utilised frequently in anion recognition, due to the strong interaction between the Lewis acid and the anionic Lewis base, such as fluoride.[54] For example, Gabbaï and co-workers have reported a cationic borane derivative (Figure 1.6b) that binds fluoride strongly in aqueous media *via* a coordinate bond to the boron centre (K_a = 10 500 M^{-1} in 9:1 H_2O/CH_3OH solution).[53]

Receptors that are capable of recognising anions in highly competitive aqueous solvent mixtures employ one or more of the aforementioned non-covalent interactions. In the following sections, the use of such intermolecular interactions within both charged and neutral anion receptors is discussed, with particular focus on those capable of binding anionic guests in water or organic–aqueous solvent mixtures.

1.2.3 Positively charged hydrogen bonding receptors for anion recognition in aqueous solvents

Positively charged motifs have been integrated into a plethora of anion receptors which are designed to function in highly competitive polar, protic solvent media such as methanol and water. The simplest conceivable receptor for anions utilises pure electrostatics to bind the anion, but frequently the association is augmented by hydrogen bonding or other non-covalent interactions (*vide supra*).

Polyammonium anion receptors: Following the seminal work of Park and Simmons in the field of anion recognition (Figure 1.1d),[5] in which a polyammonium cage was reported to bind halide anions in aqueous TFA solution *via* both electrostatics and hydrogen bonds, many other highly-charged ammonium-based receptors have been reported. Notably, Lehn and co-workers investigated the anion binding properties of a series of polyammonium cages and macrocycles in aqueous solution, such as the macrobicyclic receptor depicted in Figure 1.7a which binds the linear azide anion with high affinity and selectivity in water at pH 5 ($\log K_a = 4.6$).[55] Very recently, Amendola and co-workers reported a cryptand that recognises and senses pertechnetate anions in acidic aqueous solution ($K_a = 3.1 \times 10^5$, Figure 1.7b).[56] The recognition process is reported by means of the modulated emission from the host's integrated anthracene fluorophore. Quaternisation of the amine motif in such cage-like receptors eliminates the hydrogen bond donors, and the resulting interaction with the anion becomes purely electrostatic. Whilst this inevitably leads to a reduction in anion binding affinity, the overall charge of a quaternary ammonium host is independent of pH, with the advantageous result that anion recognition is not limited to highly acidic media. With this benefit in mind, Schmidtchen prepared a series of macrotricyclic quaternary ammonium receptors capable of binding halides within the three dimensional cavity in pure water, with the halide selectivity trend reflecting the size of the cage structure (Figure 1.7c).[57,58]

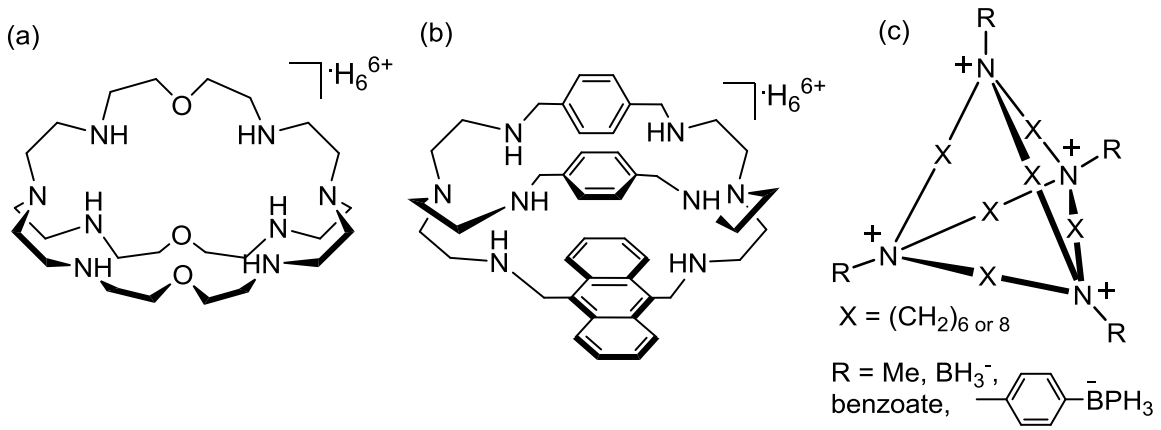

Figure 1.7 Polyammonium-based anion receptors: (a) Lehn's polyammonium cage,[55] (b) Amendola's pertechnetate receptor[56]and (c) Schmidtchen's quaternary ammonium cages.[57–61]

It should be noted that the principle disadvantage of charged anion receptors is the presence of counter-anions that can compete with the binding of the substrate. To minimise the effect of this competitive association, relatively non-coordinating counter anions are used, such as hexafluorophosphate, perchlorate or nitrate. In a novel approach, Schmidtchen prepared neutral zwitterionic quaternary ammonium cages in which negatively charged moieties such as borates or carboxylates are appended on the periphery (Figure 1.7c).[59,60,62] These hosts exhibit marked enhancement in halide association in water compared to the positively charged analogues that possess competing counter-anions.

Guanidinium-based receptors: Inspired by the anion binding capability of the arginine side-chain of the phosphate binding protein (Figure 1.3b), guanidinium motifs have been incorporated within a variety of anion receptor structural frameworks. The highly basic nature of the group ($pK_a \sim 11–13$) is particularly advantageous, with the protonated state existing over a wide pH range. Early examples of guanidinium-based receptors, such as Lehn's macrocyclic receptor shown in Figure 1.8a,[63,64] suffered from relatively poor anion binding properties, in part due to the inherent flexibility of the guanidinium motif. Anion recognition enhancement was achieved by the motif's incorporation within a pre-organised bicyclic ring (Figure 1.8b),[61] or by supplementing the interaction with additional hydrogen bond donor

groups, such as in Schmuck's tridentate guanidinium-carbonylpyrrole-based receptor (Figure 1.8c), which binds citrate in water with high affinity ($K_a > 10^5$ M^{-1}).[65]

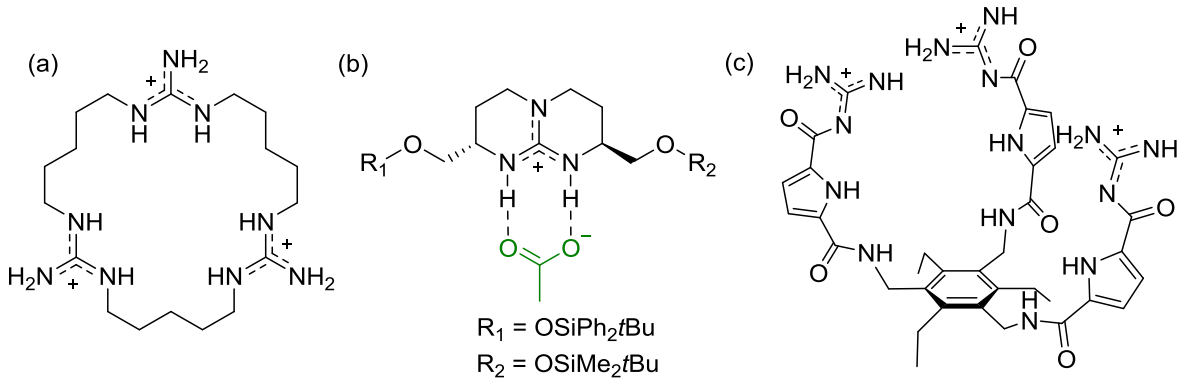

Figure 1.8 Guanidinium-based anion receptors: (a) Lehn's tris-guanidinium macrocycle,[63] (b) Schmidtchen's pre-organised bicyclic guanidinium[61] and (c) Schmuck's tridentate guanidinio-carbonylpyrrole citrate receptor.[65]

Positively charged heterocycles: A range of charged heterocyclic derivatives have been employed as anion recognition motifs, including pyridinium,[66,67] imidazolium[68–70] and triazolium,[71,72] utilising a combination of electrostatics and CH hydrogen bonding to bind the anion. For example, Kim's macrocyclic imidazolium receptor (Figure 1.9a) binds adenosine mono-phosphate (AMP) with high affinity in buffered aqueous solution,[70] whilst Beer's macrocyclic tetra-triazolium receptor has recently been demonstrated to bind halide anions in a 1:1 DMSO/water solvent mixture, with selectivity over acetate (Figure 1.9b).[72]

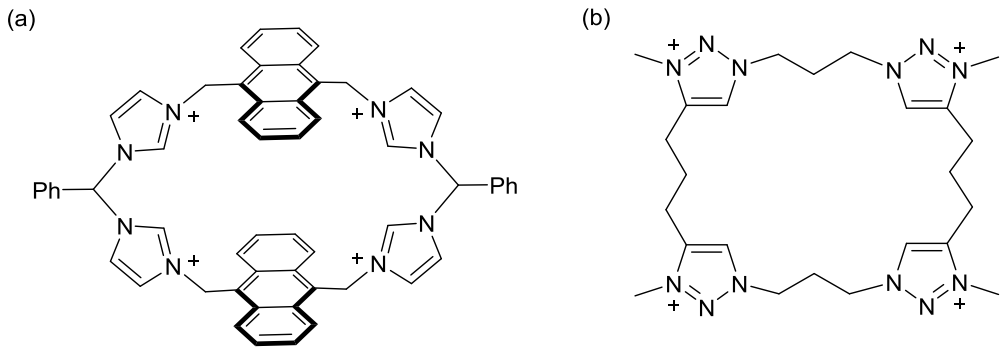

Figure 1.9 Macrocyclic (a) imidazolium[70] and (b) triazolium-based anion receptors[72] capable of anion recognition in aqueous solvents.

1.2.4 Neutral hydrogen bonding receptors for anion recognition in aqueous solvents

In contrast to the positively charged receptors discussed in the previous section which function in competitive aqueous solvents, neutral anion receptors employ weaker intermolecular interactions such as hydrogen bonds and are commonly utilised in less competitive organic solvents. Typical hydrogen bond donors incorporated into such neutral systems include amides,[73] ureas and thioureas,[74] pyrroles[75] and triazoles.[76–78] The electro-neutrality of such hosts offers an advantage over their charged analogues by eliminating the counter-anions which compete with the target guest for the binding site.

Amides and ureas: Polarised NH hydrogen bond donors, such as amides and ureas, have been used extensively in neutral anion receptors,[73] with the seminal amide-based receptor published by Pascal in 1986.[79] The major disadvantage of neutral hydrogen bonding interactions, however, is their weakness in protic solvents, and thus whilst there is a profusion of amide and urea based receptors in the literature, there are very few examples that are capable of operating in aqueous solutions.[80] A notable exception is Gale's macrocyclic host (Figure 1.10a),[81] which binds acetate with high affinity in 95:5 DMSO/H_2O solution ($K_a = 5170\ \text{M}^{-1}$), whilst Reinhoudt has demonstrated selective chloride recognition by a thiourea-functionalised cavitand host, with an association constant of 250 M^{-1} in 1:1 acetonitrile/water solution (Figure 1.10b).[82] In pioneering work, Kubik has demonstrated remarkable iodide and sulfate binding in 4:1 water–methanol solution by a neutral cyclic pseudo-peptide receptor (Figure 1.10c). The receptor forms a 2:1 host–guest complex with the anions ($K_{11} = 24\ \text{M}^{-1}$, $K_{21} = 6660\ \text{M}^{-1}$ for iodide; $K_{11} = 96\ \text{M}^{-1}$, $K_{21} = 1270\ \text{M}^{-1}$ for sulfate) through a combination of both amide-NH hydrogen bonds and the hydrophobic effect. The complexation is driven by both favourable enthalpic and entropic contributions, with the formation of the 2:1 host–guest complex being a highly cooperative process.[83,84]

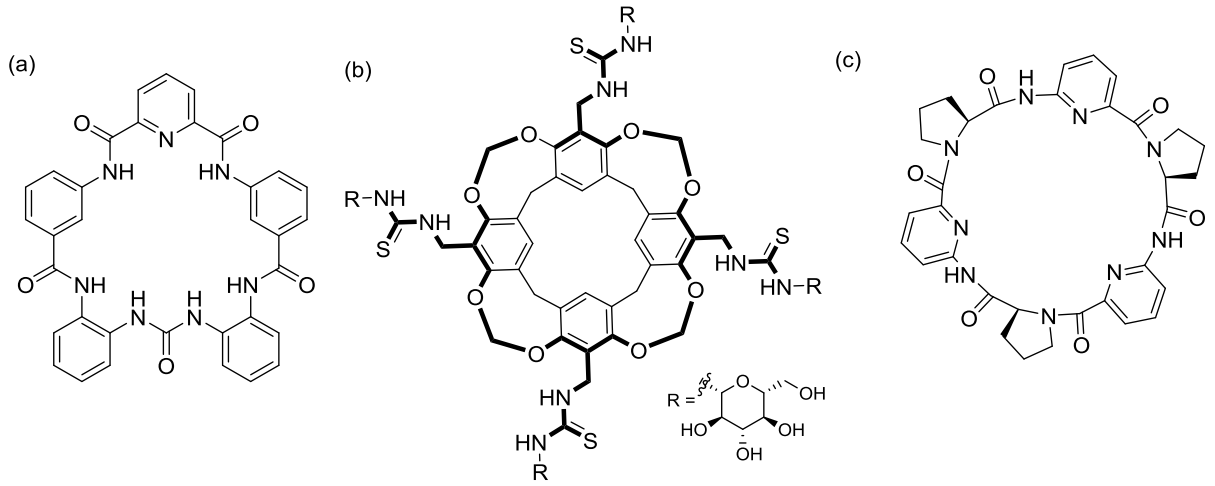

Figure 1.10 Neutral amide- and urea-based hydrogen bonding anion receptors capable of recognition in aqueous media: (a) Gale's amide-urea macrocycle,[81] (b) Reinhoudt's thiourea-functionalised cavitand,[82] (c) Kubik's cyclic peptide.[83]

Pyrrole-based anion receptors: Following the discovery of the anion binding properties of protonated sapphyrins (expanded porphyrins containing five pyrrole units),[75] and influenced by the anion binding ability of the tryptophan residue in the sulfate binding protein (Figure 1.3a),[16] extensive efforts have been applied to the development of pyrrole-containing anion receptors. Strong binding, particularly of fluoride and phosphate anions in organic solvents, has been reported by another class of macrocyclic pyrrole derivatives, the calixpyrrole.[85] However, whilst such neutral receptors are effective even in polar organic solvents such as DMSO, the interaction is, in general, too weak to operate in more competitive organic–aqueous solvent mixtures. The one notable exception to this is Sessler's fluorescent calix[4]pyrrole anion sensor (Figure 1.11a), which binds dihydrogenphosphate and hydrogenpyrophosphate in 4% water/acetonitrile solution with association constants of 6.8×10^5 M^{-1} and $>2 \times 10^6$ M^{-1} respectively.[86] It is postulated that the additional hydrogen bonds donated by the thiourea motif are responsible for the remarkably strong binding affinity observed in this competitive solvent mixture. Gale's acyclic bis-amidodipyrrolylmethane receptor also benefits from additional hydrogen bonding capability augmenting the interaction with the pyrroles, in this case from two amides (Figure 1.11b), facilitating binding of fluoride even in 25% water/DMSO solution ($K_a = 110$ M^{-1}).[87]

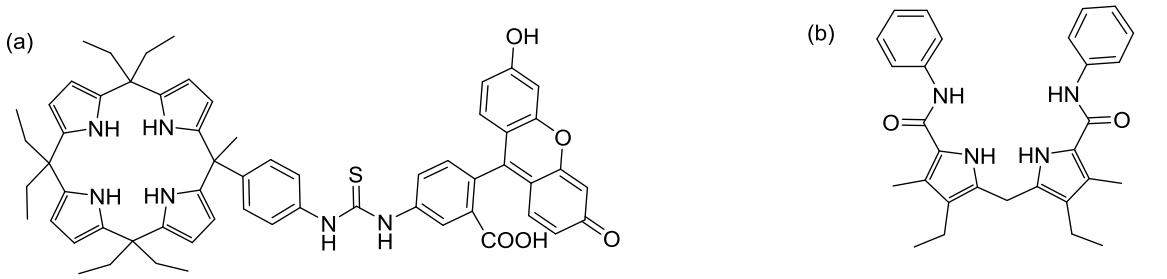

Figure 1.11 Neutral pyrrole-based hydrogen bonding anion receptors capable of recognition in aqueous media: (a) Sessler's fluorescent calix[4]pyrrole[86] and (b) Gale's acyclic bis-amido-dipyrrolylmethane receptor.[87]

1.2.5 Alternative intermolecular interactions for anion recognition in aqueous solvents

The receptors presented thus far have employed hydrogen bonds, in concert with electrostatics, to bind anions in aqueous solvents. However, alternative intermolecular interactions such as halogen bonding, anion-π and metal-ligand coordination can also be incorporated within receptor frameworks to enhance anion binding affinity and selectivity. Examples of receptors employing such intermolecular interactions are discussed in the following section.

1.2.5.1 Receptors utilising halogen bonds

Unlike the ubiquitous hydrogen bonds, the use of halogen bonds (Section 1.2.2) in solution phase anion recognition remains comparatively rare.[29] The initial step towards including halogen bonds within pre-organised anion receptor frameworks was taken by Resnati, Metrangolo and co-workers, who reported a heteroditopic ion-pair receptor (Figure 1.12a), which binds sodium in the receptor's tripodal polyether region, and the iodide counter anion by a single halogen bond (the geometry of the receptor prevents multiple halogen bonds acting in concert).[88] Taylor has more recently developed a library of multidentate iodo-tetrafluorobenzene-derived receptors capable of halide recognition in organic solvents *via* convergent halogen bonding interactions (Figure 1.12b).[30,47,89] Whilst neutral halogen bonding receptors reported to date function only in organic solvents, charged-assisted halogen bonding receptors display impressive affinities in polar organic[32,90,91] and organic–aqueous solvent

mixtures.[34,48] The strength of the interaction is exemplified in Resnati's acyclic iodoimidazolium host, which binds dihydrogen phosphate in DMSO solution (K_a = 1100 M^{-1}) by means of a single charge-assisted halogen bonding interaction (Figure 1.12c).[91] Similarly, strong binding of bromide and iodide is observed in 9:1 CH_3OH/H_2O by Beer's bis-haloimidazolium macrocycles (Figure 1.12d).[48] Interestingly, whilst the bromoimidazolium macrocycle is iodide selective, the selectivity is reversed in favour of bromide in the iodoimidazolium analogue. In both cases the halide anion guests can be sensed by means of the modulated emission of the receptor's naphthalene moiety.

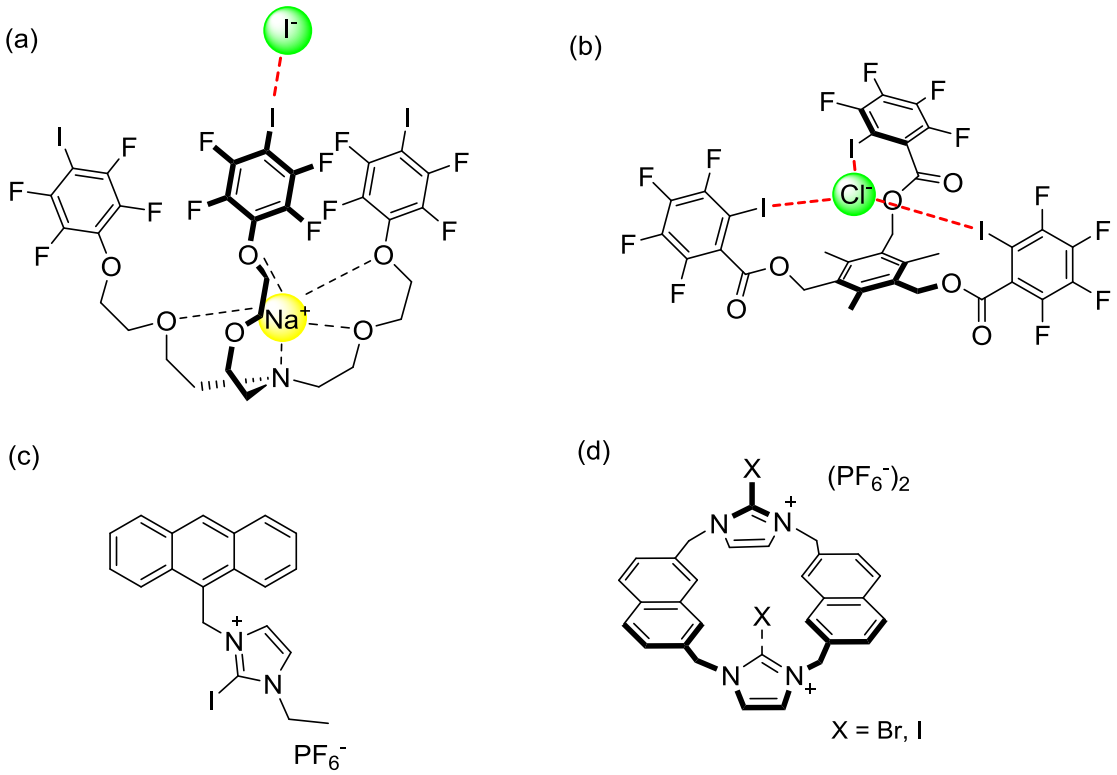

Figure 1.12 Halogen bonding anion receptors: (a) Resnati's ion-pair receptor,[88] (b) Taylor's tridentate iodotetrafluorobenzene host,[47] (c) Resnati's iodoimidazolium receptor[91] and (d) Beer's bis-iodoimidazolium macrocycle.[48]

At the commencement of the work reported in this thesis, however, the halogen bond-mediated recognition of anions in pure water was unprecedented.

1.2.5.2 Receptors utilising anion-π interactions in aqueous solution

Anion-π interactions, being relatively weak (Section 1.2.2), have not been employed to a great extent for anion recognition in competitive aqueous media and merely confined to operating in organic solvents.[50] Indeed, in a recent survey of experimental data in the literature, Ballester and co-workers concluded that in organic solvents the binding free energy contribution from anion-π interactions with substituted phenyl rings is less than −4 kJ mol^{-1}.[92] However, the binding of anions in aqueous solvent mixtures has been achieved in receptors where anion-π interactions are supplemented by additional, stronger intermolecular interactions. For example, Bianchi has very recently reported a nitroso-amino-pyrimidine receptor that binds highly charged anions such as SO_4^{2-}, SeO_4^{2-}, $S_2O_3^{2-}$ and $Co(CN)_6^{3-}$ in water, *via* electrostatics, hydrogen bonding and anion-π interactions (Figure 1.13).[93] The contribution to the total binding free energy from the anion-π interactions was determined to be in the region of −10 kJ mol^{-1}.

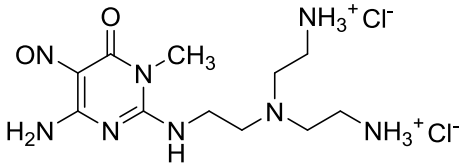

Figure 1.13 Bianchi's nitroso-amino-pyrimidine receptor that binds anions through electrostatics, hydrogen bonding and anion-π interactions.[93]

1.2.5.3 Hosts containing metal centres

Metal cations incorporated into anion receptors can play a number of different roles: (i) as a Lewis acidic coordination site for the anion; (ii) as a charged motif contributing to the anion binding affinity through electrostatics and polarisation of adjacent hydrogen bond donors; (iii) as a structure stabilising element dictating the geometry of a receptor and (iv) as a non-coordinating electrochemical or optical reporter group (Section 1.3).[94,95]

Since the early examples of dicopper(II) cryptates published by Lehn,[96] a wide variety of related transition metal-based receptors have been synthesised, including Fabbrizzi's Cu(II) trifurcate receptor that recognises citrate with high affinity in water (log K_a = 5.6),[97] and Jolliffe's bis-zinc(II)dipicolylamino-peptide which binds pyrophosphate in buffered aqueous solution (log K_a > 9, Figure 1.14b).[98] A variety of Lewis acidic receptors containing main group elements have also been reported, including boron,[54,99–101] silicon,[102] tin,[103] germanium[104], tellurium[105] and antimony.[106,107] For instance, Gabbaï has reported cationic borane receptors that recognise fluoride in water (Figure 1.6b and Figure 1.14c)[53,108] by means of a strong coordinate bond between the anion and the Lewis acidic boron atom, and very recently reported an antimony-based receptor that exhibits turn-on fluorescence emission in the presence of fluoride anions (Figure 1.14d).[107]

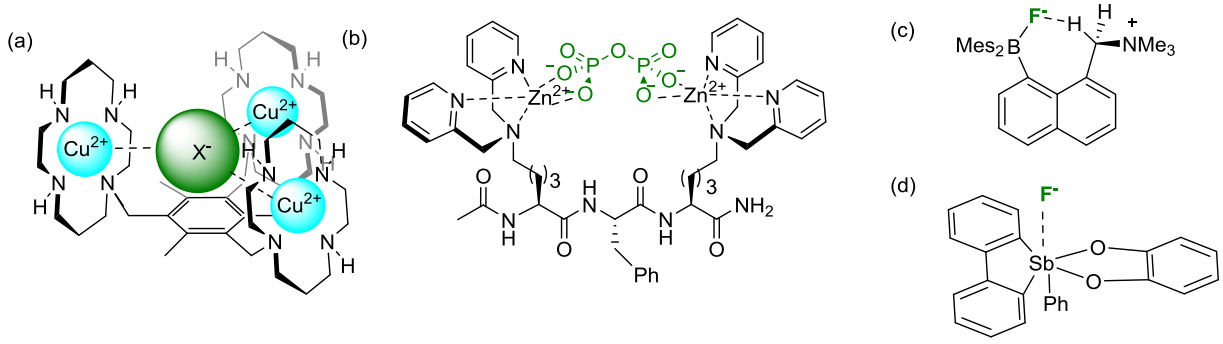

Figure 1.14 Metal-based anion receptors: (a) Fabbrizzi's trifurcate Cu(II) receptor[97] (b) Jolliffe's zinc(II)dipicolylamino peptide,[98] (c) Gabbaï's ammonium-bornane receptor and (d) stiborafluorene.[107]

Lewis acidic lanthanide cations have received much attention for anion recognition in water, in particular for anion sensing applications, as a consequence of their long-lived luminescence which is highly sensitive to the metal coordination environment.[109] These systems are discussed in more detail in Section 1.3.2.2 in the context of anion sensing.

1.3 Anion sensors

The development of selective anion *sensors* that undergo a macroscopic, detectable response upon anion binding is an area of intense interest. The most prevalent methodologies to achieve this goal are depicted schematically in Figure 1.15.

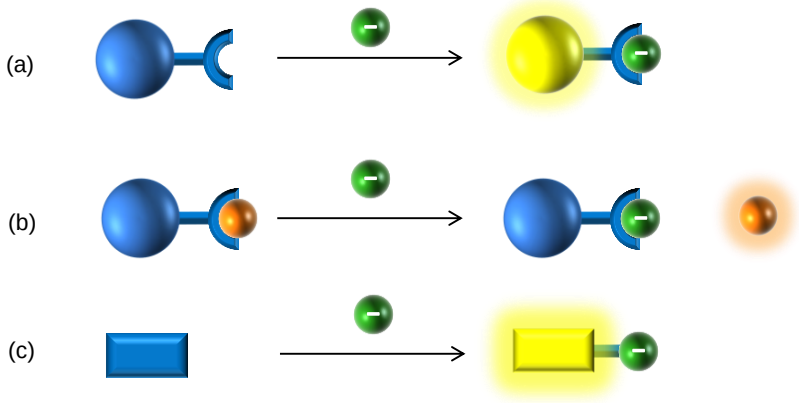

Figure 1.15 Schematic representation of the general methods of anion sensing: (a) reporter group attached to a receptor, (b) displacement assay and (c) chemo-dosimeter.

Arguably the most common system involves the appendage of an optical or electrochemical reporter group to an anion receptor motif (Figure 1.15a): anion binding perturbs either the photo-physical or electrochemical properties of the reporter group, resulting in a measurable macroscopic response. Alternatively, in a displacement assay (Figure 1.15b), the receptor is pre-formed with a bound dye guest.[110,111] The system is designed such that a target anion is bound preferentially and will displace the dye molecule, concomitant with an associated signalling response. Finally, in a chemo-dosimeter (Figure 1.15c),[112–114] the analyte reacts with the sensor molecule and induces detectable changes in the properties of the receptor.

The optimal anion sensor combines high guest affinity and selectivity with an easily detectable, sensitive response output, which necessitates careful receptor and reporter group design. This section focuses on molecular anion sensors incorporating a recognition site and appended reporter group (Figure 1.15a), which are capable of electrochemical or optical anion sensing in solution.

1.3.1 Electrochemical anion sensors

Electrochemical anion sensors incorporate a redox active reporter group in close proximity to the anion recognition site, such that guest binding perturbs the redox potential of the reporter group. The bound anion stabilises one or other of the species of the redox couple, perturbing the potential for either the oxidation (for example ferrocene to ferrocenium) or reduction (cobaltocenium to cobaltocene) process.

Since the seminal reports of cobaltocenium- and ferrocene-based electrochemical anion receptors by Beer and co-workers over two decades ago (Figure 1.16a),[115,116] many examples of acyclic, macrocyclic and mechanically interlocked anion hosts incorporating redox-active groups have been reported.[95,117] For example, Molina and co-workers recently described a bis-ferrocene-triazole anion receptor (Figure 1.16b) that senses AcO^-, $H_2PO_4^-$ and $HP_2O_7^{3-}$ by means of a large cathodic shift in the ferrocene/ferrocenium redox couple (ΔE = ~200 mV in CH_3CN / 0.1 M $TBAPF_6$),[118] whilst Becher has reported a redox-responsive mono-tetrathiafulvalene (TTF) calix[4]pyrrole which can detect chloride and bromide anions in CH_3CN solution through a ~460 mV cathodic shift of the first TTF oxidation potential (Figure 1.16c).[119]

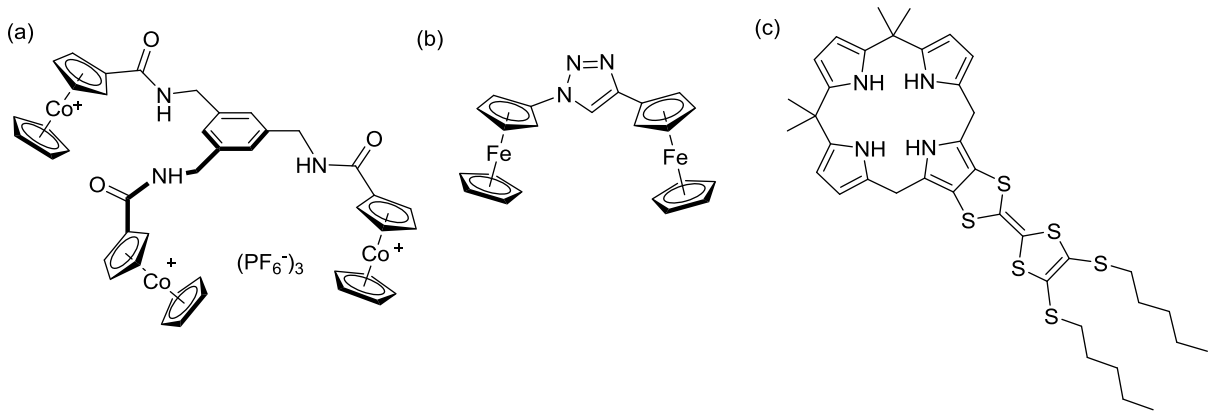

Figure 1.16 Redox-active electrochemical anion sensors: (a) Beer's cobaltocenium-based host,[115] (b) Molina's bis-ferrcoenetriazole receptor[118] and (c) Becher's tetrathiafulvalene-functionalised calix[4]pyrrole.[119]

1.3.2 Optical anion sensors

Optical anion sensors can be grouped into two classes according to their mode of signalling: in *luminescent sensors*, anion complexation causes changes to the excited-state emission (from a singlet state in the case of fluorescence, or a triplet state for phosphorescence); whilst in *colourimetric sensors* the ground-state absorption in the visible spectrum is perturbed. Luminescent sensors are desirable due to their intrinsic high sensitivity, whilst colourimetric systems have the benefit of facilitating naked-eye detection of the analyte.

1.3.2.1 Luminescent anion sensors

Luminescent reporter groups appended to an anion recognition site can signal the anion binding event *via* changes in the emission profile through a number of different signal transduction pathways: photo-induced electron transfer (PET); electronic energy transfer; switching between monomer and excimer states (or *vice versa)* and the "rigidity effect."[120]

Photo-induced electron transfer (PET) is a mechanism of fluorescence quenching in which electron transfer to the singlet excited state from a proximal orbital returns the fluorophore to the ground state without radiative emission. For example, in the unbound state of Czarnik's phosphate sensor (Figure 1.17a), the benzylic nitrogen lone pair quenches the fluorescence of the naphthalene motif *via* a PET mechanism.[121] Anion complexation is concomitant with protonation of the benzylic nitrogen atom, inhibiting the PET quenching process and turning on the fluorescence response.

The propensity of pyrene to undergo excimer formation has also been employed in the preparation of anion sensors.[122,123] In Teramae's pyrophosphate sensor,[122] anion complexation with the guanidinium-functionalised pyrene monomer results in the formation of dimeric complex in methanol solution, accompanied by the appearance of the excimer band in the pyrene emission spectrum (Figure 1.17b). The selectivity of the system for pyrophosphate stems from the geometry of the anion: the anion assembles the two pyrene derivatives in the

stacked orientation that is prerequisite for excimer formation, whereas binding of halides does not result in the correct orientation of the pyrene monomers.

Optical anion sensors have also been prepared that contain metal-based luminophores. The Ru(II) tris(bipyridyl) motif has been used extensively in such systems,[120,124–127] for example in the bis-imidazolium-functionalised sensor depicted in Figure 1.17c,[127] in which the selective binding of chloride in 9:1 CH_3CN/H_2O causes a hypsochromic (blue) shift and enhancement of the MLCT emission band of the Ru(II) centre. This enhancement is attributed to the increased rigidity of the receptor when complexed to the anion, which reduces non-radiative vibrational and rotational decay pathways.

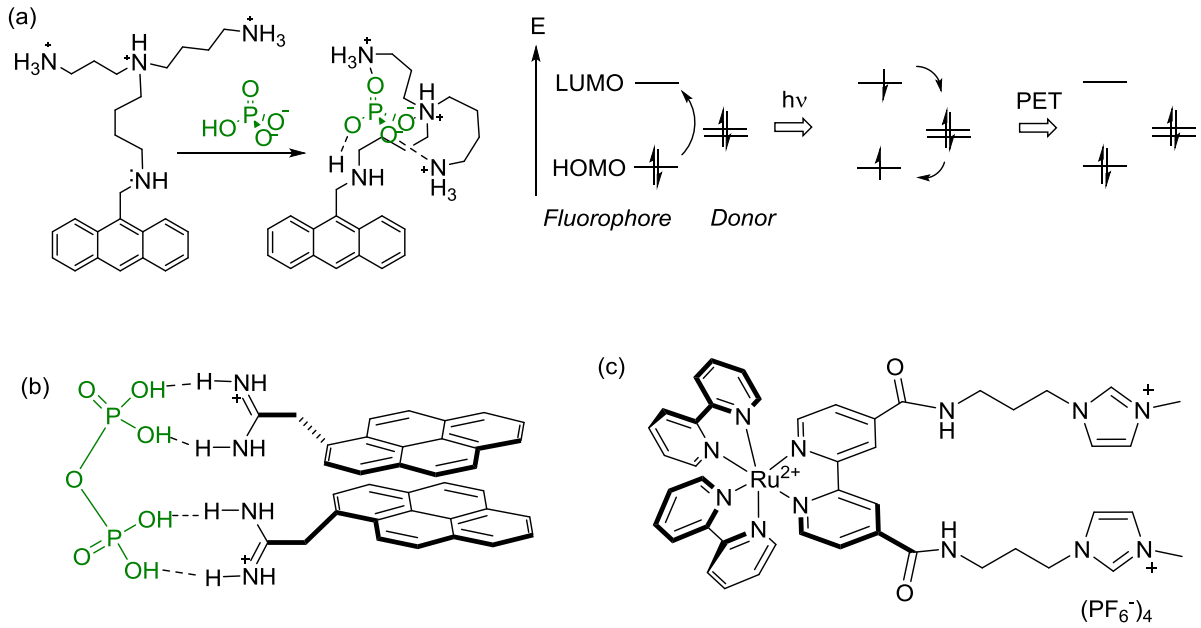

Figure 1.17 Luminescent anion sensors (a) Czarnik's anthracene-based phosphate sensor, with the mechanism for PET quenching by a proximal donor group,[121] (b) Teramae's pyrene-functionalised pyrophosphate sensor[122] and (c) Beer's bis-imidazolium $Ru(bipy)_3$ chloride receptor.

1.3.2.2 Luminescent lanthanide-based anion sensors

A distinct class of metal-based anion sensors are those containing lanthanide cations.[109] The direct excitation of lanthanide cations is very inefficient due to the Laporte forbidden f-f transitions resulting in low extinction coefficients (0.5–3 dm^{-3} mol^{-1} cm^{-1}); thus a common solution is to incorporate donor chromophore groups within the complex. These can act as an antenna to mediate the formation of the lanthanide emissive state, usually *via* the chromophore's triplet state, to achieve long-lived emission from the lanthanide centre (Figure 1.18).[128–130] Anion binding can perturb either the ligand excited state, or the lanthanide excited state, and modulate the lifetime, energy, intensity or polarization of the emitted radiation.

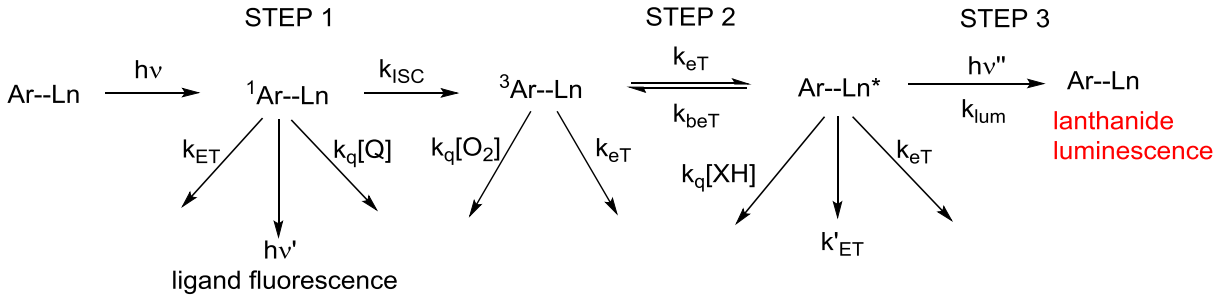

Figure 1.18 Photophysical processes occurring during sensitised lanthanide emission (eT: energy transfer; ET: electron transfer)

There are three general mechanisms through which anion sensing occurs within lanthanide-based receptors:

Displacement of a coordinated water molecule by the anion: Displacement of a coordinated water molecule results in a modification of the lanthanide coordination environment, which is manifested through a change in the spectral form of the emission. Furthermore, the overall emission intensity is enhanced due to the loss of the O–H oscillators associated with the water molecule, which contribute to non-radiative quenching of the emissive state. Such a phenomena is observed upon bicarbonate binding by Parker's europium complex (Figure 1.19a).[131]

Anion-induced perturbation of the ligand antenna ground state: The second mechanism involves the anion interacting with a ligand-based anion receptor and perturbing the ground state of the chromophore, which may result in intensity changes in the lanthanide emission spectrum due to modulation of the energy transfer processes. For example, the reversible attack of hydroxide at the phenanthridinium ligand of the europium complex shown in Figure 1.19b can be used to monitor hydroxide concentration in solution.[132]

Anion-induced perturbation of the antenna excited state: The third mechanism also involves the anion interacting with the ligand, but in this case *via* collisional quenching of the singlet excited state, resulting in a reduction of the lanthanide emission intensity. This is observed upon halide anion addition to the same phenanthridinium europium complex (Figure 1.19b).[132]

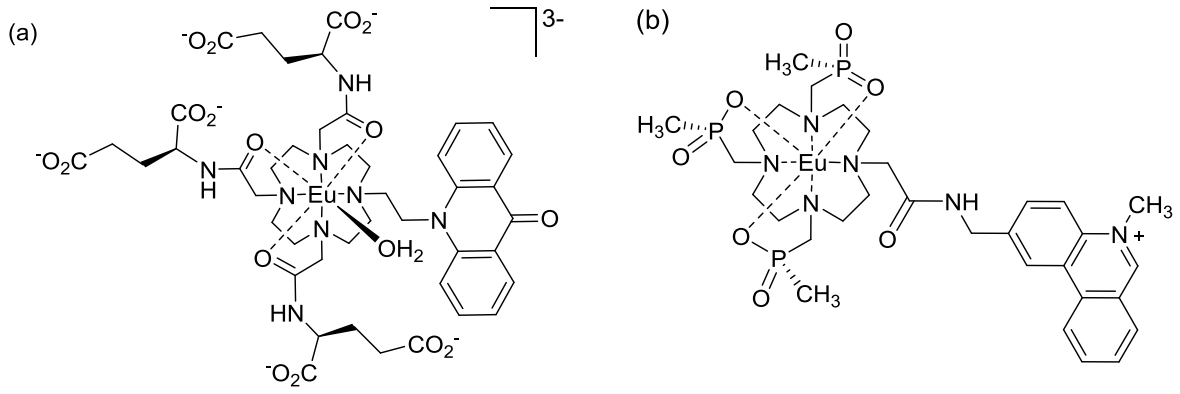

Figure 1.19 Lanthanide-based luminescent anion sensors: (a) Parker's bicarbonate sensor[131] and (b) phenanthridinium-based hydroxide and halide anion sensor.[132]

Gunnlaugsson and co-workers have demonstrated the use of sensitised lanthanide complexes in a gold nanoparticle-based *displacement assay*, capable of sensing biologically relevant phosphates such as flavin-monophosphate in water (Figure 1.20).[133] Association of the aromatic β-diketone sensitiser to the hydrated europium complex appended to the nanoparticle switches on the lanthanide luminescence. The sensitiser-lanthanide complex can sense flavin-monophosphate through displacement of the sensitiser by the anion guest, which causes the switching off of the emission.

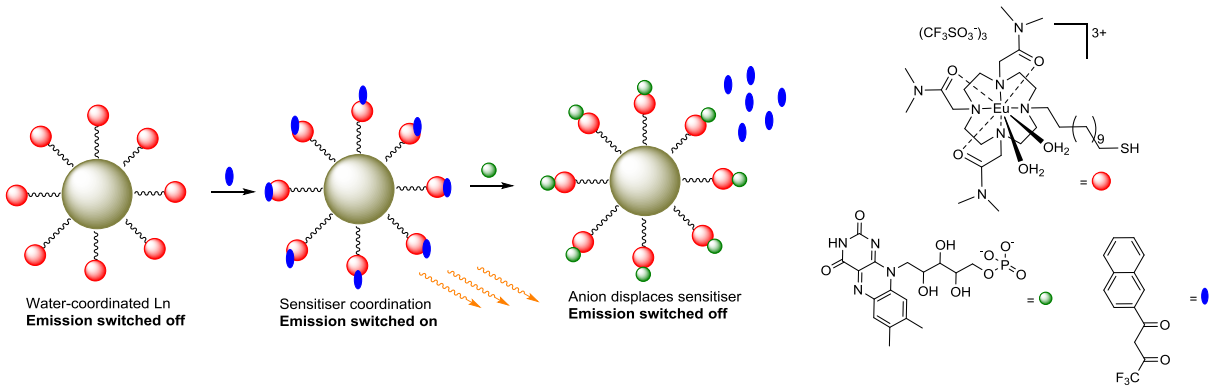

Figure 1.20 Gunnlaugsson's lanthanide-based gold nanoparticle displacement assay for flavin-monophosphate sensing.[133]

1.3.2.3 Colourimetric anion sensors

Colourimetric anion sensors, in which anion binding results in absorbance changes in the visible region of the spectrum, are particularly attractive due to the obvious advantage of naked-eye detection of anions. For example, the thiourea-based receptor shown in Figure 1.21a recognises anions in the binding cleft between the two thiourea motifs, and acts as a colorimetric sensor for fluoride anions in DMSO solution,[134] whilst fluoride binding in $CHCl_3$ by the pyridinium-borane receptor depicted in Figure 1.21b results in a "turn-on" colour change from colourless to yellow.[135] Sessler has developed a range of chromophore-appended calix[4]pyrroles, such as the hydroxyl-anthraquinone system shown in Figure 1.21c, which exhibits anion-specific colour changes for dihydrogenphosphate, chloride and fluoride in dichloromethane solution.[136]

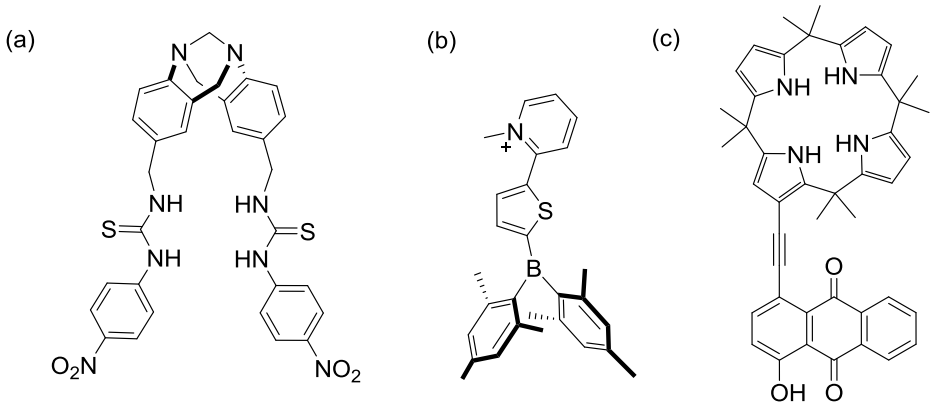

Figure 1.21 Colourimetric anion sensors: (a) thiourea-functionalised fluoride sensor,[134] (b) pyridinium-borane-based host for fluoride[135] and (c) hydroxyl-anthraquinone-appended calix[4]pyrrole anion receptor.[136]

1.4 Template synthesis of supramolecular architectures

1.4.1 Template-directed self-assembly

Self-assembly is the spontaneous association of small substrate molecules into higher-order architectures of greater complexity, utilising intermolecular attractive interactions. Control of product formation can be achieved by the addition of a templating species, and this approach will be discussed in the following sections.

Nature itself provides inspiration for template-directed synthesis, for instance in the linear template-directed replication of DNA.[18] The use of templates in synthetic chemistry was pioneered by Busch,[137,138] who coined the first definition: "*A chemical template organises an assembly of atoms, with respect to one or more geometric loci, in order to achieve a particular linking of atoms."* He further classified such species as either thermodynamic or kinetic templates: thermodynamic templates stabilise the product in an equilibrium system and drive the equilibrium in the direction of that species, whereas kinetic templates stabilise the transition states leading to the formation of the desired product in an irreversible reaction. Sanders has more recently suggested templates should be classified according to their relation to the topology of the template product species: as either linear, cyclising or interweaving templates.[139]

1.4.1.1 Cation templation

Since the pioneering work of Busch using Ni(II) cation templation to alter the product ratio of the reaction between reaction between mercapto-amines and diketones (Figure 1.22),[137] cation templation has been used extensively to construct poly-metallic supramolecular architectures of ever increasing complexity, including macrocycles,[140] grids,[141] Borromean rings (Figure 1.23a),[142] cages,[143,144] polyhedra[143-145] and nanorings.[148,149]

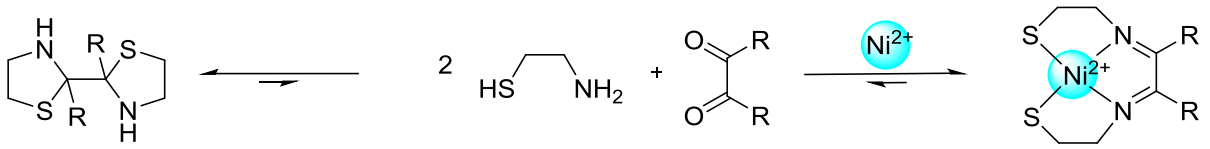

Figure 1.22 Reaction of mercapto-amines and diketones in the presence and absence of a Ni(II) cation template.[137]

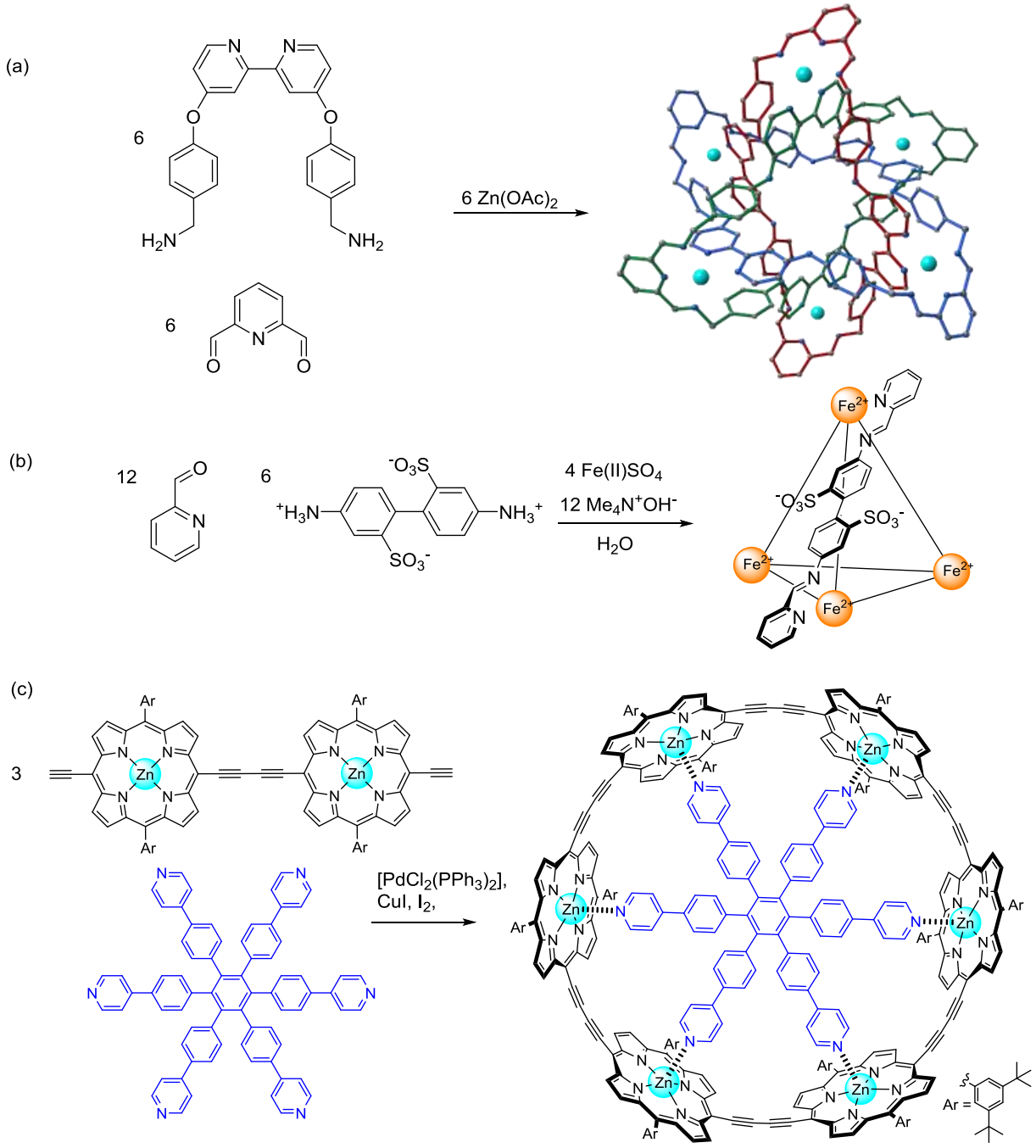

Figure 1.23 Examples of cation templation: (a) crystal structure of Stoddart's Zn(II)-templated Borromean rings,[142] (b) Nitschke's Fe(II)-templated tetrahedral cage[143] and (c) Anderson's Zn(II) porphyrin nanoring.[148]

For example, Nitschke and co-workers have reported the Fe(II) cation-templated assembly of a tetrahedral cage in aqueous solution using aldehyde-amine condensation reactions (Figure 1.23b),[143] whereas Anderson used multiple zinc-pyridine interactions to template the formation of a zinc(II)-porphyrin nanoring (Figure 1.23c).[148] These selected examples demonstrate the range of impressive architectures that can be prepared from relatively simple starting materials by exploiting the structure-directing influence of the metal cation's geometric coordination preferences.

1.4.1.2 Anion templation

As mentioned previously, the development of anion coordination chemistry has been relatively sluggish compared with the well-developed field of cation coordination chemistry, and thus examples of anion templation strategies for the formation of supramolecular architectures are much rarer. Nevertheless, the selected examples presented below (Figure 1.24) demonstrate the potential of an anion-templation approach in directing the assembly of intricate, higher-order structures.

Many examples of anion templation reported in the literature were the result of serendipitous discovery. For example, Lehn described the formation of a pentanuclear Fe(II)-helicate from a mixture of a tris-bipyridyl ligand and Fe(II) chloride (Figure 1.24a), whilst in the presence of Fe(II) sulfate the same ligand assembled into the analogous hexa-nuclear helicate structure.[150,151] Sessler discovered that nitric acid promoted the near quantitative formation of a Schiff-base macrocycle which crystallised from the reaction mixture as the nitrate salt, in dramatic contrast to the low yield obtained using hydrochloric acid (Figure 1.24b).[152] The same group later demonstrated the critical role of anions in altering the product distribution of other poly-pyrrolic macrocycles.[154] More recently, Luis and co-workers have used a terephthalate anion to template the formation of a pseudo-peptidic macrocycle in >90% yield (Figure 1.24c), whilst in the absence of the template a complex

mixture of products was formed.[153] The anion template was also shown to catalytically enhance the rate of imine bond formation during the macrocyclisation reaction.

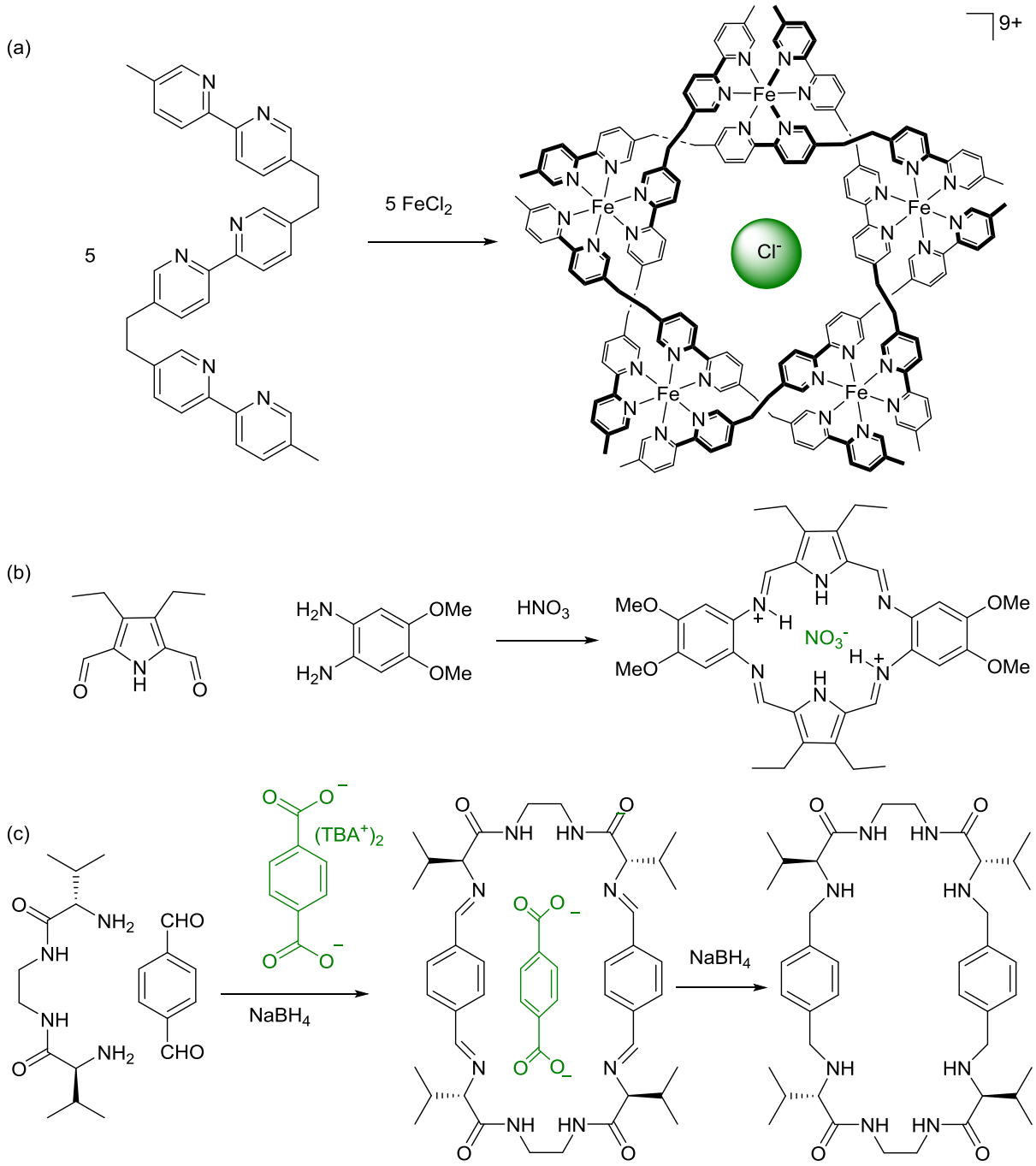

Figure 1.24 Examples of anion templation: (a) Lehn's chloride-templated Fe(II)-helicate,[150,151] (b) Sessler's nitrate templated macrocycle synthesis[152] and (c) Luis' anion templated synthesis of a pseudo-peptidic macrocycle.[153]

1.4.2 Interpenetrated and interlocked structures

Mechanically interlocked molecules have captured chemists' imaginations for decades, initially for the synthetic challenge and aesthetic appeal, but also more recently for prototypical molecular machines and other nanotechnological applications.[155] A mechanically interlocked molecule consists of two or more components, connected by a *mechanical bond*, such that they cannot be separated without cleavage of a covalent bond and yet are not themselves covalently attached. The simplest such molecules are [n]rotaxanes (a macrocycle threaded around a dumbbell) and [n]catenanes (interlocked macrocycles), where n represents the number of discrete interlocked components (Figure 1.25). A related structure is the interpenetrated [n]pseudorotaxane, in which the bulky stopper groups that are prerequisite for rotaxane formation are absent and hence is not strictly an interlocked molecule. Nevertheless, such species are useful precursors for rotaxane and catenane formation (*vide infra).*

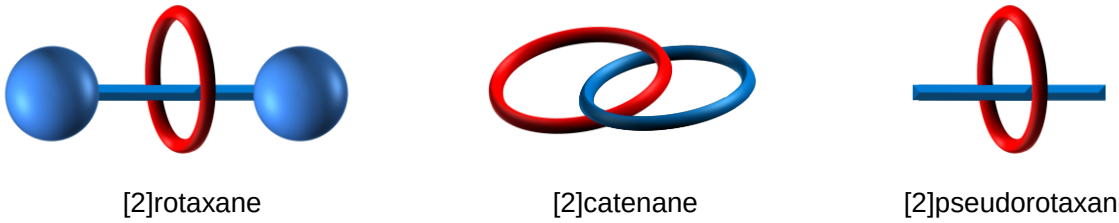

Figure 1.25 Schematic representation of interpenetrated and interlocked molecular architectures.

Other, more complex interlocked architectures are known, including knots and Borromean rings (Figure 1.23a).[142,156] The subsequent part of this section focuses on the synthesis of rotaxane and catenanes, before discussing some recent applications of such species.

1.4.3 Synthesis of rotaxanes and catenanes

The two most common strategies for rotaxane synthesis are *clipping* and *stoppering* methodologies and are also the most relevant to this thesis (Figure 1.26). Clipping requires the ring-closing of an acyclic macrocycle precursor around a stoppered-axle component, in which the stoppers are sufficiently bulky to prevent the macrocycle from subsequently de-threading. Stoppering involves the initial formation of a pseudorotaxane assembly, which is then functionalised with bulky stopper groups. Less common methodologies include *slippage,*[157] *snapping,*[158,159] *swelling*[160] and *shrinkage.*[161] Strategies for catenane synthesis include cyclisation of the threading component of a pseudorotaxane or the double cyclisation of two macrocycle precursor components arranged in an orthogonal geometry (Figure 1.26).

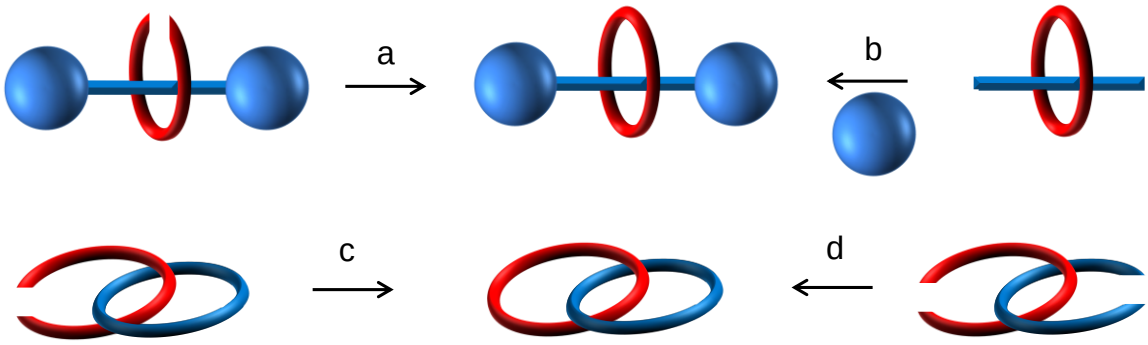

Figure 1.26 Synthetic routes for rotaxane and catenane synthesis: (a) clipping and (b) stoppering [2]rotaxane syntheses; (c) clipping and (d) double cyclisation [2]catenane syntheses.

1.4.3.1 Cation templated interlocked molecule synthesis

Early approaches to interlocked molecule synthesis relied on low yielding statistical methods[162–165] or laborious syntheses involving the covalent attachment of a template and its subsequent removal.[166] In a ground-breaking publication, Sauvage reported the seminal example of the templated synthesis of an interlocked molecule, using a discrete Cu(I) cation template: two bidentate phenanthroline ligands are held in an orthogonal arrangement by the

tetrahedral coordination preference of the templating metal cation, with a subsequent clipping reaction affording the [2]catenane (Figure 1.27).[167,168]

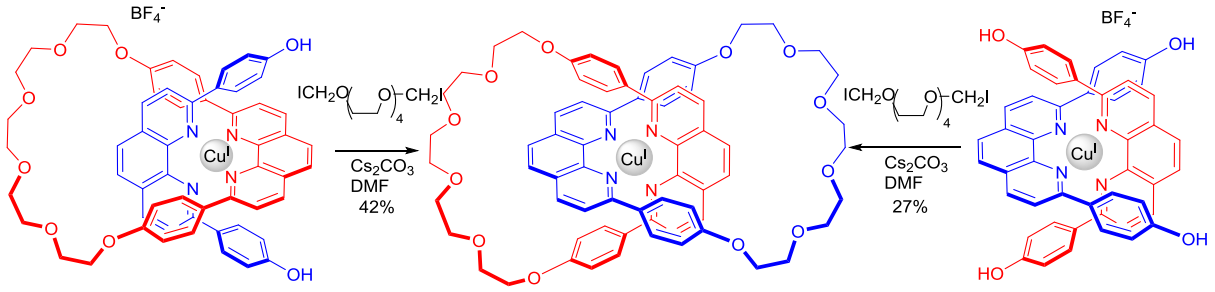

Figure 1.27 Sauvage's seminal Cu(I)-templated catenane syntheses.[167,168]

The wide-ranging utility of this Cu(I) templation approach has been subsequently exploited in the synthesis of more complex molecular architectures, such as a [3]catenane,[169] [3]rotaxane[170] and a trefoil knot.[171] Following these initial reports, a variety of other metal cations have been utilised for interlocked molecule formation, exploiting their octahedral (Ru(II)),[172] trigonal bipyramidal (Zn(II), Figure 1.28a),[173] square planar (Pd(II))[174] or linear (Au(I), Figure 1.28b) coordination geometries.[175]

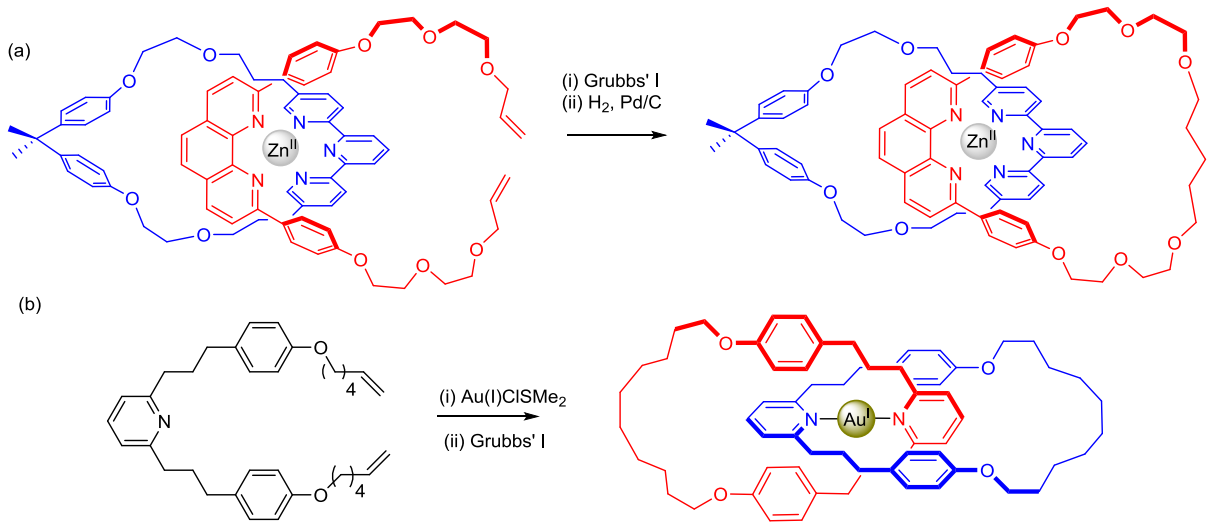

Figure 1.28 Metal-ion templated interlocked structures: (a) Zn(II) templation,[173] (b) Au(I) templation.[175]

Recently Leigh has reported the "active-metal" templation approach for the synthesis of mechanically interlocked molecules, exploiting both the defined coordination geometry and the catalytic ability of transition metal cations.[176] The metal cation is bound transiently within

the cavity of a macrocycle and catalyses covalent bond formation to form the interlocked structure (Figure 1.29).

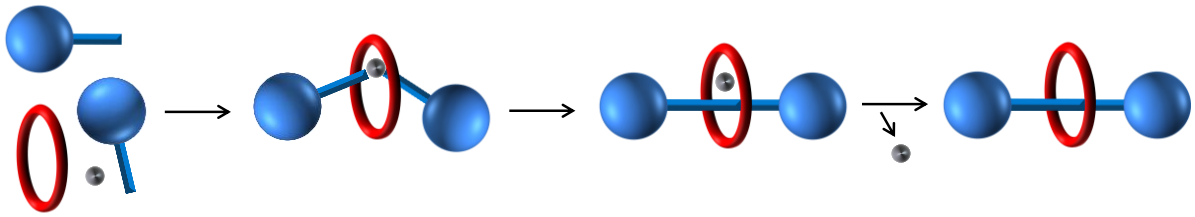

Figure 1.29 Schematic representation of active metal templation of a [2]rotaxane.[176]

Since Leigh's seminal report in 2006 of the copper(I)-catalysed alkyne–azide cycloaddition (CuAAC)[177] active-templated synthesis of a [2]rotaxane,[178] and more recently a [2]catenane (Figure 1.30a),[179] other transition-metal mediated coupling reactions have been exploited in the synthesis of mechanically interlocked architectures.

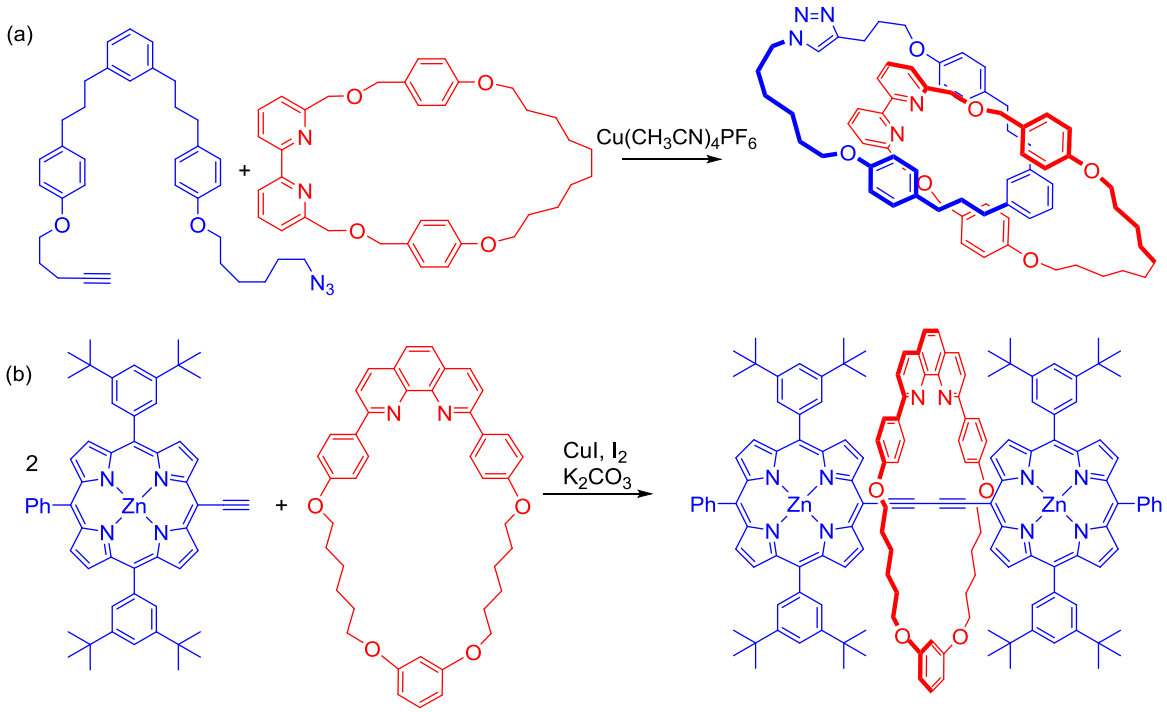

Figure 1.30 Active metal templation of interlocked molecules: (a) Leigh's CuAAC active templation of a [2]catenane[179] and (b) Anderson's butadiyne-linked porphyrin [2]rotaxane prepared *via* active-metal Glaser coupling.[180]

These include palladium-catalysed cross couplings,[181] Cu(I)[182,183] and Pd(II)[184] catalysed alkyne homo-couplings (including, for example, Anderson's butadiyne-linked porphyrin

[2]rotaxane shown in Figure 1.30b),[180] Ni(II)-catalysed C-C homo-coupling[185] and Pd(II)-mediated Michael additions.[186]

Stoddart has pioneered the use of charge-assisted aromatic donor–acceptor interactions between the 4,-4'-bipyridinium motif and an electron-rich hydroquinone derivative, facilitating the synthesis of rotaxanes, catenanes (Figure 1.31a)[187] and higher-order structures.[188] Poly-pyridinium cations, in conjunction with polyether macrocycle components, have also been utilised extensively in the preparation of interpenetrative and interlocked molecules, including pseudorotaxanes,[189,190] rotaxanes (such as Loeb's 1,2-bis(4,4'-dipyridinium)ethane-derived [3]rotaxane shown in Figure 1.31b)[191,192] and catenanes.[188]

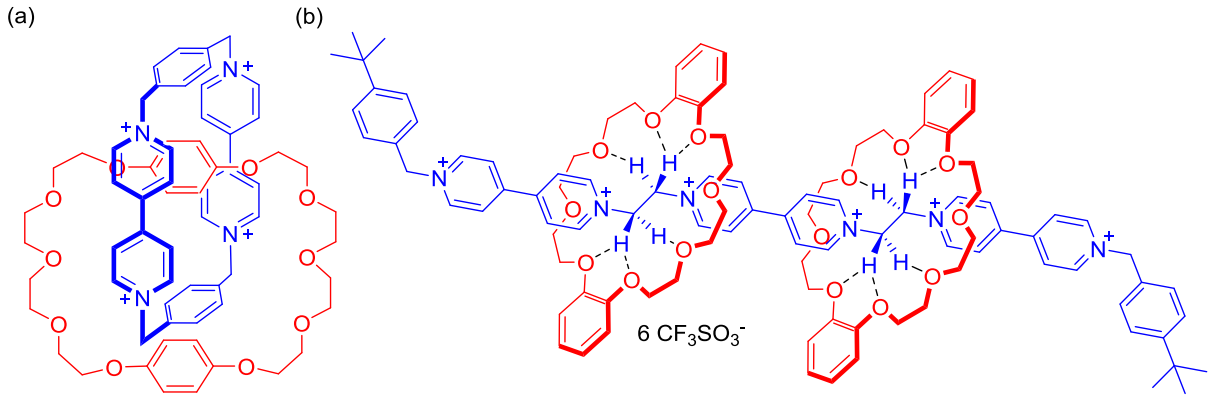

Figure 1.31 Interlocked molecules template by organic cations: (a) Stoddart's 4,4'-bipydridinium charge-assisted donor–acceptor [2]catenane[187] and (b) Loeb's 1,2-bis(4,4'-dipyridinium)ethane-derived [3]rotaxane.[192]

1.4.3.2 Assembly of interlocked architectures using neutral species

The first reports of neutral templated syntheses of interlocked molecules using hydrogen bonding interactions were published independently by Vögtle[193] and Hunter (Figure 1.32a)[194] in 1992, *via* amine–acid chloride condensation reactions. Leigh's group have also used a similar approach for the synthesis of rotaxanes and catenanes, using inter-component hydrogen bonding interactions to assemble the interlocked architectures.[195–197] Sanders has pioneered the use of neutral aromatic donor–acceptor interactions between naphthalene diimides (NDIs) and hydroquinones, to assemble catenanes from a dynamic combinatorial library (Figure 1.32b).[198,199] In a different approach, Harada has used the hydrophobic effect

to template the formation of rotaxanes by stoppering of a hydrophobic axle precursor component threaded though the cavity of cyclodextrin derivatives,[200,201] whilst Anderson has exploited such cyclodextrin-based rotaxanes in the preparation of "insulated molecular wires" (Figure 1.32c).[202,203]

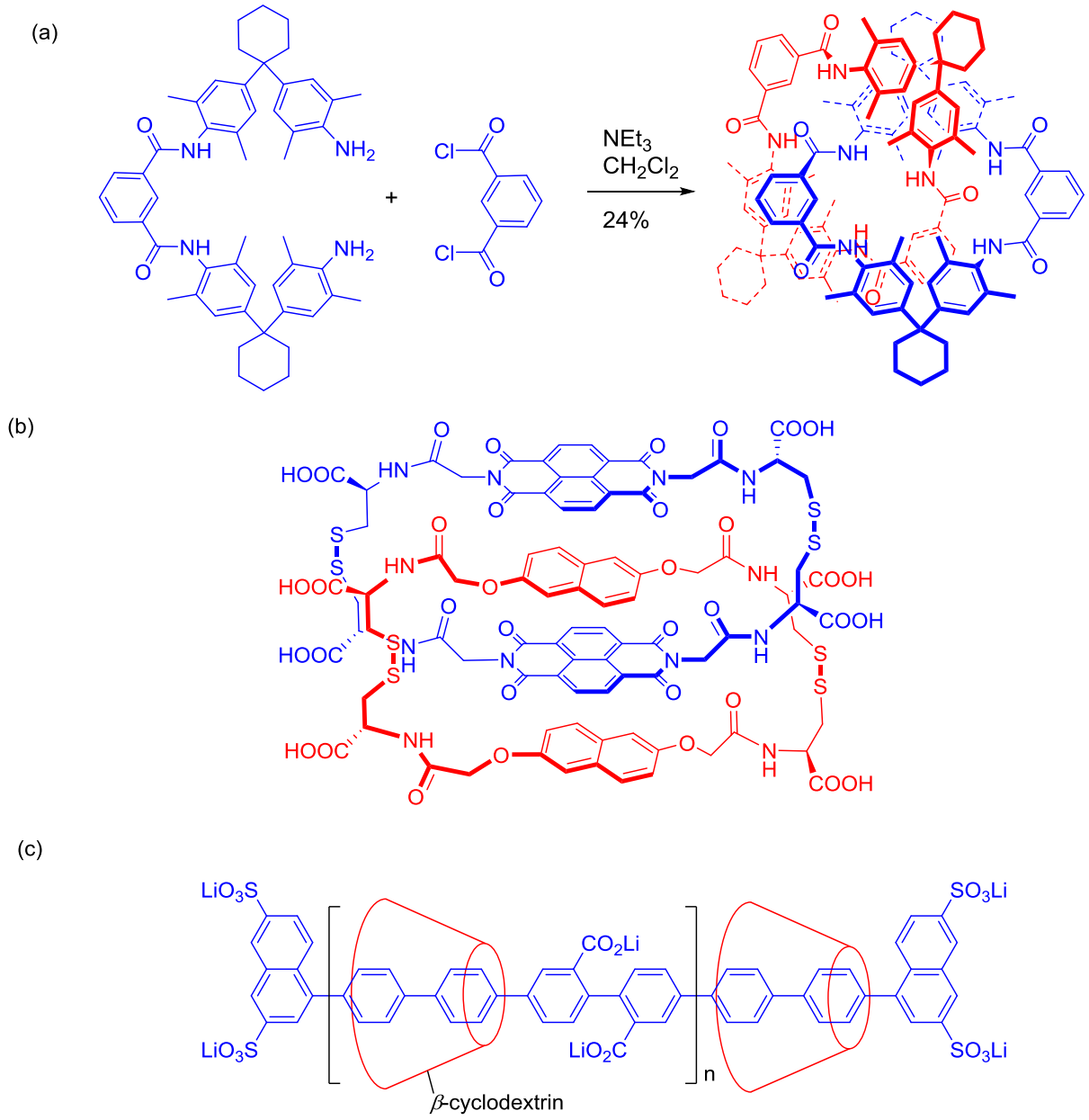

Figure 1.32 Catenanes assembled through neutral templation: (a) Hunter's hydrogen bond-templated [2]catenane,[194] (b) Sanders' donor–acceptor catenane[198] and (c) Anderson's *β*-cyclodextrin poly-rotaxane "insulated molecular wire".[202]

1.4.3.3 Anion templation of interlocked molecules

The first anion templated *interpenetrative* molecular architecture was reported by Stoddart in 1997, who demonstrated the preparation of a [5]pseudorotaxane which crystallised with a hexafluorophosphate counter anion within the cavity (Figure 1.33a).[204] The control experiment in which the assembly is conducted without the anion present was not undertaken, however, and so the role the hexafluorophosphate anion plays in templating the assembly was not fully established. The first example of an anion templated *interlocked* molecule synthesis was reported two years later by Vögtle, who demonstrated the use of a phenoxide anion to template rotaxane formation: a phenoxide-functionalised axle precursor forms hydrogen bonds to the isophthalamide amide groups of a macrocycle, before subsequently reacting with an electrophilic axle precursor component to form the interlocked structure (Figure 1.33b).[158] It is noteworthy that in this example the anion template is consumed during rotaxane construction.

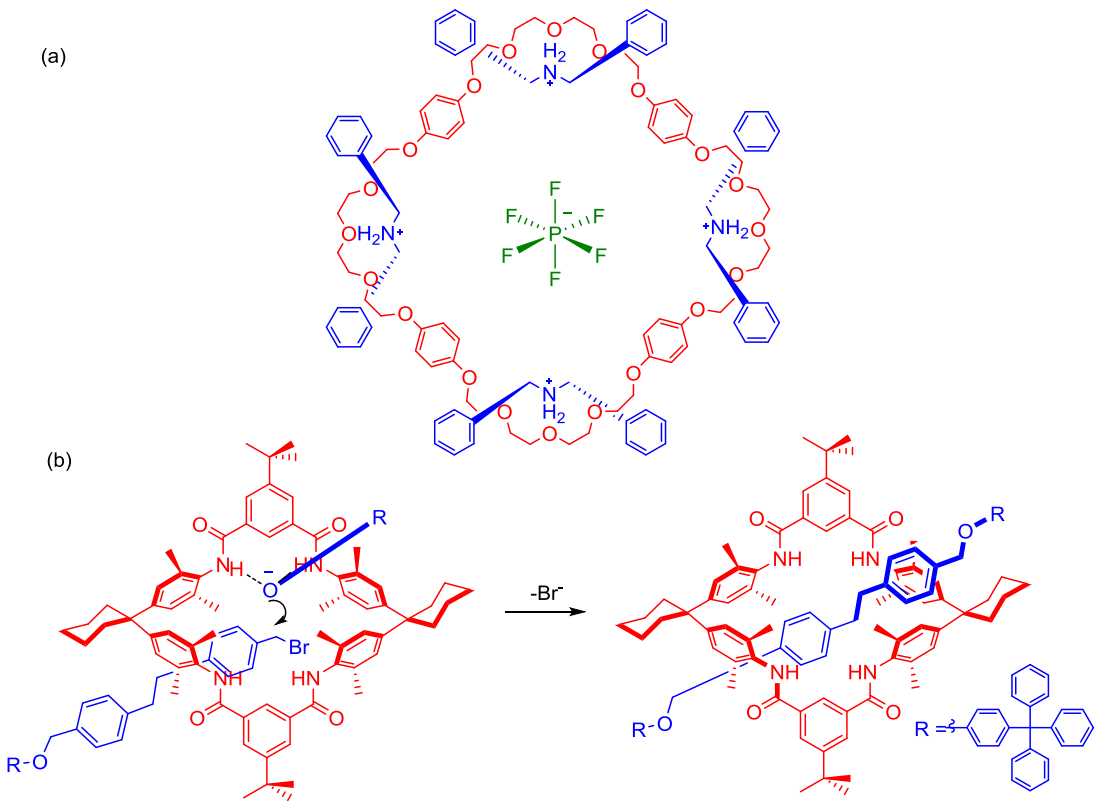

Figure 1.33 Anion templation of interpenetrative and interlocked molecular architectures: (a) Stoddart's [5]pseudorotaxane[204] and (b) Vögtle's phenoxide templation of a [2]rotaxane.[158]

More recently, the use of the zwitteranionic squaraine motif has been demonstrated by Smith and co-workers to template the condensation of isophthalolyl dichlorides with bis-amines to form both rotaxane[205–207] and catenane[208] species. In 2013, Flood and co-workers reported the dipropargylphosphate anion templated formation of a [3]rotaxane: the alkyl-phosphate anion templates the formation of an initial interpenetrative assembly with two "cyanostar" macrocycles (Figure 1.34).[209] The interlocked structure was subsequently prepared by a CuAAC click stoppering reaction with a suitable azide-functionalised stopper component.

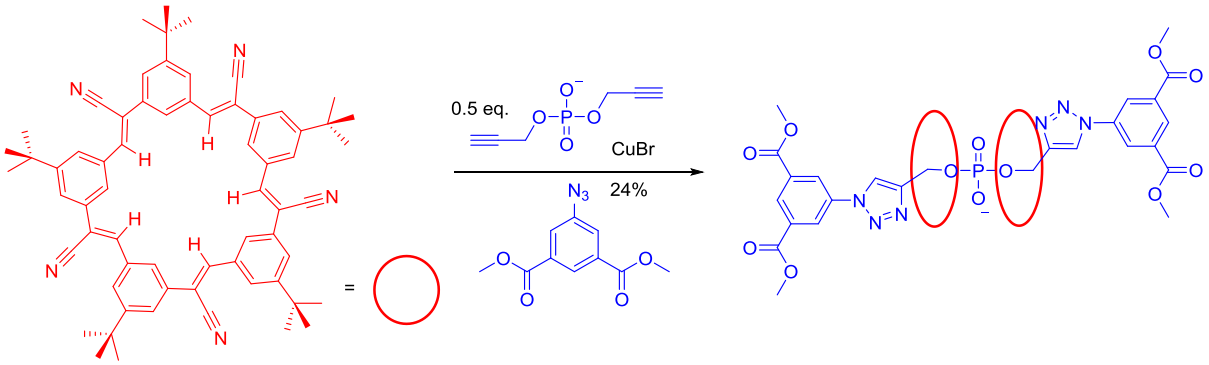

Figure 1.34 Flood's "cyanostar" phosphate-templated [3]rotaxane.[209]

In the aforementioned examples, the anionic template either forms an integral part of the resulting interlocked structure (in Smith's squaraine rotaxane and Flood's dialkylphosphate [3]rotaxane), or is consumed during the reaction (in Vögtle's phenoxide templated rotaxane). The use of a *discrete* anion template, analogous to the discrete cation templates pioneered by Sauvage (Section 1.4.3.1), has been developed by Beer and co-workers over the past few years. The initial work in this area was stimulated by the discovery that an orthogonal complex could be formed between a hydrogen-bond-donating 3,5-bis-amide pyridinium species and a neutral isophthalamide motif *via* chloride anion coordination (Figure 1.35a).[210] This three component association was initially employed in the preparation of a chloride-templated pseudorotaxane, by incorporating the isophthalamide motif within a macrocycle (Figure 1.35b).[210] The interpenetrated association is enhanced by secondary supramolecular

interactions: aromatic donor–acceptor interactions and pyridinium-*N*-methyl-polyether CH···O hydrogen bonding.

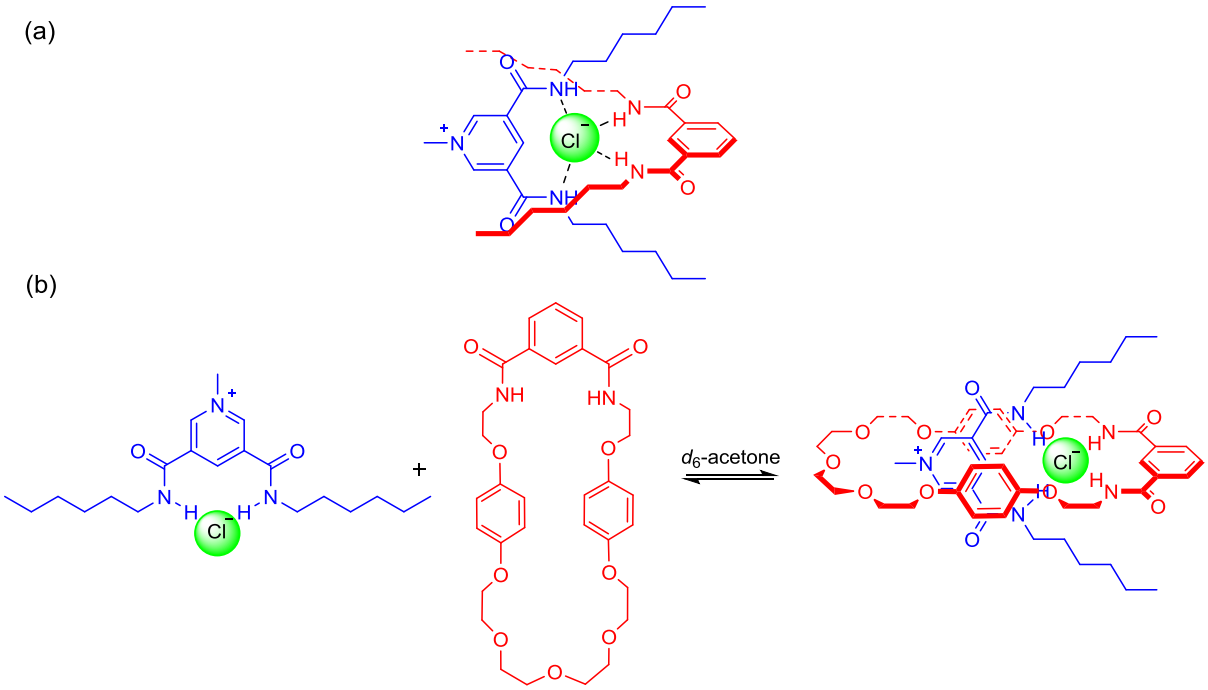

Figure 1.35 (a) Orthogonal association of hydrogen-bonding components about a chloride anion and (b) chloride-templated pseudorotaxane assembly.[210]

This strategic anion templation methodology was later exploited in the construction of a [2]rotaxane, using a ring-closing metathesis (RCM) methodology, by cyclizing a bis-vinyl-appended macrocycle precursor around a terphenyl-stoppered pyridinium chloride axle component (Figure 1.36a).[211] More recently, an alternative route for anion-templated interlocked structures was reported, templating the formation of the macrocycle using an amide condensation strategy in the presence of pyridinium chloride axle component (Figure 1.36b).[212] Discrete chloride anion templation has also been applied to the synthesis of catenanes,[213,214] and more complex molecular architectures such as a hand-cuff catenane,[215] Janus [2]rotaxane[216] and a [3]rotaxane,[217] whilst bromide[218] and sulfate[219] anions have also been utilised as templates for mechanical bond formation.

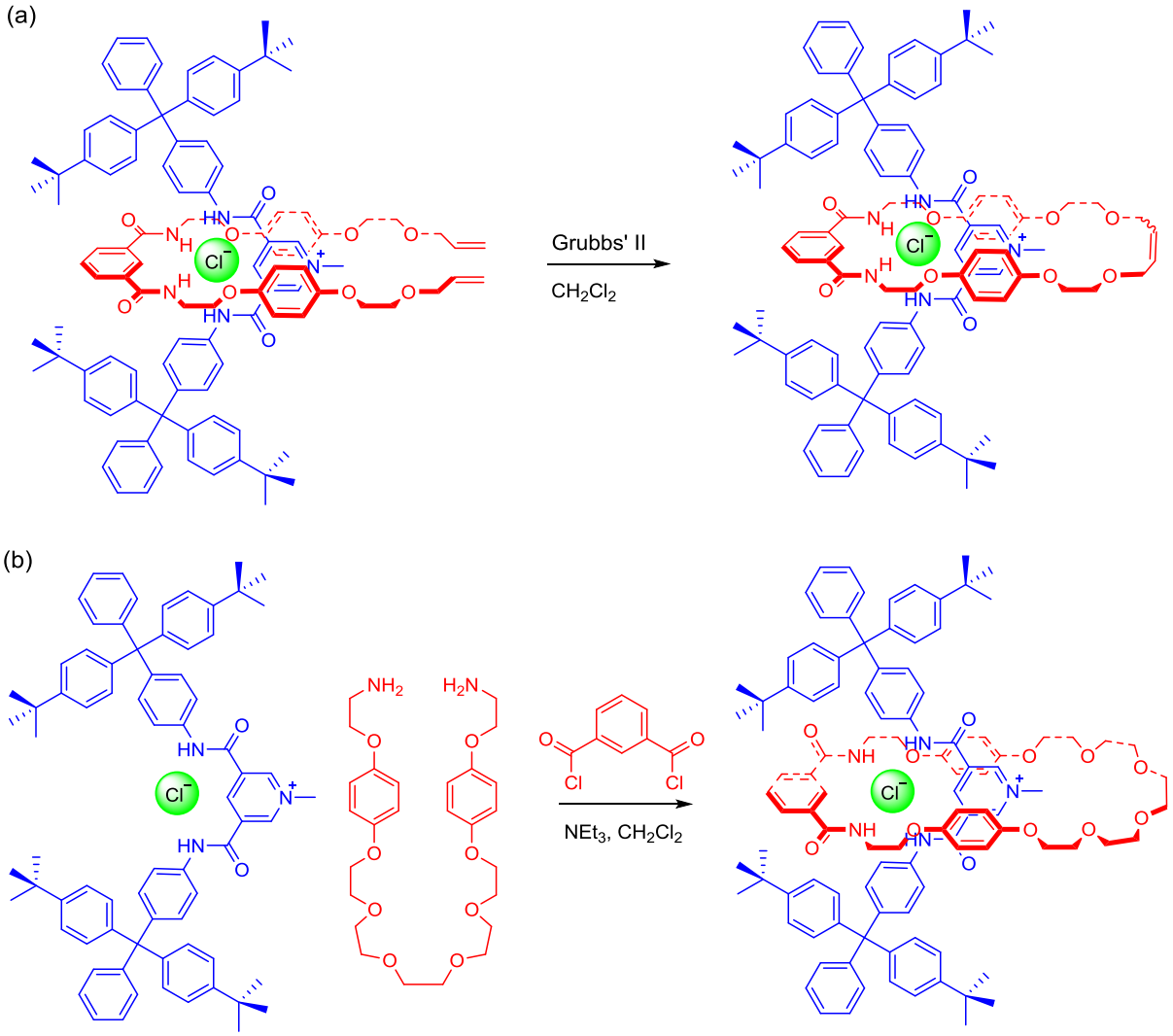

Figure 1.36 Chloride-templated [2]rotaxane synthesis *via* (a) ring closing metathesis[211] and (b) amine-acid chloride condensation.[212]

Removing the anion template from these interlocked molecular architectures, by exchanging to a non-coordinating anion such as hexafluorophosphate, reveals an anion host system which possesses a three-dimensionally restrained binding cavity formed between the interlocked components. Such hosts exhibit high selectivity for the templating anion in competitive organic–aqueous solvent mixtures. For example, the hexafluorophosphate salt of the [2]rotaxane shown in Figure 1.36b is highly selective for Cl^- in 45:45:10 $CDCl_3/CD_3OD/D_2O$ (K_a = 1500 M^{-1}) over the more basic oxoanions $H_2PO_4^-$ and AcO^- which cannot penetrate the interlocked binding cavity. It is noteworthy that this is the reverse of the anion selectivity observed for the non-interlocked axle.

1.4.4 Applications of interlocked molecules

The promise of interlocked architectures as molecular motors and machines for nanotechnological applications has stimulated an ever increasing interest in their synthesis and function. Furthermore, the unique topology of interlocked molecules has motivated their utilisation as a novel approach for molecular recognition, whilst applications in organic materials, catalysis and medicine have also been reported. Recent and important examples will be discussed in the following section, to highlight the potential of mechanically bonded molecules for practical application.

1.4.4.1 Interlocked molecules as molecular machines

Rotaxanes and catenanes have been the focus of intense research as prototypical molecular machines, due to the possibility of relative motion between their constituent parts, such as rotation and shuttling behaviour (Figure 1.37).[220]

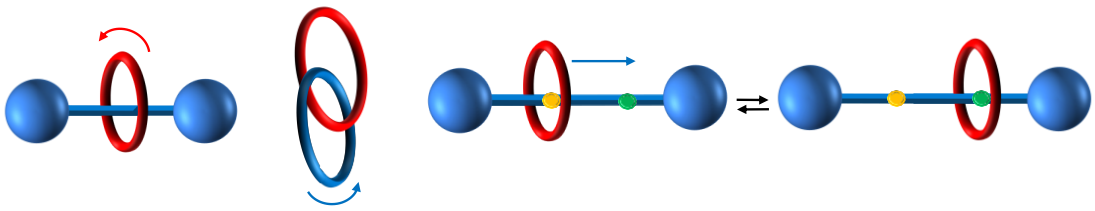

Figure 1.37 Molecular motion in rotaxanes and catenanes: rotation and shuttling motion.

Since Stoddart's seminal report of a molecular shuttle, in which the macrocycle component of a [2]rotaxane trans-located between two identical stations,[221] more elaborate and complex systems have been prepared that undergo well-defined motion controlled by external stimuli.[220,222] For example, the rotaxane shown in Figure 1.38a displays a pirouetting motion upon electrochemical switching between the Cu(I) and Cu(II) states of the cation.[223] The Cu(I) cation preferentially binds to the bidentate phenanthroline ligand to achieve a favourable four coordinate geometry. Oxidation to Cu(II) induced pirouetting of the macrocycle about the axle to facilitate binding to the terpy ligand in a preferred five coordinate geometry. Stoddart has

demonstrated the pH responsive shuttling of a so called "molecular elevator" (Figure 1.38b): the catechol-polyether macrocycles are connected in a platform-like arrangement, and reside initially over the ammonium station.[224] Addition of three equivalents of base results in deprotonation of the ammonium groups, concomitant with the translocation of the macrocycle platform to the bottom bipyridinium station.

The range of different molecular machines based on rotaxanes and catenanes continues to expand and now includes molecular muscles that expand and contract in response to external stimuli,[225,226] a rotaxane-fuctionalised surface that can "push" macroscopic droplets of liquid up an incline,[227] and a [2]rotaxane peptide synthesiser.[228]

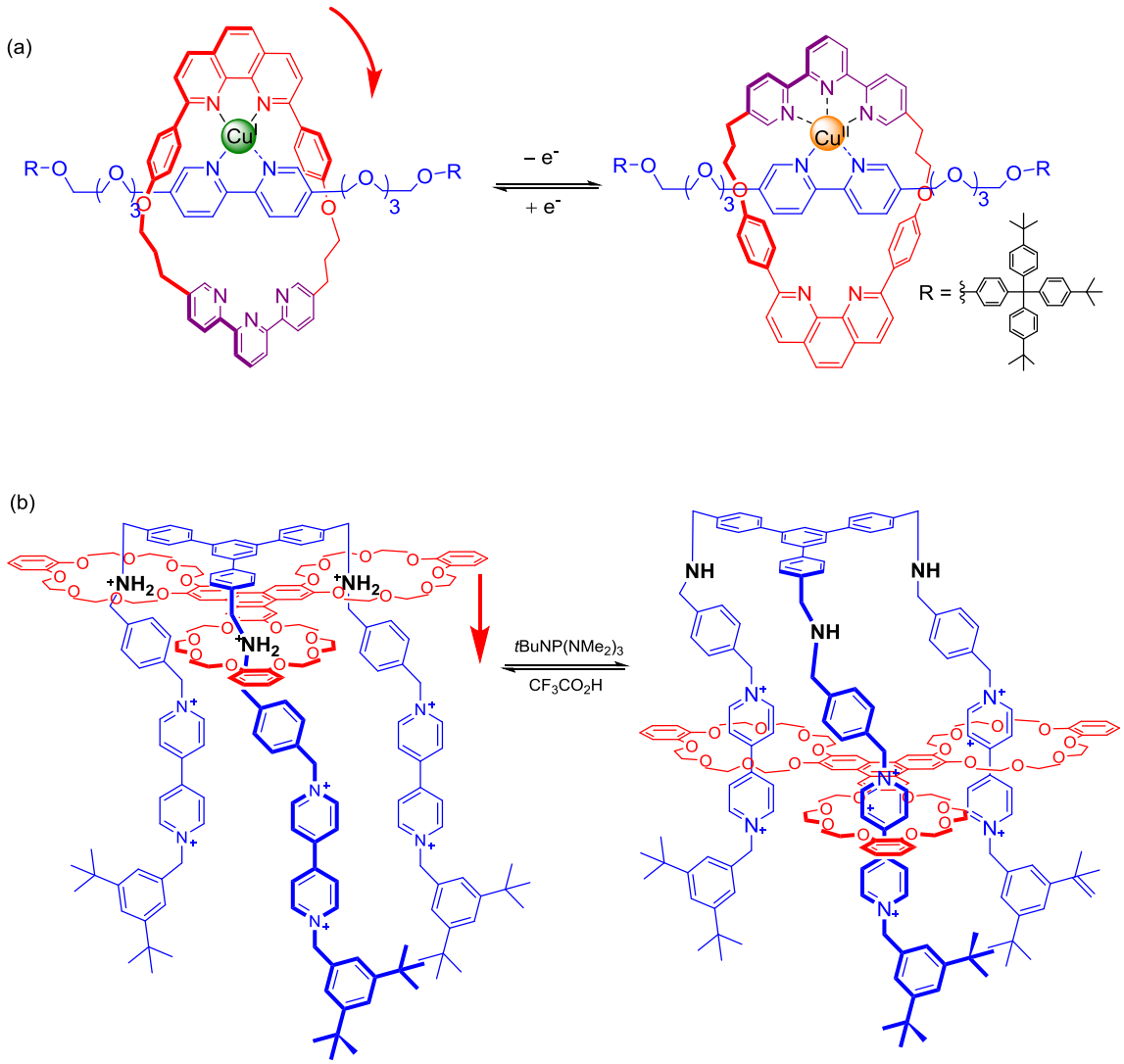

Figure 1.38 Molecular machines: (a) electrochemical stimulated pirouetting motion in a [2]rotaxane[223] and (b) Stoddart's molecular elevator.[224]

1.4.4.2 Interlocked molecules as hosts for charged guest recognition

The elaborate cavities formed between the interlocked components of mechanically bonded architectures have been utilised as binding sites for guest recognition. Sessler and co-workers have reported a pyrrole-containing [2]catenane that recognises a range of anions in d_2-1,1,2,2-tetrachloroethane solution (Figure 1.39a),[229] whilst Sanders has reported the acetylcholine-templated formation of a [2]catenane from a dynamic combinatorial library of dipeptide hydrazones, which reversibly combine through hydrazine linkages. In the presence of acetylcholine, the dominant structure at thermodynamic equilibrium was a [2]catenane consisting of interlocked macrocycle trimers (Figure 1.39b), which exhibited high affinity for the templating acetylcholine ($K_a = 10^7$ M^{-1} in 95:5 $CHCl_3$/DMSO).[230]

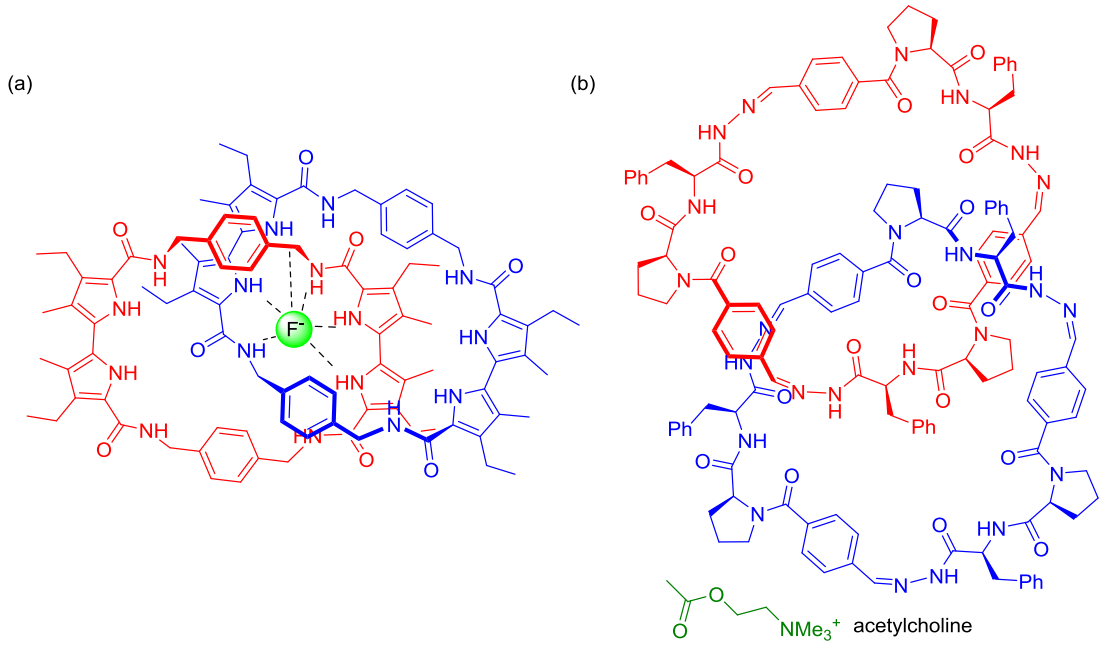

Figure 1.39 Catenane hosts: (a) Sessler's [2]catenane anion host[229] and (b) Sander's acetylcholine-binding catenane.[230]

The incorporation of reporter groups into interlocked hosts has enabled the development of a range of systems capable of sensing charged guest species.[117] The seminal work in this area was reported by Swager and co-workers in 1996, who demonstrated that a metal free polyrotaxane polymer prepared *via* cation templation could detect Cu(I) cations in solution by means of enhancement of the polymer's conductivity upon cation binding (Figure 1.40a).[231,232]

Furthermore, Cu(I) binding also resulted in an optical response, with significant red-shifting of the UV-vis absorption spectrum observed in CH_2Cl_2. Chiu and co-workers have described the sodium-templated interpenetration of both anthraquinone (Figure 1.40b) and squaraine dyes within a bis-dibenzo[18]crown-6-derived macrocycle, which led to enhancement of the dye's fluorescence emission in $CDCl_3/CD_3CN$, and thus enabled the system to act as a Na^+ sensor with high selectivity over K^+, which does not template the pseudorotaxane formation.[233] The authors later extended this methodology to the synthesis of a [2]rotaxane shuttle capable of sensing Na^+ cations in solution.[234] Hiratani has reported a fluorescent [1]rotaxane which undergoes a conformational change upon Li^+ binding in $CHCl_3/CH_3CN$, leading to the anthracene fluorophore in the thread being brought into closer proximity with the naphthalene motif within the macrocycle (Figure 1.40c).[235] Consequently, excitation of the naphthalene leads to enhanced energy transfer to the anthracene emitter, allowing the Li^+ binding event to be detected through emission intensity enhancement.

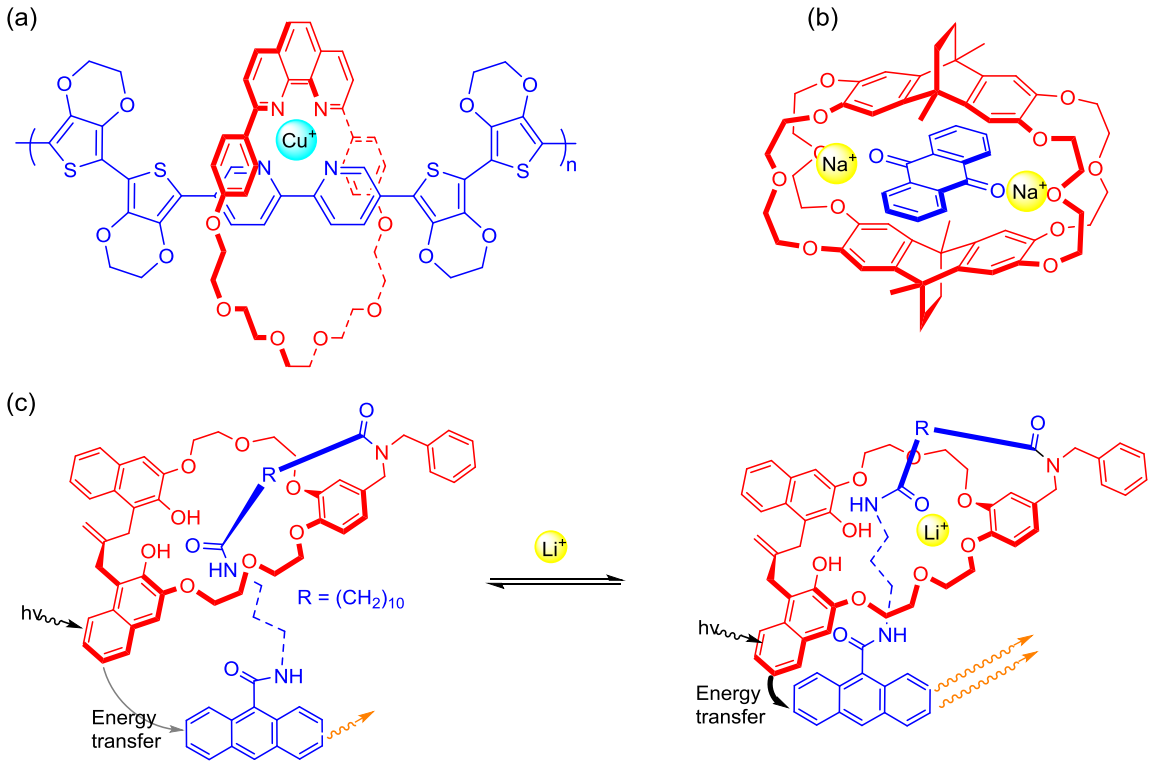

Figure 1.40 Interlocked and interpenetrative assemblies for cation sensing. (a) Swager's Cu(I)-sensing poly-rotaxane,[231] (b) Chiu optically responsive pseudorotaxane assembly[233] and (c) Hiratani's Li^+-sensing [1]rotaxane.[235]

Rotaxanes and catenanes have also been utilised for the optical sensing of anionic guest species. Notable examples include Lin's fluorescencent diketopyrrolopyrrole-based [2]rotaxane that senses fluoride anions (Figure 1.41a),[236] Jeong's chloride-sensing indolocarbazole [2]catenane (Figure 1.41b)[237] and Beer's luminescent Ru(II)-bipyridyl-functionalised rotaxane which binds Cl^- selectively over $H_2PO_4^-$ and AcO^-, and signals the binding event by means of enhancement of the Ru(II) emission intensity (Figure 1.41c).[238] Incorporation of electrochemical reporter groups within interlocked structures has also facilitated the preparation of electrochemical anion sensors, such as the ferrocene-appended rotaxane shown in Figure 1.41d, which selectively recognises Cl^- over HSO_4^-, BzO^- and $H_2PO_4^-$.[239] Importantly, the chloride selectivity is also manifested in the electrochemistry, with the maximum cathodic shift of the Fc/Fc+ couple occurring after addition of one equivalent of Cl^- in CH_3CN.

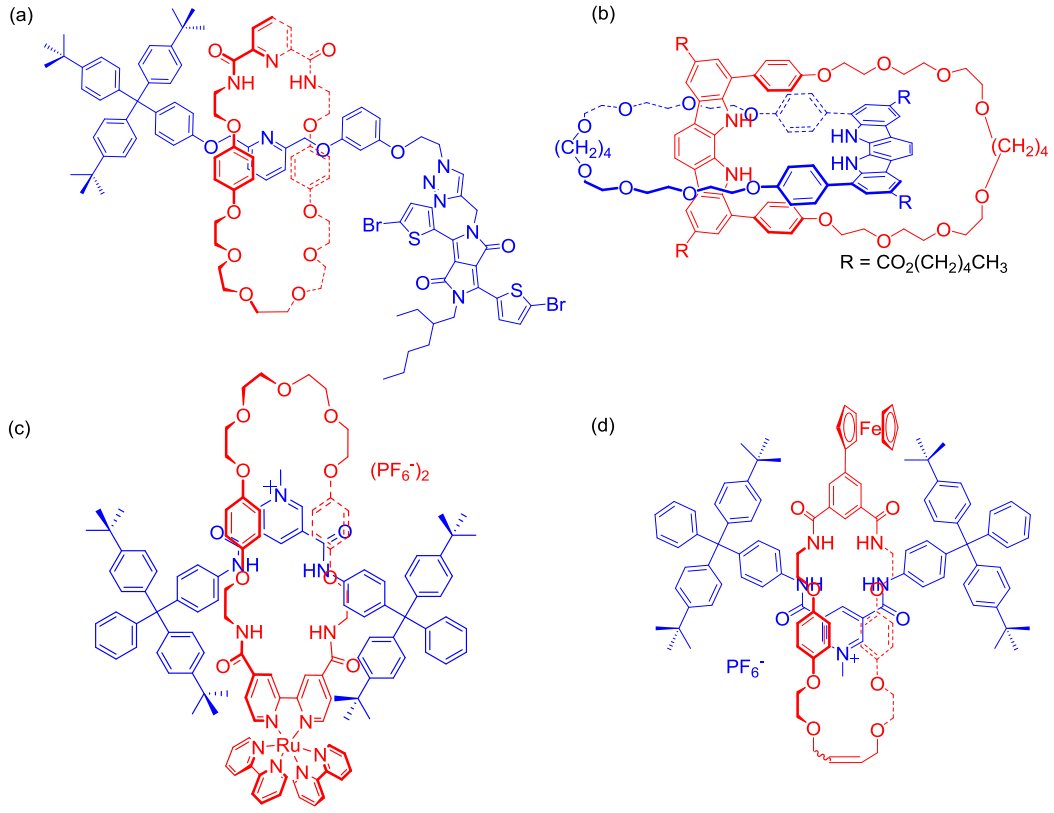

Figure 1.41 Interlocked anion sensors: (a) diketopyrrolopyrrole-based [2]rotaxane shuttle for fluoride sensing,[236] (b) Jeong's fluorescent [2]catenane,[237] (c) Beer's luminescent Ru(II)-bipyridyl-functionalised rotaxane[238] and (d) ferrocene-appended rotaxane for electrochemical chloride sensing.[239]

1.4.4.3 Interlocked molecules for functional materials, catalysis and medical applications

The encapsulation of dye molecules and conducting polymers within macrocycle components has been used to fabricate "insulated molecular wires,"[203] such as Anderson's β-cyclodextrin encapsulated polyrotaxane (Figure 1.32c), which exhibits enhanced electroluminescence efficiency compared to the free poly(para-phenylene).[202] Poly-rotaxane networks, comprising cyclodextrin-encapsulated polymers cross-linked *via* the macrocycle derivatives, have been used by Takata and co-workers to develop commercial materials with unusual properties, such as hydrogels capable of functioning as self-healing automotive coatings.[240]

Interlocked molecules have also been employed as reagents and catalysts for synthesis, taking advantage of their unique topologies to modify reactivity, stereochemistry and product distributions.[241] For example, Leigh and co-workers have demonstrated a [2]rotaxane shuttle that can act as a switchable organocatalyst for the asymmetric catalysis of a Michael addition reaction (Figure 1.42a).[242] In the protonated state, the dibenzo-24-crown-8 macrocycle resides over the catalytic site, switching off the catalytic activity. Deprotonation of the ammonium group causes the macrocycle to translocate to the triazolium motif, exposing the amine motif and turning on the catalytic activity. Loeb has recently demonstrated that rotaxanes can act as a novel approach to the preparation of frustrated Lewis pairs for H_2 activation (Figure 1.42b),[243] whilst Goldup has suggested that interlocked molecules may be employed to stabilise reactive catalytic intermediates, following the discovery of a stable rotaxane Cu(I)-triazolide species in aqueous solvent whilst preparing rotaxanes *via* a CuAAC active-template methodology (Figure 1.42c).[244]

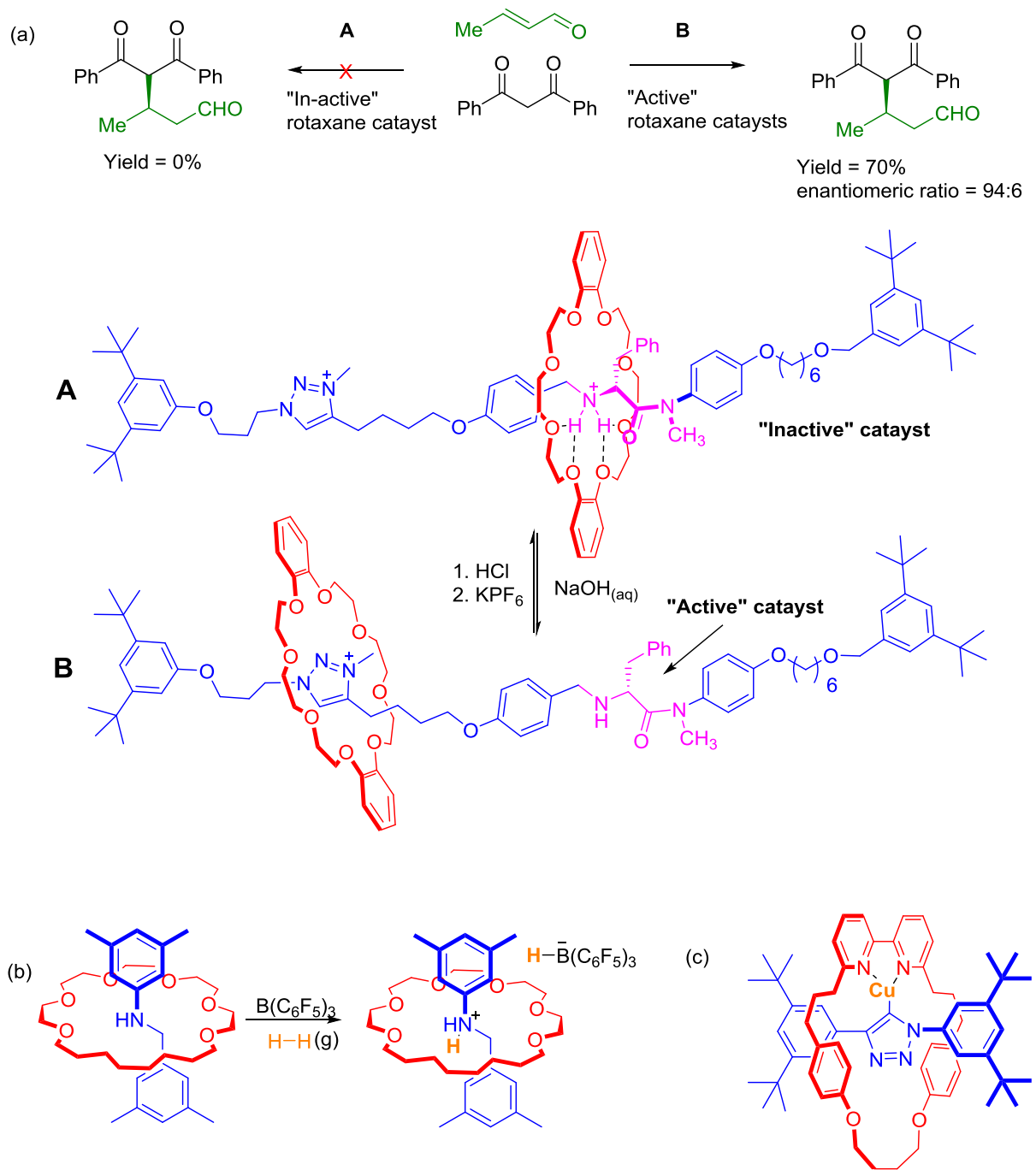

Figure 1.42 Rotaxanes for catalysis: (a) Leigh's switchable [2]rotaxane organocatayst,[242] (b) Loeb's frustrated Lewis pair for H_2 activation[243] and (c) Goldup's rotaxane-stabilised Cu(I)-triazolide[244]

Smithrud has demonstrated that crown-ether derived [2]rotaxanes may act as cellular transport agents.[245,246] The [2]rotaxane shown in Figure 1.43a binds a range of amino acids, dipeptides and fluorophores in aqueous solution, and is capable of transporting both fluorescein and a fluorescein-functionalised protein kinase C inhibitor into eukaryotic cells, including into the nucleus.[245]

Recently, the same group prepared a related [2]rotaxane capable of binding calcium cations in a crown-ether stoppered axle component, and showed that the rotaxane induced apoptosis in ovarian cancer cells. This effect was believed to be due to rotaxane-mediated transport of calcium cations across the cell membrane.[246]

The enhanced stability of interlocked structures has also been exploited in several studies in which a rotaxane can act as a pro-drug.[247–249] For example, Leigh's rotaxane pro-peptide shown in Figure 1.43b contains the bioactive peptide Met-encephalin (depicted in blue) and exhibits enhanced stability compared to both the parent peptide and the non-interlocked axle component.[248] *β*-Galactosidase-mediated enzymatic hydrolysis removes the monosaccharide stopper component (black), releasing the bioactive peptide molecule by a de-threading process.

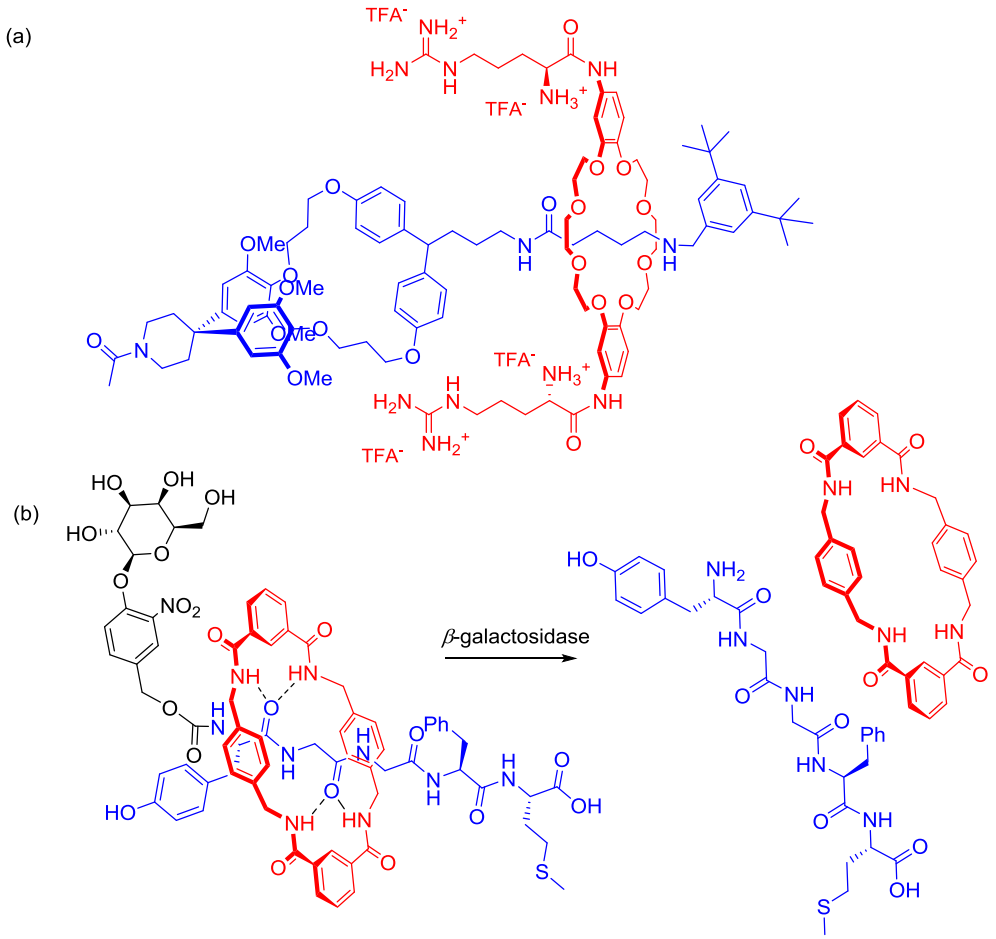

Figure 1.43 Bioactive-[2]rotaxanes: (a) Smithrud's fluorescein cellular transport agent[245] and (b) Leigh's rotaxane pro-peptide.[248]

1.5 Project aims

The broad aims of the project are to develop mechanically bonded host molecules for anion recognition and sensing that are capable of functioning in competitive organic–aqueous solvent mixtures, with the aim of ultimately achieving strong recognition even in pure water. In particular, both hydrogen and halogen bonding will be exploited as intermolecular interactions for anion guest recognition in such host systems. Novel approaches to the incorporation of lanthanide complexes within interlocked host frameworks for anion sensing applications will also be investigated.

Chapter 2 details the synthesis of hydrogen bonding mechanically bonded hosts for recognising oxoanions in competitive aqueous solvent media. A novel nitrate anion templated synthesis of rotaxane and catenane host systems is presented and the nitrate anion recognition capabilities of these systems investigated. The anion recognition and optical sensing capability of a sulfate selective [3]rotaxane host, incorporating a fluorescent naphthalene reporter group, is also examined.

Chapter 3 focuses on preparing water soluble *β*-cyclodextrin stoppered rotaxane-based receptors for halide anion recognition in pure water. Specifically, both hydrogen and halogen bonding anion hosts are prepared, and a detailed examination of the relative capabilities of both intermolecular interactions for binding anions in water is presented.

Chapter 4 investigates the unprecedented integration of luminescent lanthanide complexes into the binding domain of interlocked molecules for anion sensing applications. The novel use of lanthanide cation templation for mechanical bond formation is presented initially and investigations into the structure and anion sensing properties of the rotaxane using the luminescence from the lanthanide centre are detailed. Finally, novel anion templation strategies to prepare lanthanide-based rotaxanes are discussed, and the luminescence anion sensing capabilities of the interlocked hosts explored.

1.6 References for Chapter 1

1. J. W. Steed and J. L. Atwood, *Supramolecular Chemistry*, Wiley, Chichester, UK, 2nd Edition., 2009.
2. J.-M. Lehn, *Angew. Chem. Int. Ed. Engl.*, 1988, **27**, 89–112.
3. D. J. Cram, *Angew. Chem. Int. Ed. Engl.*, 1988, **27**, 1009–1020.
4. C. J. Pedersen, *Angew. Chem. Int. Ed. Engl.*, 1988, **27**, 1021–1027.
5. C. H. Park and H. E. Simmons, *J. Am. Chem. Soc.*, 1968, **90**, 2431–2432.
6. J. L. Sessler, P. A. Gale, and W.-S. Cho, *Anion Receptor Chemistry*, RSC, Cambridge, 2006.
7. F. Delange, *Thyroid*, 1994, **4**, 107–128.
8. M. P. Anderson, R. J. Gregory, S. Thompson, D. W. Souza, S. Paul, R. C. Mulligan, A. E. Smith, and M. J. Welsh, *Science*, 1991, **253**, 202–205.
9. V. H. Smith and D. W. Schindler, *Trends Ecol Evol*, 2009, **24**, 201–207.
10. R. F. Follett and J. L. Hatfield, *Nitrogen in the environment sources, problems, and management,*, Elsevier, New York, 2001.
11. S. G. Chang, D. Littlejohn, and K. Y. Hu, *Science*, 1987, **237**, 756–758.
12. K. Yoshihara and T. Omori, *Top. Curr. Chem.*, 1996, **176**, 17–35.
13. P. D. Beer and P. A. Gale, *Angew. Chem. Int. Ed.*, 2001, **40**, 486–516.
14. F. Hofmeister, *Arch. Exp. Pathol. Pharmacol.*, 1888, **24**, 247–260.
15. S. Goldman and R. G. Bates, *J. Am. Chem. Soc.*, 1972, **94**, 1476–1484.
16. J. W. Pflugrath and F. A. Quiocho, *Nature*, 1985, **314**, 257–260.
17. H. Luecke and F. A. Quiocho, *Nature*, 1990, **347**, 402–406.
18. J. D. Watson and F. H. C. Crick, *Nature*, 1953, **171**, 737–738.
19. P. Metrangolo, F. Meyer, T. Pilati, G. Resnati, and G. Terraneo, *Angew. Chem. Int. Ed.*, 2008, **47**, 6114–6127.
20. P. Politzer, P. Lane, M. C. Concha, Y. Ma, and J. S. Murray, *J. Mol. Model.*, 2007, **13**, 305–311.
21. G. R. Desiraju, P. S. Ho, L. Kloo, A. C. Legon, R. Marquardt, P. Metrangolo, P. Politzer, G. Resnati, and K. Rissanen, *Pure Appl. Chem.*, 2013, **85**, 1711–1713.
22. R. Bertani, P. Sgarbossa, A. Venzo, F. Lelj, M. Amati, G. Resnati, T. Pilati, P. Metrangolo, and G. Terraneo, *Coord. Chem. Rev.*, 2010, **254**, 677–695.
23. K. Rissanen, *CrystEngComm*, 2008, **10**, 1107–1113.
24. L. C. Roper, C. Präsang, V. N. Kozhevnikov, A. C. Whitwood, P. B. Karadakov, and D. W. Bruce, *Cryst. Growth Des.*, 2010, **10**, 3710–3720.
25. D. Cinčić, T. Friščić, and W. Jones, *Chem. – Eur. J.*, 2008, **14**, 747–753.
26. R. Liantonio, P. Metrangolo, T. Pilati, G. Resnati, and A. Stevenazzi, *Cryst. Growth Des.*, 2003, **3**, 799–803.
27. J. Xu, X. Liu, J. K.-P. Ng, T. Lin, and C. He, *J. Mater. Chem.*, 2006, **16**, 3540–3545.
28. C. B. Aakeröy, M. Baldrighi, J. Desper, P. Metrangolo, and G. Resnati, *Chem. – Eur. J.*, 2013, **19**, 16240–16247.
29. T. M. Beale, M. G. Chudzinski, M. G. Sarwar, and M. S. Taylor, *Chem. Soc. Rev.*, 2013, **42**, 1667–1680.
30. M. G. Sarwar, B. Dragisic, L. J. Salsberg, C. Gouliaras, and M. S. Taylor, *J. Am. Chem. Soc.*, 2010, **132**, 1646–1653.
31. L.-Y. You, S.-G. Chen, X. Zhao, Y. Liu, W.-X. Lan, Y. Zhang, H.-J. Lu, C.-Y. Cao, and Z.-T. Li, *Angew. Chem. Int. Ed.*, 2012, **51**, 1657–1661.
32. N. L. Kilah, M. D. Wise, C. J. Serpell, A. L. Thompson, N. G. White, K. E. Christensen, and P. D. Beer, *J. Am. Chem. Soc.*, 2010, **132**, 11893–11895.

33. C. J. Serpell, N. L. Kilah, P. J. Costa, V. Félix, and P. D. Beer, *Angew. Chem. Int. Ed.*, 2010, **49**, 5322–5326.
34. A. Caballero, F. Zapata, N. G. White, P. J. Costa, V. Félix, and P. D. Beer, *Angew. Chem. Int. Ed.*, 2012, **51**, 1876–1880.
35. R. Wilcken, M. O. Zimmermann, A. Lange, A. C. Joerger, and F. M. Boeckler, *J. Med. Chem.*, 2013, **56**, 1363–1388.
36. L. A. Hardegger, B. Kuhn, B. Spinnler, L. Anselm, R. Ecabert, M. Stihle, B. Gsell, R. Thoma, J. Diez, J. Benz, J.-M. Plancher, G. Hartmann, D. W. Banner, W. Haap, and F. Diederich, *Angew. Chem. Int. Ed.*, 2011, **50**, 314–318.
37. R. D. Carpenter, A. Natarajan, E. Y. Lau, M. Andrei, D. M. Solano, F. C. Lightstone, S. J. DeNardo, K. S. Lam, and M. J. Kurth, *Cancer Res.*, 2010, **70**, 5448–5456.
38. C. T. Lemke, N. Goudreau, S. Zhao, O. Hucke, D. Thibeault, M. Llinàs-Brunet, and P. W. White, *J. Biol. Chem.*, 2011, **286**, 11434–11443.
39. R. Wilcken, X. Liu, M. O. Zimmermann, T. J. Rutherford, A. R. Fersht, A. C. Joerger, and F. M. Boeckler, *J. Am. Chem. Soc.*, 2012, **134**, 6810–6818.
40. A. Vargas Jentzsch, D. Emery, J. Mareda, P. Metrangolo, G. Resnati, and S. Matile, *Angew. Chem. Int. Ed.*, 2011, **50**, 11675–11678.
41. A. V. Jentzsch, D. Emery, J. Mareda, S. K. Nayak, P. Metrangolo, G. Resnati, N. Sakai, and S. Matile, *Nat. Commun.*, 2012, **3**, 905–913.
42. A. Vargas Jentzsch, A. Hennig, J. Mareda, and S. Matile, *Acc. Chem. Res.*, 2013, **46**, 2791–2800.
43. A. Bruckmann, M. Pena, and C. Bolm, *Synlett*, 2008, **2008**, 900–902.
44. F. Kniep, S. H. Jungbauer, Q. Zhang, S. M. Walter, S. Schindler, I. Schnapperelle, E. Herdtweck, and S. M. Huber, *Angew. Chem. Int. Ed.*, 2013, **52**, 7028–7032.
45. A. R. Voth, F. A. Hays, and P. S. Ho, *Proc. Natl. Acad. Sci.*, 2007, **104**, 6188–6193.
46. M. Carter, A. R. Voth, M. R. Scholfield, B. Rummel, L. C. Sowers, and P. S. Ho, *Biochemistry (Mosc.)*, 2013, **52**, 4891–4903.
47. M. G. Sarwar, B. Dragisic, S. Sagoo, and M. S. Taylor, *Angew. Chem. Int. Ed.*, 2010, **49**, 1674–1677.
48. F. Zapata, A. Caballero, N. G. White, T. D. W. Claridge, P. J. Costa, V. Félix, and P. D. Beer, *J. Am. Chem. Soc.*, 2012, **134**, 11533–11541.
49. L. C. Gilday, N. G. White, and P. D. Beer, *Dalton Trans.*, 2012, **41**, 7092–7097.
50. H. T. Chifotides and K. R. Dunbar, *Acc. Chem. Res.*, 2013, **46**, 894–906.
51. D. Quiñonero, C. Garau, C. Rotger, A. Frontera, P. Ballester, A. Costa, and P. M. Deyà, *Angew. Chem. Int. Ed.*, 2002, **41**, 3389–3392.
52. R. E. Dawson, A. Hennig, D. P. Weimann, D. Emery, V. Ravikumar, J. Montenegro, T. Takeuchi, S. Gabutti, M. Mayor, J. Mareda, C. A. Schalley, and S. Matile, *Nat. Chem.*, 2010, **2**, 533–538.
53. Y. Kim and F. P. Gabbaï, *J. Am. Chem. Soc.*, 2009, **131**, 3363–3369.
54. C. R. Wade, A. E. J. Broomsgrove, S. Aldridge, and F. P. Gabbaï, *Chem. Rev.*, 2010, **110**, 3958–3984.
55. E. Graf and J. M. Lehn, *J. Am. Chem. Soc.*, 1976, **98**, 6403–6405.
56. V. Amendola, G. Bergamaschi, M. Boiocchi, R. Alberto, and H. Braband, *Chem. Sci.*, 2014, **5**, 1820–1826.
57. F. P. Schmidtchen, *Angew. Chem. Int. Ed. Engl.*, 1977, **16**, 720–721.
58. F. P. Schmidtchen, *Chem. Ber.*, 1981, **114**, 597–607.
59. K. Worm and F. P. Schmidtchen, *Angew. Chem. Int. Ed. Engl.*, 1995, **34**, 65–66.
60. K. Worm, F. P. Schmidtchen, A. Schier, A. Schäfer, and M. Hesse, *Angew. Chem. Int. Ed. Engl.*, 1994, **33**, 327–329.
61. M. Berger and F. P. Schmidtchen, *J. Am. Chem. Soc.*, 1999, **121**, 9986–9993.

62. A. Cattani and F. P. Schmidtchen, *J. Prakt. Chem.*, 1999, **341**, 291–296.
63. B. Dietrich, D. L. Fyles, T. M. Fyles, and J.-M. Lehn, *Helv. Chim. Acta*, 1979, **62**, 2763–2787.
64. B. Dietrich, T. M. Fyles, J.-M. Lehn, L. G. Pease, and D. . Fyles, *J. Chem. Soc. Chem. Commun.*, 1978, 934–936.
65. C. Schmuck and M. Schwegmann, *J. Am. Chem. Soc.*, 2005, **127**, 3373–3379.
66. S. Shinoda, M. Tadokoro, H. Tsukube, S. Shinoda, and R. Arakawa, *Chem. Commun.*, 1998, 181–182.
67. W. J. Belcher, M. Fabre, T. Farhan, and J. W. Steed, *Org. Biomol. Chem.*, 2006, **4**, 781–786.
68. E. Alcalde, N. Mesquida, L. Pérez-García, C. Alvarez-Rúa, S. García-Granda, and E. García-Rodriguez, *Chem. Commun.*, 1999, 295–296.
69. Z. Xu, S. K. Kim, and J. Yoon, *Chem. Soc. Rev.*, 2010, **39**, 1457–1466.
70. M. Yousuf, N. Ahmed, B. Shirinfar, V. M. Miriyala, I. S. Youn, and K. S. Kim, *Org. Lett.*, 2014, **16**, 2150–2153.
71. A. Kumar and P. S. Pandey, *Org. Lett.*, 2008, **10**, 165–168.
72. N. G. White, S. Carvalho, V. Félix, and P. D. Beer, *Org. Biomol. Chem.*, 2012, **10**, 6951–6959.
73. C. R. Bondy and S. J. Loeb, *Coord. Chem. Rev.*, 2003, **240**, 77–99.
74. V. Amendola, L. Fabbrizzi, and L. Mosca, *Chem. Soc. Rev.*, 2010, **39**, 3889–3915.
75. J. L. Sessler, S. Camiolo, and P. A. Gale, *Coord. Chem. Rev.*, 2003, **240**, 17–55.
76. Y. Li and A. H. Flood, *Angew. Chem. Int. Ed.*, 2008, **47**, 2649–2652.
77. H. Juwarker, J. M. Lenhardt, D. M. Pham, and S. L. Craig, *Angew. Chem. Int. Ed.*, 2008, **47**, 3740–3743.
78. Y. Hua and A. H. Flood, *Chem. Soc. Rev.*, 2010, **39**, 1262–1271.
79. R. A. Pascal Jr., J. Spergel, and D. Van Engen, *Tetrahedron Lett.*, 1986, **27**, 4099–4102.
80. S. Kubik, *Chem. Soc. Rev.*, 2010, **39**, 3648–3663.
81. S. J. Brooks, P. A. Gale, and M. E. Light, *Chem. Commun.*, 2006, 4344–4346.
82. G. V. Oshovsky, W. Verboom, R. H. Fokkens, and D. N. Reinhoudt, *Chem. – Eur. J.*, 2004, **10**, 2739–2748.
83. S. Kubik, R. Goddard, R. Kirchner, D. Nolting, and J. Seidel, *Angew. Chem. Int. Ed.*, 2001, **40**, 2648–2651.
84. S. Kubik and R. Goddard, *Proc. Natl. Acad. Sci.*, 2002, **99**, 5127–5132.
85. P. A. Gale, J. L. Sessler, V. Král, and V. Lynch, *J. Am. Chem. Soc.*, 1996, **118**, 5140–5141.
86. P. Anzenbacher, K. Jursíková, and J. L. Sessler, *J. Am. Chem. Soc.*, 2000, **122**, 9350–9351.
87. I. E. D. Vega, S. Camiolo, P. A. Gale, M. B. Hursthouse, and M. E. Light, *Chem. Commun.*, 2003, 1686.
88. A. Mele, P. Metrangolo, H. Neukirch, T. Pilati, and G. Resnati, *J. Am. Chem. Soc.*, 2005, **127**, 14972–14973.
89. M. G. Sarwar, B. Dragisić, E. Dimitrijević, and M. S. Taylor, *Chem. – Eur. J.*, 2013, **19**, 2050–2058.
90. S. M. Walter, F. Kniep, L. Rout, F. P. Schmidtchen, E. Herdtweck, and S. M. Huber, *J. Am. Chem. Soc.*, 2012, **134**, 8507–8512.
91. M. Cametti, K. Raatikainen, P. Metrangolo, T. Pilati, G. Terraneo, and G. Resnati, *Org. Biomol. Chem.*, 2012, **10**, 1329–1333.
92. P. Ballester, *Acc. Chem. Res.*, 2013, **46**, 874–884.

93. P. Arranz-Mascarós, C. Bazzicalupi, A. Bianchi, C. Giorgi, M.-L. Godino-Salido, M.-D. Gutiérrez-Valero, R. Lopez-Garzón, and M. Savastano, *J. Am. Chem. Soc.*, 2013, **135**, 102–105.
94. P. A. Gale, *Coord. Chem. Rev.*, 2003, **240**, 191–221.
95. P. D. Beer and E. J. Hayes, *Coord. Chem. Rev.*, 2003, **240**, 167–189.
96. R. J. Motekaitis, A. E. Martell, B. Dietrich, and J. M. Lehn, *Inorg. Chem.*, 1984, **23**, 1588–1591.
97. L. Fabbrizzi, F. Foti, and A. Taglietti, *Org. Lett.*, 2005, **7**, 2603–2606.
98. K. K. Y. Yuen and K. A. Jolliffe, *Chem. Commun.*, 2013, **49**, 4824–4826.
99. M. Melaimi and F. P. Gabbaï, *J. Am. Chem. Soc.*, 2005, **127**, 9680–9681.
100. T. W. Hudnall, C.-W. Chiu, and F. P. Gabbaï, *Acc. Chem. Res.*, 2009, **42**, 388–397.
101. F. Cheng, E. M. Bonder, and F. Jäkle, *J. Am. Chem. Soc.*, 2013, **135**, 17286–17289.
102. K. Tamao, T. Hayashi, and Y. Ito, *J. Organomet. Chem.*, 1996, **506**, 85–91.
103. M. Newcomb, J. H. Horner, and M. T. Blanda, *J. Am. Chem. Soc.*, 1987, **109**, 7878–7879.
104. S. Aoyagi, K. Tanaka, and Y. Takeuchi, *J. Chem. Soc. Perkin Trans. 2*, 1994, 1549–1553.
105. H. Zhao and F. P. Gabbaï, *Nat. Chem.*, 2010, **2**, 984–990.
106. C. R. Wade, I.-S. Ke, and F. P. Gabbaï, *Angew. Chem. Int. Ed.*, 2012, **51**, 478–481.
107. M. Hirai and F. P. Gabbaï, *Chem. Sci.*, 2014, **5**, 1886–1893.
108. C.-W. Chiu and F. P. Gabbaï, *J. Am. Chem. Soc.*, 2006, **128**, 14248–14249.
109. S. J. Butler and D. Parker, *Chem. Soc. Rev.*, 2013, **42**, 1652–1666.
110. S. L. Wiskur, H. Ait-Haddou, J. J. Lavigne, and E. V. Anslyn, *Acc. Chem. Res.*, 2001, **34**, 963–972.
111. X. Lou, D. Ou, Q. Li, and Z. Li, *Chem. Commun.*, 2012, **48**, 8462–8477.
112. J. Du, M. Hu, J. Fan, and X. Peng, *Chem. Soc. Rev.*, 2012, **41**, 4511–4535.
113. D.-G. Cho, J. H. Kim, and J. L. Sessler, *J. Am. Chem. Soc.*, 2008, **130**, 12163–12167.
114. Y. Willener, K. M. Joly, C. J. Moody, and J. H. R. Tucker, *J. Org. Chem.*, 2008, **73**, 1225–1233.
115. P. D. Beer and A. D. Keefe, *J. Organomet. Chem.*, 1989, **375**, C40–C42.
116. P. D. Beer, D. Hesek, J. Hodacova, and S. E. Stokes, *J. Chem. Soc. Chem. Commun.*, 1992, 270.
117. M. J. Langton and P. D. Beer, *Acc. Chem. Res.*, 2014, DOI:10.1021/ar500012a.
118. T. Romero, R. A. Orenes, A. Tárraga, and P. Molina, *Organometallics*, 2013, **32**, 5740–5753.
119. K. A. Nielsen, J. O. Jeppesen, E. Levillain, and J. Becher, *Angew. Chem. Int. Ed.*, 2003, **42**, 187–191.
120. R. Martínez-Máñez and F. Sancenón, *Chem Rev*, 2003, **103**, 4419–4476.
121. M. E. Huston, E. U. Akkaya, and A. W. Czarnik, *J. Am. Chem. Soc.*, 1989, **111**, 8735–8737.
122. S. Nishizawa, Y. Kato, and N. Teramae, *J. Am. Chem. Soc.*, 1999, **121**, 9463–9464.
123. Z. Xu, N. J. Singh, J. Lim, J. Pan, H. N. Kim, S. Park, K. S. Kim, and J. Yoon, *J. Am. Chem. Soc.*, 2009, **131**, 15528–15533.
124. S. Watanabe, O. Onogawa, Y. Komatsu, and K. Yoshida, *J. Am. Chem. Soc.*, 1998, **120**, 229–230.
125. P. D. Beer, *Acc. Chem. Res.*, 1998, **31**, 71–80.
126. Pavel Anzenbacher, D. S. Tyson, K. Jursíková, and F. N. Castellano, *J. Am. Chem. Soc.*, 2002, **124**, 6232–6233.
127. M. S. Vickers, K. S. Martindale, and P. D. Beer, *J. Mater. Chem.*, 2005, **15**, 2784–2790.

128. D. Parker, R. S. Dickins, H. Puschmann, C. Crossland, and J. A. K. Howard, *Chem. Rev.*, 2002, **102**, 1977–2010.
129. S. Faulkner, S. J. A. Pope, and B. P. Burton-Pye, *Appl. Spectrosc. Rev.*, 2005, **40**, 1–31.
130. J.-C. G. Bünzli, S. Comby, A.-S. Chauvin, and C. D. B. Vandevyver, *J. Rare Earths*, 2007, **25**, 257–274.
131. Y. Bretonniere, M. J. Cann, D. Parker, and R. Slater, *Chem. Commun.*, 2002, 1930–1931.
132. D. Parker, P. K. Senanayake, and J. A. G. Williams, *J. Chem. Soc. Perkin Trans. 2*, 1998, 2129–2140.
133. J. Massue, S. J. Quinn, and T. Gunnlaugsson, *J. Am. Chem. Soc.*, 2008, **130**, 6900–6901.
134. E. M. Boyle, S. Comby, J. K. Molloy, and T. Gunnlaugsson, *J. Org. Chem.*, 2013, **78**, 8312–8319.
135. C. R. Wade and F. P. Gabbaï, *Dalton Trans.*, 2009, 9169–9175.
136. H. Miyaji, W. Sato, and J. L. Sessler, *Angew. Chem. Int. Ed.*, 2000, **39**, 1777–1780.
137. M. C. Thompson and D. H. Busch, *J. Am. Chem. Soc.*, 1962, **84**, 1762–1763.
138. D. H. Busch, *J. Incl. Phenom. Macrocycl. Chem.*, 1992, **12**, 389–395.
139. S. Anderson, H. L. Anderson, and J. K. M. Sanders, *Acc. Chem. Res.*, 1993, **26**, 469–475.
140. N. F. Curtis, *Coord. Chem. Rev.*, 1968, **3**, 3–47.
141. M.-T. Youinou, N. Rahmouni, J. Fischer, and J. A. Osborn, *Angew. Chem. Int. Ed. Engl.*, 1992, **31**, 733–735.
142. K. S. Chichak, S. J. Cantrill, A. R. Pease, S.-H. Chiu, G. W. V. Cave, J. L. Atwood, and J. F. Stoddart, *Science*, 2004, **304**, 1308–1312.
143. P. Mal, D. Schultz, K. Beyeh, K. Rissanen, and J. R. Nitschke, *Angew. Chem. Int. Ed.*, 2008, **47**, 8297–8301.
144. P. Mal, B. Breiner, K. Rissanen, and J. R. Nitschke, *Science*, 2009, **324**, 1697–1699.
145. Q.-F. Sun, J. Iwasa, D. Ogawa, Y. Ishido, S. Sato, T. Ozeki, Y. Sei, K. Yamaguchi, and M. Fujita, *Science*, 2010, **328**, 1144–1147.
146. Q. Sun, T. Murase, S. Sato, and M. Fujita, *Angew. Chem. Int. Ed.*, 2011, **50**, 10318–10321.
147. Q.-F. Sun, S. Sato, and M. Fujita, *Nat. Chem.*, 2012, **4**, 330–333.
148. M. Hoffmann, C. J. Wilson, B. Odell, and H. L. Anderson, *Angew. Chem. Int. Ed.*, 2007, **46**, 3122–3125.
149. M. C. O' Sullivan, J. K. Sprafke, D. V. Kondratuk, C. Rinfray, T. D. W. Claridge, A. Saywell, M. O. Blunt, J. N. O' Shea, P. H. Beton, M. Malfois, and H. L. Anderson, *Nature*, 2011, **469**, 72–75.
150. B. Hasenknopf, J.-M. Lehn, B. O. Kneisel, G. Baum, and D. Fenske, *Angew. Chem. Int. Ed. Engl.*, 1996, **35**, 1838–1840.
151. B. Hasenknopf, J.-M. Lehn, N. Boumediene, A. Dupont-Gervais, A. Van Dorsselaer, B. Kneisel, and D. Fenske, *J. Am. Chem. Soc.*, 1997, **119**, 10956–10962.
152. J. L. Sessler, T. D. Mody, and V. Lynch, *Inorg. Chem.*, 1992, **31**, 529–531.
153. M. Bru, I. Alfonso, M. I. Burguete, and S. V. Luis, *Angew. Chem. Int. Ed.*, 2006, **45**, 6155–6159.
154. E. A. Katayev, G. D. Pantos, M. D. Reshetova, V. N. Khrustalev, V. M. Lynch, Y. A. Ustynyuk, and J. L. Sessler, *Angew. Chem. Int. Ed.*, 2005, **44**, 7386–7390.
155. J.-P. Sauvage and C. O. Dietrich-Buchecker, *Molecular Catenanes, Rotaxanes and Knots,*, Wiley-VCH, Weinheim, 1999.

156. J.-F. Ayme, J. E. Beves, C. J. Campbell, and D. A. Leigh, *Chem. Soc. Rev.*, 2013, **42**, 1700–1712.
157. P. R. Ashton, M. Belohradsky, D. Philp, and J. F. Stoddart, *J. Chem. Soc. Chem. Commun.*, 1993, 1269.
158. G. M. Hübner, J. Gläser, C. Seel, and F. Vögtle, *Angew. Chem. Int. Ed.*, 1999, **38**, 383–386.
159. V. Aucagne, J. Berná, J. D. Crowley, S. M. Goldup, K. D. Hänni, D. A. Leigh, P. J. Lusby, V. E. Ronaldson, A. M. Z. Slawin, A. Viterisi, and D. B. Walker, *J. Am. Chem. Soc.*, 2007, **129**, 11950–11963.
160. C.-W. Chiu, C.-C. Lai, and S.-H. Chiu, *J. Am. Chem. Soc.*, 2007, **129**, 3500–3501.
161. I. Yoon, M. Narita, T. Shimizu, and M. Asakawa, *J. Am. Chem. Soc.*, 2004, **126**, 16740–16741.
162. E. Wasserman, *J. Am. Chem. Soc.*, 1960, **82**, 4433–4434.
163. I. T. Harrison and S. Harrison, *J. Am. Chem. Soc.*, 1967, **89**, 5723–5724.
164. G. Agam, D. Graiver, and A. Zilkha, *J. Am. Chem. Soc.*, 1976, **98**, 5206–5214.
165. G. Agam and A. Zilkha, *J. Am. Chem. Soc.*, 1976, **98**, 5214–5216.
166. G. Schill and A. Lüttringhaus, *Angew. Chem. Int. Ed. Engl.*, 1964, **3**, 546–547.
167. J.-P. Sauvage and C. O. Dietrich-Buchecker, *Tetrahedron Lett*, 1983, **24**, 5091–5094.
168. C. O. Dietrich-Buchecker, J. P. Sauvage, and J. M. Kern, *J. Am. Chem. Soc.*, 1984, **106**, 3043–3045.
169. J. P. Sauvage and J. Weiss, *J. Am. Chem. Soc.*, 1985, **107**, 6108–6110.
170. A. Joosten, Y. Trolez, J.-P. Collin, V. Heitz, and J.-P. Sauvage, *J. Am. Chem. Soc.*, 2012, **134**, 1802–1809.
171. C. O. Dietrich-Buchecker and J.-P. Sauvage, *Angew. Chem. Int. Ed. Engl.*, 1989, **28**, 189–192.
172. J. P. Sauvage and M. Ward, *Inorg. Chem.*, 1991, **30**, 3869–3874.
173. C. Hamann, J.-M. Kern, and J.-P. Sauvage, *Inorg. Chem.*, 2003, **42**, 1877–1883.
174. A.-M. Fuller, D. A. Leigh, P. J. Lusby, I. D. H. Oswald, S. Parsons, and D. B. Walker, *Angew. Chem. Int. Ed.*, 2004, **43**, 3914–3918.
175. S. M. Goldup, D. A. Leigh, P. J. Lusby, R. T. McBurney, and A. M. Z. Slawin, *Angew. Chem. Int. Ed.*, 2008, **47**, 6999–7003.
176. J. D. Crowley, S. M. Goldup, A.-L. Lee, D. A. Leigh, and R. T. McBurney, *Chem. Soc. Rev.*, 2009, **38**, 1530–1541.
177. H. C. Kolb, M. G. Finn, and K. B. Sharpless, *Angew. Chem. Int. Ed.*, 2001, **40**, 2004–2021.
178. V. Aucagne, K. D. Hänni, D. A. Leigh, P. J. Lusby, and D. B. Walker, *J. Am. Chem. Soc.*, 2006, **128**, 2186–2187.
179. S. M. Goldup, D. A. Leigh, T. Long, P. R. McGonigal, M. D. Symes, and J. Wu, *J. Am. Chem. Soc.*, 2009, **131**, 15924–15929.
180. M. J. Langton, J. D. Matichak, A. L. Thompson, and H. L. Anderson, *Chem. Sci.*, 2011, **2**, 1897.
181. J. D. Crowley, K. D. HÃ¤nni, A.-L. Lee, and D. A. Leigh, *J. Am. Chem. Soc.*, 2007, **129**, 12092–12093.
182. S. Saito, E. Takahashi, and K. Nakazono, *Org. Lett.*, 2006, **8**, 5133–5136.
183. Y. Sato, R. Yamasaki, and S. Saito, *Angew. Chem. Int. Ed.*, 2009, **48**, 504–507.
184. J. Berná, J. D. Crowley, S. M. Goldup, K. D. Hänni, A.-L. Lee, and D. A. Leigh, *Angew. Chem. Int. Ed.*, 2007, **46**, 5709–5713.
185. D. A. Leigh, V. E. Ronaldson, and A. M. Z. Slawin, *J. Am. Chem. Soc.*, 2010, **132**, 6243–6248.

186. S. M. Goldup, D. A. Leigh, P. J. Lusby, R. T. McBurney, and A. M. Z. Slawin, *Angew. Chem. Int. Ed. Engl.*, 2008, **120**, 3429–3432.
187. P. R. Ashton, O. A. Matthews, S. Menzer, F. M. Raymo, N. Spencer, J. F. Stoddart, and D. J. Williams, *Liebigs Ann.*, 1997, **1997**, 2485–2494.
188. M. E. Belowich, C. Valente, R. A. Smaldone, D. C. Friedman, J. Thiel, L. Cronin, and J. F. Stoddart, *J. Am. Chem. Soc.*, 2012, **134**, 5243–5261.
189. S. J. Loeb and J. A. Wisner, *Angew. Chem. Int. Ed.*, 1998, **37**, 2838–2840.
190. W. Jiang, D. Sattler, K. Rissanen, and C. A. Schalley, *Org. Lett.*, 2011, **13**, 4502–4505.
191. M.-V. Martínez-Díaz, N. Spencer, and J. F. Stoddart, *Angew. Chem. Int. Ed. Engl.*, 1997, **36**, 1904–1907.
192. S. J. Loeb and J. A. Wisner, *Chem. Commun.*, 2000, **10**, 845–846.
193. F. Vögtle, S. Meier, and R. Hoss, *Angew. Chem. Int. Ed. Engl.*, 1992, **31**, 1619–1622.
194. C. A. Hunter, *J. Am. Chem. Soc.*, 1992, **114**, 5303–5311.
195. A. G. Johnston, D. A. Leigh, R. J. Pritchard, and M. D. Deegan, *Angew. Chem. Int. Ed. Engl.*, 1995, **34**, 1209–1212.
196. D. M. D'Souza, D. A. Leigh, L. Mottier, K. M. Mullen, F. Paolucci, S. J. Teat, and S. Zhang, *J. Am. Chem. Soc.*, 2010, **132**, 9465–9470.
197. R. Ahmed, A. Altieri, D. M. D'Souza, D. A. Leigh, K. M. Mullen, M. Papmeyer, A. M. Z. Slawin, J. K. Y. Wong, and J. D. Woollins, *J. Am. Chem. Soc.*, 2011, **133**, 12304–12310.
198. F. B. L. Cougnon, H. Y. Au-Yeung, G. D. Pantoş, and J. K. M. Sanders, *J. Am. Chem. Soc.*, 2011, **133**, 3198–3207.
199. S. P. Black, J. K. M. Sanders, and A. R. Stefankiewicz, *Chem. Soc. Rev.*, 2014, **43**, 1861–1872.
200. A. Harada, J. Li, and M. Kamachi, *Chem. Commun.*, 1997, **15**, 1413–1414.
201. A. Miyawaki, M. Miyauchi, Y. Takashima, H. Yamaguchi, and A. Harada, *Chem. Commun.*, 2008, **4**, 456–458.
202. P. N. Taylor, M. J. O'Connell, L. A. McNeill, M. J. Hall, R. T. Aplin, and H. L. Anderson, *Angew. Chem. Int. Ed.*, 2000, **39**, 3456–3460.
203. M. J. Frampton and H. L. Anderson, *Angew. Chem. Int. Ed.*, 2007, **46**, 1028–1064.
204. M. C. T. Fyfe, P. T. Glink, S. Menzer, J. F. Stoddart, A. J. P. White, and D. J. Williams, *Angew. Chem. Int. Ed. Engl.*, 1997, **36**, 2068–2070.
205. E. Arunkumar, C. C. Forbes, B. C. Noll, and B. D. Smith, *J. Am. Chem. Soc.*, 2005, **127**, 3288–3289.
206. J. J. Gassensmith, J. M. Baumes, and B. D. Smith, *Chem. Commun.*, 2009, 6329–6338.
207. J. J. Gassensmith, S. Matthys, J. Lee, A. Wojcik, P. V. Kamat, and B. D. Smith, *Chem. - Eur. J.*, 2010, **16**, 2916–2921.
208. J.-J. Lee, J. M. Baumes, R. D. Connell, A. G. Oliver, and B. D. Smith, *Chem. Commun.*, 2011, **47**, 7188–7190.
209. S. Lee, C.-H. Chen, and A. H. Flood, *Nat. Chem.*, 2013, **5**, 704–710.
210. J. A. Wisner, P. D. Beer, and M. G. B. Drew, *Angew. Chem. Int. Ed.*, 2001, **40**, 3606–3609.
211. J. A. Wisner, P. D. Beer, M. G. B. Drew, and M. R. Sambrook, *J Am Chem Soc*, 2002, **124**, 12469–12476.
212. L. M. Hancock and P. D. Beer, *Chem. - Eur. J.*, 2008, **15**, 42–44.
213. N. H. Evans, E. S. H. Allinson, M. D. Lankshear, K.-Y. Ng, A. R. Cowley, C. J. Serpell, S. M. Santos, P. J. Costa, V. Félix, and P. D. Beer, *RSC Adv.*, 2011, **1**, 995–1003.

214. L. M. Hancock, L. C. Gilday, N. L. Kilah, C. J. Serpell, and P. D. Beer, *Chem. Commun.*, 2011, **47**, 1725–1727.
215. N. H. Evans, C. J. Serpell, and P. D. Beer, *Angew. Chem. Int. Ed.*, 2011, **50**, 2507–2510.
216. N. H. Evans and P. D. Beer, *Chem. – Eur. J.*, 2011, **17**, 10542–10546.
217. N. H. Evans, C. J. Serpell, and P. D. Beer, *Chem. Commun.*, 2011, **47**, 8775–8777.
218. K. M. Mullen, J. Mercurio, C. J. Serpell, and P. D. Beer, *Angew. Chem. Int. Ed.*, 2009, **48**, 4781–4784.
219. K. M. Mullen and P. D. Beer, *Chem. Soc. Rev.*, 2009, **38**, 1701–1713.
220. E. R. Kay, D. A. Leigh, and F. Zerbetto, *Angew. Chem. Int. Ed.*, 2007, **46**, 72–191.
221. P. L. Anelli, N. Spencer, and J. F. Stoddart, *J. Am. Chem. Soc.*, 1991, **113**, 5131–5133.
222. V. Balzani, A. Credi, S. Silvi, and M. Venturi, *Chem. Soc. Rev.*, 2006, **35**, 1135–1149.
223. U. Létinois-Halbes, D. Hanss, J. M. Beierle, J.-P. Collin, and J.-P. Sauvage, *Org. Lett.*, 2005, **7**, 5753–5756.
224. J. D. Badjić, V. Balzani, A. Credi, S. Silvi, and J. F. Stoddart, *Science*, 2004, **303**, 1845–1849.
225. M. C. Jiménez, C. Dietrich-Buchecker, and J.-P. Sauvage, *Angew. Chem. Int. Ed.*, 2000, **39**, 3284–3287.
226. C. J. Bruns and J. F. Stoddart, *Acc. Chem. Res.*, 2014.
227. J. Berná, D. A. Leigh, M. Lubomska, S. M. Mendoza, E. M. Pérez, P. Rudolf, G. Teobaldi, and F. Zerbetto, *Nat. Mater.*, 2005, **4**, 704–710.
228. B. Lewandowski, G. D. Bo, J. W. Ward, M. Papmeyer, S. Kuschel, M. J. Aldegunde, P. M. E. Gramlich, D. Heckmann, S. M. Goldup, D. M. D'Souza, A. E. Fernandes, and D. A. Leigh, *Science*, 2013, **339**, 189–193.
229. A. Andrievsky, F. Ahuis, J. L. Sessler, F. Vögtle, D. Gudat, and M. Moini, *J. Am. Chem. Soc.*, 1998, **120**, 9712–9713.
230. R. T. S. Lam, A. Belenguer, S. L. Roberts, C. Naumann, T. Jarrosson, S. Otto, and J. K. M. Sanders, *Science*, 2005, **308**, 667–669.
231. S. S. Zhu, P. J. Carroll, and T. M. Swager, *J. Am. Chem. Soc.*, 1996, **118**, 8713–8714.
232. S. S. Zhu and T. M. Swager, *J. Am. Chem. Soc.*, 1997, **119**, 12568–12577.
233. S.-Y. Hsueh, C.-C. Lai, Y.-H. Liu, S.-M. Peng, and S.-H. Chiu, *Angew. Chem. Int. Ed.*, 2007, **46**, 2013–2017.
234. S.-Y. Hsueh, C.-C. Lai, and S.-H. Chiu, *Chem. – Eur. J.*, 2010, **16**, 2997–3000.
235. K. Hiratani, M. Kaneyama, Y. Nagawa, E. Koyama, and M. Kanesato, *J. Am. Chem. Soc.*, 2004, **126**, 13568–13569.
236. M. V. R. Raju and H.-C. Lin, *Org. Lett.*, 2013, **15**, 1274–1277.
237. M. K. Chae, J. Suk, and K.-S. Jeong, *Tetrahedron Lett.*, 2010, **51**, 4240–4242.
238. L. M. Hancock, E. Marchi, P. Ceroni, and P. D. Beer, *Chem. – Eur. J.*, 2012, **18**, 11277–11283.
239. N. H. Evans and P. D. Beer, *Org. Biomol. Chem.*, 2010, **9**, 92–100.
240. M. Ogawa, A. Kawasaki, Y. Koyama, and T. Takata, *Polym. J.*, 2011, **43**, 909–915.
241. E. A. Neal and S. M. Goldup, *Chem. Commun.*, 2014, **50**, 5128–5142.
242. V. Blanco, D. A. Leigh, V. Marcos, J. A. Morales-Serna, and A. L. Nussbaumer, *J. Am. Chem. Soc.*, 2014, **136**, 4905–4908.
243. C. B. Caputo, K. Zhu, V. N. Vukotic, S. J. Loeb, and D. W. Stephan, *Angew. Chem. Int. Ed.*, 2013, **52**, 960–963.
244. J. Winn, A. Pinczewska, and S. M. Goldup, *J. Am. Chem. Soc.*, 2013, **135**, 13318–13321.

245. V. Dvornikovs, B. E. House, M. Kaetzel, J. R. Dedman, and D. B. Smithrud, *J. Am. Chem. Soc.*, 2003, **125**, 8290–8301.
246. D. B. Smithrud, X. Wang, P. Tarapore, and S. Ho, *ACS Med. Chem. Lett.*, 2013, **4**, 27–31.
247. A. G. Cheetham, M. G. Hutchings, T. D. W. Claridge, and H. L. Anderson, *Angew. Chem.*, 2006, **118**, 1626–1629.
248. A. Fernandes, A. Viterisi, F. Coutrot, S. Potok, D. A. Leigh, V. Aucagne, and S. Papot, *Angew. Chem. Int. Ed.*, 2009, **48**, 6443–6447.
249. A. Fernandes, A. Viterisi, V. Aucagne, D. A. Leigh, and S. Papot, *Chem. Commun.*, 2012, **48**, 2083–2085.

CHAPTER 2

Chapter 2 Hydrogen bonding interlocked host systems for oxoanion recognition in aqueous solvent mixtures

2.1 Introduction

2.1.1 Anion templation of interlocked molecules

In 2002 Beer and co-workers reported the seminal example of the anion templated synthesis of a [2]rotaxane,[1] using a chloride templation approach (*vide supra*). This methodology was subsequently used in the synthesis of a wide range of interlocked architectures including rotaxanes,[2,3] catenanes,[4,5] a Janus [2]rotaxane[6] and a [3]rotaxane.[7] Removing the anion template from these interlocked molecular architectures, by exchanging to a non-coordinating anion such as hexafluorophosphate, reveals an anion host system which possesses a three-dimensionally restrained binding cavity formed between the interlocked components. Such hosts exhibit high selectivity for the templating anion in competitive organic–aqueous solvent mixtures. For example, the dicationic chloride templated rotaxane shown in Figure 2.1a is highly selective for Cl^- in 65:35 d_6-acetone/D_2O (K_a = 500 M^{-1}) over the more basic oxoanions $H_2PO_4^-$ and AcO^-, which do not bind since they cannot penetrate the interlocked binding cavity. Importantly, this is the reverse of the anion selectivity observed for the non-interlocked axle. Furthermore, as was discussed in Chapter 1, by incorporating electrochemical or optical reporter groups within the interlocked host architecture, such hosts can be employed as selective anion sensors that report anion binding by means of a change in the redox or optical properties of the system.[8]

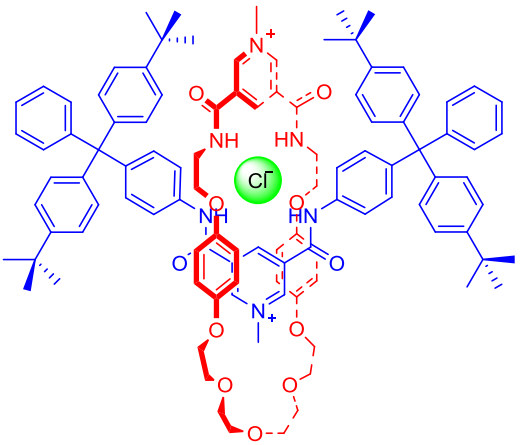

Figure 2.1 Dicationic hydrogen bonding rotaxane for selective chloride recognition in aqueous solution.[3]

The utilisation of anion templates other than chloride for the synthesis of mechanically bonded molecules has, however, been less extensively explored. Only two other templating anions have been exploited to date: bromide has been employed to template both rotaxane[9] and catenane formation,[10] whilst sulfate has been shown to be highly effective in templating catenane assembly.[11,12] The use of other oxoanions, including nitrate, for anion templated synthesis of mechanically bonded structures is, however, unprecedented.

2.1.2 Higher order interlocked architectures for guest recognition

Higher order interlocked architectures, specifically those structures containing more than two discrete interlocked components, provide intriguing opportunities for forming host–guest complexes with elaborate binding modes, and yet there are relatively few reported examples in the literature.[13–21] A notable example, however, was described by Sauvage and co-workers (Figure 2.2),[18] who prepared a [3]rotaxane that is capable of binding small, ditopic pyridyl guests, such as 4,4'-bipyridine, between the two zinc(II) metallo-porphyrin moieties of the macrocycle components. Upon removal of Cu(I), the macrocycles are free to translocate along the axle, facilitating the binding of larger ditopic pyridyl guest species between the zinc(II) metallo-porphyrin components.

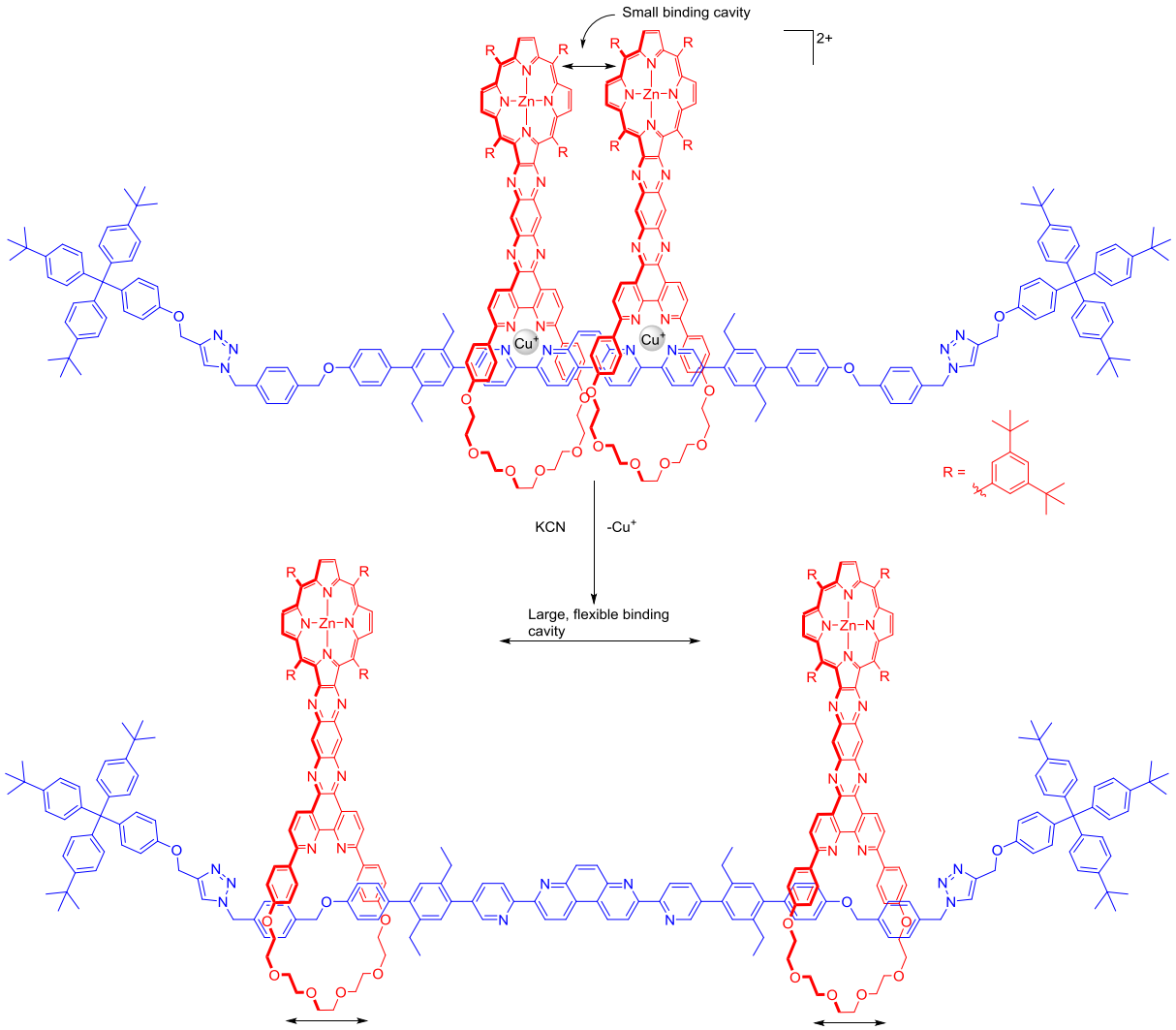

Figure 2.2 Sauvage's adjustable [3]rotaxane host for ditopic pyridyl guests.[18]

Examples of higher order structures capable of charged guest *sensing* are particularly rare, with only two examples reported in the literature to date (Figure 2.3). Beer's ferrocene-functionalised [3]rotaxane can bind and electrochemically sense chloride and sulfate by means of a cathodic shift in the ferrocene/ferrocenium redox couple of the metallocene axle (Figure 2.3a),[7] whilst Hiratani's anthracene-functionalised [3]rotaxane is capable of binding and sensing caesium cations by means of enhancement of the axle's anthracene emission (Figure 2.3b).[15] Whilst there are a handful of interlocked optical anion sensors, however,[8] at the commencement of the work in this thesis, higher order analogues had not been reported.

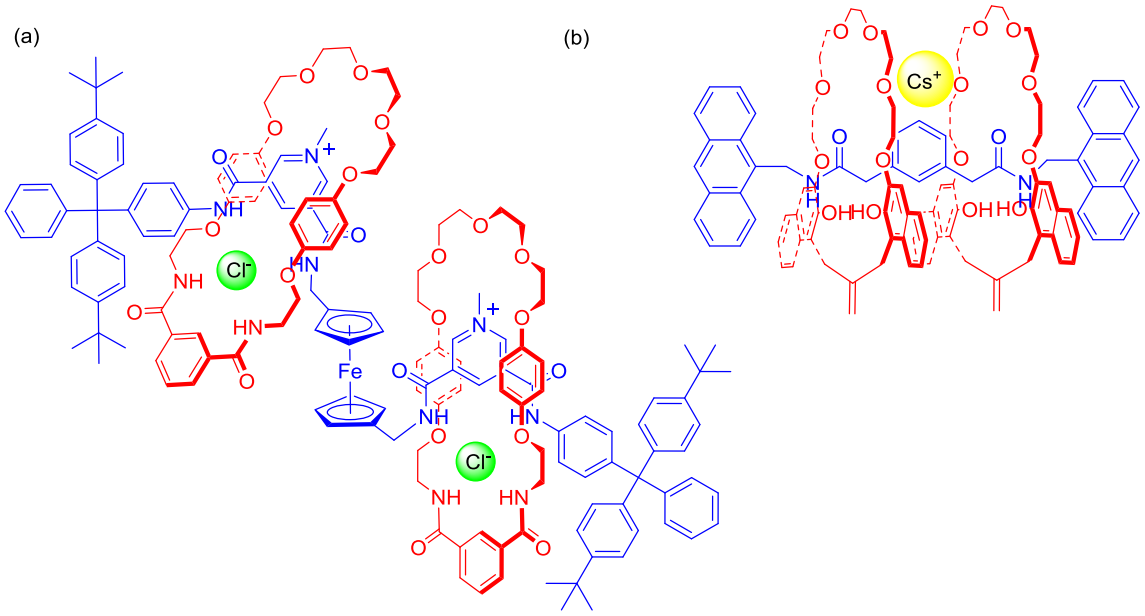

Figure 2.3 [3]rotaxanes for charged guest sensing: Evans and Beer's [3]rotaxane for electrochemical sensing of chloride and sulfate anions[7] and Hiratani's Cs^+-sensing [3]rotaxane.[15]

2.1.3 Chapter aims

The overall goal of the research conducted in this chapter is to prepare novel interlocked host molecules for the selective recognition of oxoanion guests in competitive organic–aqueous solvent mixtures. The chapter concerns two specific objectives related to this theme: firstly, to prepare and investigate higher order interlocked host molecules for anion *sensing* applications, and secondly, to examine approaches to synthesising mechanically bonded hosts capable of selective nitrate anion recognition.

In particular, a [3]rotaxane host system incorporating a fluorescent naphthalene motif will be prepared, and the anion recognition and sensing properties will be probed. Selective nitrate recognition by both rotaxane and catenane host systems will also be explored, using an unprecedented nitrate anion templation strategy to form interlocked host molecules with a complementary binding site for the recognition of the trigonal nitrate anion in highly competitive organic–aqueous solvent mixtures.

2.2 Synthesis of a fluorescent [3]rotaxane for anion recognition and optical sensing in aqueous solvent mixtures[†]

2.2.1 Design, synthesis and characterisation

Inspired by Hiratani's [3]rotaxane that binds caesium cations in a 1:1 stoichiometric "sandwich" complex (Figure 2.3b), and senses such charged guest species by means of modulation of the anthracene emission, an analogous [3]rotaxane receptor capable of the selective sensing of anions was targeted. The rotaxane design was based broadly on the previously reported ferrocene-containing [3]rotaxane (Figure 2.3a), replacing the electrochemical reporter group with a fluorescent naphthalene motif, to facilitate optical anion sensing. It was envisaged that the dicationic rotaxane host would bind two halide anions, one in each of the interlocked cavities, but the larger, doubly charged sulfate anion would associate in a 1:1 stoichiometric fashion between the two macrocycles (Figure 2.4), reminiscent of the "sandwich complex" formed with a caesium cation guest in Hiratani's receptor. These two binding modes could conceivably result in discrete and distinguishable modulation of the naphthalene emission, facilitating the selective optical sensing of the two guest species.

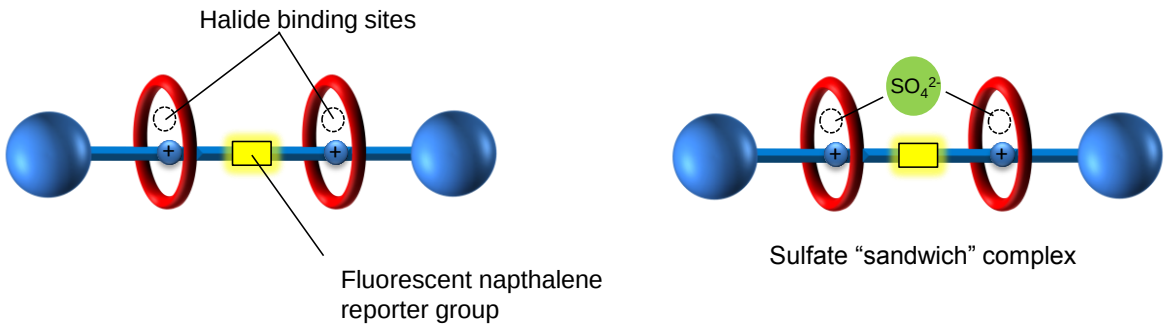

Figure 2.4 Schematic representation of the target fluorescent [3]rotaxane for anion sensing.

[†] The work in the following section was published as a full paper in the journal *Chemistry, A European Journal:* M. J. Langton and P. D. Beer, *Chem. Eur. J.,* 2012, **18**, 14406–14412.

The target rotaxane **1·(Cl)$_2$** is depicted in Figure 2.5. The novel axle consists of two 3,5-bis-amide pyridinium chloride motifs each covalently attached to a bulky terphenyl stopper group, which are themselves linked by a 2,7-bis(aminomethyl)naphthalene spacer unit. The macrocycle incorporates a hydrogen bond donating isophthalamide motif to coordinate to an anion, whilst hydroquinone groups provide secondary stabilisation through aromatic donor–acceptor interactions with the electron-deficient pyridinium moieties in the axle component.

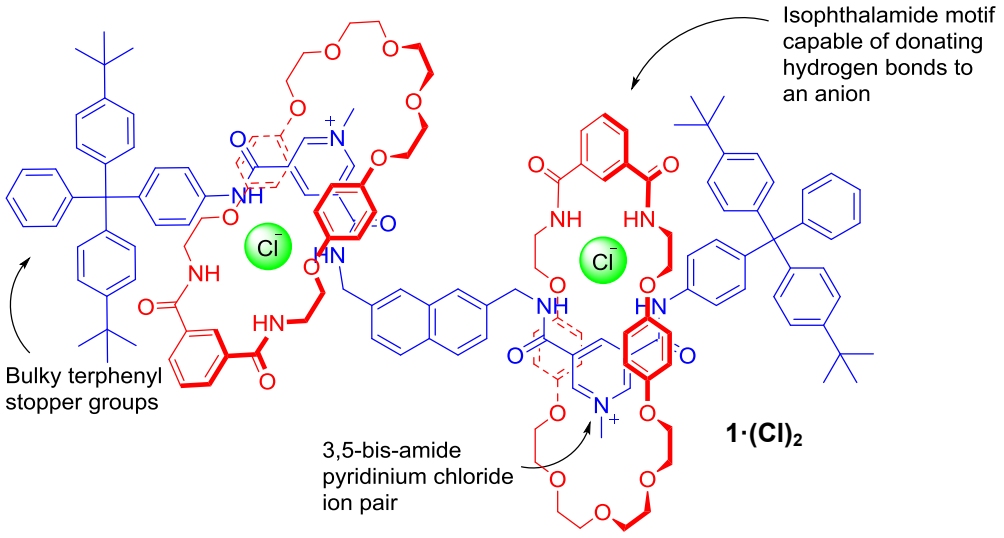

Figure 2.5 Target naphthalene-containing [3]rotaxane **1·(Cl)$_2$**.

The initial stage of the axle synthesis involved the preparation of the asymmetric stopper intermediate **7**, derived from an asymmetrically substituted pyridine-3,5-dicarboxylic acid moiety, using the procedure developed by Hancock and Beer.[22] The aniline-derived terphenyl stopper component **3**[23] was prepared initially by the reaction of methyl benzoate with the Grignard reagent derived from 4-*tert*-butyl-bromobenzene to afford tertiary alcohol **2**, in 90% yield (Scheme 2.1). This was subsequently activated with acetyl chloride to facilitate electrophilic substitution of aniline, affording stopper **3** in 52% yield.

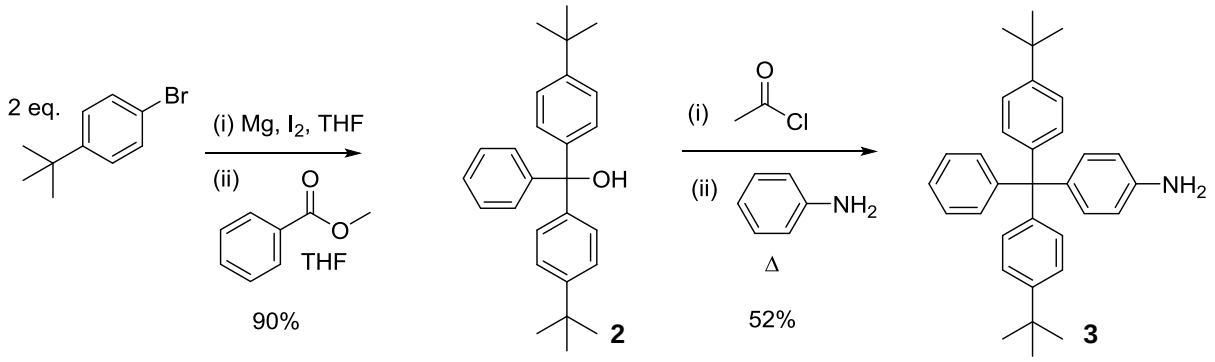

Scheme 2.1 Synthesis of aniline-derived terphenyl stopper component **3**.

Dimethyl ester **4** was prepared from pyridine-3,5-dicarboxylic acid by microwave irradiation in methanol in the presence of concentrated H_2SO_4 (Scheme 2.2). Mono-hydrolysis was achieved using 1.1 equivalents of KOH in methanol to afford monoester **5**, which upon condensation with amine stopper **3** gave compound **6** in 92% yield. Saponification with KOH produced the target asymmetric stopper component **7**.

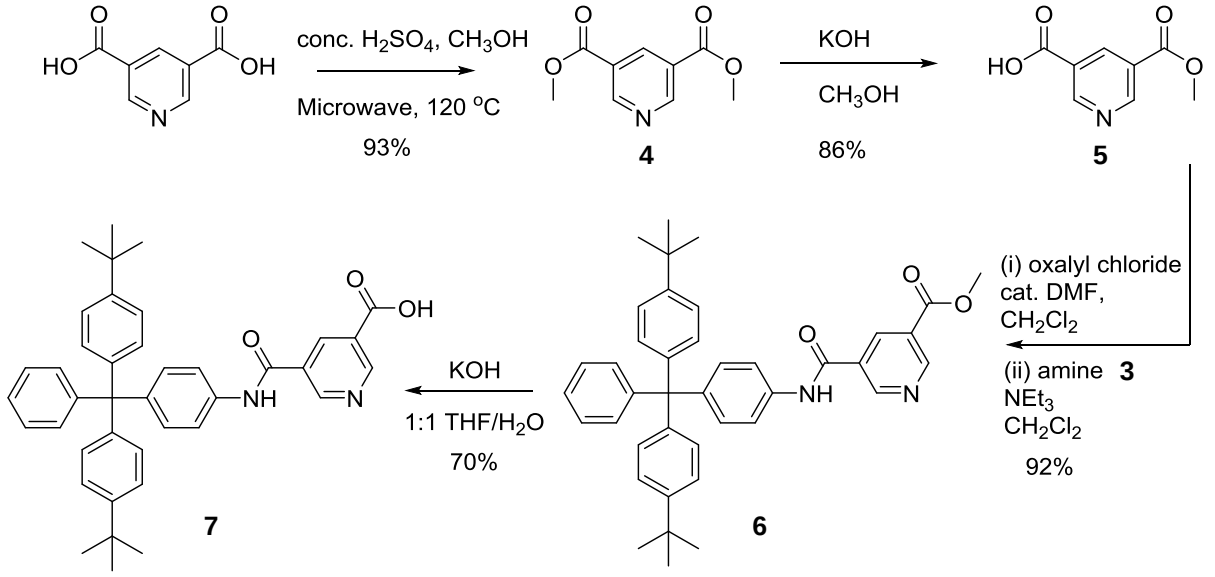

Scheme 2.2 Synthesis of asymmetric stopper component **7**.

2,7-Bis(aminomethyl)napthalene, which forms the central portion of the target axle component, was prepared from 2,7-dimethylnapthalene using literature procedures (Scheme 2.3).[24] 2,7-Bis(bromomethyl)naphthalene **8** was prepared initially from the dimethyl naphthalene precursor according to a modification of the procedure reported by Choi *et al.*,[24]

using *N*-bromosuccinimide (NBS) and azobisisobutyronitrile AIBN as the radical initiator. Purification by recrystallisation from hot ethanol afforded compound **8** in 64% yield. A nucleophilic substitution reaction between compound **8** and sodium azide in dimethyl sulfoxide afforded the bis-azide **9**, which was converted to the target bis-amine **10** *via* hydrogenation in a near quantitative yield.

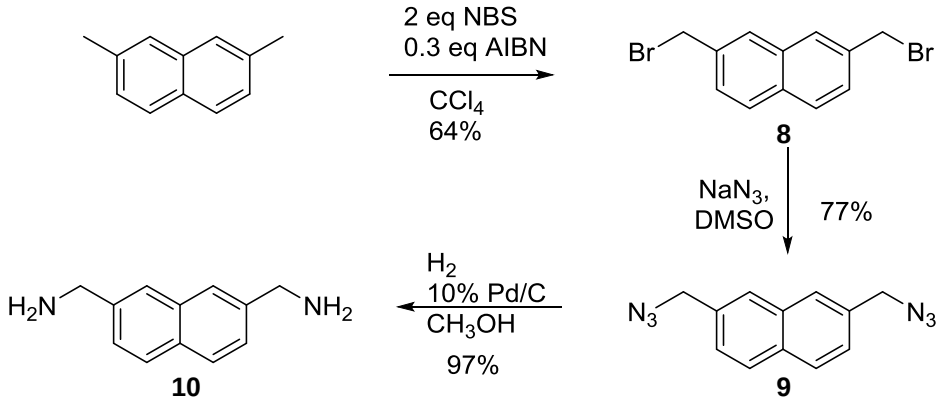

Scheme 2.3 Synthesis of 2,7-bis(aminomethyl)naphthalene **10**.

Axle precursor component **11** was synthesised by the reaction of bis-amine **10** with two equivalents of asymmetric stopper **7** using 1-ethyl-3-(3-dimethylaminopropyl)carbodiimide (EDC) mediated amide coupling (Scheme 2.4). Methylation with CH_3I afforded axle **12·(I)$_2$**, with the chloride salt **12·(Cl)$_2$** being prepared by washing a chloroform solution of the iodide salt with 1M $NH_4Cl_{(aq)}$, in preparation for chloride-templated rotaxane synthesis.[25]

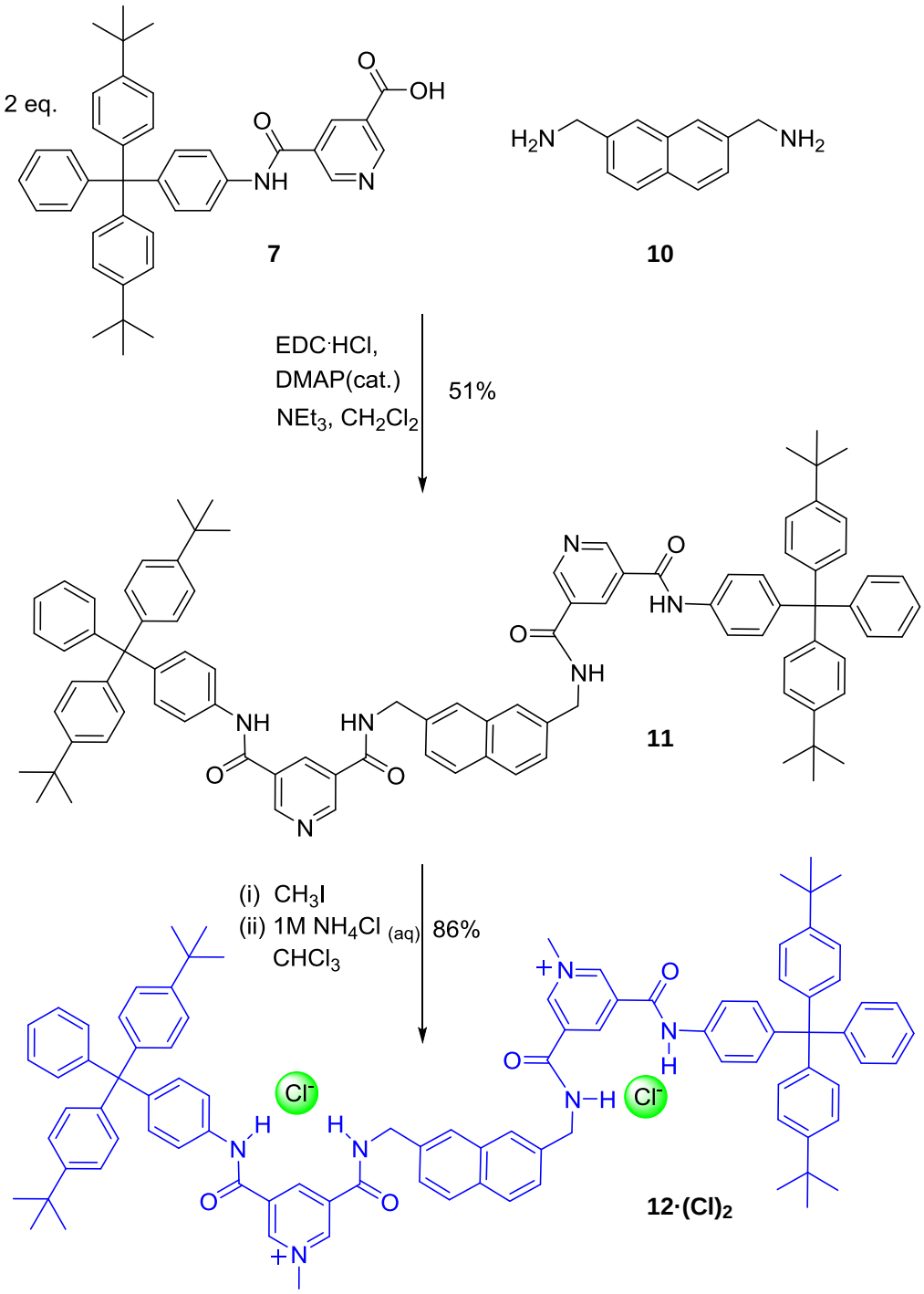

Scheme 2.4 Synthesis of axle **12·(Cl)$_2$**.

Before embarking on the rotaxane synthesis, it was necessary to prepare the appropriate bis-amine macrocycle precursor **16**, using the procedure reported by Hancock *et al.* (Scheme 2.5).[25] Initial mono-functionalisation of hydroquinone with under basic conditions afforded compound **13** in 63% yield. Two equivalents of **13** were reacted with **14**, synthesised from

tetraethylene glycol and mesyl chloride, to form bis-nitrile **15** in 81% yield. Reduction using borane in THF gave bis-amine macrocycle precursor **16** in 51% yield**.**

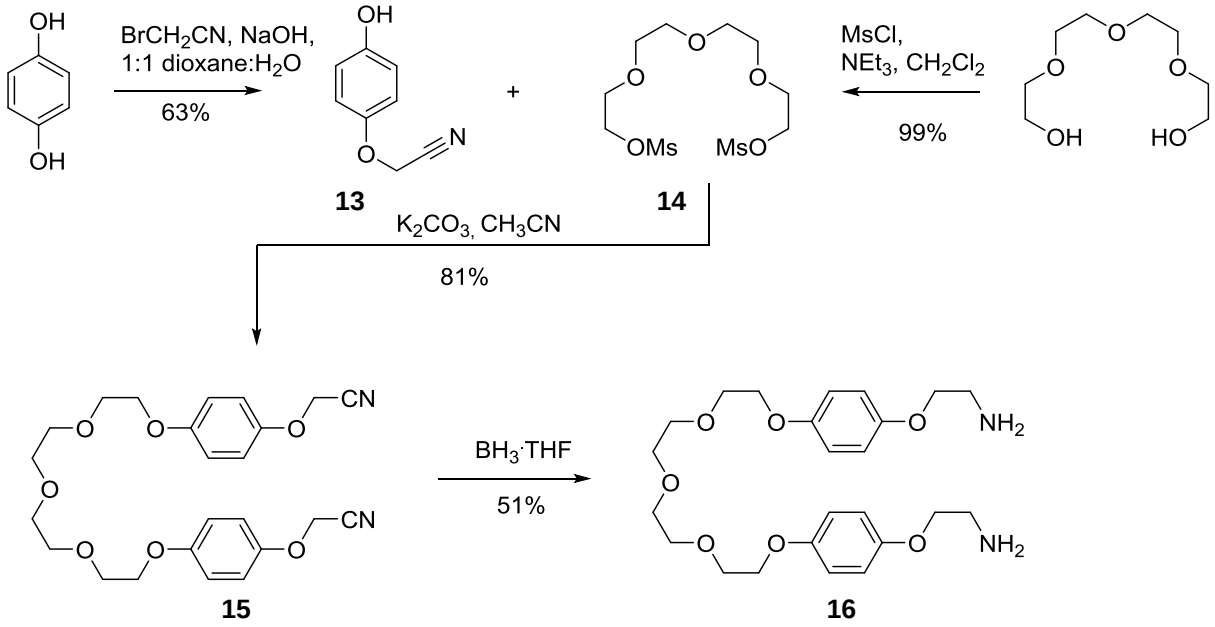

Scheme 2.5 Synthesis of bis-amine macrocycle precursor **16**.

Synthesis of [3]rotaxane **1·(Cl)$_2$** was achieved using a chloride templation procedure developed previously in these laboratories,[7,25] by stirring one equivalent of axle **12·(Cl)$_2$** with three equivalents of bis-amine **16** and three equivalents of isophthaloyl dichloride in the presence of NEt_3 in CH_2Cl_2 (Scheme 2.6). After purification by preparatory silica gel chromatography which removed residual axle, followed by size exclusion chromatography to separate the macrocycle byproduct **17**, [3]rotaxane **1·(Cl)$_2$** was isolated in 33% yield and characterised by ^{1}H and ^{13}C NMR spectroscopy, and high resolution electrospray mass spectrometry (HRMS).

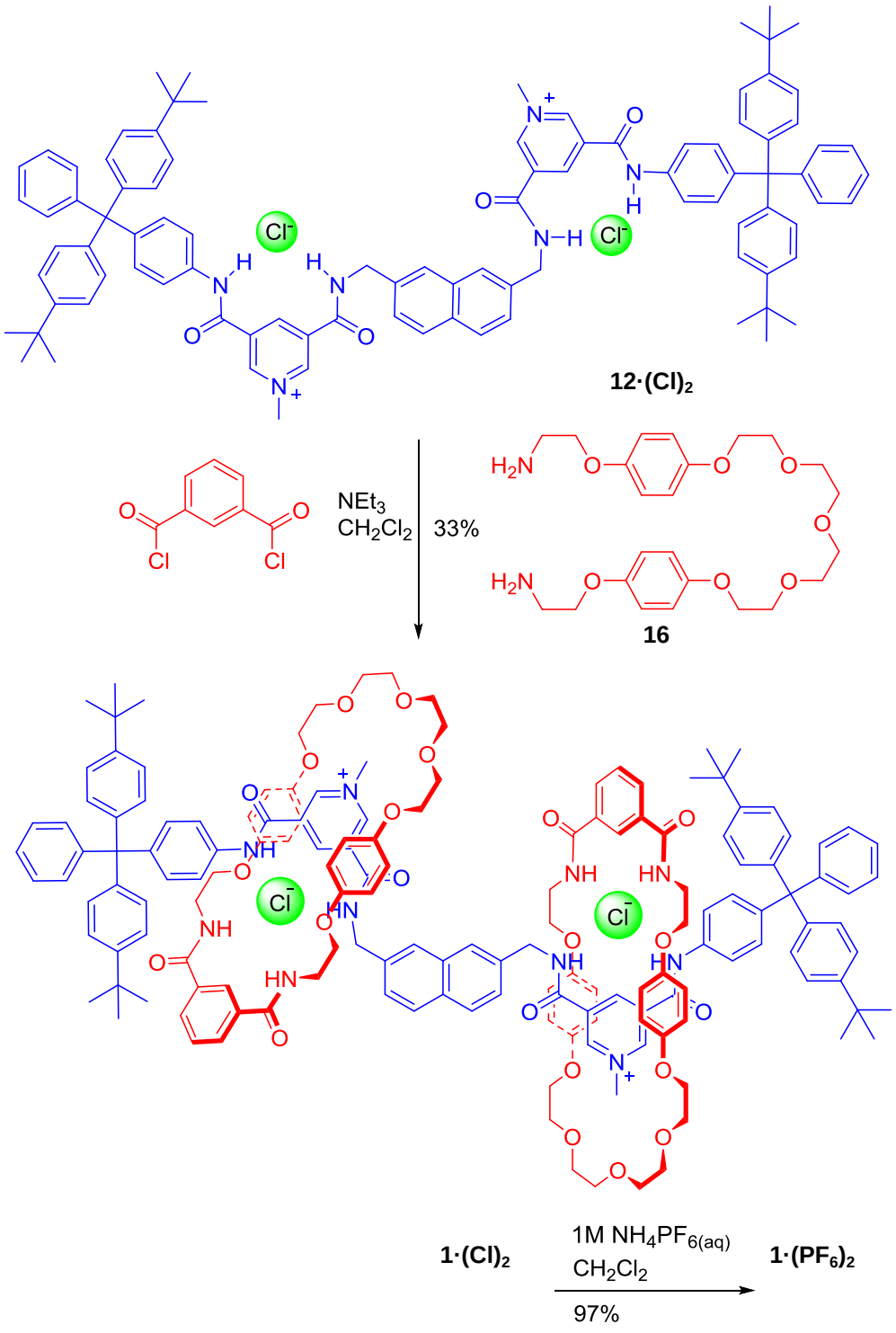

Scheme 2.6 Synthesis of [3]rotaxane **1·(Cl)$_2$**.

The ^{1}H NMR spectrum of **1·(Cl)$_2$** is compared to the spectra of the non-interlocked axle and free macrocycle components in Figure 2.6,‡ and exhibits several distinct features that are consistent with the formation of the interlocked species. Upfield shifts of the cavity axle pyridinium protons *3* and the downfield shift of cavity macrocycle isophthalamide proton *c* are indicative of the hydrogen bonding interactions with the chloride anion template. Importantly, the macrocycle hydroquinone protons *e* and *f* are shifted upfield and split, which is characteristic of aromatic donor–acceptor interactions between the electron rich hydroquinone groups of the macrocycles and the electron deficient pyridinium moieties in the axle. The presence of two macrocycle components was confirmed by integration of signals associated with the macrocycle in the ^{1}H NMR spectrum, and by high resolution mass spectrometry which verified the molecular mass of the [3]rotaxane.

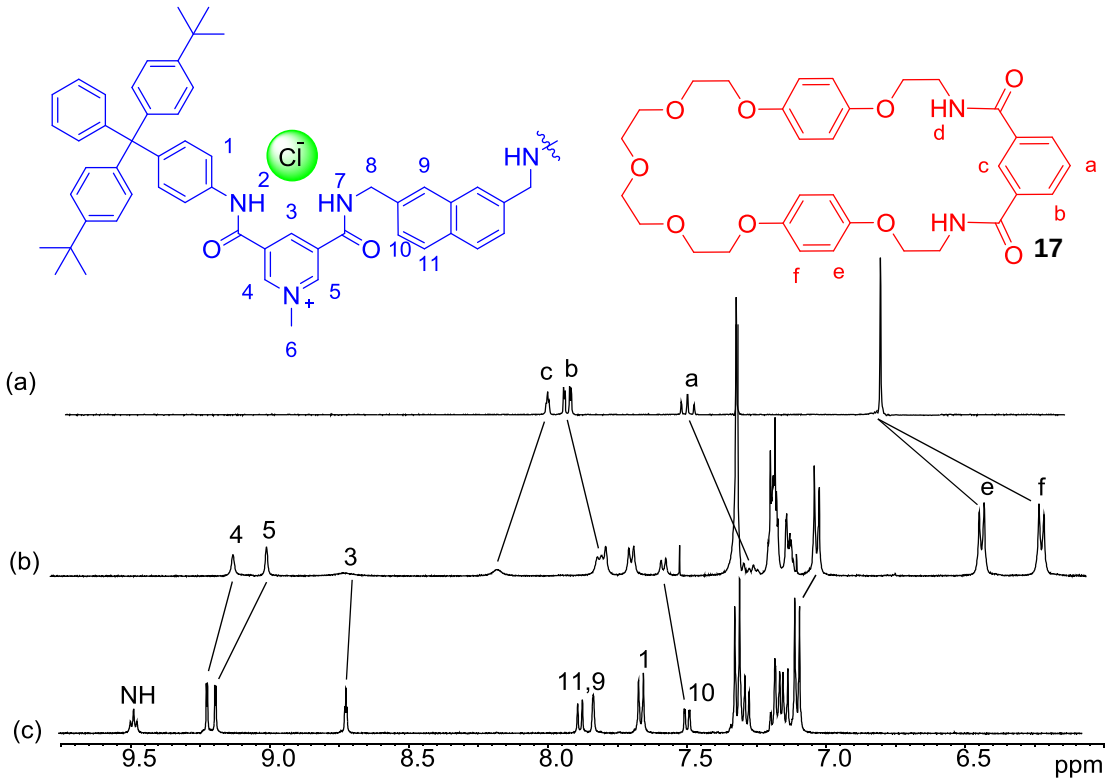

Figure 2.6 Comparison of ^{1}H NMR spectra of (a) unthreaded macrocycle **17**, (b) [3]rotaxane **1·(Cl)$_2$** and (c) axle **12·(Cl)$_2$** in 1:1 $CDCl_3/CD_3OD$ (300 MHz, 298 K).

‡ A pure sample of the free macrocycle component was isolated from the reaction mixture in low yield (<10%), and its identity confirmed by comparison of the ^{1}H NMR and mass spectra with an authentic sample kindly donated by Dr Lydia Gilday.

Conclusive evidence of the mechanically bonded structure was obtained in the ^{1}H ROESY NMR spectrum of **1·(Cl)$_2$**, in which multiple through-space interactions are observed (Figure 2.7). Of particular note are the interactions between protons *e* and *f* of the hydroquinone moieties, and pyridinium protons *3*, *4* and *5*, which are consistent with the axle pyridinium motif intercalating between the hydroquinone groups of the macrocycle in the interlocked structure.

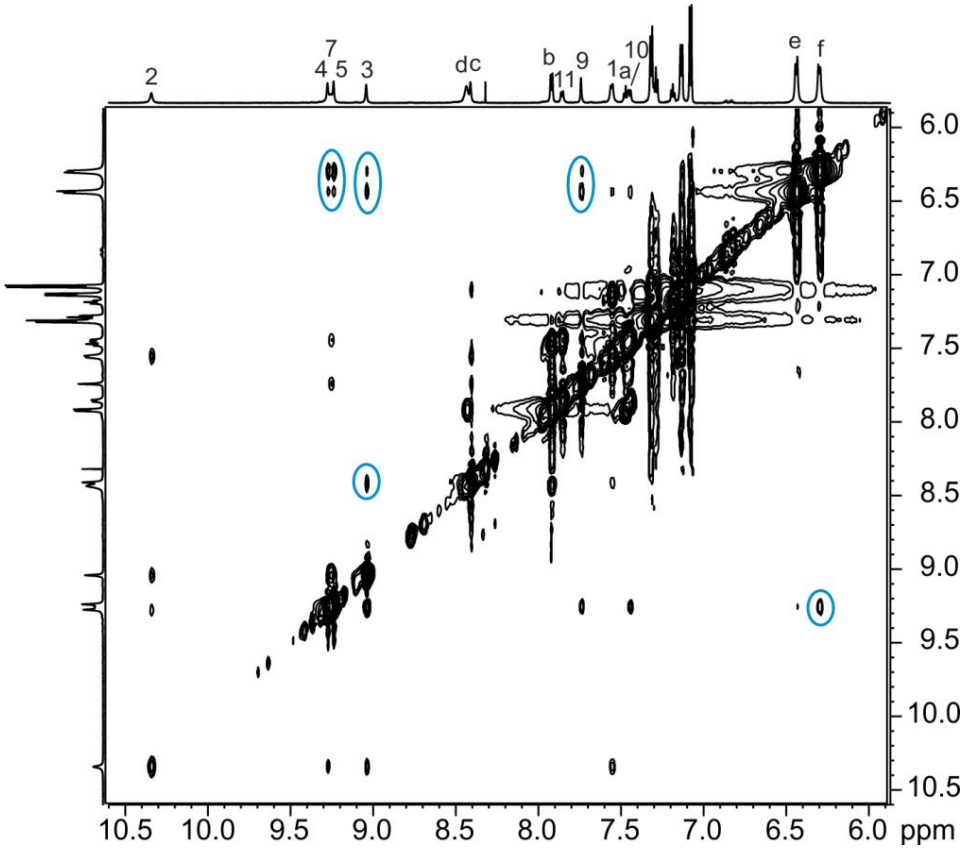

Figure 2.7 Section of the ^{1}H ROESY NMR spectrum of **1·(Cl)$_2$** in d_6-DMSO (700 MHz, 298 K). Selected cross-peaks indicating through space interactions between the interlocked macrocycle and axle components are highlighted. For atom labels see Figure 2.6.

2.2.2 Anion recognition properties of [3]Rotaxane $\mathbf{1\cdot(PF_6)_2}$

The chloride anion template was removed by washing a solution of rotaxane $\mathbf{1\cdot(Cl)_2}$ in CH_2Cl_2 with a 1M aqueous ammonium hexafluorophosphate solution to afford $\mathbf{1\cdot(PF_6)_2}$ which was characterised by ^{1}H, ^{13}C, ^{19}F and ^{31}P NMR, and HRMS. The removal of the chloride anion template from the two rotaxane cavities may be inferred by the upfield shifts of the cavity proton resonances *4, 5, 3* and *c*. It is noteworthy that, whilst moving slightly upfield, the hydroquinone protons *e* and *f* remain split (Figure 2.8), indicating that the pyridinium moieties remain intercalated between the hydroquinones of the macrocycle components, demonstrating that the interlocked nature of the rotaxane is preserved.

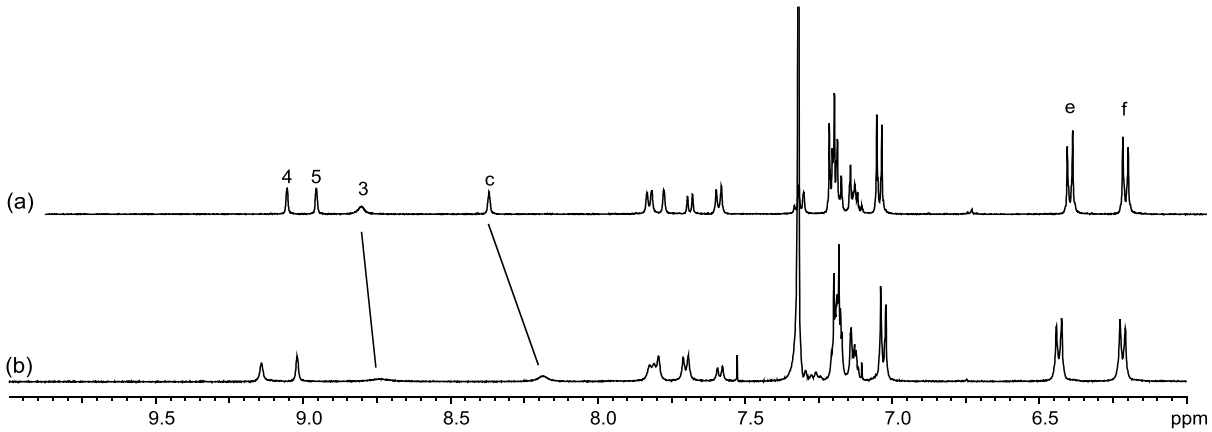

Figure 2.8 ^{1}H NMR spectra of (a) [3]rotaxane $\mathbf{1\cdot(Cl)_2}$, and (b) [3]rotaxane $\mathbf{1\cdot(PF_6)_2}$ in 1:1 $CDCl_3/CD_3OD$ (300 MHz, 298 K). For atom labels see Figure 2.6.

2.2.2.1 ^{1}H NMR anion binding studies

The anion recognition capabilities of rotaxane **1·(PF$_6$)$_2$** were probed initially *via* a series of ^{1}H NMR titration experiments. Preliminary sulfate binding studies were conducted in 1:1 $CDCl_3/CD_3OD$, by adding increasing amounts of the anion as the tetrabutylammonium salt (TBA) to a 1.5 mM solution of **1·(PF$_6$)$_2$** (Figure 2.9).

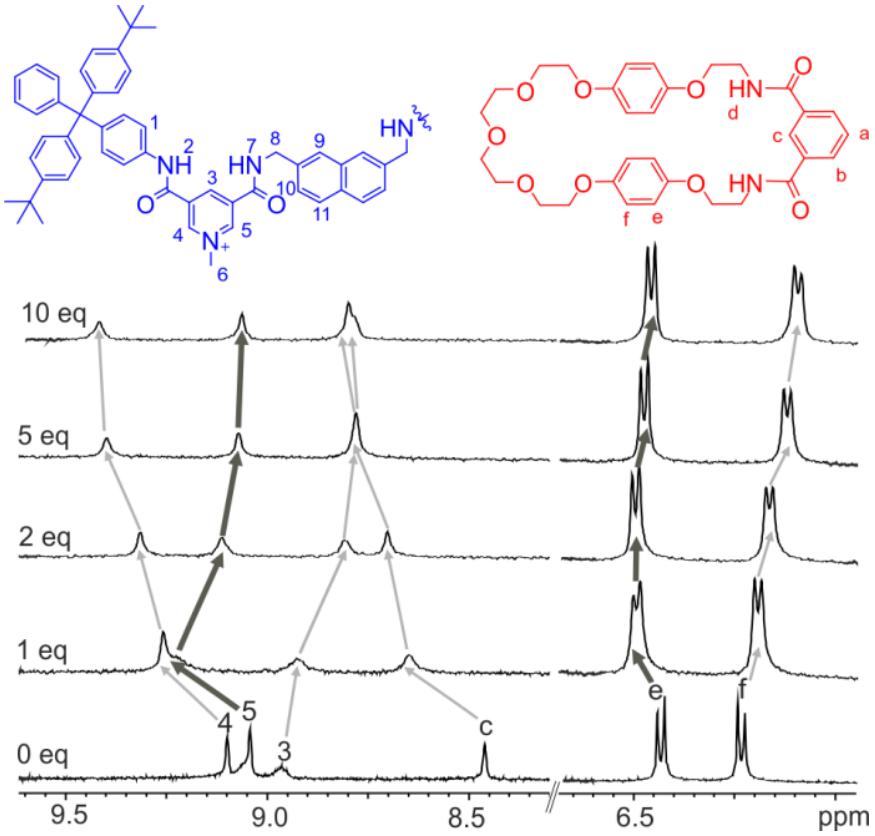

Figure 2.9 Changes in the ^{1}H NMR spectrum of **1·(PF$_6$)$_2$** upon addition of TBA_2SO_4 (1:1 $CDCl_3/CD_3OD$, 500 MHz, 298 K).

Addition of 1 equivalent of sulfate to **1·(PF$_6$)$_2$** resulted in downfield shifts for axle *ortho*-pyridinium protons *4* and *5*, and macrocycle isophthalamide proton *c*, whilst the axle *para*-pyridinium protons *3* shifted upfield. The hydroquinone protons *e* and *f* in the macrocycle exhibited increased splitting when compared to the free rotaxane **1·(PF$_6$)$_2$**. On addition of further equivalents of SO_4^{2-}, pyridinium protons *5* and hydroquinone protons *e* then moved upfield, i.e. in the opposite direction. This surprising result suggests a change in the geometry of the rotaxane host, which is consistent with the binding process depicted in Scheme 2.7.

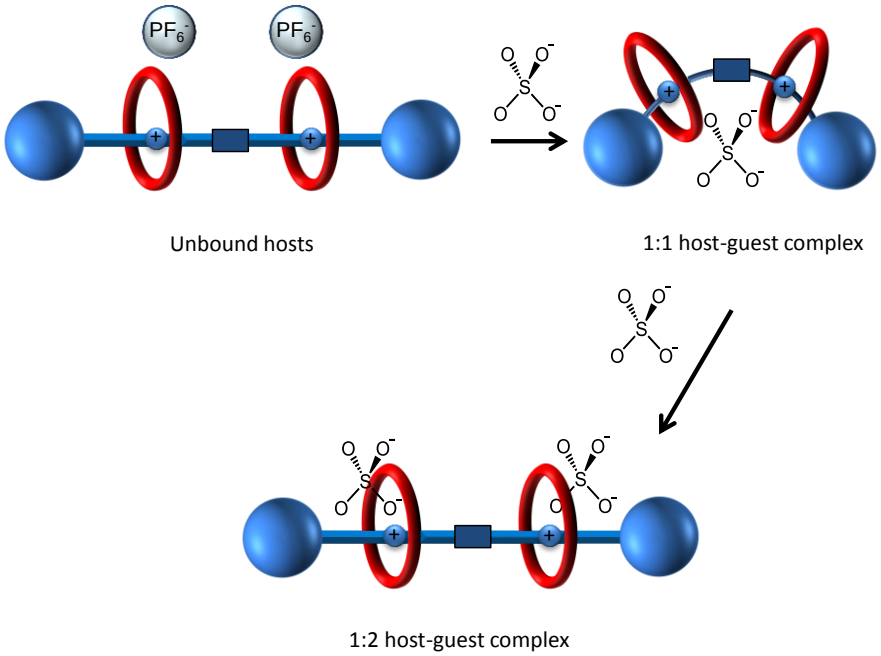

Scheme 2.7 Schematic representation of successive sulfate binding by [3]rotaxane **1·(PF$_6$)$_2$**.

Upon addition of one equivalent of sulfate to the dicationic rotaxane host, a 1:1 stoichiometric complex is formed in which the sulfate anion guest is bridged between the two macrocycle components. This conformation is facilitated by the rotary flexibility of the 2,7-substituted naphthalene moiety in the axle, allowing the rotaxane to fold around the anion. The change in perturbation direction of protons *5* and *e* following addition of the second equivalent of oxodianion is consistent with a change of stoichiometry from a 1:1 to 1:2 stoichiometric host–guest complex, where the binding of the second equivalent of sulfate causes the rotaxane to adopt a more open conformation with one anion associated with each macrocycle. This conformation is expected to be more favourable for the 1:2 stoichiometric complex because it maximises the inter-anion distances and thus minimises unfavourable intramolecular anion–anion electrostatic interactions. Importantly, the internal cavity protons *3* and *c* continue to shift upfield and downfield respectively as further equivalents of sulfate are added, indicating that the anions remain associated with the rotaxane's interlocked cavities.

Due to the apparent strong binding of sulfate in 1:1 $CDCl_3/CD_3OD$, quantitative anion binding data were determined in the more competitive organic–aqueous solvent mixture of 45:45:10 $CDCl_3/CD_3OD/D_2O$. The signals in the ^1H NMR spectra for cavity protons *3 (*axle internal pyridinium) and *c* (macrocycle internal isophthalamide) were perturbed by the binding of anion guests and were monitored as a function of anion concentration (Figure 2.10).

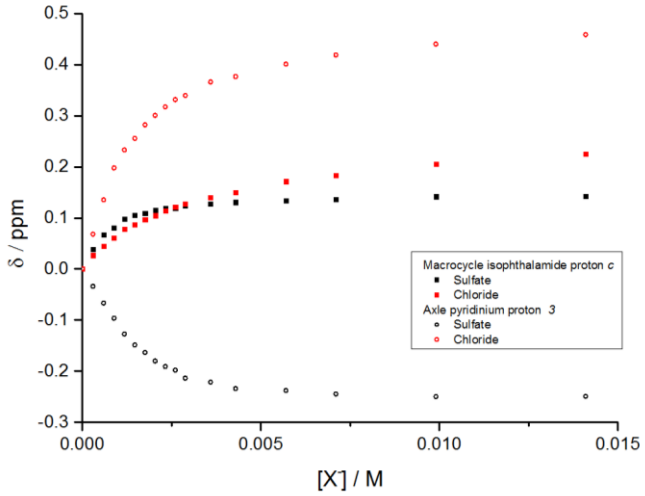

Figure 2.10 Plots of change in chemical shift for protons *c* and *3* upon addition of chloride and sulfate to [3]rotaxane **1·(PF$_6$)$_2$** (45:45:10 $CDCl_3/CD_3OD/D_2O$, 298 K).

Downfield perturbations were observed for macrocycle isophthalamide proton *c* upon addition of both chloride and sulfate, and for internal pyridinium axle proton *3* upon chloride binding, indicative of hydrogen bonding of the halide anion guest within the interlocked cavity.[§] In contrast, upon addition of sulfate, macrocycle isophthalamide proton *c* was perturbed upfield, which is consistent with the proposed formation of the 1:1 stoichiometric sandwich complex, in which the SO_4^{2-} anion bridges the two macrocycle components and associates at the periphery of each interlocked cavity. Addition of bromide to **1·(PF$_6$)$_2$** also resulted in downfield perturbation of protons *c* and *3*, indicative of binding of the larger halide

[§] Previous crystal structures and molecular modelling studies of related rotaxane and catenane host systems which possess similar binding cavity dimensions and hydrogen bond donor functionality, indicate that halide anions bind within the interlocked cavity. In contrast, oxoanions such as dihydrogen phosphate and acetate bind more weakly, which is believed to be due to poor complementarity with the binding domain resulting in weak association on the periphery.[1,3]

anion within the interlocked binding cavity, whilst AcO^-, BF_4^-, HSO_4^-, ClO_4^-, $H_2PO_4^-$ caused no measurable change to the spectra, indicating that these anions are not bound in this aqueous solvent mixture.

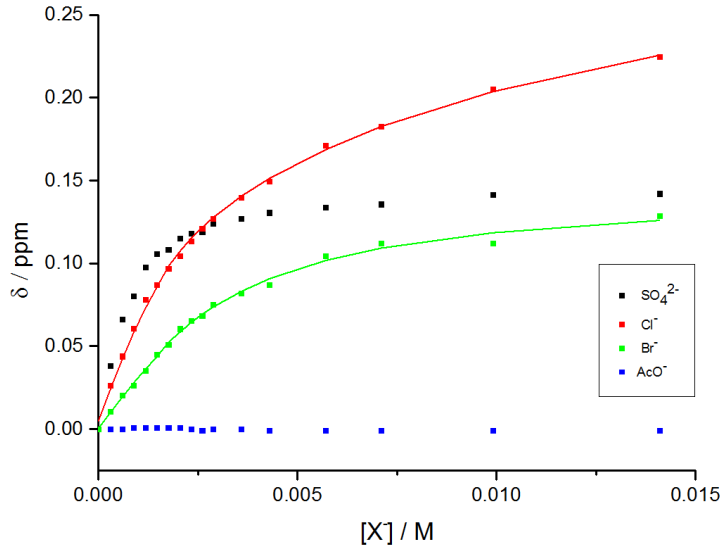

Figure 2.11 Plots of chemical shift change against anion concentration in 45:45:10 $CDCl_3/CD_3OD/D_2O$ for macrocycle proton *c* of rotaxane **1·(PF$_6$)$_2$**. Actual data represented by solid symbols, calculated 1:2 host–guest binding isotherms represented by solid lines. $T = 298$ K.

WinEQNMR2[26] analysis of the titration data, monitoring the chemical shift of macrocycle isophthalamide proton c (Figure 2.11), determined the anion association constants shown in Table 2.1. The binding isotherms for the halides were consistent with the formation of a 1:2 stoichiometric host–guest complex.

Table 2.1 Anion association constants of rotaxane **1·(PF$_6$)$_2$** and axle **12·(PF$_6$)$_2$** in 45:45:10 $CDCl_3/CD_3OD/D_2O$

Anion [a]	[3]Rotaxane **1·(PF$_6$)$_2$**		Axle **12·(PF$_6$)$_2$**	
	K_1 [M^{-1}]	K_2 [M^{-1}]	K_1 [M^{-1}]	K_2 [M^{-1}]
Cl^-	3.0×10^3	1.2×10^2	1.5×10^3	6.0×10^1
Br^-	3.7×10^3	2.7×10^2	- [c]	- [c]
SO_4^{2-}	$>10^4$	- [b]	$>10^4$	- [b]

[a] Anions added as TBA salts. $T = 298$ K. Anion association constants calculated using winEQNMR2[26] and chemical shift data of the macrocycle isophthalamide proton *c* (estimated errors <10 %). [b] No evidence of 2:1 binding. [c] Not determined. Shifts were too small to infer a binding event for AcO^-, BF_4^-, HSO_4^-, ClO_4^- and $H_2PO_4^-$.

The ratio of K_1/K_2 suggests binding of the first anion inhibits the binding of the second, which can be attributed to unfavourable intramolecular anion–anion electrostatic interactions. It is noteworthy that upon sulfate binding in this competitive organic–aqueous solvent mixture there is no evidence of a change in the perturbation direction of any of the proton signals, suggesting that there is no switch in stoichiometry from 1:1 to 2:1 binding as was observed in the less competitive 1:1 $CDCl_3/CD_3OD$ solvent mixture. Indeed, the binding isotherm was consistent with the formation of a 1:1 host–guest stoichiometric complex, indicating that in this more competitive solvent mixture K_2 for the divalent sulfate anion is negligible. Importantly, the rotaxane exhibits an excellent selectivity for binding sulfate over the halides, and a modest selectivity for Br^- over Cl^-, which is presumably due, in part, to the larger halide being less heavily solvated.

Analogous titrations with chloride and sulfate were conducted in 45:45:10 $CDCl_3/CD_3OD/D_2O$ with the non-interlocked axle component **12·(PF$_6$)$_2$**, prepared from the chloride salt by washing a chloroform solution with 1M aqueous ammonium hexafluorophosphate solution. Chloride was bound more weakly than with the rotaxane, demonstrating the role of the interlocked binding cavities in enhancing the anion association (Table 2.1). Sulfate was bound strongly ($K_a > 10^4$ M^{-1}), however poor solubility of both the rotaxane and axle prevented comparison of association constants in a more competitive solvent media containing a higher percentage of water.

2.2.2.2 Optical anion sensing studies

The anion sensing capability of [3]rotaxane **1·(PF$_6$)$_2$** was investigated using fluorescence spectroscopy. The rotaxane (1×10^{-5} M solution in chloroform) exhibited a broad emission band following excitation at 263 nm, with two maxima observed at $\lambda = 410$ and 432 nm which were attributed to the monomer emission of the integrated naphthalene moiety of the axle component (Figure 2.12).[**] Addition of increasing quantities of the anions Cl^-, Br^- and AcO^- to a chloroform solution of rotaxane **1·(PF$_6$)$_2$** revealed in all three cases a small blue-shift of the two maxima, concomitant with a modest increase in the fluorescence intensity, of up to 15% enhancement with Cl^- (Figure 2.12), 7% with Br^- and 4% with AcO^-.

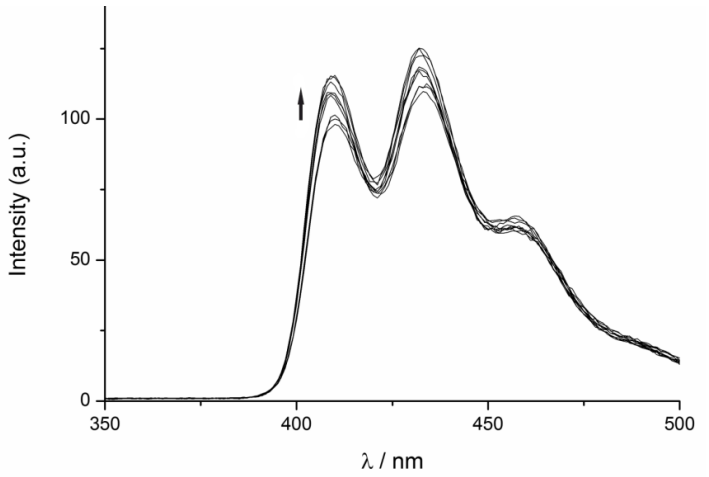

Figure 2.12 Changes in the emission spectrum of [3]rotaxane **1·(PF$_6$)$_2$** (1×10^{-5} M, $CHCl_3$, 298 K) upon addition of increasing amounts of TBACl.

In contrast, addition of sulfate to **1·(PF$_6$)$_2$** in chloroform solution led to a 3 nm blue shift in the naphthalene emission and a dramatic quenching of the fluorescence intensity (Figure 2.13a), with the minimum intensity occurring after the addition of four equivalents of anion. Addition of further equivalents of the oxodianion led to restoration of the emission, and eventual enhancement of the fluorescence intensity, peaking at a maximum of 15% increase on the initial value after addition of 15 equivalents of anion (Figure 2.12).

[**] The TBA salts of the anions were dissolved in a 1×10^{-5} M solution of rotaxane in $CHCl_3$, and added to a fluorescence cuvette containing a 1×10^{-5} M $CHCl_3$ solution of the rotaxane. This ensured that the total rotaxane host concentration remained constant throughout the titration, and thus emission intensity changes were reasonably attributed to anion complexation and not dilution effects

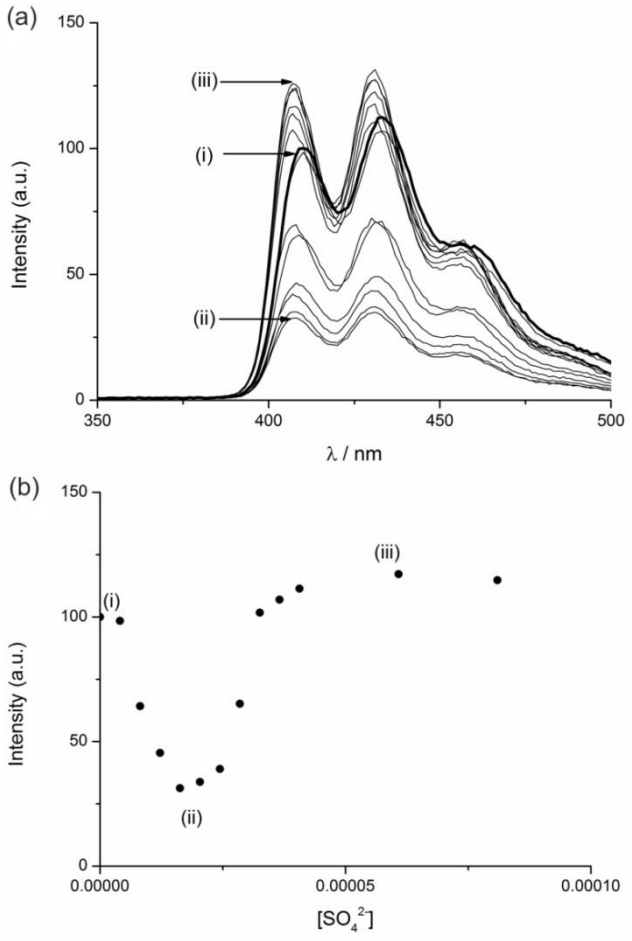

Figure 2.13 Changes in the emission spectrum of [3]rotaxane **1·(PF$_6$)$_2$** (1×10^{-5} M, $CHCl_3$, 298 K) upon addition of increasing amounts of TBA_2SO_4: (a) (i) non-complexed rotaxane (bold); (ii) 1:1 host–guest complex; (iii) 1:2 host–guest complex. (b) Change in emission intensity at 410 nm with increasing [SO_4^{2-}].

These observations can be rationalised with the binding process proposed in Scheme 2.8, which is consistent with that proposed on the basis of the NMR titration results (**Scheme 2.7**). Initially the 1:1 stoichiometric complex with sulfate is formed, in which the sulfate guest is bridged between the two macrocycles, and held in close proximity to the naphthalene unit, leading to a quenching of the fluorescence. Further addition of sulfate results in the rotaxane changing conformation in order to bind a second anion, with the effect that sulfate is no longer bound in the vicinity of the naphthalene motif and so a restoration of the fluorescence intensity is observed. Given that the naphthalene reporter group is not conjugated with the isophthalamide and 3,5-bis-amide pyridinium anion receptor motifs, such a quenching phenomenon may be tentatively attributed to a through-space photo-induced electron transfer (PET) process between the anion-receptor complex and the naphthalene excited state. Anion

binding enhances the PET process by modulating the reduction potential of the receptor motif, leading to a switching off of the emission.[††] The 2:1 complex presumably does not adopt a geometry that facilitates efficient PET quenching, and so in contrast, a fluorescence enhancement is observed for the of all four anion guests, which may be attributed to increased rigidity of the system that reduces the efficiency of the vibrational relaxation pathway of the naphthalene excited state.[28] As such, by exploiting the unique anion-induced conformational changes exhibited by the novel [3]rotaxane host structure, a selective optical response signalling the binding of sulfate has been obtained. Indeed, exploiting such guest-induced geometrical changes within receptors may prove to be a more general method for obtaining selective supramolecular sensors.

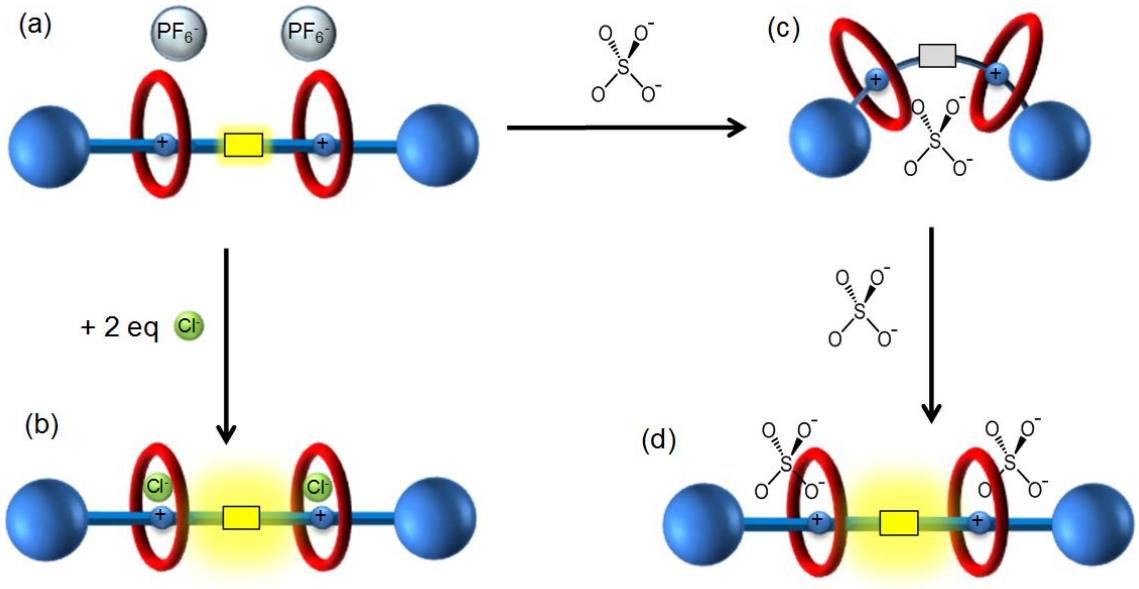

Scheme 2.8 Schematic representation of anion binding by [3]rotaxane **1·(PF$_6$)$_2$**: (a) emissive unbound host; (b) enhanced emission in the 2:1 stoichiometric mono-charged anion/host complex; (c) quenched emission in the 1:1 stoichiometric sandwich complex with sulfate; (d) enhanced emission in the 2:1 stoichiometric complex with sulfate

[††]Gunnlaugson and co-workers have reported various hydrogen bonding anion receptors in which anion binding results in quenching of the aromatic fluorophore excited state by a PET quenching mechanism.[27] Such a mechanism would appear to be consistent with the results presented here: fluorescence quenching is observed in the 1:1 complex with sulfate, in which the geometry is presumably optimal for a PET quenching process of the naphthalene excited state by the anion-receptor complex.

2.3 Nitrate anion templated assembly of interlocked host molecules for selective nitrate recognition in aqueous solvent media[‡‡]

2.3.1 Nitrate recognition

It was demonstrated in the first half of this chapter that the sulfate anion was recognised selectively by a dicationic [3]rotaxane host, with excellent selectivity over the halides and mono-anionic oxoanions in terms of both strong anion association and the optical output of the sensor. It could be argued, however, that achieving selective recognition of one mono-charged oxoanion over another is a much greater challenge, which necessitates the careful design of a highly complementary receptor in order to achieve discrimination on the basis of the target anion geometry.

The nitrate anion is a species of significant importance in environmental and medical contexts, and so it is surprising that little attention has been paid to its selective binding by synthetic anion receptors. As alluded to in Chapter 1, the over-use of nitrate in fertilisers has led to the eutrophication of natural water courses, and increased nitrate levels have been implicated in the formation of carcinogenic nitrosamines and cause methemoglobinemia (blue-baby syndrome) in infants. The design of nitrate receptors is particularly challenging, however, due to a combination of high hydration energy ($\Delta G_{hyd} = -300$ kJ mol^{-1}) and low basicity of the anion (conjugate acid p$K_a = -1.4$), which results in a low affinity for hydrogen bonds.[29]

[‡‡] Some of the work in the remainder of this chapter was conducted in collaboration with Part II undergraduate student Lucy Duckworth, and published as two communications in the journal *Chemical Communications:*
M. J. Langton, L. C. Duckworth and P. D. Beer, *Chem. Commun.,* 2013, **49**, 8608–8610 and
M. J. Langton and P. D .Beer, *Chem. Commun.,* 2014, **50**, 8124–8127

The trigonal planar geometry of the nitrate anion has been exploited in the design of a handful of tripodal, macrocyclic and cage-like host systems, in which the hydrogen bond donors are arranged in a complementary trigonal geometric arrangement (Figure 2.14).[30–36]

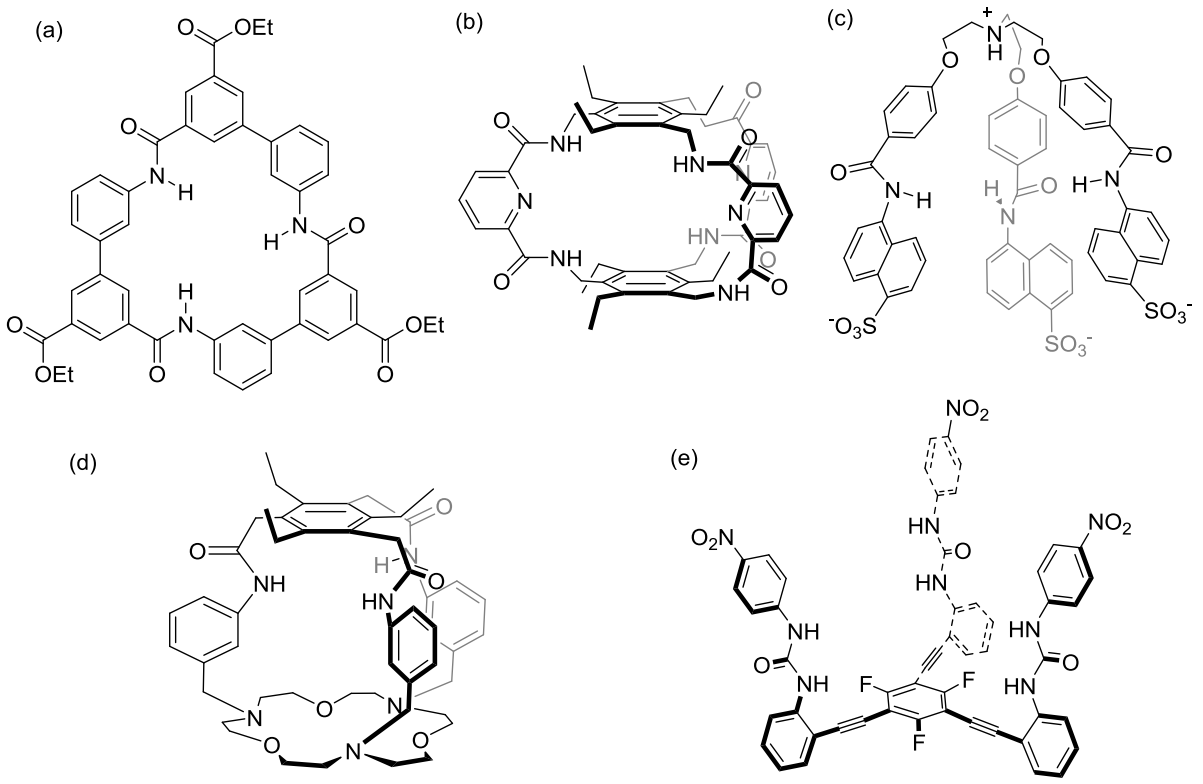

Figure 2.14 Examples of hydrogen bonding nitrate receptors: (a) Hamilton's tri-amide macrocycle,[31] (b) Anslyn's bucyclic cyclophane,[30] (c) Singh's fluorescent nitrate sensor,[34] (d) Romański's heteroditopic receptor[35] and (e) Johnson and Haley's tripodal urea receptor[36]

For example, Hamilton has synthesised a tridentate macrocycle (Figure 2.14a) that recognises nitrate in 98:2 $CDCl_3/d_6$-DMSO ($K_a = 4.6 \times 10^5$ M^{-1}),[31] whilst Anslyn has reported a bicyclic cyclophane receptor with six converging amide hydrogen bonds (Figure 2.14b), which binds nitrate selectively over halide anions ($K_a = 300$ M^{-1} in 3:1 CD_3CN/CD_2Cl_2), however, the more basic acetate anion was found to bind more strongly ($K_a = 770$ M^{-1}).[30] Singh has designed a tripodal C_3 symmetric tri-amide receptor with appended fluorescent dansyl groups (Figure 2.14c**)**:[34] nitrate binding in d_6-DMSO solution ($K_a = 550$ M^{-1}) is reported by quenching of the emission from the dansyl fluorophores. A macrotricyclic heteroditopic receptor has been synthesised by Romański and Piątek (Figure 2.14d**),** which incorporates a triaza-18-crown-6

motif cation binding site and a tripodal 1,3,5-tris-amide-benzene capping group to bind nitrate through three convergent hydrogen bonds in d_6-DMSO solution ($K_a = 280$ M^{-1}).[35] Ammonium cation binding within the crown-6 motif results in a significant enhancement in the nitrate binding affinity due to strong ion-pairing within the host ($K_a = 1050$ M^{-1}). Very recently, Johnson and Haley have shown that a tripodal urea architecture can recognise nitrate anions in 9:1 $CDCl_3/d_6$-DMSO ($K_a = 24\ 000$ M^{-1}), through six hydrogen bonds, with a postulated contribution from anion–π interactions (Figure 2.14e).[36]

At the commencement of the work conducted in the following section, Romański's heteroditopic receptor exhibits the strongest binding affinity reported for nitrate recognition in a competitive polar–organic solvent. High levels of nitrate selectivity, however, have yet to be achieved, whilst the recognition of nitrate in aqueous media by synthetic organic host molecules remains elusive.

2.3.2 Design strategy for the preparation of a nitrate-selective rotaxane host

It has been shown previously that mechanically interlocked molecules, such as rotaxanes and catenanes, can be prepared by anion templation (*vide supra*), and that the resulting host molecules can encapsulate halide anion guests with a high degree of selectivity for the templating anion, through convergent hydrogen or halogen bonding interactions.[37] Such structures, however, bound oxoanions with very low affinity as a result of the three-dimensionally restrained binding cavity being too small to encapsulate the larger oxoanion guest species. It was anticipated that, in principle, interlocked hosts could be designed to be selective for the nitrate anion, if the individual components were carefully conceived such that the binding domain formed between the interlocked components was of the optimum geometry for binding of the trigonal nitrate anion. Indeed, such a host system could also be prepared using an unprecedented nitrate templating strategy, to afford an interlocked host that was selective for the templating nitrate anion.

During the course of a crystallographic investigation into the structures of triazole- and amide-containing anion templated pseudorotaxanes, Dr Nick White, at the time a DPhil student in the group, crystallised a range of pseudorotaxanes consisting of a simple 3,5-bis-amide pyridinium thread $\mathbf{18}^+$ and an isophthalamide-containing macrocycle **19** with a range of anions (Cl^-, Br^-, I^-, AcO^-, NO_3^-, HSO_4^- and BzO^-).[38] It was demonstrated that all of the anions investigated in qualitative ^1H NMR pseudorotaxane assembly experiments templated pseudorotaxane formation to some extent in d_6-acetone solution. This was surprising given that the corresponding rotaxane and catenane hosts are selective for halides, whilst binding the larger oxoanions with very low affinity. Presumably, the interpenetrated assemblies are more accommodating of a range of anion geometries than the analogous interlocked structures, and the oxoanion is able to perch out of the plane of the macrocycle, with the oxygen atoms pointing into the cavity. Unfortunately, quantitative comparison of the

templating ability of the anions could not be obtained due to poor solubility of the 3,5-bis-amide pyridinium threading components. The crystal structure of the nitrate salt of pseudorotaxane **18·19**$^{+}$ is shown in Figure 2.15: the bis-amide hydrogen bond donor motifs incorporated within the thread and macrocycle components form hydrogen bonds to two of the nitrate anion's oxygen atoms, whilst the third oxygen is non-coordinating.

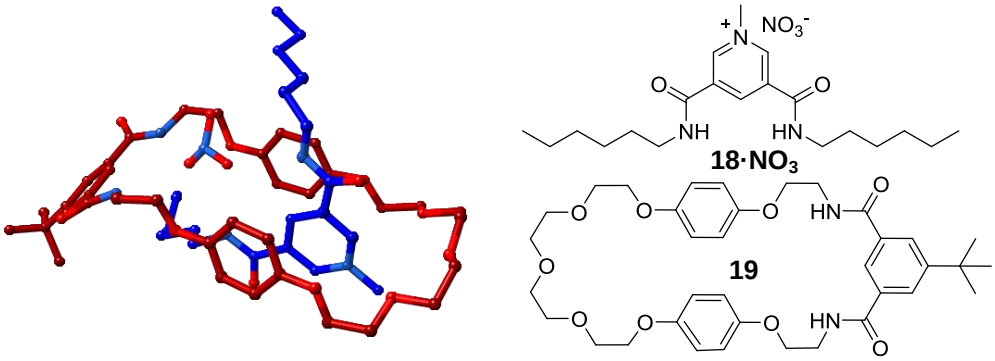

Figure 2.15 Solid state structure of pseudorotaxane **18·19·NO$_3$**.[38] Solvent molecules and most hydrogen atoms omitted for clarity.

This structure inspired the development of a strategy to prepare a nitrate selective rotaxane: it was envisaged that a complementary threading component could be designed to contain *two* hydrogen bond donor sites for coordinating to two of the oxygen atoms of the nitrate anion (Figure 2.16). The remaining oxygen atom would be free to accept hydrogen bonds from a suitable donor motif that is integrated into a macrocycle component, thus fulfilling the maximum tri-dentate coordination of the oxoanion, and facilitate the trigonal nitrate anion templated assembly of a rotaxane.

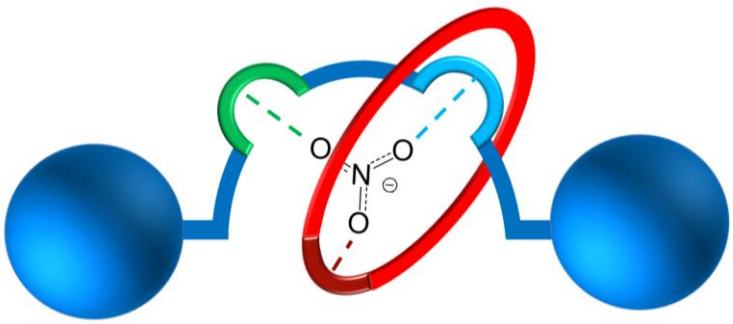

Figure 2.16 Schematic representation of a nitrate templated [2]rotaxane, with two hydrogen-bonding recognition sites in the axle (blue and green) and one in the macrocycle (red), forming a complementary binding site for the trigonal nitrate anion between the interlocked components.

2.3.3 Nitrate templated pseudorotaxane assembly

2.3.3.1 Design and synthesis of pseudorotaxane components

The utilisation of nitrate as a pseudorotaxane templating anion with bidentate threading components was investigated initially. To this end two novel bidentate hydrogen bonding threading motifs were devised: the mono-cationic asymmetric isophthalamide-3,5-bis-amide pyridinium thread **20·PF$_6$** and the symmetric dicationic 3,5-bis-amide pyridinium thread **21·(PF$_6$)$_2$**, both terminated with non-interacting hexyl chains (Figure 2.17). The macrocycle component **19** for this investigation has previously been utilised for pseudorotaxane assembly studies,[39] and features an isophthalamide motif to coordinate to the nitrate anion *via* hydrogen bonds, and is functionalised with a *tert*-butyl group to enhance solubility. Hydroquinone groups provide secondary stabilisation of the pseudorotaxane assembly through aromatic donor–acceptor interactions with the electron-deficient pyridinium moieties in the threading components. Further stabilisation may arise from CH···O hydrogen bonding between the thread pyridinium *N*-methyl group and the macrocycle polyether linkage.

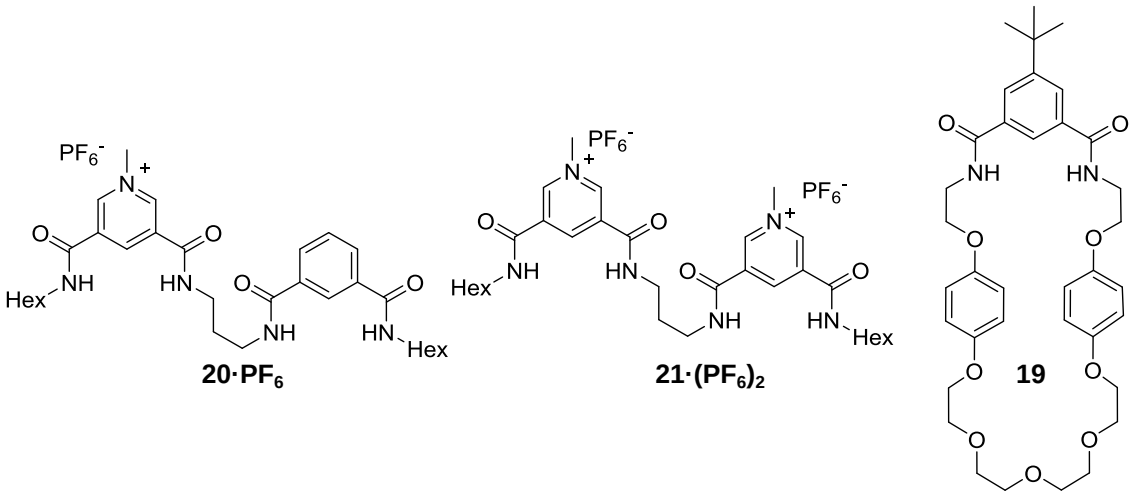

Figure 2.17 Target thread components and macrocycle for nitrate templated pseudorotaxane assembly studies.

The multistep synthetic procedure for the synthesis of the asymmetric thread component **20·PF$_6$** is shown in Scheme 2.9 and Scheme 2.10. Pyridine mono-ester **5**,[22] and isophthalate-derived mono-ester **24**, prepared from the commercially available 3,5-dimethyl isophthalate

by KOH-mediated mono-hydrolysis,[40] were activated to the respective acid chlorides by the use of oxalyl chloride and subsequently condensed with hexylamine to afford compounds **22** and **25**. Selective hydrolysis with KOH in methanol solution afforded the asymmetric acids **23**[41] and **26**, which form the essential precursors for the target threading components.

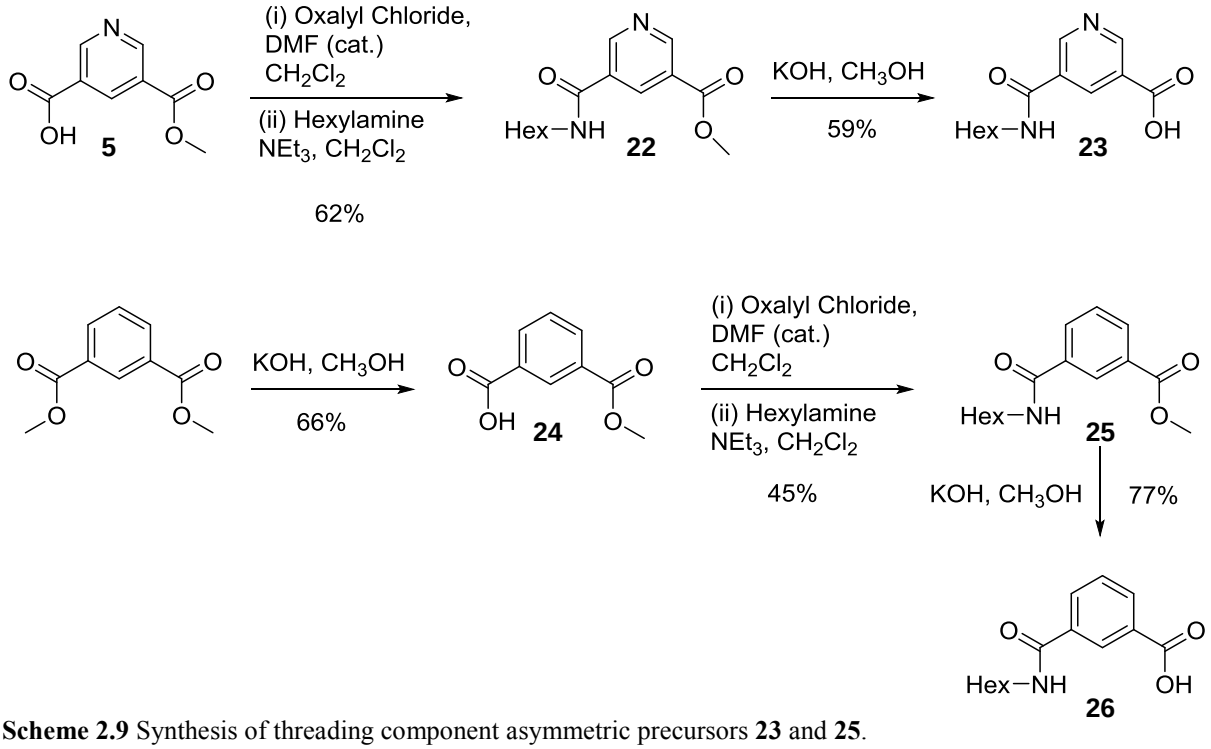

Scheme 2.9 Synthesis of threading component asymmetric precursors **23** and **25**.

To synthesise the asymmetric threading component **20·PF$_6$**, it was necessary to mono-protect the core 1,3-diaminopropane moiety, which was achieved by reaction with di-*tert*-butyl bicarbonate (Boc_2O) to form amine **27** in 43% yield (Scheme 2.10).[42] EDC-mediated amide coupling of amine **27** with pyridine mono-acid **23** afforded Boc-protected amine **28** in 60% yield, which was subsequently deprotected using trifluoroacetic acid (TFA) to afford **29·CF$_3$CO$_2$**.

Initial attempts to form thread intermediate **30** involved the condensation of the acid chloride of **25** with **29·CF$_3$CO$_2$** in a basic DMF/CH_2Cl_2 solution. Analysis of the crude reaction mixture by both ^{1}H NMR and mass spectrometry, however, revealed no evidence of the desired product. An EDC-mediated amide coupling approach proved more successful, by

stirring a suspension of acid **25** with EDC·HCl in CH_2Cl_2, before subsequent addition of a solution of **29·CF_3CO_2** in DMF, in addition to catalytic 4-(dimethylamino)pyridine (DMAP) and 1-hydroxybenzotriazole hydrate (HOBt), which acts as a nucleophilic catalyst and minimises the rearrangement of EDC intermediates to urea by-products. Thread intermediate **30** was isolated in 54% yield following purification by silica gel column chromatography. Methylation using CH_3I in DMF afforded **20·I**, which was converted to the hexafluorophosphate salt by washing with $NH_4PF_{6(aq)}$ to give **20·PF_6** in a 77% yield.

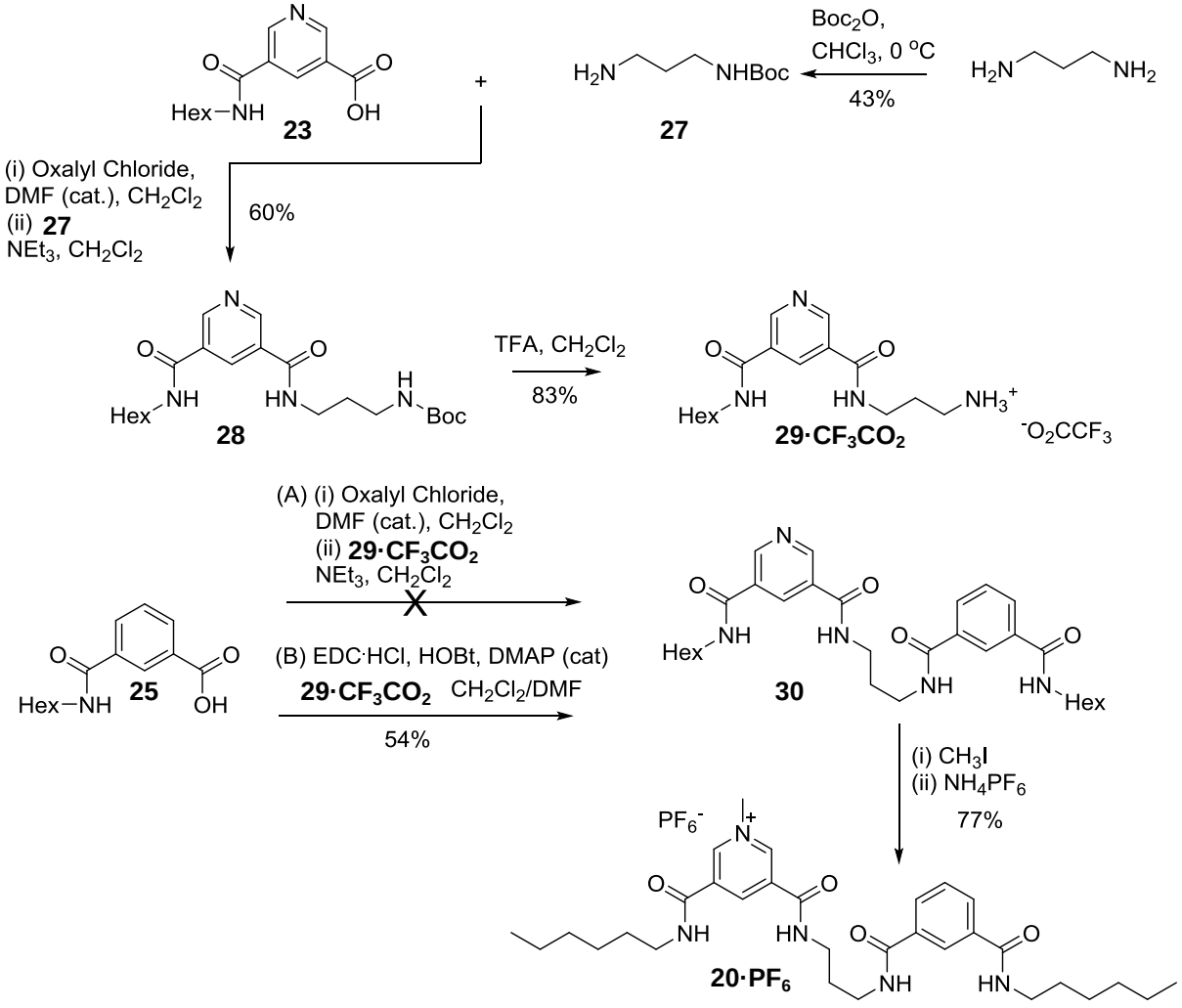

Scheme 2.10 Synthesis of thread **20·PF_6**.

The synthesis of the symmetrical thread intermediate **21·$(PF_6)_2$** was attempted initially by reaction of two equivalents of the acid chloride form of **23** and 1,3-diaminopropane in CH_2Cl_2 solution, but no product was detected by either ^{1}H NMR or mass spectrometry (Scheme 2.11).

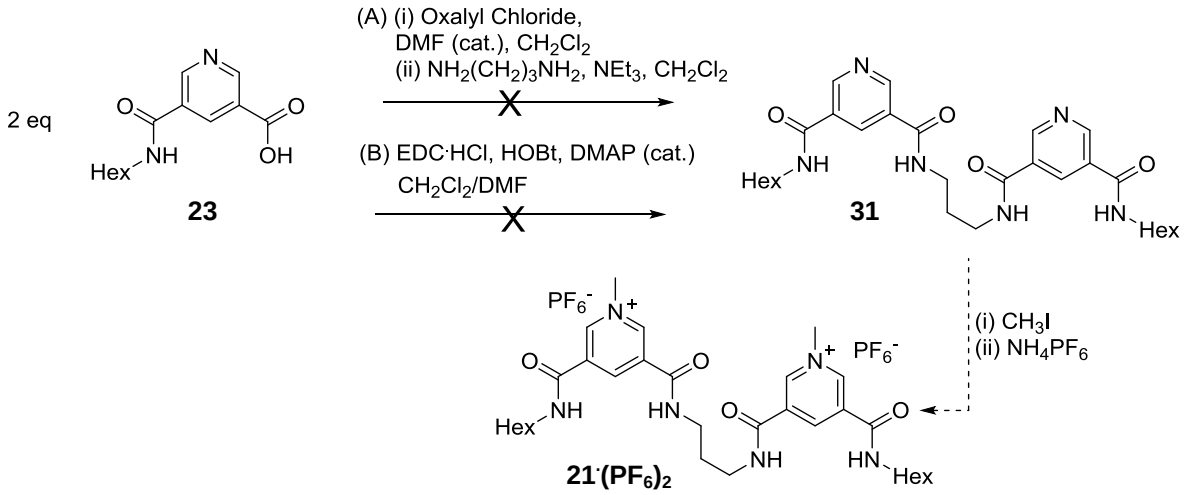

Scheme 2.11 Attempted synthesis of symmetric thread $\mathbf{21\cdot(PF_6)_2}$.

As an alternative route, the reaction of 1,3-diaminopropane with two equivalents of pyridine mono-acid **23** using EDC-mediated amide coupling in DMF was also attempted, however the formation of a precipitate which was insoluble in all common solvents prevented further characterisation.

The final component required for the nitrate-templated pseudorotaxane assembly studies, macrocycle **19**, was prepared as shown in Scheme 2.12, by the condensation of bis-amine **16** with the corresponding acid chloride of 5-(*tert*-butyl)isophthalic acid in the presence of pyridinium chloride template **18** (kindly donated by Dr Jim Mercurio).[25]

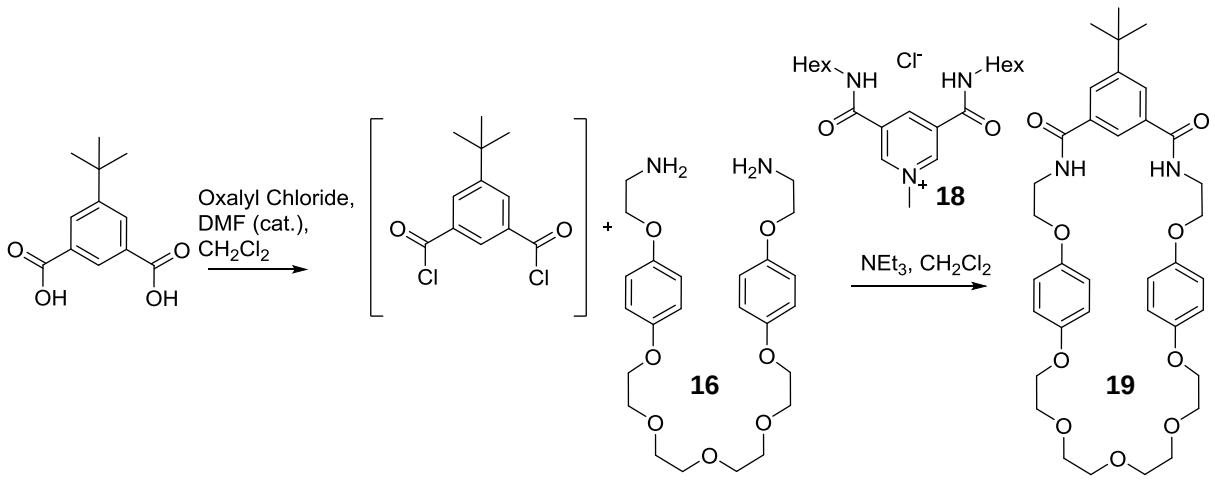

Scheme 2.12 Synthesis of macrocycle **19**.[25]

2.3.3.2 Pseudorotaxane assembly studies

With the asymmetric thread component **20·PF$_6$** and macrocycle **19** in hand, initial qualitative ^{1}H NMR pseudorotaxane assembly studies were conducted in d_6-acetone (Scheme 2.13).

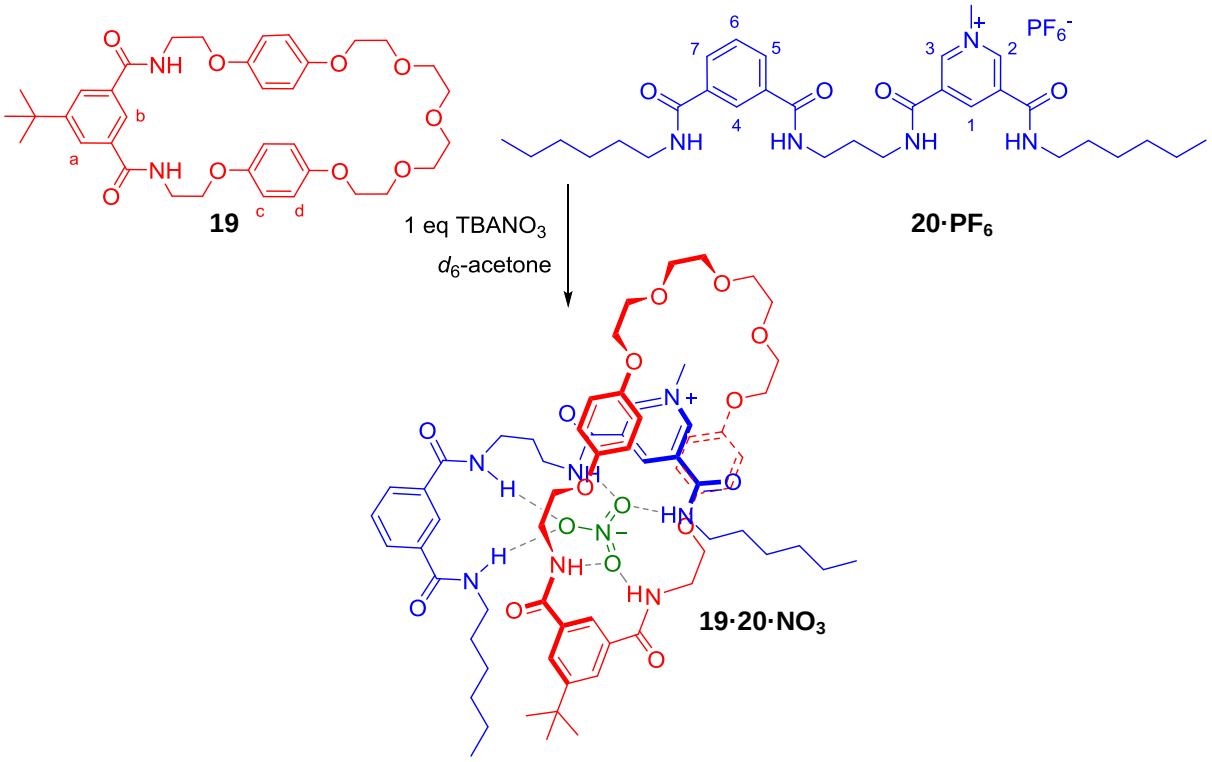

Scheme 2.13 Assembly of nitrate templated pseudorotaxane **19·20·NO$_3$**.

Addition of one equivalent of tetrabutylammonium nitrate to an acetone solution of macrocycle **19** resulted in downfield perturbation of the isophthalamide internal proton *b* and amide protons, indicative of binding of the oxoanion within the bis-amide binding cleft (Figure 2.18). Upon addition of one equivalent of thread **20·PF$_6$**, downfield shifts of the thread protons *1* and *4*, in addition to the amide protons, were observed which is indicative anion complexation. This demonstrates that both the isophthalamide and the 3,5-bis-amide pyridinium moieties of the thread component are involved in hydrogen bonding to the nitrate anion, which in turn remains hydrogen bonded to the isophthalamide motif of the macrocycle. Importantly, the macrocycle hydroquinone protons *c* and *d* undergo upfield perturbation and increased splitting, which is characteristic of aromatic donor–acceptor interactions between

the electron rich hydroquinone groups of the macrocycle and the electron deficient pyridinium motif of the thread, and confirms the formation of pseudorotaxane **19·20·NO$_3$** (Scheme 2.13).

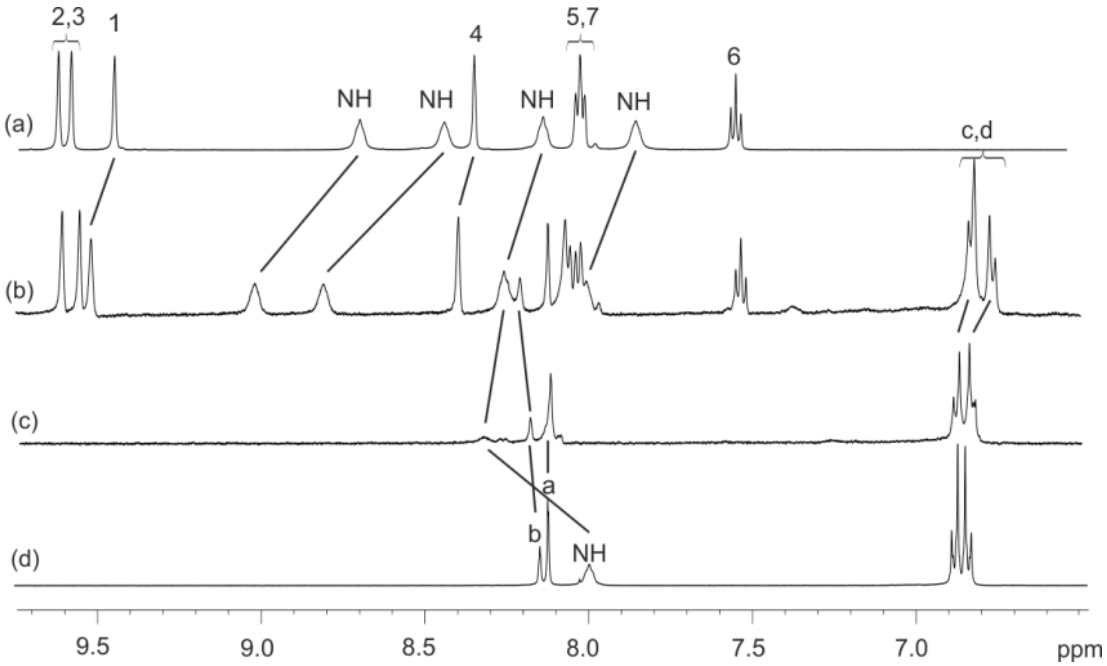

Figure 2.18 ^{1}H NMR spectra of (a) thread **20·PF$_6$**, (b) **19·20·PF$_6$**, (c) macrocycle **19** + 1 eq. TBANO$_3$ and (d) macrocycle **19** in d_6-acetone (500 MHz, 298 K). For atom labels see Scheme 2.13.

The crucial role of the nitrate anion in templating the formation of the interpenetrative assembly was established by a conducting a ^{1}H NMR pseudorotaxane titration experiment in which one equivalent of thread **20PF$_6$** was added to a d_6-acetone solution of macrocycle **19** in the absence of the nitrate anion. No perturbations of the thread or macrocycle protons were observed, which indicates a lack of pseudorotaxane formation in the absence of the nitrate anion, and conclusively demonstrates the pivotal templating role of the nitrate anion in the formation of the interpenetrative assembly.

2.3.4 Nitrate templated synthesis of a [2]rotaxane

The successful formation of the nitrate templated pseudorotaxane assembly **19·20·NO$_3$** suggested that the synthesis of a [2]rotaxane would be possible using nitrate templation *via* a stoppering strategy in a non-competitive solvent (Scheme 2.14).

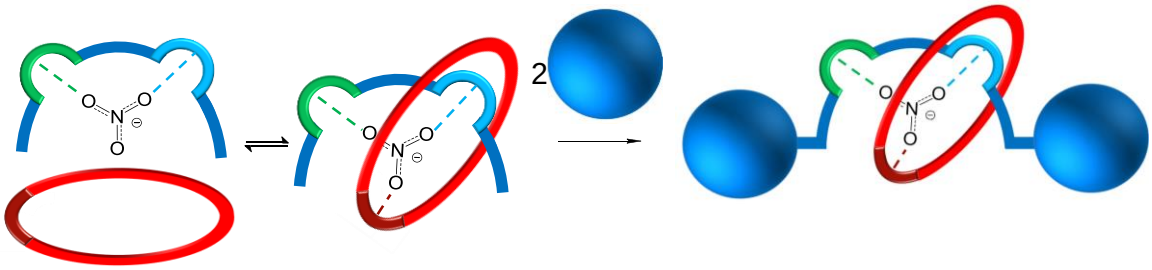

Scheme 2.14 Schematic representation of the nitrate templated synthesis of a [2]rotaxane *via* stoppering of a pseudorotaxane assembly.

To this end an azide-terminated axle precursor **32·NO$_3$** (Figure 2.20) was synthesised, in preparation for a copper(I)-catalysed azide–alkyne (CuAAC) click stoppering rotaxanation strategy[43] with a suitably alkyne-functionalised stopper component. This CuAAC methodology has been used in the preparation of a wide range of organic molecules that incorporate heteroatom linkages, including many examples of interlocked molecules.[44]

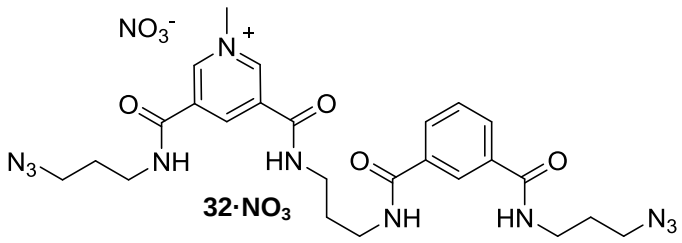

Figure 2.19 Target axle precursor component **32·NO$_3$**.

2.3.4.1 Synthesis and characterisation of nitrate templated [2]rotaxane

The multistep synthetic procedure for the synthesis of the asymmetric thread component **32·NO$_3$** is shown in Scheme 2.15 and Scheme 2.16. Azides **33** and **34** were prepared from the mono-acid precursors **24** and **5** respectively, by reaction of 3-bromo-propylamino hydrobromide with the corresponding acid chloride. The crude products were reacted immediately with sodium azide in DMF at 70 ºC, to afford the desired azide products **33** and **34** following purification by silica gel column chromatography. Subsequent de-esterification with KOH in methanol solution afforded the asymmetric acids **35** and **36**. Using an analogous procedure to that employed in the synthesis of the asymmetric thread **20·PF$_6$**, the acid chloride of compound **36** was reacted with mono-Boc-protected amine **27** to yield compound **37** in 69% yield, which was subsequently deprotected using trifluoroacetic acid to give **38·CF$_3$CO$_2$**.

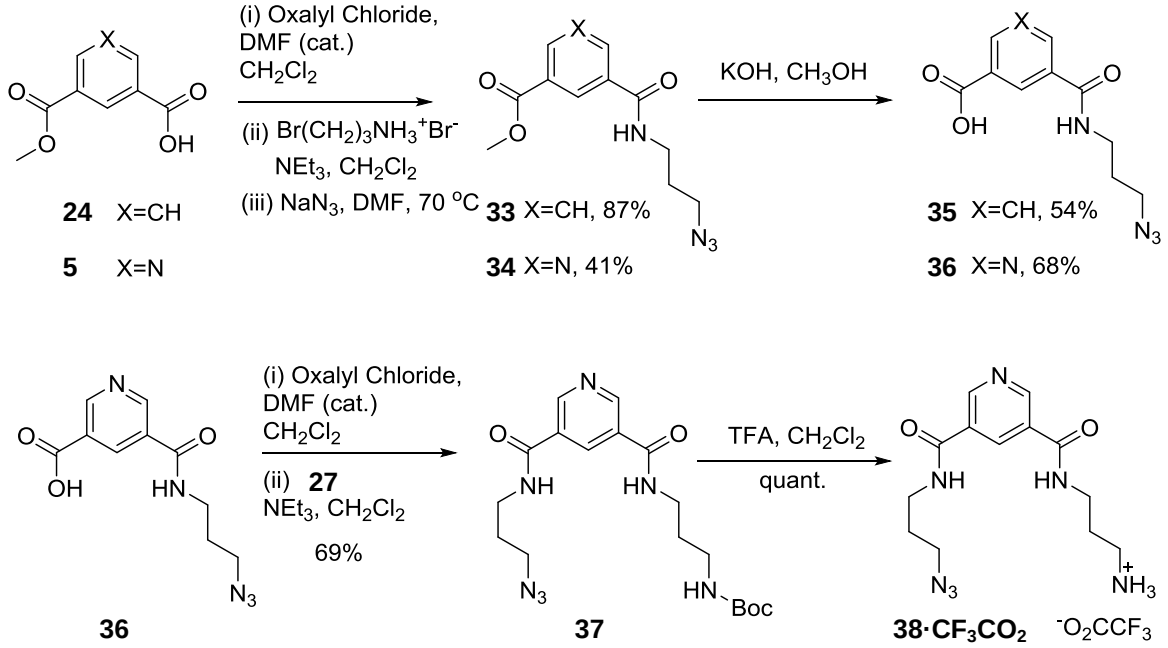

Scheme 2.15 Synthesis of asymmetric azide precursors **35** and **38·CF$_3$CO$_2$**.

The penultimate step in the synthesis of the target axle precursor **32·NO$_3$** involved the EDC-mediated amide coupling of acid **35** with **38·CF$_3$CO$_2$**, affording compound **39** in 38% yield, which was methylated using CH_3I to give axle precursor **32·I**. Anion exchange to the nitrate salt was achieved by passing down a nitrate-loaded Amberlite® column in 9:1 acetone/water to afford **32·NO$_3$**.

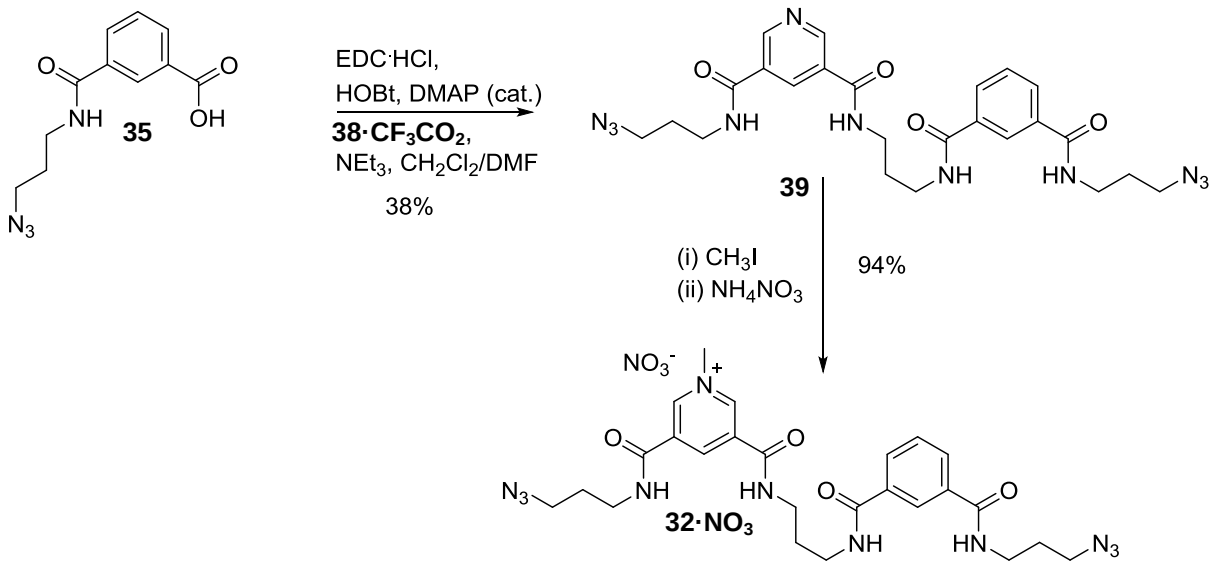

Scheme 2.16 Synthesis of axle precursor **32·NO$_3$**.

The final component required for the rotaxane synthesis was alkyne-functionalised terphenyl stopper **41**, which was prepared according to literature procedures as shown in Scheme 2.17.[45] Reaction of stopper-alcohol **40**, prepared by Dr Fabiola Zapata, with propargyl bromide in DMF at 80 ºC in the presence of K_2CO_3 afforded the desired alkyne-functionalised stopper **41**.[45]

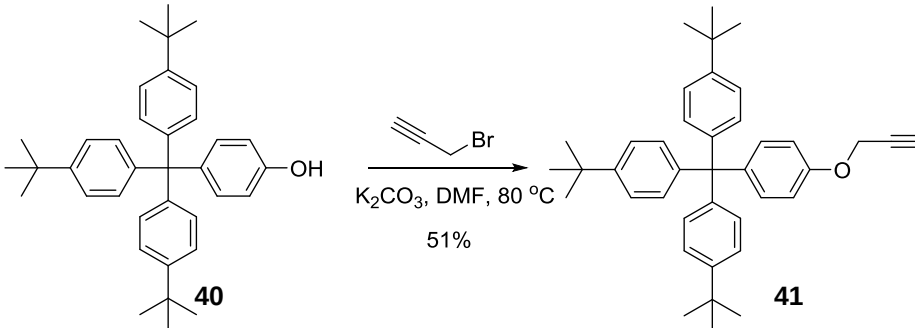

Scheme 2.17 Synthesis of alkyne stopper **41**.

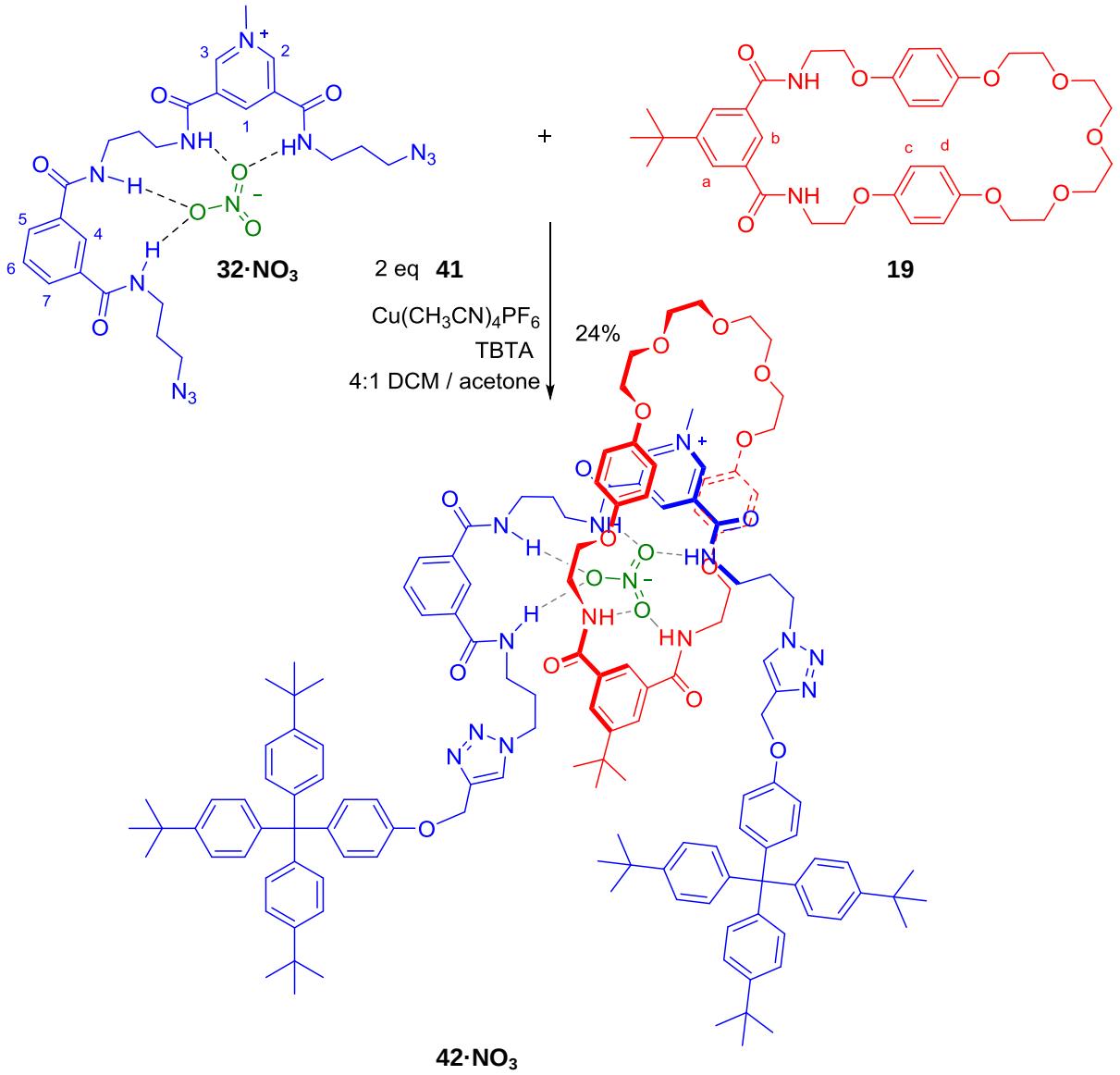

Scheme 2.18 Synthesis of rotaxane **42·NO$_3$** *via* nitrate templation.

The nitrate templated synthesis of rotaxane **42·NO$_3$** was achieved by mixing one equivalent of bis-azide functionalised axle precursor **32·NO$_3$** with 1.1 equiv. of macrocycle **19** in 4:1 CH_2Cl_2/acetone to form the initial pseudorotaxane assembly.[§§] Catalytic $Cu(CH_3CN)_4PF_6$, tris-(benzyltriazolylmethyl)amine (TBTA) and one equivalent of stopper alkyne **41** were then added, and the reaction mixture allowed to stir for one hour, to encourage the formation of a mono-stoppered axle precursor, which would further enhance the solubility of the pseudo-

[§§] Axle precursor **32·NO$_3$** was not sufficiently soluble in neat $CHCl_3$ to attempt rotaxane formation in this solvent, necessitating the addition of 20% acetone to enhance the solubility, at the expense of increasing the competitive nature of the solvent.

rotaxane. A further 1.2 equivalents of stopper alkyne **41** was then added and the reaction mixture allowed to stir for four days, to afford rotaxane **42·NO$_3$** (Scheme 2.18).[***]

Analysis of the ^{1}H NMR spectrum of the crude reaction mixture revealed that the rotaxane was formed in approximately 35% yield, the other products being non-interlocked macrocycle and axle components. Purification by size exclusion chromatography and silica gel chromatography gave rotaxane **42·NO$_3$** in an isolated yield of 24%, which was fully characterised by ^{1}H, ^{13}C and ^{1}H ROESY NMR, and HRMS. The ^{1}H NMR spectra of rotaxane **42·NO$_3$**, macrocycle **19** and axle precursor **32·NO$_3$** are compared in Figure 2.20.

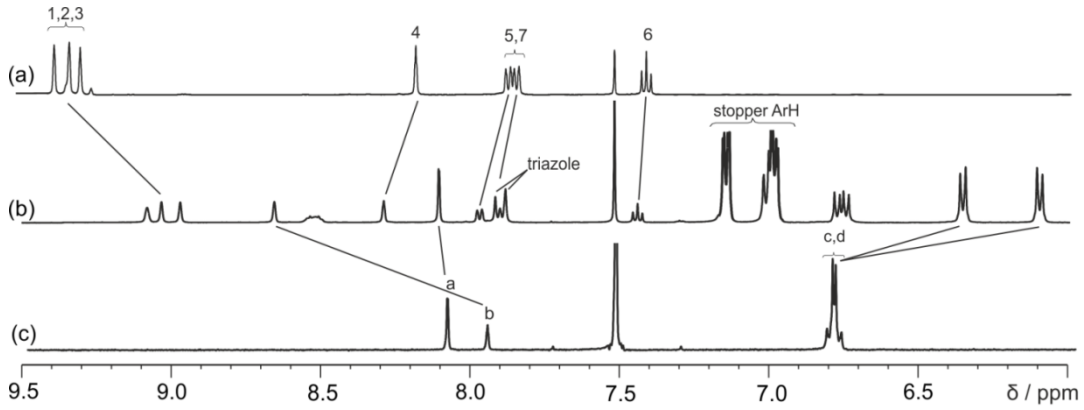

Figure 2.20 ^{1}H NMR spectra of (a) axle precursor **32·NO$_3$**, (b) rotaxane **42·NO$_3$** (c) macrocycle **19** in 1:1 $CDCl_3/CD_3OD$ (500 MHz, 298 K). For atom labels see Scheme 2.18.

Upfield perturbation of axle pyridinium proton *1*, and downfield shifts of axle isophthalamide proton *4* and macrocycle proton *b* are observed, due to hydrogen bonding interactions with the nitrate anion. Notably, the macrocycle hydroquinone protons *c* and *d* are split and shifted upfield, which is diagnostic of the aromatic donor–acceptor interactions between the macrocycle hydroquinone groups and the axle pyridinium motif. Further evidence for the interlocked nature of the rotaxane was obtained in the ^{1}H ROESY NMR spectrum, in which through-space interactions between the macrocycle hydroquinone protons *c* and *d* and axle protons *1*, *2*, *3* and *7* are observed (Figure 2.21).

[***] Initial attempts involved using diisopropylethylamine (DIPEA) as a base to enhance the rate of the reaction, but it was found to cause decomposition of the pyridinium motif and thus it was excluded from the reaction in subsequent attempts.

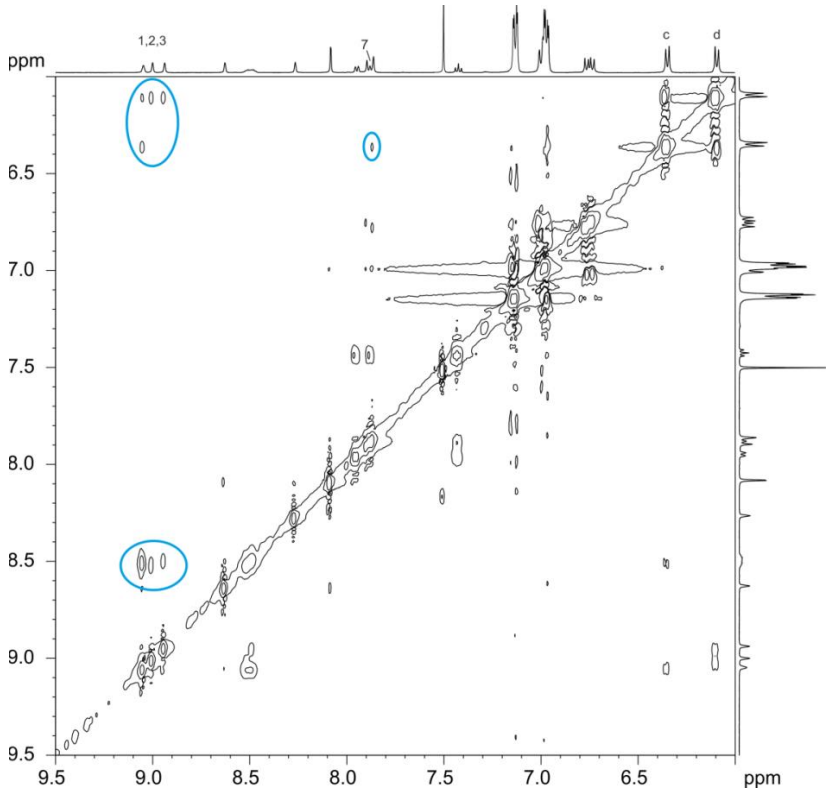

Figure 2.21 ^{1}H ROESY NMR spectrum of **42·NO$_3$** (1:1 $CDCl_3$/CD_3OD, 500 MHz, 298 K). Selected cross-peaks indicating through-space interactions between the interlocked macrocycle and axle components are highlighted. For atom labels see Scheme 2.18.

To probe the role of the nitrate anion in templating the formation of the rotaxane, analogous rotaxane synthesis experiments were conducted on a test scale with a range of other anions, and the crude reaction mixture analysed initially by mass spectrometry. In the cases where rotaxane was observed by this technique, the estimated yield of rotaxane formation was determined by analysis of the ^{1}H NMR spectrum of the crude reaction mixture. The control experiment using the non-coordinating hexafluorophosphate salt of the axle precursor **32·PF$_6$** afforded no rotaxane, highlighting the crucial role of the templating nitrate anion in the synthesis of **42·NO$_3$**. Furthermore, no rotaxane was produced in the presence of acetate, whilst dihydrogenphosphate and hydrogen carbonate were found to be poor templates, resulting in the formation of <5% of the interlocked product. Chloride was found to be an intermediate case, templating rotaxane formation in 15% yield (compared to 35% for nitrate). These observations serve to further highlight the importance of the trigonal nitrate anion in the efficient templation of rotaxane **42**$^+$.

2.3.4.2 Anion binding studies

In order to conduct anion binding studies, it was necessary to exchange the nitrate anion to the non-coordinating hexafluorophosphate counter anion, and this was achieved by washing a solution of rotaxane **42·NO$_3$** in CH_2Cl_2 with aqueous NH_4PF_6. The nitrate recognition properties of rotaxane **42·PF$_6$** were investigated using ^{1}H NMR titrations, initially in the competitive polar organic solvent mixture of 1:1 $CDCl_3/CD_3OD$.

The observation of significant upfield shifts of internal axle pyridinium proton *1* upon addition of $TBANO_3$ to rotaxane **42·PF$_6$** is indicative of binding of the nitrate anion within the rotaxane's interlocked cavity (Figure 2.22).

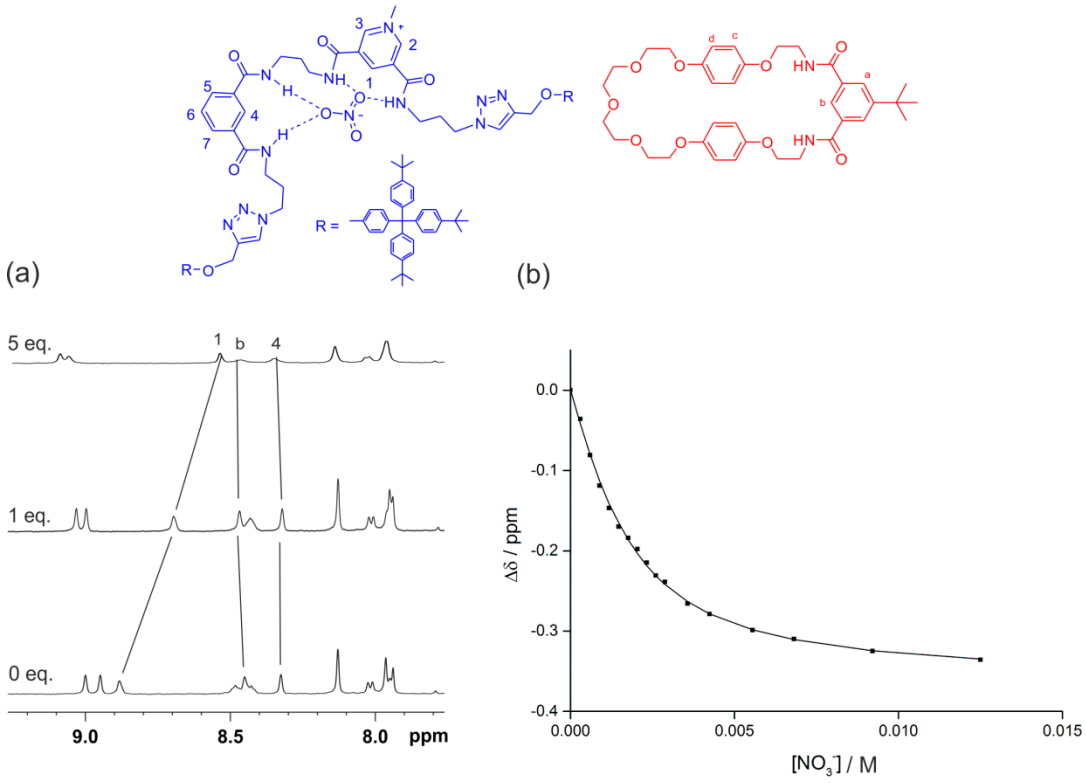

Figure 2.22 (a) Changes in the ^{1}H NMR spectrum of **42·PF$_6$** upon addition of increasing equivalents of $TBANO_3$ (1:1 $CDCl_3/CD_3OD$, 500 MHz, 298 K), (b) plots of chemical shift change against anion concentration for proton *1*. Actual data represented by solid symbols, calculated 1:1 host–guest binding isotherm represented by solid lines.

This was also confirmed by the, albeit modest, perturbations of the macrocycle internal isophthalamide proton *b* and the internal isophthalamide axle proton *4*. The perturbation of axle proton *4* suggests some hydrogen bonding of this motif to the nitrate anion; however, the

shift is much smaller than for pyridinium proton *1* ($\Delta\delta(2) = 0.34$ ppm, $\Delta\delta(4) = 0.05$ ppm after 10 equivalents of anion) implying that the nitrate anion is bound more tightly to the charged pyridinium motif. Nonetheless, the importance of the axle's isophthalamide group in nitrate recognition was demonstrated in the pseudo-rotaxane assembly studies described in Section 2.3.3.2 wherein significant perturbation of proton *4* upon interpenetration revealed the association of this motif to the nitrate anion. WinEQNMR2[26] analysis of the titration data (Figure 2.22b), monitoring proton *1*, revealed that the nitrate anion bound with an impressive association constant of 1050 M^{-1}. The strong association of nitrate within the rotaxane host, indeed one of the strongest reported to date in a competitive polar organic solvent, suggested that the unprecedented possibility of nitrate recognition in a more competitive organic–aqueous solvent mixture was achievable. To this end analogous titrations were conducted with nitrate, and a range of other mono-charged oxoanions, in 45:45:10 $CDCl_3/CD_3OD/D_2O$ (Figure 2.23).

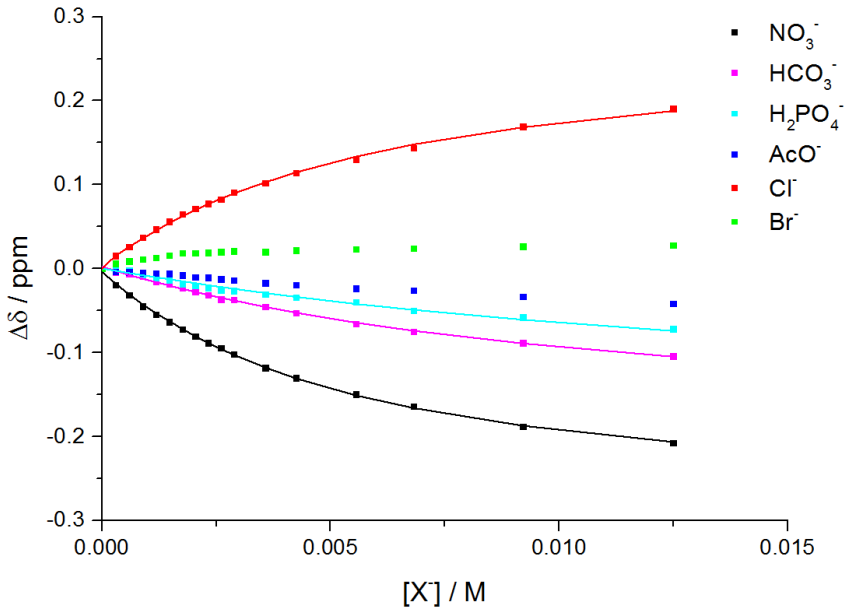

Figure 2.23 Plots of chemical shift change against anion concentration in 45:45:10 $CDCl_3/CD_3OD/D_2O$ for proton *1* of rotaxane **42·PF$_6$**. Actual data represented by solid symbols, calculated 1:1 host–guest binding isotherm represented by solid lines. $T = 298$ K.

Upon nitrate binding in this solvent mixture, strong upfield perturbation of the axle pyridinium proton *1* was again observed, whilst addition of other oxoanions led to smaller perturbation of the same proton (Table 2.2). Stoichiometric 1:1 association constants were determined by WinEQNMR2 analysis of the titration data, monitoring proton *1*, and are shown in Table 2.2.

Table 2.2 Anion association constants of rotaxane **42·PF$_6$** in 45:45:10 $CDCl_3/CD_3OD/D_2O$ and complexation induced chemical shift changes of proton *1*.

Anion[a]	NO_3^-	HCO_3^-	$H_2PO_4^-$	AcO^-	Cl^-	Br^-
K_a (M^{-1})[b]	430	100	50	-[c]	490	-[c]
$\Delta\delta(1)$[d]	−0.19	−0.10	−0.07	−0.02	0.21	0.02

T = 298 K. [a] Anions added as TBA salts, except for HCO_3^- which was added as the TEA salt. [b] Calculated using chemical shift data of proton *1*. Errors estimated to be <10%. [c] Binding too weak to be quantified. [d] Chemical shift change of proton *1* after addition of 10 equivalent of anion.

The trigonal nitrate anion guest binds strongly within the rotaxane host's complementary tridentate hydrogen bond donor binding cavity, even in this highly competitive aqueous–polar-organic solvent mixture (K_a = 430 M^{-1}). The rotaxane exhibits impressive selectivity for the templating nitrate anion over a range of other more basic oxoanions: the pseudo-trigonal hydrogen carbonate anion bound considerably more weakly, whilst acetate and dihydrogenphosphate resulted in very weak association, which in the case of acetate was too weak to be quantified. The selectivity for nitrate over acetate is particularly notable, given that acetate is 10^5 times more basic,[46] and reflects in part the geometric complementarity of the rotaxane binding cavity for the nitrate anion. To the best of our knowledge this is the first example of a synthetic anion receptor capable of nitrate recognition in aqueous solvent mixtures, and represents one of the highest levels of nitrate selectivity reported to date.

The binding of the spherical chloride anion, which is of comparable size to nitrate but lacks the trigonal geometric preference, was determined for comparison in the same solvent mixture, and found to associate with a similar affinity to nitrate. Addition of the larger

bromide anion led to very small perturbations of the internal cavity proton *1* and the binding could not be quantified.

Analogous titrations with NO_3^- and Cl^- were also conducted with the hexafluorophosphate salt of the non-interlocked axle precursor **32·PF$_6$** (Figure 2.24), which revealed no binding of nitrate in the same solvent mixture, but significantly stronger binding of chloride (K_a = 150 M^{-1}). These results highlight the crucial role of the interlocked binding cavity of **42·PF$_6$** in the enhancement of the nitrate binding affinity with respect to that of the non-interlocked pyridinium receptor **32·PF$_6$**.

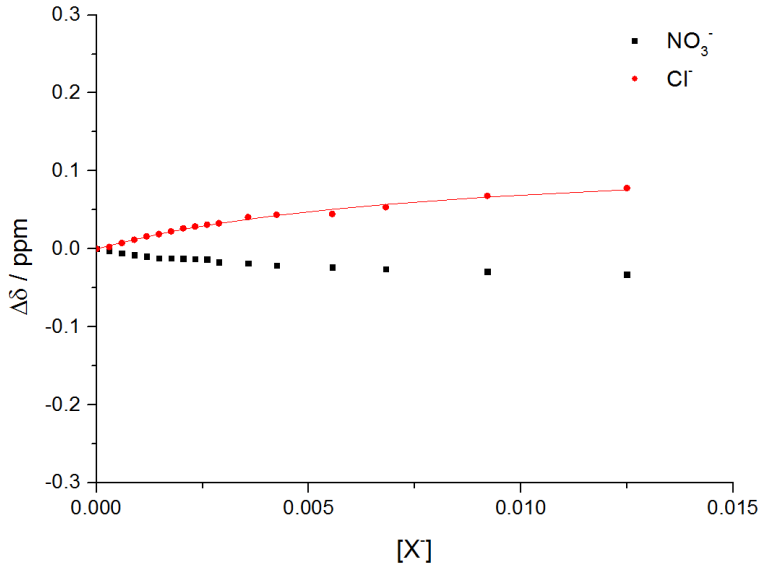

Figure 2.24 Plots of chemical shift change against anion concentration in 45:45:10 $CDCl_3/CD_3OD/D_2O$ for proton *1* of axle precursor **32·PF$_6$**. Actual data represented by solid symbols, calculated 1:1 host–guest binding isotherm represented by solid lines. T = 298 K.

2.3.5 Nitrate templated catenane synthesis

In the previous section it was shown that nitrate anion templation could be used as an effective strategy for the synthesis of a [2]rotaxane, *via* the stoppering of an initial pseudorotaxane assembly formed between suitably designed macrocycle and axle precursor components. Considering the utility of this approach for rotaxane formation, attention was turned to extending this methodology to investigate the nitrate anion templated synthesis of a [2]catenane. Examples of catenane host structures for molecular recognition are relatively rare compared to their rotaxane counterparts,[47] especially those capable of binding anionic guests.[4,10,11,48]

The strategy was to prepare a macrocycle precursor component incorporating the same asymmetric isophthalamide−3,5-bis-amide pyridinium hydrogen bond donor motifs integrated within in axle precursor **32·NO$_3$**, and terminal vinyl groups to facilitate "clipping" ring closing metathesis (RCM) catenane formation when threaded through a suitable macrocycle component. The macrocycle component **17** used in the catenane formation was isolated in sufficient quantity as a by-product from the preparation of [3]rotaxane **1·(Cl)$_2$**.

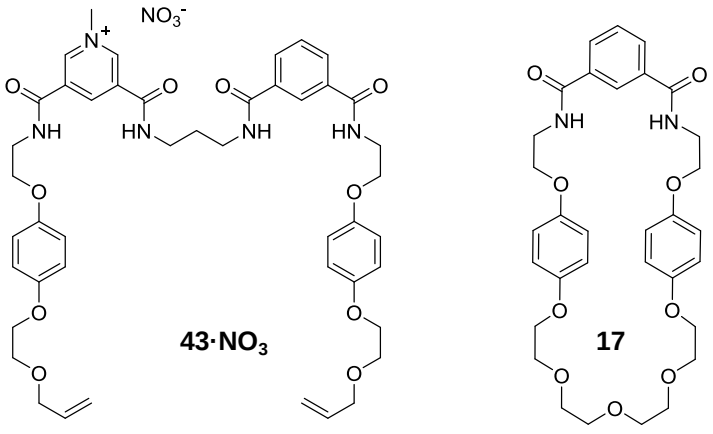

Figure 2.25 Target macrocycle precursor component **43·NO$_3$** and macrocycle **17** for nitrate templated catenane synthesis.

2.3.5.1 Synthesis and characterisation of nitrate templated [2]catenane

The synthesis of the target macrocycle precursor component **43·NO$_3$** is shown in Scheme 2.19 and Scheme 2.20. Mono-esters **5** and **24** were reacted with amine **44**[1] (kindly provided by Dr Fabiola Zapata) using EDC-mediated amide coupling to afford esters **45** and **46** in 60% and 45% yield respectively (Scheme 2.19), which were de-esterified to the acid forms **47** and **48** using KOH in methanol. Coupling of **47** mono-Boc protected 1,3-diamine **27** afforded **49**, from which the Boc protecting group was cleaved using TFA to afford amine **50·CF$_3$CO$_2$** in near quantitative yield.

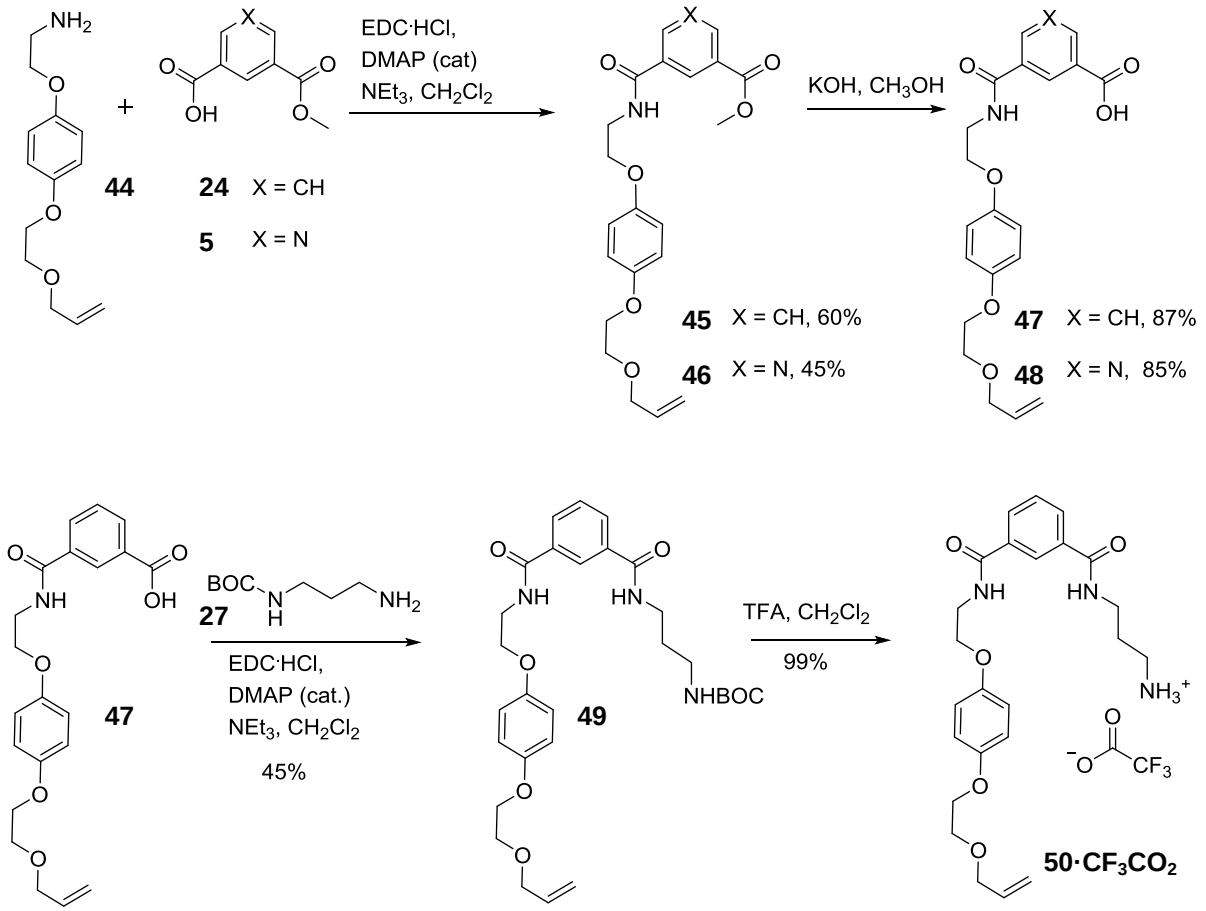

Scheme 2.19 Synthesis of asymmetric catenane precursors **48** and **50·CF$_3$CO$_2$**.

Amine **50·CF_3CO_2** was coupled to **48** to give the neutral pyridine compound **51** (Scheme 2.20), and methylated using CH_3I to produce the asymmetric isophthalamide−3,5-bis-amide pyridinium macrocycle precursor **43·I**. Anion exchange using a nitrate-loaded Amberlite® anion exchange column afforded the nitrate salt **43·NO_3**.

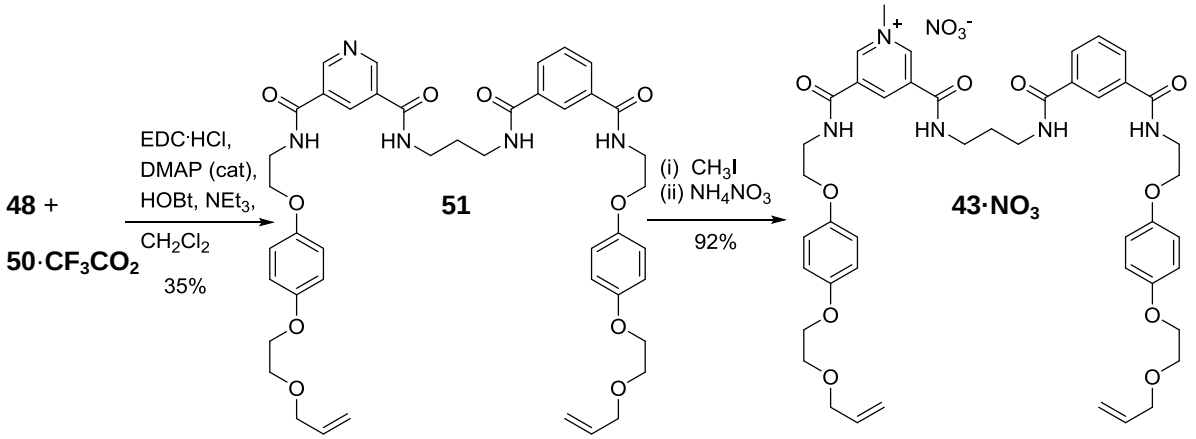

Scheme 2.20 Synthesis of macrocycle precursor **43·NO_3**.

The nitrate templated synthesis of the target [2]catenane was achieved using a ring closing metathesis (RCM) strategy. An initial nitrate templated pseudorotaxane assembly **17·51·NO_3** was prepared by mixing macrocycle precursor **51** with macrocycle **17** in dry CH_2Cl_2 (Scheme 2.21). Addition of Grubbs' second generation catalyst (10 wt%) afforded [2]catenane **52·NO_3**. Analysis of the ^{1}H NMR spectrum of the crude reaction mixture revealed that the rotaxane was formed in approximately 25% yield, the other products being the non-interlocked cyclised form of **43**$^+$ and macrocycle **17**. Purification by silica gel chromatography gave catenane **52·NO_3** in an isolated yield of 20%, which was fully characterised by ^{1}H, ^{13}C and ^{1}H ROESY NMR, and HRMS.

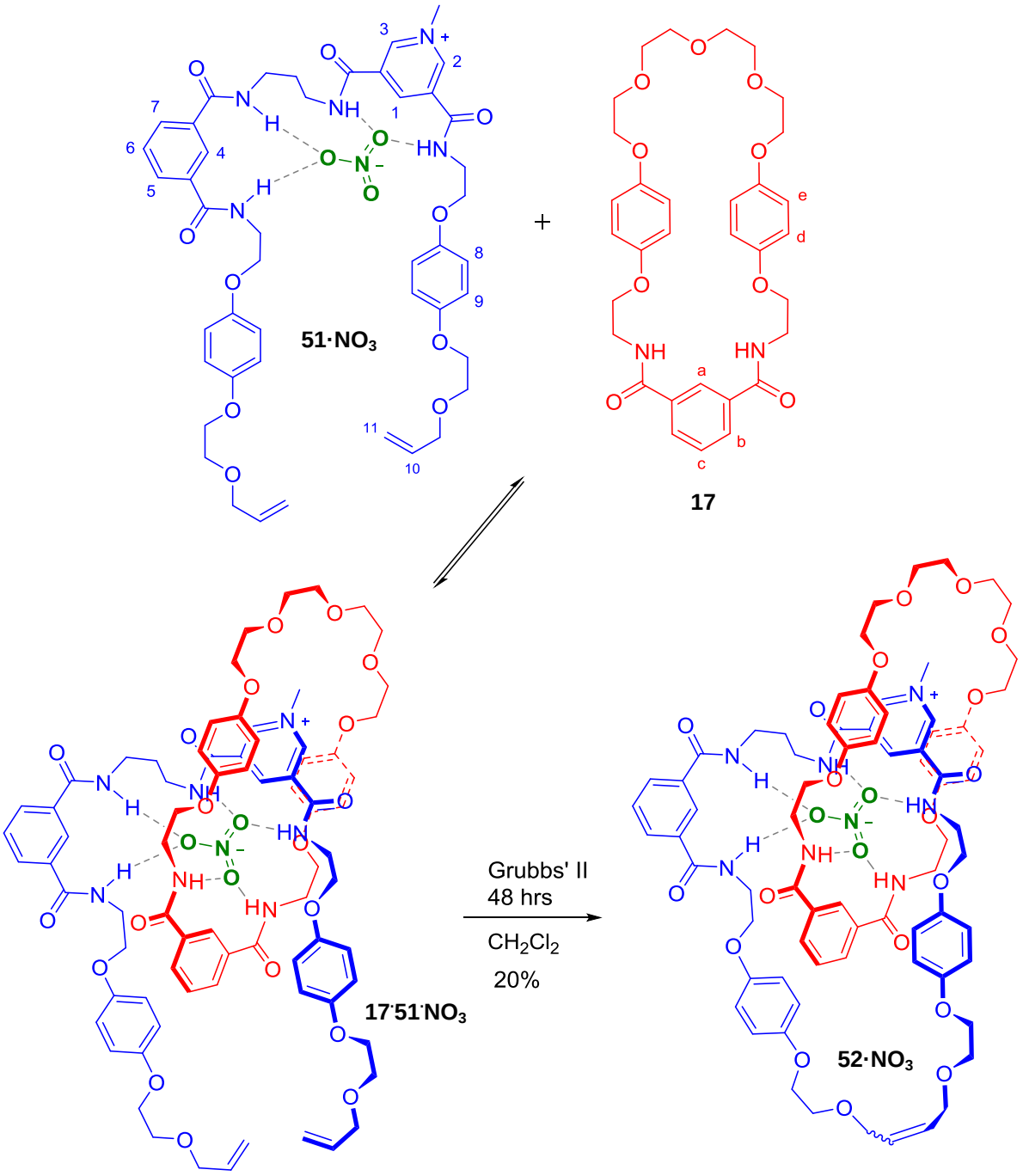

Scheme 2.21 Synthesis of nitrate templated catenane **52·NO_3**.

The ^{1}H NMR spectra of macrocycle **17**, catenane **52·NO$_3$**, and macrocycle precursor **51·NO$_3$** are compared in Figure 2.26.

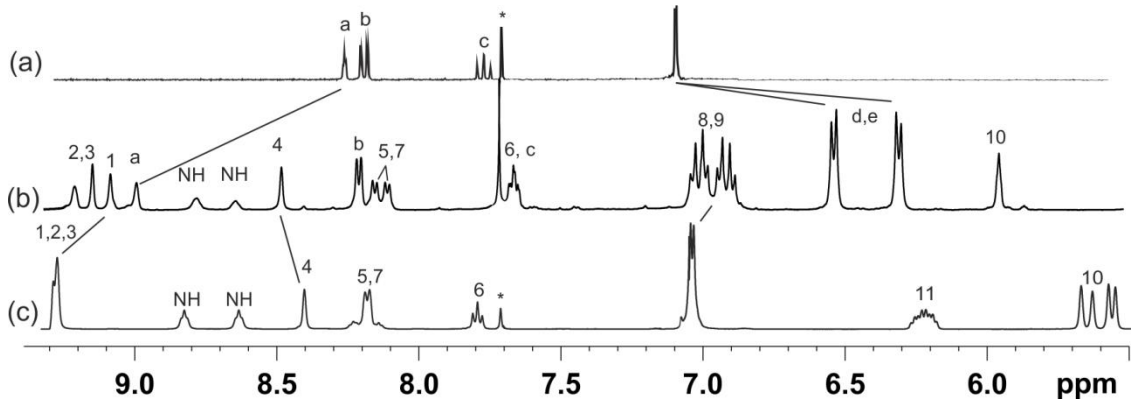

Figure 2.26 Partial ^{1}H NMR spectra of (a) macrocycle **17**, (b) catenane **52·NO$_3$** and (c) macrocycle precursor **51·NO$_3$** in 1:1 $CDCl_3/CD_3OD$ (500 MHz, 298 K). For atom labels see Scheme 2.21, *denotes residual solvent peak.

Upfield perturbation of pyridinium proton *1*, and downfield perturbation of internal isophthalamide protons *a* and *4*, are indicative of hydrogen bonding interactions with the nitrate anion template. Of particular note is the upfield shift and splitting of the hydroquinone protons *d* and *e*, which is diagnostic of aromatic donor–acceptor interactions between the hydroquinone groups in macrocycle **17** and the electron-deficient pyridinium motif in the other macrocycle. This confirms the interlocked nature of the catenane, which is further supported by the observation of through-space interactions between the pyridinium protons *1, 2* and *3* of the larger macrocycle with the hydroquinone protons *d* and *e* of the other macrocycle in the ^{1}H ROESY NMR spectrum of **52·NO$_3$** (Figure 2.27).

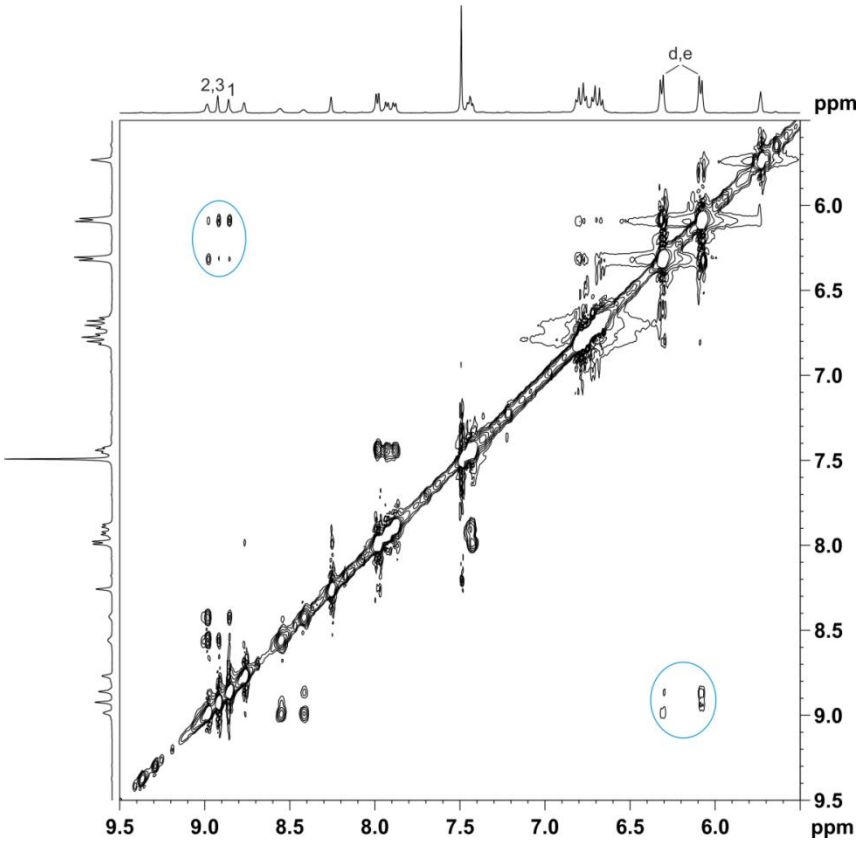

Figure 2.27 ^{1}H ROESY NMR spectrum of **52·NO$_3$** (1:1 $CDCl_3/CD_3OD$, 500 MHz, 298 K). Cross-peaks indicating through space interactions between the interlocked macrocycle and axle components are highlighted. For atom labels see Scheme 2.21.

For comparison, synthesis of the catenane was also attempted using both the chloride and hexafluorophosphate salts of macrocycle precursor **51**$^+$. Analysis of the ^{1}H NMR spectrum of the crude reaction mixture revealed a yield of catenane of <10% with chloride, and the predominant formation of the cyclised form of **51**$^+$. Presumably the bidentate nature of **51**$^+$ fulfils the coordination of the spherical chloride anion and competes with the association of macrocycle **17**, resulting in minimal pseudorotaxane formation. No interlocked product was formed in the case of the non-coordinating hexafluorophosphate anion, highlighting the pivotal templating role of the nitrate anion in the synthesis of the catenane.

2.3.5.2 Anion binding studies

Anion exchange to the non-coordinating hexafluorophosphate salt, in preparation for anion binding studies, was achieved by washing a CH_2Cl_2 solution of catenane **52·NO$_3$** with aqueous NH_4PF_6. To enable a direct comparison with the anion recognition properties of rotaxane **42·PF$_6$**, analogous ^{1}H NMR titrations with catenane **52·PF$_6$** were conducted in 45:45:10 $CDCl_3/CD_3OD/D_2O$ (Figure 2.28).

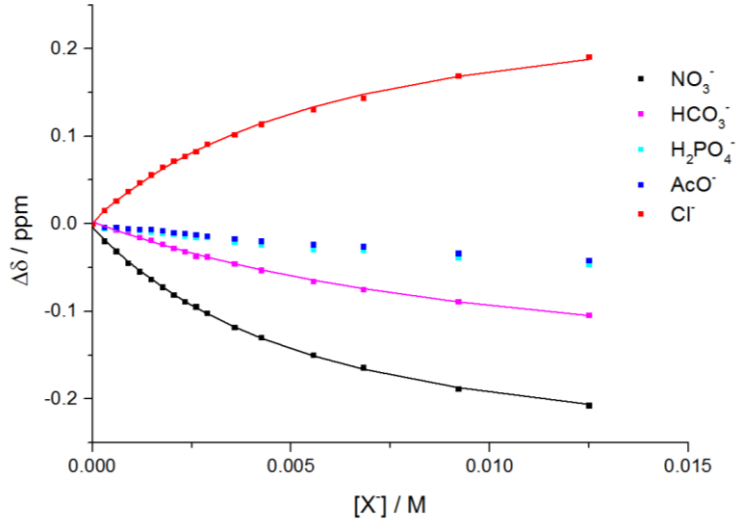

Figure 2.28 Plots of chemical shift change against anion concentration in 45:45:10 $CDCl_3/CD_3OD/D_2O$ for proton *1* of catenane **52·PF$_6$**. Actual data represented by solid symbols, calculated 1:1 host–guest binding isotherm represented by solid lines. *T* = 298 K.

Nitrate binding results in strong upfield perturbation of the internal pyridinium proton *1* ($\Delta\delta$ = 0.21 ppm after 10 equivalents of anion), which is indicative of anion binding within the cavity formed between the interlocked macrocycle components. Addition of other oxoanions led to much smaller perturbation of the same proton (Table 2.3). WinEQNMR2[26] analysis of the titration data, monitoring proton *1*, determined the 1:1 stoichiometric association constants shown in Table 2.3.

Table 2.3 Anion association constants of catenane **52·NO$_3$** in 45:45:10 $CDCl_3/CD_3OD/D_2O$, and complexation induced chemical shift changes of proton *1*.

Anion[a]	NO_3^-	HCO_3^-	$H_2PO_4^-$	AcO^-	Cl^-
K_a (M^{-1})[b]	250	80	-[c]	-[c]	200
$\Delta\delta(1)$[d]	0.21	0.10	0.04	0.04	0.19

T = 298 K. [a] Anions added as TBA salts, except for HCO_3^- which was added as the TEA salt. [b] Calculated using chemical shift data of proton *1*. Errors estimated to be <10%. [c] Binding too weak to be quantified. [d] Chemical shift change of proton *1*after addition of 10 equivalent of anion.

The anion selectivity of catenane **52·PF$_6$** closely resembles that of rotaxane **42·PF$_6$**, in that the interlocked host displays impressive selectivity for nitrate over the other more basic oxoanions. The association constants were lower than in the analogous rotaxane for all of the anions measured: this presumably reflects the greater steric constraint to anion binding in the catenane compared to the rotaxane. As with rotaxane **42·PF$_6$**, the binding of chloride was found to be of similar magnitude to that of nitrate. Bearing in mind that the analogous non-interlocked isophthalamide−3,5-bis-amide pyridinium motif (Section 2.3.4.2, compound **32·PF$_6$**) recognises chloride selectively over nitrate in the same solvent mixture, this result highlights the role of the interlocked binding domain of the catenane in enhancing the nitrate recognition.

2.4 Chapter conclusions

The work reported in this chapter demonstrates that careful design of interlocked hosts can facilitate unprecedented levels of anion recognition, such that selective binding of the target oxoanion guest in competitive aqueous solvent mixtures may be achieved.

In the first section, it was shown that a naphthalene-containing [3]rotaxane host, prepared by chloride anion templation, selectively senses sulfate by means of an anion-induced quenching of the fluorescence emission. Binding of mono-charged anionic guests, by contrast, resulted in enhancement of the emission.

In the second section, the novel use of nitrate templation for the synthesis of rotaxane and catenanes was presented. Formation of a [2]rotaxane was achieved by a stoppering reaction of a nitrate templated pseudorotaxane assembly consisting of a suitable bidentate hydrogen bonding axle precursor threaded through an isophthalamide-containing macrocycle. In a similar fashion, the nitate anion templated [2]catenane synthesis involved a "clipping" RCM cyclisation of a bis-vinyl-appended macrocycle precursor threaded through a macrocycle. The rotaxane and catenane host structures were shown to bind nitrate in a $CDCl_3/CD_3OD/D_2O$ solvent mixture, which represents the first reports of an anion receptors capable of recognising nitrate in organic–aqueous solvent media. Furthermore, unprecedented levels of selectivity for nitrate over a range of considerably more basic oxoanions was observed in both mechanically bonded host systems.

2.5 References for Chapter 2

1. J. A. Wisner, P. D. Beer, M. G. B. Drew, and M. R. Sambrook, *J Am Chem Soc*, 2002, **124**, 12469–12476.
2. M. R. Sambrook, P. D. Beer, M. D. Lankshear, R. F. Ludlow, and J. A. Wisner, *Org. Biomol. Chem.*, 2006, **4**, 1529.
3. L. M. Hancock, L. C. Gilday, S. Carvalho, P. J. Costa, V. Félix, C. J. Serpell, N. L. Kilah, and P. D. Beer, *Chem. - Eur. J.*, 2010, **16**, 13082–13094.
4. L. M. Hancock, L. C. Gilday, N. L. Kilah, C. J. Serpell, and P. D. Beer, *Chem. Commun.*, 2011, **47**, 1725–1727.
5. N. H. Evans, H. Rahman, A. V. Leontiev, N. D. Greenham, G. A. Orlowski, Q. Zeng, R. M. J. Jacobs, C. J. Serpell, N. L. Kilah, J. J. Davis, and P. D. Beer, *Chem. Sci.*, 2012, **3**, 1080.
6. N. H. Evans and P. D. Beer, *Chem. – Eur. J.*, 2011, **17**, 10542–10546.
7. N. H. Evans, C. J. Serpell, and P. D. Beer, *Chem. Commun.*, 2011, **47**, 8775–8777.
8. M. J. Langton and P. D. Beer, *Acc. Chem. Res.*, 2014, DOI:10.1021/ar500012a.
9. K. M. Mullen, J. Mercurio, C. J. Serpell, and P. D. Beer, *Angew. Chem. Int. Ed.*, 2009, **48**, 4781–4784.
10. A. Caballero, F. Zapata, N. G. White, P. J. Costa, V. Félix, and P. D. Beer, *Angew. Chem. Int. Ed.*, 2012, **51**, 1876–1880.
11. B. Huang, S. M. Santos, V. Felix, and P. D. Beer, *Chem. Commun.*, 2008, 4610.
12. K. M. Mullen and P. D. Beer, *Chem. Soc. Rev.*, 2009, **38**, 1701–1713.
13. D. B. Amabilino, P. R. Ashton, A. S. Reder, N. Spencer, and J. F. Stoddart, *Angew. Chem. Int. Ed. Engl.*, 1994, **33**, 433–437.
14. T. J. Huang, B. Brough, C.-M. Ho, Y. Liu, A. H. Flood, P. A. Bonvallet, H.-R. Tseng, J. F. Stoddart, M. Baller, and S. Magonov, *Appl. Phys. Lett.*, 2004, **85**, 5391–5393.
15. Y. Nagawa, J. Suga, K. Hiratani, E. Koyama, and M. Kanesato, *Chem. Commun.*, 2005, 749–751.
16. J.-P. Collin, F. Durola, J. Frey, V. Heitz, F. Reviriego, J.-P. Sauvage, Y. Trolez, and K. Rissanen, *J. Am. Chem. Soc.*, **132**, 6840–6850.
17. J.-S. Marois, K. Cantin, A. Desmarais, and J.-F. Morin, *Org Lett*, 2007, **10**, 33–36.
18. J.-P. Collin, J. Frey, V. Heitz, J.-P. Sauvage, C. Tock, and L. Allouche, *J Am Chem Soc*, 2009, **131**, 5609–5620.
19. Q. Jiang, H.-Y. Zhang, M. Han, Z.-J. Ding, and Y. Liu, *Org Lett*, 2010, **12**, 1728–1731.
20. M. J. Langton, J. D. Matichak, A. L. Thompson, and H. L. Anderson, *Chem. Sci.*, 2011, **2**, 1897.
21. A. Joosten, Y. Trolez, J.-P. Collin, V. Heitz, and J.-P. Sauvage, *J. Am. Chem. Soc.*, 2012, **134**, 1802–1809.
22. L. M. Hancock and P. D. Beer, *Chem. Commun.*, 2011, **47**, 6012.
23. H. W. Gibson, S. H. Lee, P. T. Engen, P. Lecavalier, J. Sze, Y. X. Shen, and M. Bheda, *J. Org. Chem.*, 1993, **58**, 3748–3756.
24. I. S. Choi, X. Li, E. E. Simanek, R. Akaba, and G. M. Whitesides, *Chem. Mater.*, 1999, **11**, 684–690.
25. L. M. Hancock and P. D. Beer, *Chem. – Eur. J.*, 2009, **15**, 42–44.
26. M. J. Hynes, *J. Chem. Soc. Dalton Trans.*, 1993, **2**, 311–312.
27. T. Gunnlaugsson, H. D. P. Ali, M. Glynn, P. E. Kruger, G. M. Hussey, F. M. Pfeffer, C. M. G. dos Santos, and J. Tierney, *J. Fluoresc.*, 2005, **15**, 287–299.

28. P. D. Beer, F. Szemes, V. Balzani, C. M. Salà, M. G. B. Drew, S. W. Dent, and M. Maestri, *J. Am. Chem. Soc.*, 1997, **119**, 11864–11875.
29. J. W. Steed and J. L. Atwood, *Supramolecular Chemistry*, Wiley, Chichester, UK, 2nd Edition., 2009.
30. A. P. Bisson, V. M. Lynch, M.-K. C. Monahan, and E. V. Anslyn, *Angew. Chem. Int. Ed. Engl.*, 1997, **36**, 2340–2342.
31. K. Choi and A. D. Hamilton, *J. Am. Chem. Soc.*, 2001, **123**, 2456–2457.
32. R. Herges, A. Dikmans, U. Jana, F. Köhler, P. G. Jones, I. Dix, T. Fricke, and B. König, *Eur. J. Org. Chem.*, 2002, **2002**, 3004–3014.
33. P. Blondeau, J. Benet-Buchholz, and J. de Mendoza, *New J. Chem.*, 2007, **31**, 736–740.
34. A. S. Singh and S.-S. Sun, *J. Org. Chem.*, 2012, **77**, 1880–1890.
35. J. Romański and P. Piątek, *J. Org. Chem.*, 2013, **78**, 4341–4347.
36. M. M. Watt, L. N. Zakharov, M. M. Haley, and D. W. Johnson, *Angew. Chem. Int. Ed.*, 2013, **52**, 10275–10280.
37. G. T. Spence and P. D. Beer, *Acc. Chem. Res.*, 2013, **46**, 571–586.
38. N. G. White, C. J. Serpell, and P. D. Beer, *Cryst. Growth Des.*, 2014.
39. M. R. Sambrook, P. D. Beer, J. A. Wisner, R. L. Paul, A. R. Cowley, F. Szemes, and M. G. B. Drew, *J. Am. Chem. Soc.*, 2005, **127**, 2292–2302.
40. S. Umbreen, M. Brockhaus, H. Ehrenberg, and B. Schmidt, *Eur. J. Org. Chem.*, 2006, **2006**, 4585–4595.
41. G. T. Spence, C. Chan, F. Szemes, and P. D. Beer, *Dalton Trans.*, 2012, **41**, 13474–13485.
42. D. Muller, I. Zeltser, G. Bitan, and C. Gilon, *J. Org. Chem.*, 1997, **62**, 411–416.
43. H. C. Kolb, M. G. Finn, and K. B. Sharpless, *Angew. Chem. Int. Ed.*, 2001, **40**, 2004–2021.
44. D. A. Leigh and K. D. Hanni, *Chem. Soc. Rev.*, 2010, **39**, 1240–1251.
45. V. Aucagne, K. D. Hänni, D. A. Leigh, P. J. Lusby, and D. B. Walker, *J. Am. Chem. Soc.*, 2006, **128**, 2186–2187.
46. C. E. Housecroft and A. G. Sharpe, *Inorganic Chemistry*, Pearson Harlow, UK, 3rd edn., 2008.
47. N. H. Evans and P. D. Beer, *Chem. Soc. Rev.*, 2014.
48. N. H. Evans, H. Rahman, A. V. Leontiev, N. D. Greenham, G. A. Orlowski, Q. Zeng, R. M. J. Jacobs, C. J. Serpell, N. L. Kilah, J. J. Davis, and P. D. Beer, *Chem. Sci.*, 2012, **3**, 1080–1089.

CHAPTER 3

Chapter 3 Hydrogen and halogen bonding rotaxane hosts for anion recognition in water†

3.1 Introduction

3.1.1 Anion recognition in pure water

The field of anion supramolecular chemistry has grown rapidly over recent years, driven by the need to recognise, sense and sequester anions of biological and environmental importance. Whilst there are a plethora of anion receptors capable of anion recognition in organic or organic–aqueous solvent mixtures, relatively few systems have been demonstrated to function in pure water (Chapter 1).[1] The majority of these hosts possess high charges in order to overcome the significant hydration energy of the anion, and operate over a restricted pH range whilst undergoing multiple protonation equilibria. In pioneering work, Kubik has demonstrated that even neutral host systems, in the form of macrocyclic peptides, can be used to recognise anions in aqueous solvents through a combination of hydrogen bonding interactions and the hydrophobic effect.[2,3] For example, the cyclic peptide host shown in Figure 3.1a binds halides and sulfate anions in pure water, albeit with low affinities (K_a = 5, 10, 14 and 52 M^{-1} for Cl^-, Br^-, I^- and SO_4^{2-}, respectively).[3] In the interests of comparison, Lehn's azacryptand in the hexa-protonated form (Figure 3.1b) binds the same anions in water with considerably higher affinity (K_a = 1000, 400, 140 and 79000 M^{-1} for Cl^-, Br^-, I^- and SO_4^{2-}, respectively).[4] More recently, Jeong has prepared a foldamer structure incorporating three indolocarbazole units (Figure 3.1c), which is capable of halide anion complexation in pure water by encapsulation of the anion within a hydrophobic cavity

† The work described in this chapter was published as an article in the journal *Nature Chemistry:*
M. J. Langton, S. W. Robinson, I. Marques, V. Félix and P. D. Beer, ***Nat. Chem.,*** in press, 2014, DOI: 10.1038/NCHEM.2111

shielded from competing solvent molecules (K_a = 65, 19 and <1 M^{-1} for Cl^-, Br^- and I^-).[5] Whilst the recognition of halide anions in water with a neutral receptor is indeed impressive, the difference in binding affinities between such receptors and analogous highly charged, yet pH-dependent systems is significant, and the preparation of anion receptors that are capable of the pH-independent binding of anions with high affinity remains a challenge. It is noteworthy that both the neutral peptidic receptor and the highly charged azacryptand receptor both bound sulfate with significantly greater affinity than the halide anions. Reversing this selectivity trend poses a great challenge to the design of receptors for the selective recognition of halide anions over polyanionic oxoanions.

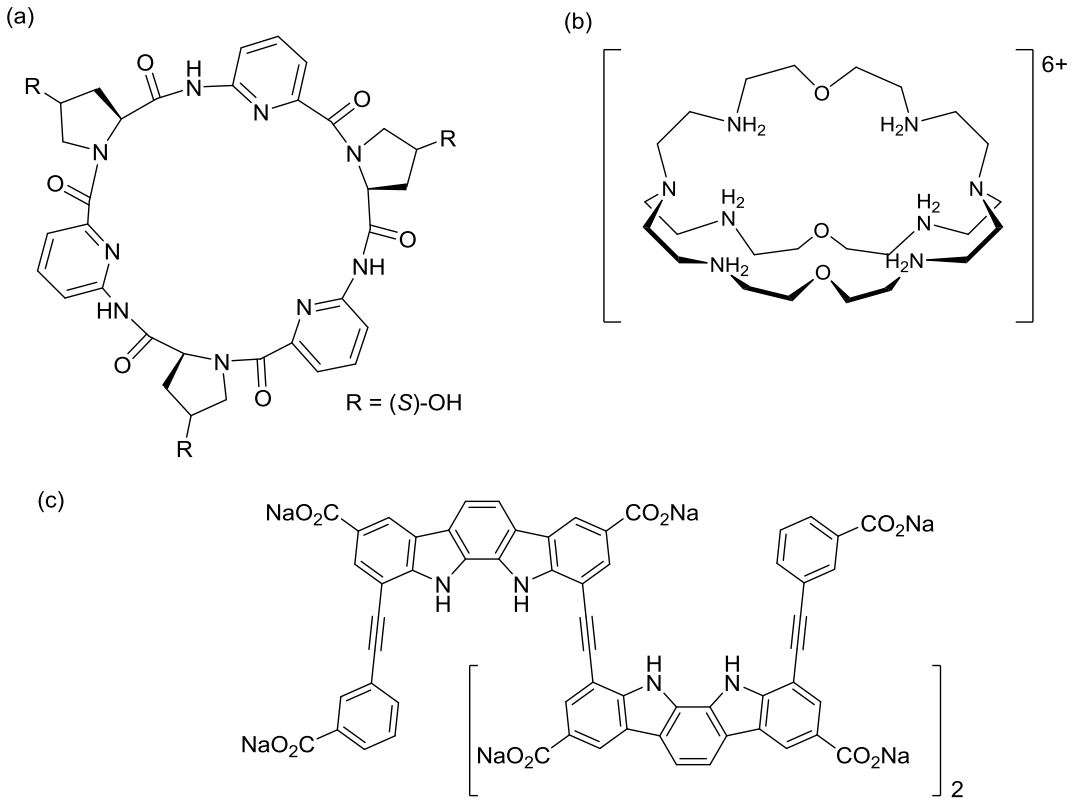

Figure 3.1 Examples of anion receptors capable of halide recognition in water: (a) Kubik's neutral cyclic peptide receptor,[3] (b) Lehn's hexa-protonated receptor[4] and (c) Jeong's neutral foldamer.[5]

As was discussed previously, interlocked molecular architectures are effective anion hosts by virtue of the unique three-dimensional binding cavity formed between the interlocked components. The host encapsulates the anion guest and enhances both the binding affinity and selectivity, relative to the acyclic analogues. The recognition of anions in pure water using such mechanically bonded receptors has, however, been hampered by poor solubility. To date, effective recognition has been achieved in organic–aqueous solvent mixtures containing up to 35% water: the dicationic rotaxane shown in Figure 3.2 prepared by Laura Hancock within this laboratory[6] was shown to bind chloride in 65:35 d_6-acetone/D_2O (K_a = 500 M^{-1}), with impressive selectivity over acetate and dihydrogenphosphate, which did not bind in this solvent mixture. Complexation of anions in pure water by rotaxane or catenane hosts, however, remains unprecedented.

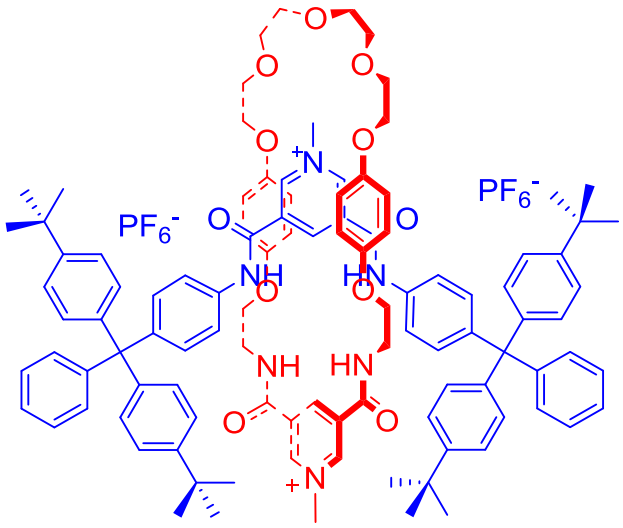

Figure 3.2 Hancock's dicationic rotaxane host capable of chloride binding in 65:35 d_6-acetone/D_2O.[6]

3.1.2 Halogen bonding as an intermolecular interaction for anion recognition

The use of halogen bonds (XB) as intermolecular interactions for anion recognition is in its infancy, with the seminal examples of XB-mediated anion binding reported only very recently. As discussed in Chapter 1, neutral halogen bonding anion hosts only function in organic solvents, yet charge-assisted halogen bonding receptors have been shown to display impressive affinities in polar organic and organic–aqueous solvent mixtures. Furthermore, XB-donor motifs have been incorporated into macrocyclic and interlocked anion receptors to further enhance the anion recognition capability. For example, the iodoimidazolium macrocycle[7] and bromoimidazolium catenane[8] shown in Figure 3.3 recognise anions through two convergent halogen bonds, and sense the guest species by means of modulation of the emission from the integrated naphthalene reporter groups. The iodoimidazolium (Figure 3.3a) macrocycle recognises Br^- and I^- with high affinity in a competitive 9:1 methanol/water mixture (log K_a = 5.9 and 4.6 for Br^- and I^- respectively), whilst the catenane (Figure 3.3b) recognises Cl^- and Br^- in CH_3CN solution.

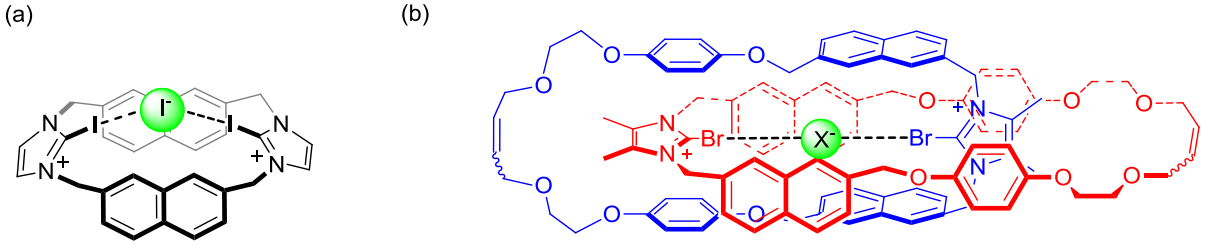

Figure 3.3 Beer's macrocyclic and interlocked halogen bonding anion hosts: (a) iodo-imidazolium macrocycle[7] and (b) bromo-imidazolium catenane.[8]

A pertinent consideration when designing supramolecular systems utilising halogen bonds in solution is the relative strengths of both XB and the ubiquitous HB interactions. From the point of view of anion recognition, in the past few years a number of groups have independently demonstrated that, in organic solvents, replacing a HB-donor with a like-for-like halogen bond donor can dramatically increase the anion binding affinity. For instance, in the bis-iodoimidazolium macrocycle discussed earlier (Figure 3.3a), replacing the iodine

atoms with hydrogen atoms results in a dramatic decrease in the anion binding affinity by three orders of magnitude. Likewise, in the triazolium-containing rotaxane shown in Figure 3.4a the binding affinities of the halides in 1:1 $CDCl_3/CD_3OD$ are enhanced by at least an order of magnitude when the prototriazolium HB-donor is replaced by an iodotriazolium XB-donor group.[9,10] A similar effect is observed in Resnati's halogen bonding dihydrogenphosphate receptor (Figure 3.4b), where replacing the hydrogen atom with a halogen atom significantly increases the anion binding affinity in DMSO solution ($K_{a\,[X=I]} = 1100\ M^{-1}$, $K_{a\,[X=H]} = 26\ M^{-1}$).[11] The XB-mediated enhancement of chloride binding affinity in acetone by Taylor's tripodal halogen bonding host is even more dramatic (Figure 3.4c), with a four order-of-magnitude enhancement over the HB analogue ($K_{a\,[X=I]} = 19\,000\ M^{-1}$, $K_{a\,[X=H]} = <5\ M^{-1}$).[12]

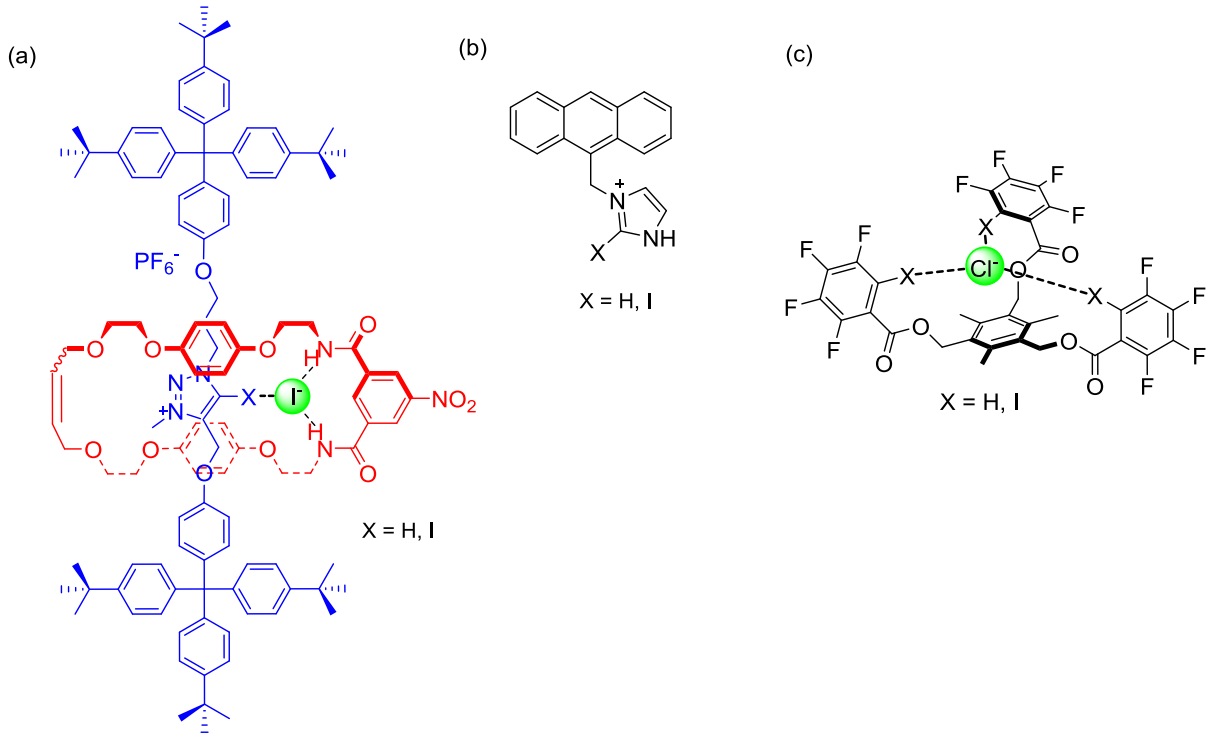

Figure 3.4 (a) Beer's triazolium-containing rotaxane host,[9] (b) Resnati's dihydrogenphosphate receptor[11] and (c) Taylor's tripodal anion host.[12]

It is clear that incorporating XB-donor groups within anion receptors can significantly enhance the binding affinity of anions in polar organic solvents with respect to the hydrogen bonding analogues. Experimental data quantifying the thermodynamics of halogen bonding interactions remains surprisingly limited however, particularly in the case of charge-assisted halogen bonding, and confined merely to selected measurements in organic solvents.[13–18] Furthermore, the recognition of anions using XB interactions in water has yet to be reported, despite the importance of developing supramolecular systems for applications in this biologically and environmentally relevant solvent medium.

3.1.3 Chapter aims

The aim of the work described in this chapter was to prepare water soluble, halogen bonding rotaxane hosts, capable of strong anion recognition in pure water. A cyclodextrin-stoppered 3,5-bis-amide pyridinium rotaxane is prepared initially, and its anion binding properties in water determined. The synthesis of analogous interlocked hosts containing bis-prototriazole pyridinium HB-donors, and bis-iodotriazole pyridinium XB-donors is then discussed.

A comparison of the anion binding properties of these structurally related XB- and HB-donor rotaxane host systems aims to facilitate a greater understanding about the nature of halogen bonding functioning in pure water.

3.2 Solubilising hydrogen bonding rotaxane hosts to facilitate anion recognition in water

Despite the superior levels of recognition that is achievable using sophisticated interlocked host structures, the binding of anions in pure water has remained elusive. The primary handicap to investigating the anion binding ability of such hosts has been their lack of aqueous solubility. The terphenyl stopper components utilised in anion-binding rotaxanes, such as Hancock's dicationic rotaxane (Figure 3.2), are highly hydrophobic and therefore the starting point for the research was to replace these groups with hydrophilic stopper analogues. Suitable candidates for a hydrophilic stopper should fulfil a number of criteria: impart aqueous solubility onto the structure; be synthetically accessible with a range of functional groups; and be of sufficient bulky size to prevent the de-threading of the rotaxane (Figure 3.5).

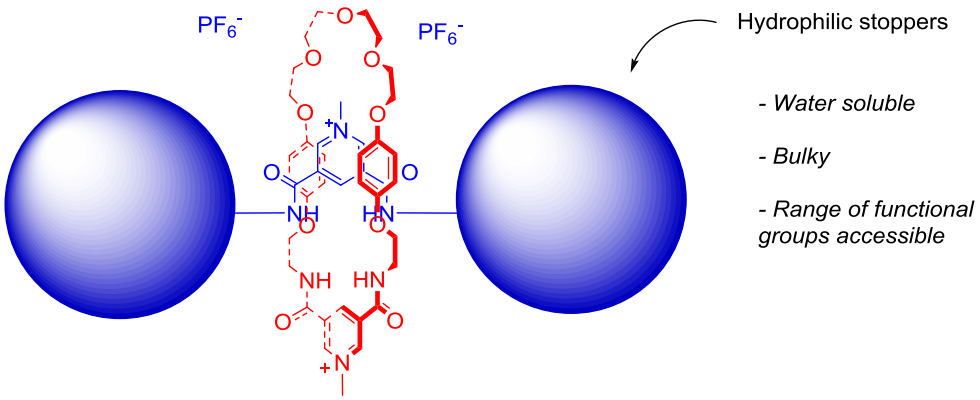

Figure 3.5 Schematic representation of the target water-soluble rotaxane, featuring hydrophilic stopper components.

It was anticipated that these three criteria would be satisfied by using mono-functionalised permethylated *β*-cyclodextrin. Cyclodextrins (CD) are cyclic oligosaccharides which are most commonly found in three forms, *α*, *β* (Figure 3.6a), and *γ*, consisting of 6, 7 or 8 glucose units respectively, and are produced through the degradation of starch by the enzyme CD transglycosylase obtained from the bacterium *Bacillus macerans*. They are truncated cone-shaped macrocycles (Figure 3.6b), in which the narrow rim is comprised of primary hydroxyl

groups and the larger rim made up of secondary hydroxyls. The central tapered cavity is hydrophobic in nature and can bind hydrophobic aliphatic and aromatic guests, such as adamantane and naphthalene, and this inclusion chemistry has been extensively studied.[19,20] Of the three common forms of cyclodextrin, the host–guest chemistry of *β*-cyclodextrin is arguably the most exploited since its internal cavity is of optimum size to complex a wide range of aromatic guest species.

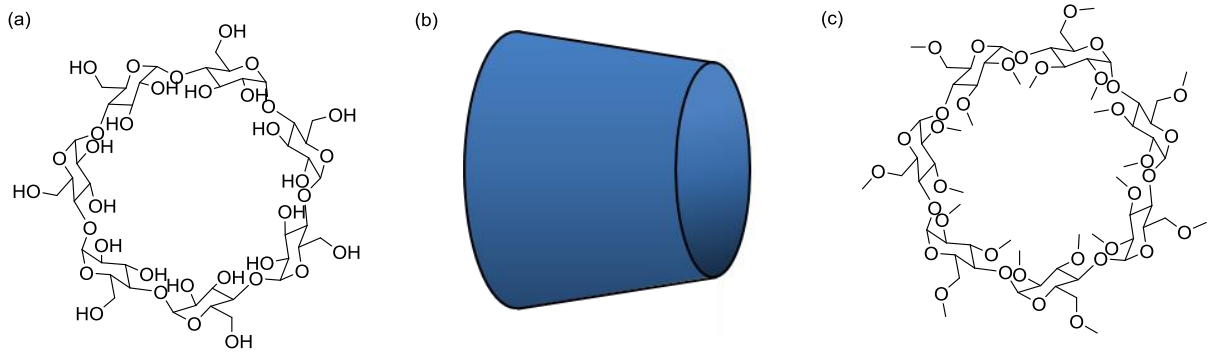

Figure 3.6 (a) *β*-Cyclodextrin, (b) schematic representation of the truncated cone geometry adopted by cyclodextrin derivatives and (c) permethylated *β*-cyclodextrin.

Whilst all forms of cyclodextrin are water soluble to some extent, the solubility of *β*-cyclodextrin is considerably less than its homologues (18.5 mg/L compared to 145 and 232 mg/L for the *α* and *γ* forms respectively).[21] Modification of the parent cyclodextrins, however, by substitution of any of the hydrogen bonding hydroxyl groups, even by hydrophobic moieties such as methoxy groups, results in a dramatic enhancement in the water solubility (>500 mg/L for permethylated *β*-cyclodextrin, Figure 3.6c). An additional benefit of permethylation is that the product is rendered highly soluble in a wide range of polar organic solvents, including CH_3Cl, CH_2Cl_2, THF, EtOAc, DMF and DMSO. As such, permethylated *β*-cyclodextrin represents an ideal solubilising stopper component: the external diameter determined from crystal structure data is 12–13 Å,[22] larger than that of the commonly used terphenyl stopper components (~11 Å) and hence is expected to prevent macrocycle slippage; whilst solubility in organic solvents will facilitate synthetic manipulation, and importantly,

anion-templated rotaxane assembly in non-competitive solvents. Furthermore, the mono-functionalisation of *β*-cyclodextrin has been previously reported in the literature.[23,24]

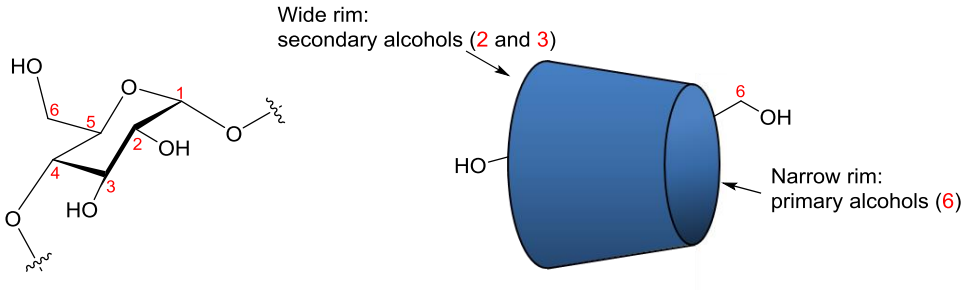

Figure 3.7 Distribution of alcohol functionalities in the *β*-cyclodextrin truncated cone.

The differing nucleophilicity and basicity of the primary and secondary alcohols allows synthetic discrimination between the two rims of the truncated cone: reaction with an electrophile leads to preferential alkylation of the primary alcohols of the narrow rim, while initial deprotonation of the more acidic secondary alcohols and subsequent reaction with a suitable electrophile facilitates alkylation on the wider rim. Functionalisation of just one of the identical alcohols on either rim is inevitably a statistical reaction however, requiring laborious chromatographic purification to isolate the desired mono-functionalised product from a complex mixture. Selectively alkylating just one of the two possible secondary alcohols (2-*O* or 3-*O*, Figure 3.7) on the wide rim is challenging, and correspondingly, the simpler alkylation of the primary rim is most commonly reported in the literature, and will be utilised in the following work.

Cyclodextrins have been incorporated extensively as the macrocycle component within rotaxanes and catenanes by forming an initial pseudorotaxane with an electron rich aromatic threading component, driven by the hydrophobic effect.[25] A notable example is Anderson's polyrotaxane "insulated molecular wire" (Chapter 1), in which multiple *β*-cyclodextrin derivatives are threaded on a poly(*para*-phenylene) axle component.[26] Although there are a plethora of rotaxanes and catenanes containing cyclodextrins as the

macrocycle component(s), only a handful of examples of rotaxanes in which the cyclodextrins act as the *stopper* component have been reported to date.

In 2006, Harada described a rotaxane architecture in which *β*-cyclodextrin derivatives form both the macrocycle and stopper components of a oligo(thiophene)-derived rotaxane (Scheme 3.1a).[27] Suzuki coupling of an oligothiophene diboric-ethylene-glycolester component, threaded through dimethyl-*β*-cyclodextrin, with 6-*O*-(4-iodophenyl)-*β*-CD formed the [2]rotaxane shown in Scheme 3.1a, in addition to other [2]- and [3]rotaxanes consisting of different numbers of thiophene units in the axle component.

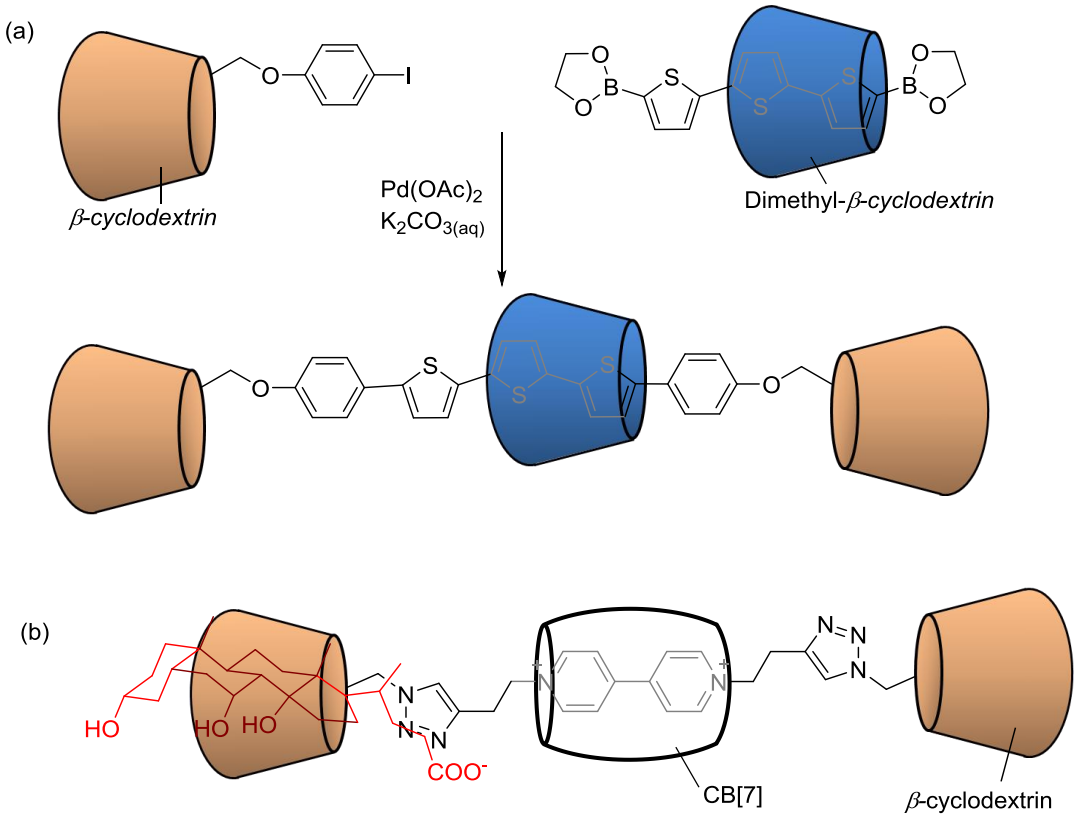

Scheme 3.1 Cyclodextrin-stoppered rotaxanes: (a) Harada's synthesis of a *β*-cyclodextrin stoppered oligo(thiphene) rotaxane.[27] Dimethyl-*β*-cyclodextrin forms the macrocycle component [*β*-cyclodextrin in which the hydroxyl groups 2-*O* and 6-*O* are methylated on each glucose monomer unit (Figure 3.7)]; (b) Liu's steroid-binding [2]rotaxane.[28]

Very recently, Liu and co-workers also reported a *β*-CD-stoppered [2]rotaxane, containing a cucurbit[7]uril macrocycle component, which was demonstrated to bind steroid guests by means of complexation within the cavity of the *β*-cyclodextrin stoppers (Scheme 3.1b).[28]

3.2.1 Synthesis of mono-functionalised permethylated *β*-cyclodextrin derivatives

The initial route undertaken to synthesise mono-functionalised *β*-cyclodextrin derivatives is shown in Scheme 3.2. Preparation of the primary rim mono-tosyl derivative (6^{A-}*O*-tosyl-*β*-CD)‡ **53** was conducted according to literature procedures.[24,29] *β*-Cyclodextrin and excess toluene-*para*-sulfonylchloride were stirred as a suspension in water for 3 hours, before the addition of 2 M aqueous sodium hydroxide. Ammonium chloride was added to adjust the solution to pH 8, and upon cooling the desired product **53** precipitated from solution in approximately 50% yield and 90% purity (as determined by ^{1}H NMR); the other major products being the parent cyclodextrin and a mixture of double-substituted products. Unfortunately, despite repeated recrystallisations from water, the purity of **53** could not be improved beyond around 95%. The synthesis was continued however, with the intention of conducting chromatographic purification following the methylation step. Conversion to the corresponding azide **54** was achieved by reaction with sodium azide in water, followed by permethylation with sodium hydride and CH_3I to afford **55**, as a mixture of the desired product, the bis-azide substituted product and permethylated *β*-cyclodextrin. Separation of the three components using silica gel column chromatography proved impossible however, due to the identical retention times of the two azide derivatives in the mixture.

‡ By convention, the glucose monomer in which substitution occurs is denoted *A*, the other six units are denoted *B* – *G*. Thus 6^A-*O*-tosyl-*β*-CD denotes that the tosylate group is on the oxygen atom bonded to carbon *6*, on glucose unit *A*.

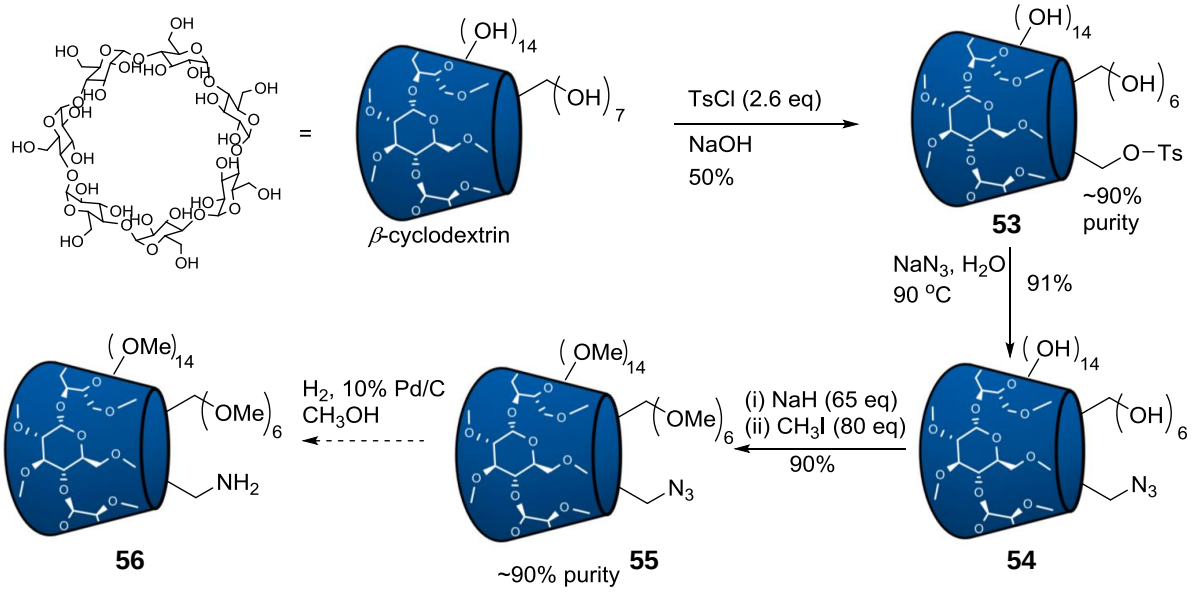

Scheme 3.2 Attempted synthesis of 6^{A}-amino-permethyl-*β*-cyclodextrin **56**.

Attention was then turned to an alternative synthetic procedure to prepare the target mono-functionalised derivatives. Bradshaw reported a one-pot method to afford 6^{A}-hydroxy-permethylated-*β*-CD **57**,[23] which is a useful precursor for the synthesis of a wide range of functional groups. The procedure involved selectively attaching a *tert*-butyldimethylsilyl group, which is relatively stable under normal conditions, to the primary 6-*O* hydroxy group of the glucose moieties. This silane protecting group can be easily removed using a fluoride source, avoiding the use of acid which may lead to decomposition of the cyclodextrin itself. Thus the initial step in the synthesis involved the statistical protection of one of the primary 6-*O* hydroxyl groups, by using a slight excess of *tert*-butyldimethylsilyl chloride in the presence of imidazole in DMF (Scheme 3.3). One-pot methylation of the mixture of silane-protected CD derivatives with NaH/CH_3I, followed by subsequent cleavage of the silyl groups with NH_4F in methanol, afforded the target 6^{A}-hydroxy-permethylated-*β*-CD, in addition to permethylated *β*-cyclodextrin and products containing two or more 6-*O* hydroxyl derivatives. In this case, the desired product could be separated from the by-products by careful silica gel column chromatography, using a 50:1 CH_3Cl/CH_3OH eluent, to afford compound **57** in 20% yield. A pure sample of permethylated *β*-cyclodextrin **58** was also isolated in 20% yield.

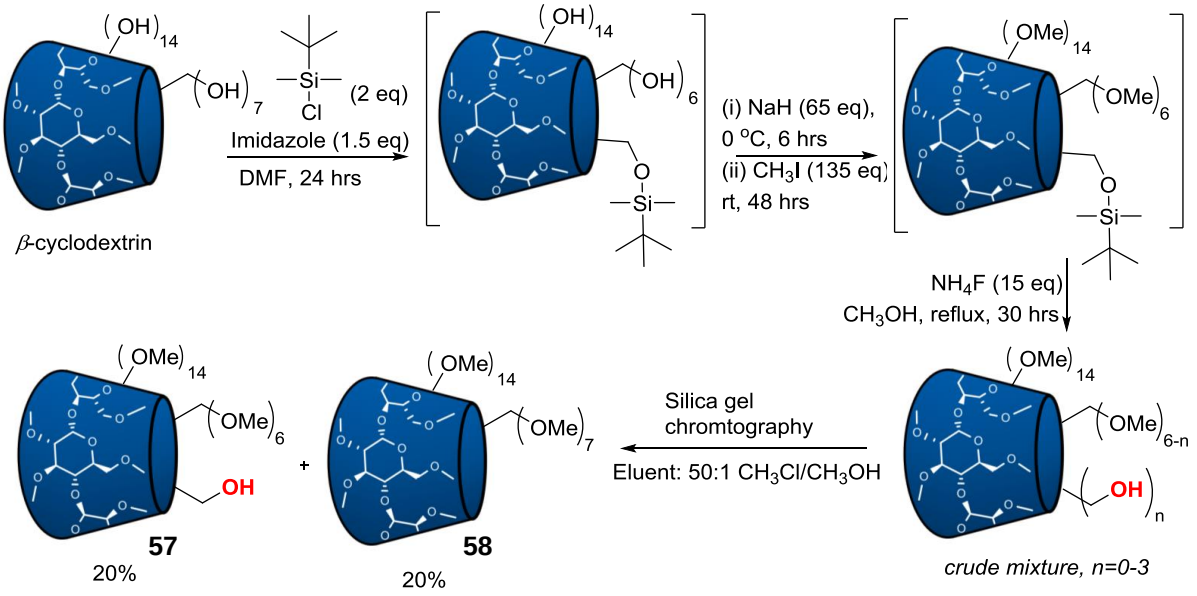

Scheme 3.3 Synthesis of 6^{A}-hydroxy-permethylated-*β*-CD **57** using Bradshaw's method.[23]

The principle disadvantage of this methodology, however, is its sensitivity to water which leads to reproducibility issues. It is believed that small quantities of water, trapped in the *β*-cyclodextrin cavity, react with sodium hydride in the methylation step to form a reactive hydroxide species that cleaves the silyl protecting groups, resulting in the overall formation of permethylated *β*-cyclodextrin **58**. Indeed, it was determined that commercial *β*-cyclodextrin contains 600 mol% water, and thus it proved necessary to dry the starting material under high vacuum and over phosphorus pentoxide for seven days prior to reaction.

As a consequence of the moisture sensitivity of this reaction, in addition to the long timescale of the procedure (six days from the initial silane addition to the final workup of the deprotected mixture), a third and final approach to mono-functionalisation of *β*-cyclodextrin was investigated. This method, reported by Sinaÿ and co-workers,[30] is conceptually distinct from the previous syntheses discussed above in that mono-functionalisation is achieved by de-*O*-methylation of permethylated *β*-cyclodextrin, as opposed to a statistical reaction being conducted prior to permethylation. This was achieved by the addition of seven equivalents of diisobutylaluminium hydride (DIBAL) to a toluene solution of **58** (prepared from *β*-cyclodextrin by methylation with NaH/CH_3I) and stirred at 50 ºC for three hours, before

quenching with 1 M $HCl_{(aq)}$ (Scheme 3.4). Purification by silica gel column chromatography using a 50:1 CH_3Cl/CH_3OH eluent afforded the desired 6^A-hydroxy-permethylated-*β*-CD **57** in 20% yield. The major product of the reaction is the $2^A,3^B$-diol **59**, isolated in 43% yield, whilst other by-products containing three or more de-alkylated hydroxyl groups were detected by mass spectrometry but not isolated. The isolated yields were comparable to those reported for this reaction in the literature.

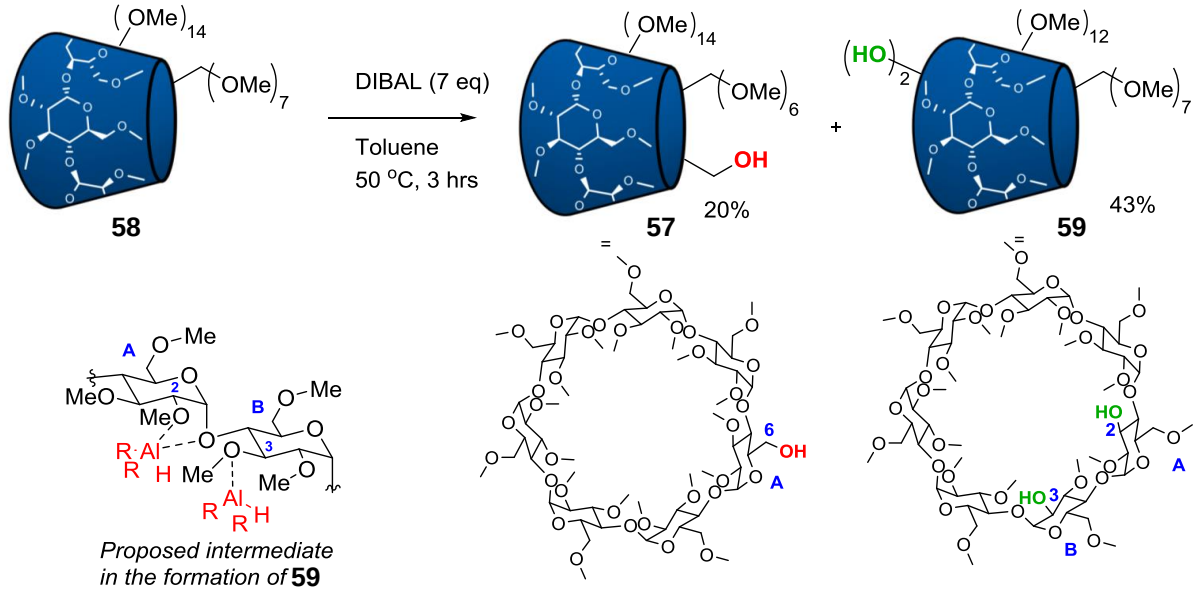

Scheme 3.4 Synthesis of 6^A-hydroxy-permethylated-*β*-CD **57** *via* DIBAL-promoted de-*O*-methylation of permethylated *β*-cyclodextrin **58**.[30] Inset: proposed bis-aluminium intermediate in the formation of $2^A,3^B$-diol **59**.[31]

The authors have proposed that the de-methylation reaction involves two molecules of aluminium reagent, and that the observed $2^A,3^B$ selectivity is a result of the preferential initial chelation of an active aluminium species by the 2^A-*O* and 3^B-*O* atoms, which point away from the cavity of the cyclodextrin (Scheme 3.4, inset).[31] Subsequent rate-limiting de-alkylation of 3^B-*O* is followed by a faster, second de-alkylation of 2^A-*O* to afford $2^A,3^B$-diol **59** following acidic work up. De-alkylation of the less hindered, primary 6-*O* hydroxy groups competes with this process, resulting in the formation of 6^A-hydroxy-permethylated-*β*-CD **57**.

This route to mono-functionalisation of permethylated *β*-cyclodextrin, affords **57** in comparable yield to the silyl-protection route and offers considerable advantages. Firstly,

although the cyclodextrin needs to be dried under vacuum prior to the reaction, the procedure is less sensitive to moisture owing to the presence of an excess of aluminium reagent, and secondly, the reaction time is significantly reduced from an overall time of six days to just three hours. Attempts to alter the product distribution of the reaction in favour of **57** over diol **59** by reducing the number of equivalents of DIBAL were unsuccessful, merely lowering the overall yield whilst the ratio of cyclodextrin derivative products **57–59** remained unchanged.

With 6^A-hydroxy-permethylated-*β*-CD **57** in hand, functional group inter-conversion to the desired amino-derivative **56** was achieved (Scheme 3.5) using standard literature procedures.[29] Conversion to the azide **55**, *via* the intermediate mesylate **60**, proceeded in high yield. Initial attempts to prepare the target amine **56** using the reported reduction conditions of H_2 (5 atm), Pd/C (10wt%) in ethanol solution failed to realise greater than 50% conversion, even after seven days. Pleasingly, however, reduction using hydrazine hydrate at 50 ºC, in the presence of Pd/C (10wt%), afforded the target amine **56** in a near quantitative yield after one hour without the need for additional purification.

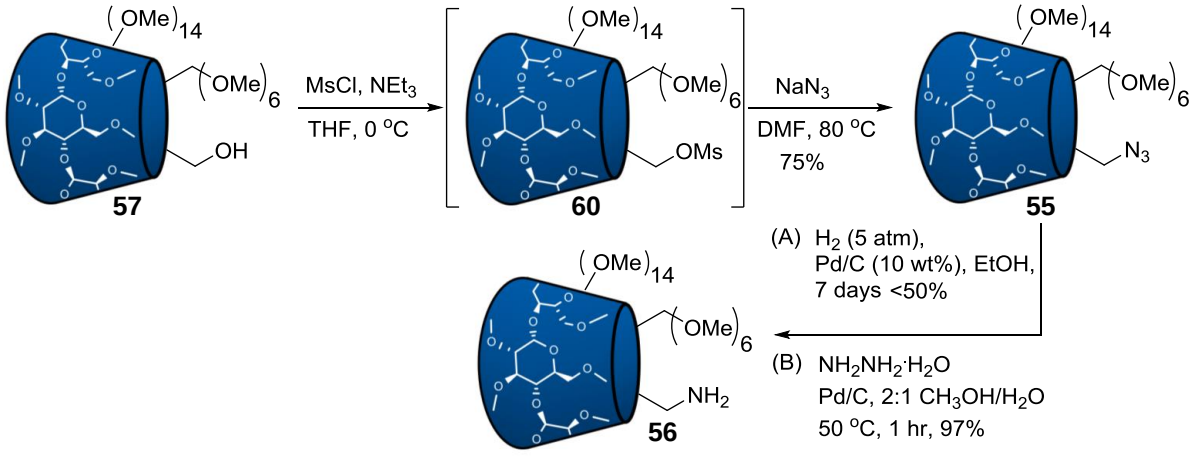

Scheme 3.5 Synthesis of 6^A-amino-permethyl-*β*-cyclodextrin **56**.[29]

3.2.2 Synthesis of water soluble hydrogen bonding 3,5-bis-amide pyridinium rotaxane

Initially the synthesis of a permethylated-*β*-CD-stoppered 3,5-bis-amide pyridinium rotaxane was attempted to ascertain whether cyclodextrin moieties imparted water solubility on the structure and were sufficiently large to prevent de-threading of the macrocycle.

The permethylated-*β*-CD-stoppered 3,5-bis-amide pyridinium axle component **62·Cl** was prepared as shown in Scheme 3.6. An EDC-mediated amide coupling reaction of 3,5-pyridine dicarboxylic acid with two equivalents of 6^A-amino-permethyl-*β*-cyclodextrin **56** afforded pyridine axle precursor **61**, which was methylated with CH_3I to give **62·I**. Anion exchange to the chloride salt, in preparation for chloride-templated rotaxane formation, was achieved by passing down a chloride-loaded Amberlite® column in 7:3 acetone/water, to afford **62·Cl** in 90% yield over two steps.

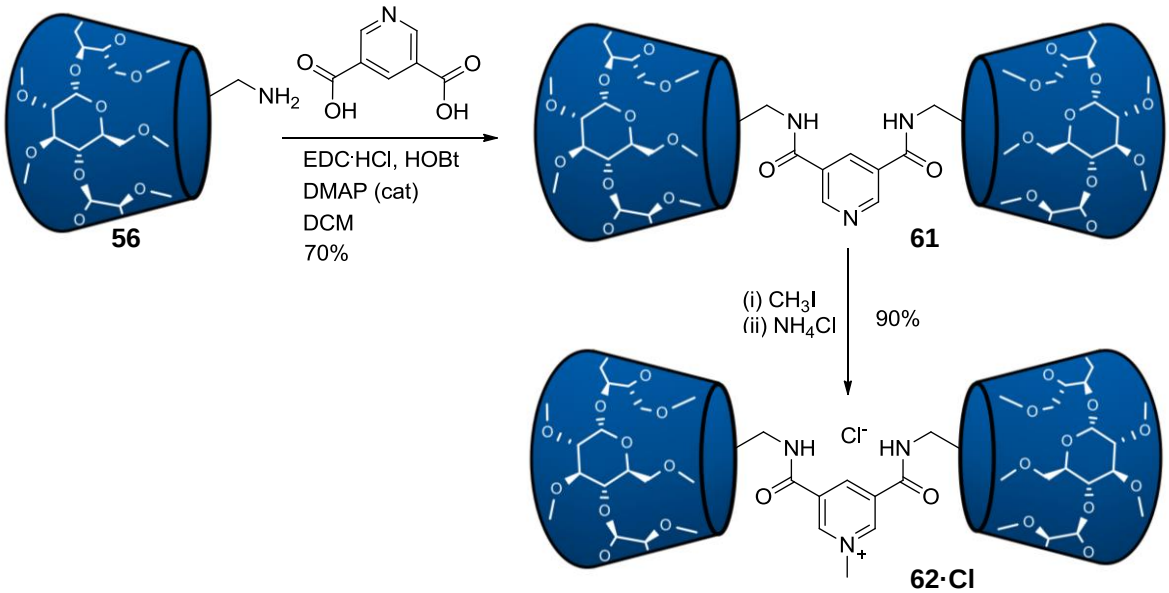

Scheme 3.6 Synthesis of 3,5-bisamide pyridinium axle **62·Cl**.

Rotaxane synthesis was achieved *via* the chloride templation approach[32] used in the synthesis of [3]rotaxane **1·(Cl)$_2$** (Chapter 2), by stirring one equivalent of axle **62·Cl** with one equivalent of bis-amine **16** in the presence of 3,5-bis-chlorocarbonyl pyridine and NEt_3 in dry dichloromethane for three hours (Scheme 3.7). The target rotaxane **63·Cl** was formed in approximately 5% yield, as determined by analysis of the ^{1}H NMR spectrum of the crude reaction mixture. Significant improvement of the yield could be achieved, however, by adding an excess (10 equivalents) of bis-amine **16** and 3,5-bis-chlorocarbonyl pyridine, affording **63·Cl** in an isolated yield of 33% following purification by preparative TLC and size-exclusion chromatography.

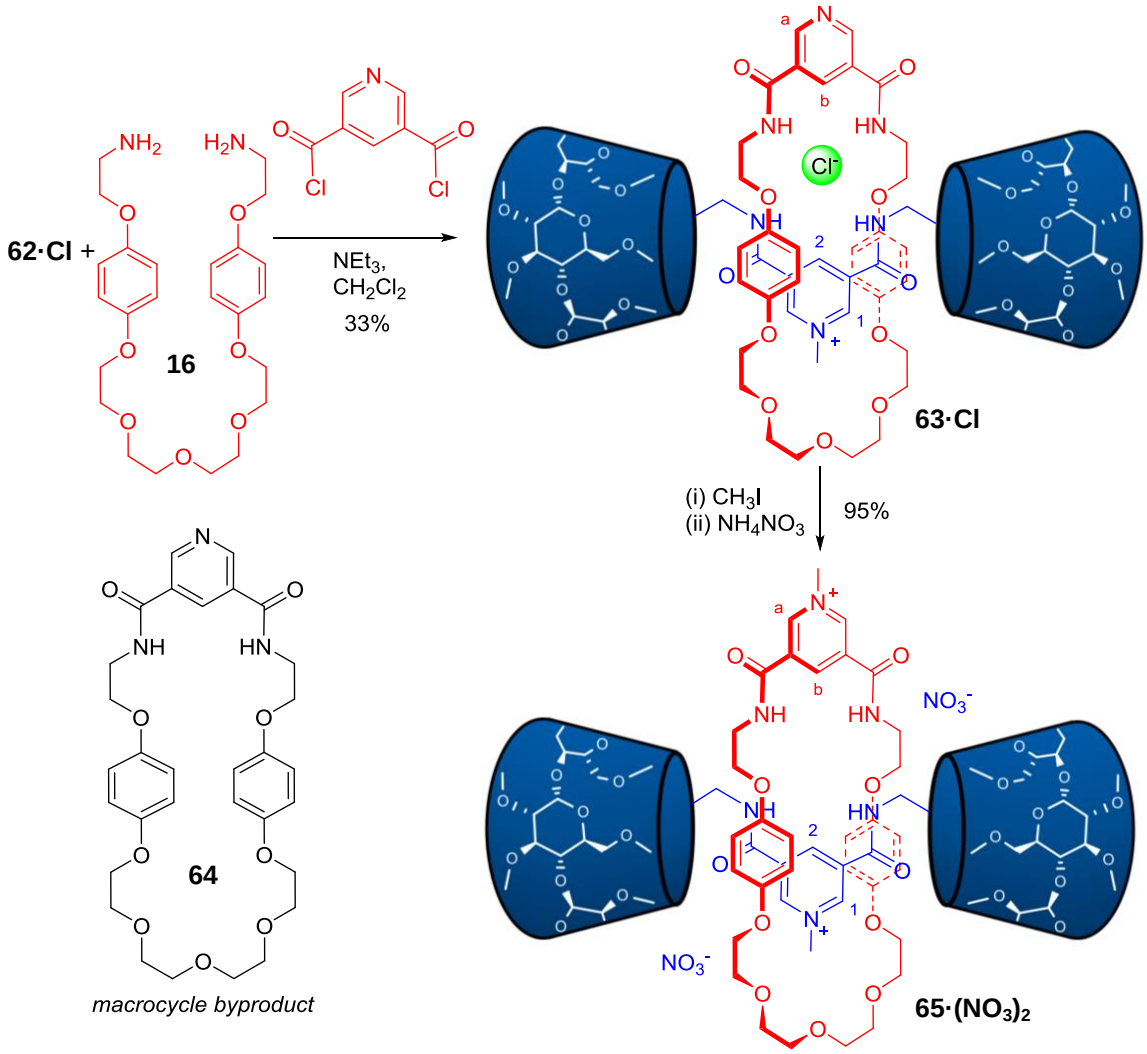

Scheme 3.7 Synthesis of 3,5-bis-amide pyridinium rotaxane **65·(NO$_3$)$_2$**.

The other products from the reaction were non-interlocked axle **62·Cl** and ring-closed pyridine macrocycle **64**. Presumably, the bulky cyclodextrin stoppers hinder the cyclisation of the macrocycle precursors around the axle component, resulting in a lower yield than reported for the analogous terphenyl-stoppered rotaxane (56%, with one equivalent of macrocycle precursors).[6]

The ^{1}H NMR spectra of rotaxane **63·Cl**, macrocycle **64**, and axle **62·Cl** are compared in Figure 3.8. Protons *b* and *2* shift significantly downfield in the rotaxane, whilst macrocycle hydroquinone protons *c* and *d* are split and perturbed upfield, which is characteristic of aromatic donor–acceptor interactions between the electron rich hydroquinones in the macrocycle and the electron-deficient pyridinium motif in the axle, and is consistent with the pyridinium motif intercalating between the macrocycle hydroquinone groups in the rotaxane structure.

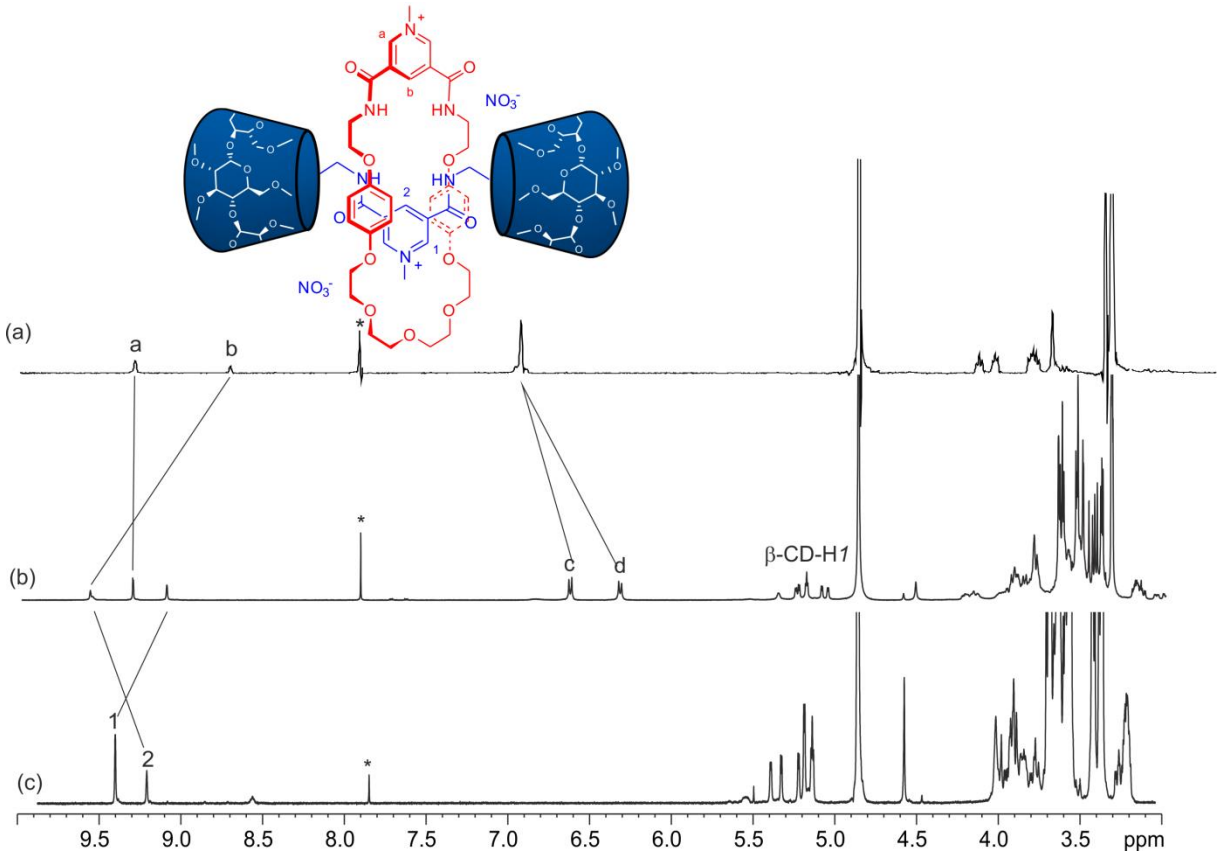

Figure 3.8 ^{1}H NMR spectra of (a) macrocycle **64**, (b) rotaxane **63·Cl** and (c) axle **62·Cl** in 1:1 $CDCl_3/CD_3OD$ (500 MHz, 298 K).

Additional evidence for the interlocked nature of the rotaxane was found in the two dimensional ^{1}H ROESY NMR spectrum of **63·Cl**, in which through-space interactions are obserevd between the macrocycle hydroquinone protons and the pyridinium protons of the axle component (Figure 3.9a).

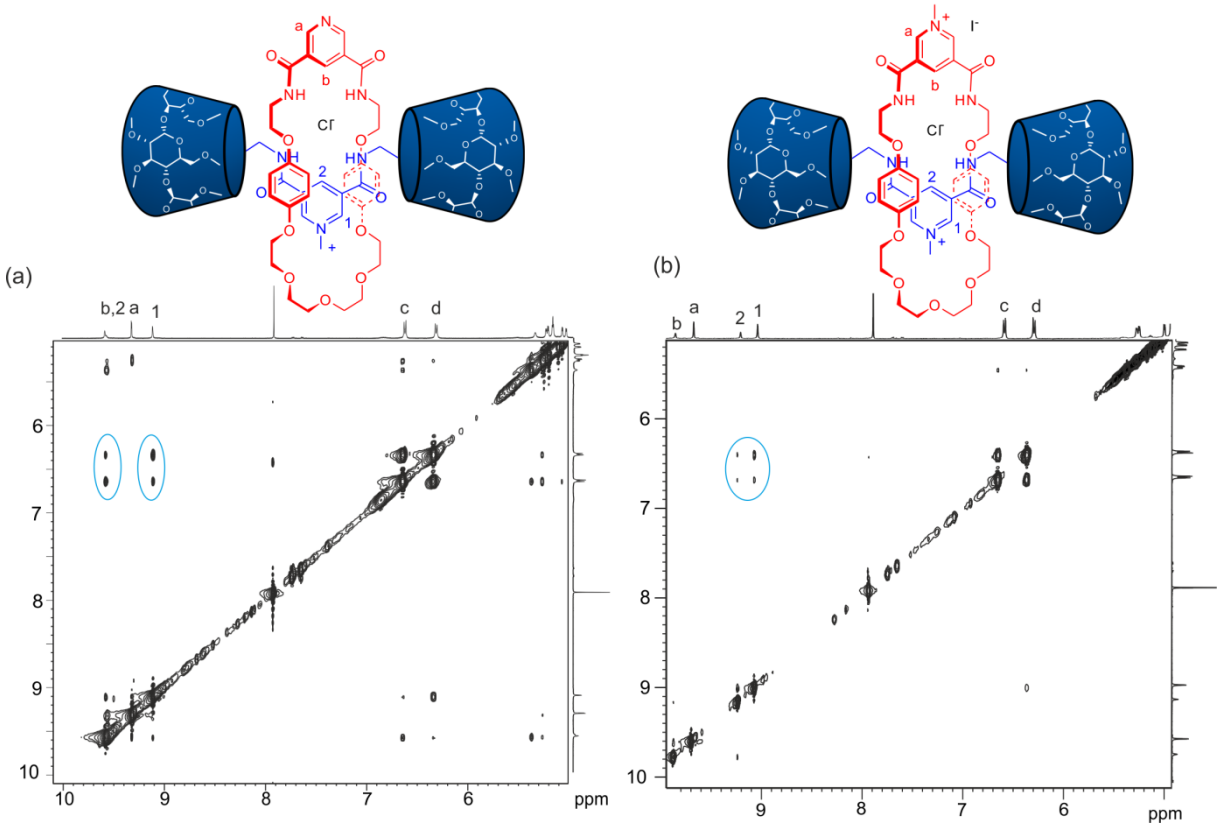

Figure 3.9 Section of the ^{1}H ROESY NMR spectrum in 1:1 $CDCl_3/CD_3OD$ (500 MHz, 298 K) of: (a) mono-cationic rotaxane **63·Cl** and (b) dicationic rotaxane **65·I·Cl**. Selected cross-peaks indicating through-space interactions between the interlocked macrocycle and axle components are highlighted

The dicationic rotaxane **65**$^{2+}$ (Scheme 3.7) was prepared by methylation of the pyridine moiety of the macrocycle component of rotaxane **63·Cl** using CH_3I, to give the dicationic rotaxane as the mixed chloride-iodide salt. The hydroquinone protons of rotaxane **65·I·Cl** remain upfield shifted, and through-space interactions in the ^{1}H ROESY NMR spectrum between the macrocycle and axle components are observed, indicating that the interlocked nature of the rotaxane is preserved upon methylation (Figure 3.9b).

In order to probe the anion binding properties in water of rotaxane **65**$^{2+}$, it was necessary to exchange the halide counter anions for the corresponding water-soluble, weakly coordinating nitrate anion. This was achieved by passing a solution of **65·I·Cl** in 7:3 acetone/water through a nitrate-loaded Amberlite® column, to afford **65·(NO$_3$)$_2$**. Pleasingly, the rotaxane nitrate salt was sufficiently soluble in D_2O to obtain a ^{1}H NMR spectrum at 1.5 mM concentration (Figure 3.10).

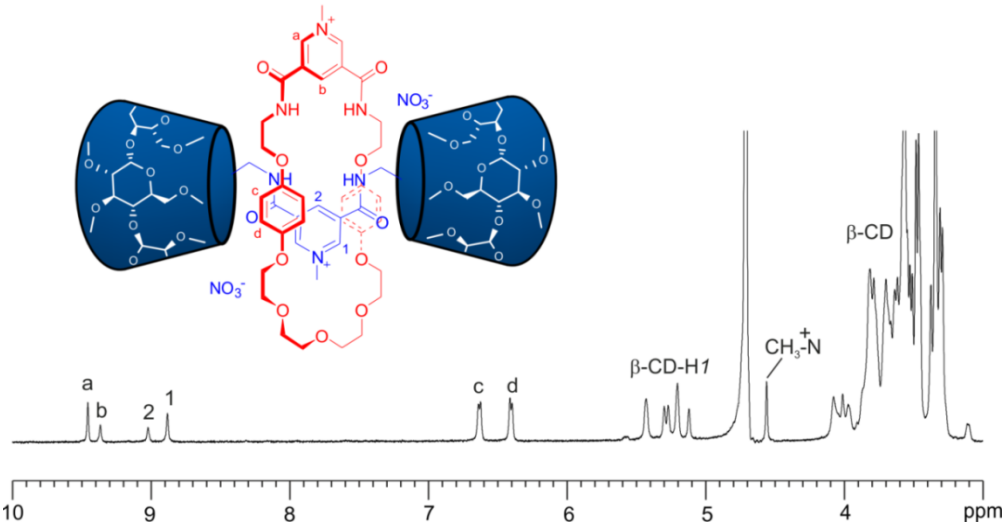

Figure 3.10 ^{1}H NMR of dicationic [2]rotaxane **65·(NO$_3$)$_2$** in D_2O (500 MHz, 298 K).

3.2.3 Anion recognition studies on 3,5-bis-amide pyridinium receptors

The anion recognition properties of rotaxane **65·(NO$_3$)$_2$** were investigated using ^{1}H NMR titration experiments, by adding increasing amounts of the sodium salts of Cl^-, Br^-, I^- and SO_4^{2-} to a 1.5 mM solution of rotaxane in D_2O.

Addition of halide anions caused downfield perturbations of the chemical shift of the pyridinium protons, the largest magnitude of which occurred with the macrocycle proton *b*, indicative of halide anion binding within the interlocked cavity (representative spectra from the titration with iodide are shown in Figure 3.11a).

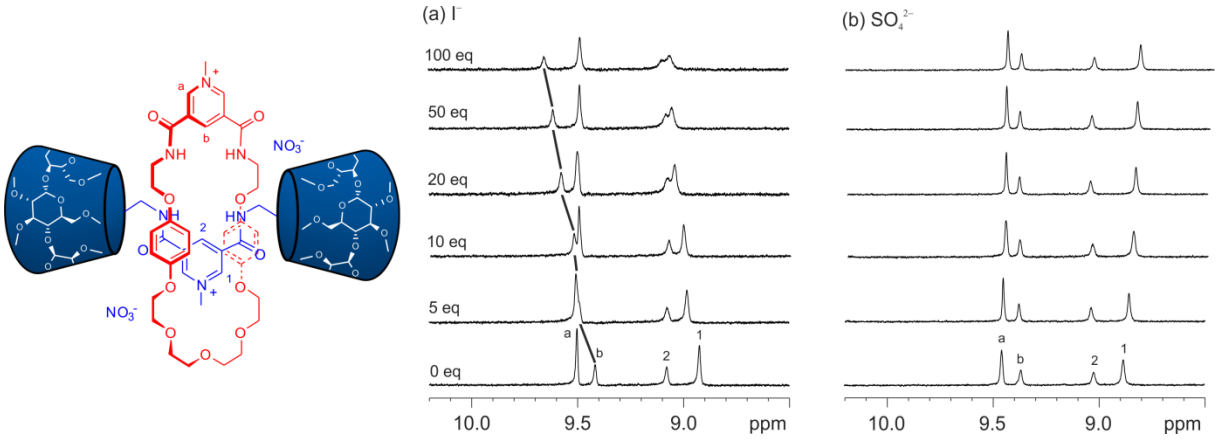

Figure 3.11 Changes in the ^{1}H NMR spectrum of rotaxane **65·(NO$_3$)$_2$** in D_2O (500 MHz, 298 K) upon addition of (a) NaI and (b) Na_2SO_4.

In contrast, addition of sulfate resulted in negligible perturbation of these protons, suggesting that the oxo-dianion is not bound by the rotaxane host (Figure 3.11b). The chemical shift perturbations of proton *b* upon halide anion addition was monitored as a function of anion concentration (Figure 3.12), and WinEQNMR2[33] analysis of the titration data determined the 1:1 stoichiometric association constants reported in Table 3.1.

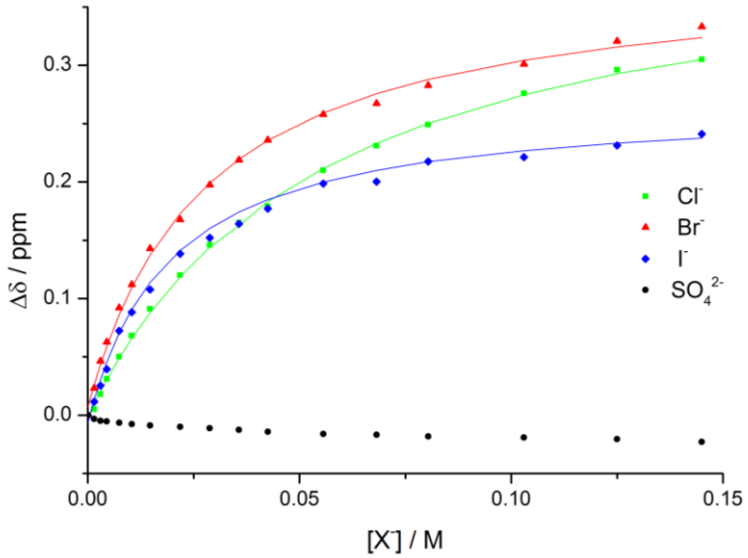

Figure 3.12 Plots of chemical shift change against anion concentration in D_2O (T = 298 K) for proton *b* of rotaxane **65·(NO$_3$)$_2$**. Actual data represented by solid symbols, calculated 1:1 host–guest binding isotherm represented by solid lines.

The halide anions are bound in the order $Cl^- < Br^- < I^-$. This binding selectivity is presumably dominated by the Hofmeister series[34] bias towards the larger, less highly solvated halide anions. The sulfate anion is too large to penetrate the binding cavity, which, combined with a high solvation energy, results in no binding of the anion by the rotaxane host.

Table 3.1 Anion association constants (K_a) in D_2O.

	K_a (M^{-1})[a]			
	Cl^-	Br^-	I^-	SO_4^{2-}
Rotaxane **65·(NO$_3$)$_2$**	15	35	50	-[b]
Axle **62·NO$_3$**	-[b]	-[b]	-[b]	-[b]

T = 298 K, anions added as the sodium salt. [a] Calculated using chemical shift data of proton *b*. Errors estimated to be <10%. [b] No binding.

For comparison, analogous titrations were conducted with the nitrate salt of the non-interlocked axle component **62·NO$_3$**. No perturbations of the pyridinium protons *1* and *2* were observed upon addition of either the halides or sulfate, indicating that this simple hydrogen bonding receptor is unable to complex these anionic species in pure water.

Receptors reported to date that are capable of recognition of halides in pure water typically bind sulfate with much higher affinity and therefore the selectivity of the rotaxane for the halides over sulfate is particularly notable. For instance, the ratio of $K_a(SO_4^{2-})/K_a(I^-)$ for Kubik's neutral cyclo-peptide (Figure 3.1a) is ~4 (the best yet reported), whilst for Lehn's hexa-protonated aza-cryptand (Figure 3.1b) the ratio is much higher (~60). The unprecedented selectivity for the halides observed in rotaxane **65·(NO$_3$)$_2$** results in part from the large sulfate anion being unable to penetrate the geometrically restrained interlocked binding cavity, which suggests that this strategy may prove fruitful for designing halide receptors that function in biological and environmental media, where competing oxoanions are prevalent. The magnitude of the halide association constants however, are relatively low, and reflecting the energetic penalty of anion desolvation in water. It would be advantageous to enhance these values further whilst maintaining the selectivity over the sulfate anion; and strategies to achieve this goal are discussed in the following sections.

3.2.4 Towards enhanced anion recognition in rotaxane hosts by exploiting the host–guest chemistry of cyclodextrins

In the work discussed so far in this chapter, the permethylated *β*-cyclodextrin derivatives have been utilised as water-solubilising stopper components for rotaxane synthesis. As was eluded to in Section 3.2, the host–guest chemistry of cyclodextrin derivatives is well established, with both the parent *β*-cyclodextrin and functionalised derivatives able to complex hydrophobic guest molecules within the cavity in aqueous solution, with association constants in the region of log K_a = 2–4. It was envisaged that by including hydrogen-bond-donating guest species within the cyclodextrin stopper components of rotaxane **65·(NO$_3$)$_2$**, the anion association strength within the interlocked binding cavity may be enhanced by virtue of the additional stabilising hydrogen bond (HB) interactions (Figure 3.13).

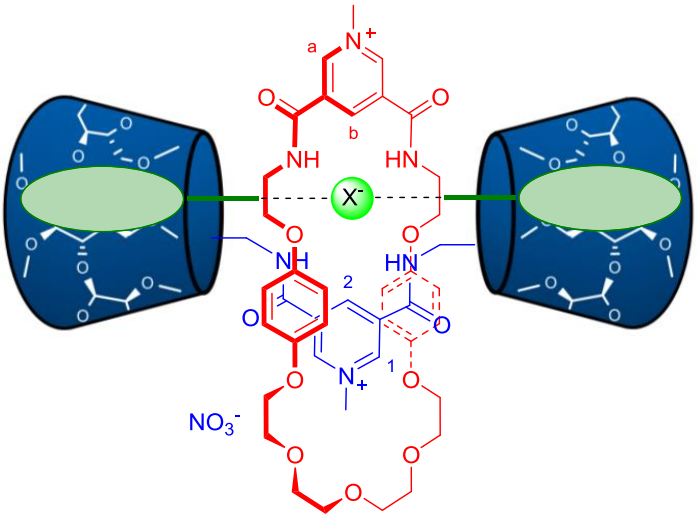

Figure 3.13 Schematic representation of the target quaternary complex formed between rotaxane **65·(NO$_3$)$_2$**, an anion and two hydrogen-bond-donating aromatic guests (green) included within the cyclodextrin stopper components.

To this end, ^{1}H NMR titrations were conducted to determine the iodide binding affinity of rotaxane **65·(NO$_3$)$_2$** in the presence of HB-donating species that are known to be encapsulated within *β*-cyclodextrin derivatives. A variety of HB-donor guests were screened, by preparing a solution of rotaxane **65·(NO$_3$)$_2$** and guest in D_2O at concentrations of 1.5 mM and 3 mM respectively, before conducting the iodide binding titration as previously described. The association constants for the aromatic guest binding within the cyclodextrin stoppers were expected to be of the order of log K_a = 3, based on values for similar aromatic compounds reported in the literature,[20] and thus the rotaxane–guest ternary complex could be assumed to be the dominant species in solution at this concentration. In each case changes in the chemical shift of the guest's aromatic protons upon complexation with the rotaxane provided qualitative evidence as to the formation of the inclusion complex. It is important to note, however, that the anion association constants determined by monitoring the rotaxane's cavity protons reflects the binding of the anion by the equilibrium mixture in solution (namely the rotaxane·guest(s) complexes and free rotaxane) and not one discrete species. The HB-donor guest species used in this study are shown in Figure 3.14, and were converted to the weakly-coordinating nitrate salt, where necessary, using a nitrate-loaded Amberlite® column. The bis-guanidinium biphenyl compound **68·(NO$_3$)$_2$** was prepared from the corresponding bis-amine (kindly donated by Dr Thomas Lang) using 1*H*-pyrazole-1-carboxamidine hydrochloride in DMF.[35]

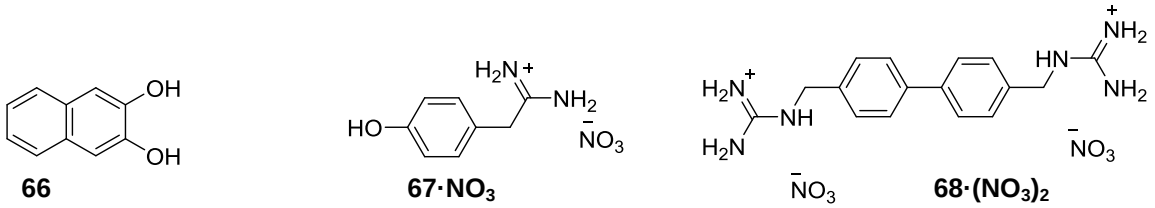

66 **67·NO$_3$** **68·(NO$_3$)$_2$**

Figure 3.14 Hydrogen bonding aromatic guests.

Cyclodextrin derivatives are known to be unable to bind positively charged aromatics, and hence in both amidinium **67**$^{+}$ and guanidinium **68**$^{2+}$ the positively charged moieties are not conjugated to the aromatic core, which itself remains relatively electron rich, to ensure that inclusion within the cyclodextrin stopper cavities remains favourable. In the case of the neutral naphthalene guest **66** the determined apparent association constant value with iodide was of similar magnitude (K_a = 50 M^{-1}) to that obtained with the free rotaxane. In contrast, with the charged HB-donor derivatives **67·NO$_3$** and **68·(NO$_3$)$_2$**, the association constants were found to be diminished (K_a = 35 and 30 M^{-1} respectively, compared to K_a = 50 M^{-1} with the free rotaxane host). Presumably this results from the charged amidinium and guanidinium motifs competing with the iodide binding within the rotaxane cavity. This suggests that the geometry of the host–guest complex is not as depicted in Figure 3.13: indeed the structure may adopt a geometry in which the charged HB-donor groups are not directed into the binding cavity. Furthermore, the asymmetric guests **66** and **67·NO$_3$** can be included within the cyclodextrins in two possible orientations, such that the HB-donor groups are directed out of either the narrow or wide rim, of which the latter is more favourable on steric grounds. A possible solution may involve preparing the analogous rotaxane host in which the cyclodextrins are functionalised on the wide rim, such that the HB-donors converge into the rotaxane's anon binding cavity.

Due to the low anion binding constants obtained in D_2O for hydrogen bonding rotaxane **65·(NO$_3$)$_2$**, and the failure to improve the recognition properties by using additional hydrogen bond donors included within the rotaxane's cyclodextrin stopper motifs, attention turned to incorporating halogen bond donors within the rotaxane architecture, to investigate the possibility of enhancing anion association using this underexplored intermolecular interaction.

3.3 Incorporating halogen bond donors within acyclic and rotaxane hosts for enhanced anion recognition in water

3.3.1 Halogen bonding anion receptor design

Since the development of the copper(I) catalysed azide–alkyne (CuAAC) click reaction in 2002 by Sharpless and co-workers,[36] in which a regioselective [3+2] cycloaddition of azides and terminal alkynes affords 1,4-disubstituted-1,2,3-triazole compounds in the presence of a copper(I) catalyst, the reaction has been exploited extensively across a wide range of chemical sciences.[37] Of particular relevance to the field of anion coordination is work by Flood and co-workers, who in 2008 established that pre-organised anion receptors incorporating the 1,2,3-triazole group are capable of binding anions in CH_2Cl_2 solely through polarized C–H hydrogen bonds.[38] Subsequently, numerous anion receptors containing these heterocycles have been reported.[39] In particular, White and Beer described the bidentate bis-triazole pyridinium motif, which recognises anions through two polarised convergent C–H hydrogen bonds (Figure 3.15a).[40] Furthermore, the recent development of synthetic strategies to prepare the 5-halo-1,2,3-triazole motif[41,42] has opened up the possibility of preparing halogen bonding analogues of such receptors. In recent unpublished work, Sean Robinson, a DPhil student working in these laboratories, prepared 3,5-bis-iodotriazole pyridinium acyclic and catenane based anion receptors, which recognise anions through two convergent C–I halogen bonds (Figure 3.15b).

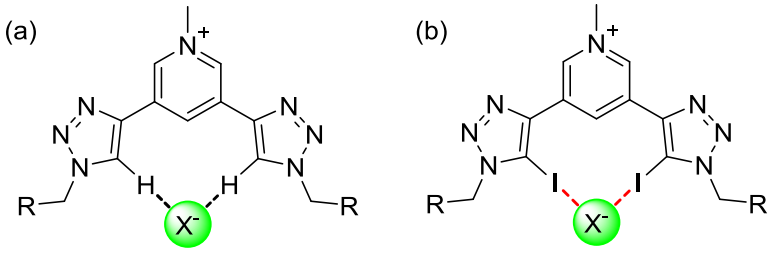

Figure 3.15 3,5-Bis-triazole pyridinium anion receptor motif: (a) bis-*proto*triazole hydrogen bond donor and (b) bis-*iodo*triazole halogen bond donor analogue.

In essence, replacing the triazole protons of the prototriazole-based receptor with iodine atoms directly interchanges HB-donors with XB-donors within an otherwise identical structural framework, and thus facilitates the direct comparison of the two intermolecular interactions with anions in solution. Importantly, in unpublished work, the solid state structure of the chloride salt of an octyl-appended 3,5-bis-iodotriazole pyridinium receptor (Figure 3.16) reveals the XB-donor bis-iodotriazole pyridinium motif remain planar, whilst forming two strong XB interactions with the halide anion, as deduced from the short $I^{\cdots}Cl^{-}$ contacts, which vary between 3.120(2)–3.195(2) Å, equivalent to 84–86% of the sum of the van der Waals radii. This indicates that this XB-donor motif is iso-structural with the prototriazole HB-donor system, in which the bis-triazole pyridinium motif is also planar, forming two hydrogen bonds to the anion guest.[43] The integration of the bis-prototriazole and bis-iodotriazole pyridinium motifs into permethylated-β-CD stoppered axle components, in preparation for rotaxane synthesis, is described in the following section, and was carried out in collaboration with Sean Robinson.

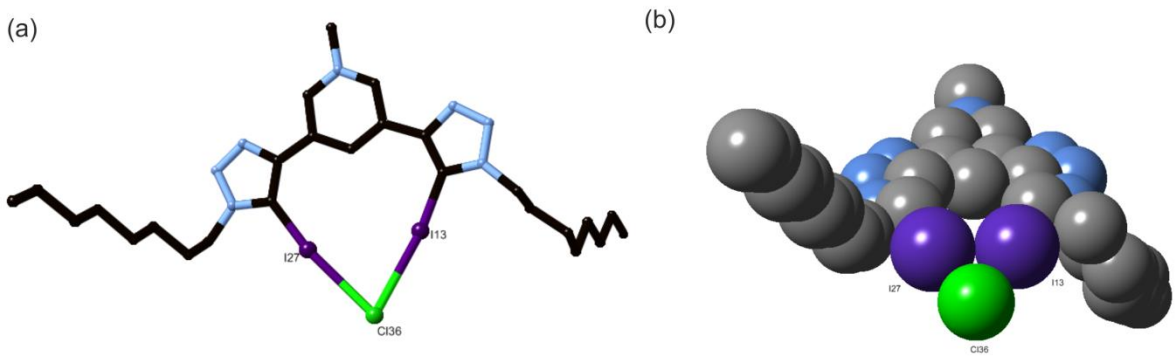

Figure 3.16 (a) Solid state structure of the chloride salt of octyl-appended 3,5-bis-iodotriazole pyridinium receptor and (b) space filling model. *d* ($I^{\cdots}Cl^{-}$) = 3.120(2)–3.195(2) Å, ΣvdW = 84–86%.

3.3.2 Synthesis of cyclodextrin-stoppered bis-prototriazole and bis-iodotriazole pyridinium rotaxanes

The synthetic procedure used to prepare the cyclodextrin-appended bis-prototriazole and bis-iodotriazole pyridinium axle components **72·Cl** and **73·Cl** is shown in Scheme 3.8. 3,5-Diethynylpyridine was prepared by Sean Robinson in two steps from 3,5-dibromopyridine by a Sonogashira[44] reaction with TMS-acetylene to afford the TMS-protected alkyne,[45] which was subsequently deprotected using KOH in methanol[46] to give the desired bis-alkyne **69** in 55% yield.

Synthesis of the 3,5-bis-triazole pyridine intermediates **70** and **71** was achieved using modified copper(I)-catalysed azide–alkyne (CuAAC) click reactions between just over two equivalents of 6^A-azido-permethylated-*β*-cyclodextrin **55** and 3,5-diethynylpyridine **69** (Scheme 3.8). The iodotriazole product **70** was prepared according to the one-pot procedure reported by Zhu and co-workers,[42] using a copper(II) perchlorate hexahydrate catalyst in the presence of sodium iodide, diazabicyclo[5.4.0]undec-7-ene (DBU) and tris-(benzyltriazolylmethyl)amine (TBTA). The reaction was initially conducted in THF, as per Zhu's reported procedure, which afforded the desired compound **70** in 25% yield. In contrast, when the reaction was conducted in acetonitrile a complex mixture of the desired 3,5-bis-*iodo*triazole pyridine product, 3-*iodo*triazole-5-*proto*triazole pyridine and 3,5-bis-*proto*triazole pyridine was obtained, which could not be separated by chromatographic methods. Pleasingly, when the reaction was repeated in a 1:1 THF/CH_3CN solvent mixture, however, the yield was significantly enhanced, affording compound **70** in 65% yield.

The synthesis of analogous 3,5-bis-*proto*triazole pyridine intermediate **71** from the same starting materials was achieved in 52% yield using a $Cu(CH_3CN)_4PF_6$ catalyst in the presence of TBTA and diisopropylethylamine (DIPEA) in CH_2Cl_2 solution.

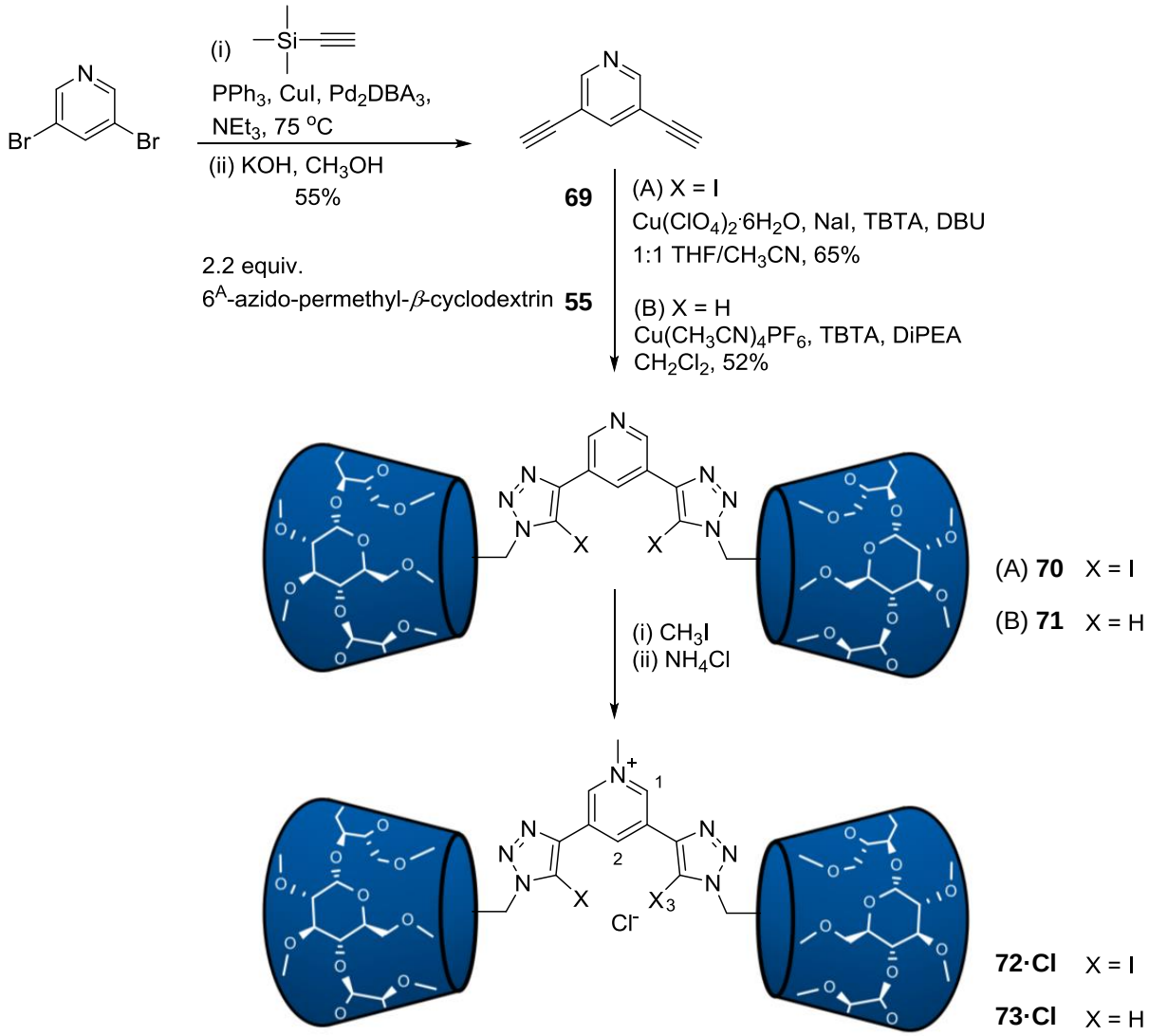

Scheme 3.8 Synthesis of 3,5-bistriazole pyridinium axle components **72·Cl** and **73·Cl**.

The bis-triazole pyridine intermediates were subsequently methylated using CH_3I to afford **72·I** and **73·I** and the iodide counter anions exchanged using a chloride-loaded Amberlite® column in 7:3 acetone/water, to afford **72·Cl** and **73·Cl**, respectively, in preparation for chloride-templated rotaxane synthesis.

Further samples of both compounds were converted to the weakly coordinating nitrate salts in readiness for anion recognition studies, by passing down a nitrate-loaded Amberlite® column to yield **72·NO_3** and **73·NO_3**.

Rotaxane formation was achieved using the same chloride templation methodology used to prepare permethylated-*β*-cyclodextrin stoppered rotaxane **63·Cl** (*vide supra*). The chloride salts of axles **72·Cl** and **73·Cl** were stirred with 10 equivalents of bis-amine macrocycle precursor **16** and 3,5-bis-chlorocarbonyl pyridine in dry CH_2Cl_2, in the presence of NEt_3 (Scheme 3.9).

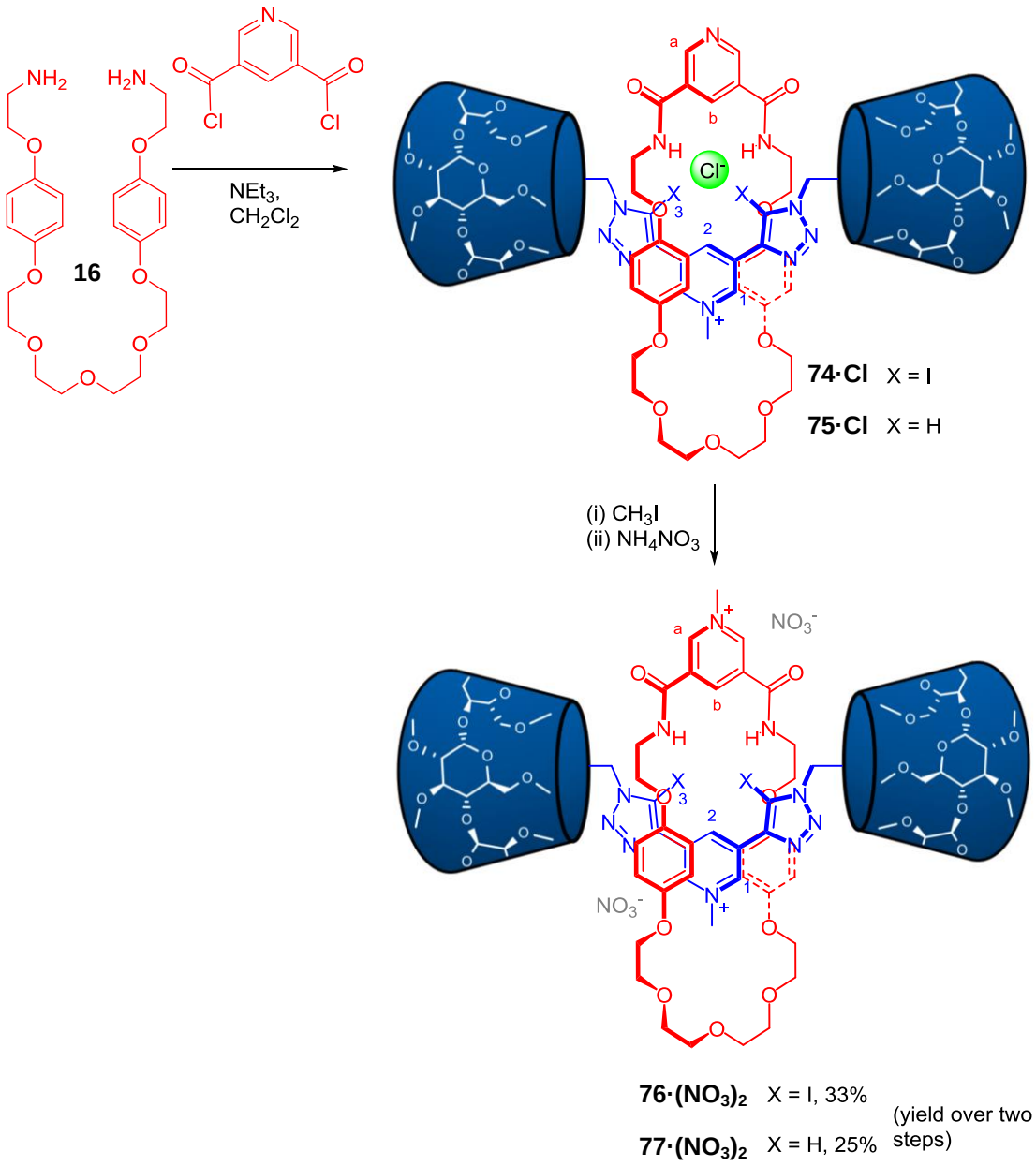

Scheme 3.9 Chloride-anion templated synthesis of XB and HB rotaxanes **76·$(NO_3)_2$** and **77·$(NO_3)_2$**.

Purification by preparative TLC allowed the isolation of the corresponding mono-cationic halogen bonding rotaxane **74·Cl** in 37% yield, the major byproducts being the respective non-interlocked components (axle **72·Cl** and macrocycle **64**). In the case of the analogous mono-cationic hydrogen bonding rotaxane **75·Cl**, attempted purfication by both preparative TLC and size exclusion chromatography failed to remove the macrocycle byproduct entirely. ^{1}H NMR analysis of the rotaxane–macrocycle mixture, however, revealed that the rotaxane was formed in appoximately 26% yield. Methylation of XB rotaxane **74·Cl** with CH_3I afforded the dicationic rotaxane **76**$^{2+}$ in 96% yield, as the mixed chloride–iodide salt. The impure HB rotaxane **75·Cl** was also subjected to the same conditions to afford pure **77**$^{2+}$ as the mixed halide salt in a yield of 25% over two steps, following successful purification using preparative TLC. Anion exchange of both rotaxanes to the nitrate salts in preparation for anion recognition studies was achieved by passing a solution of the respective rotaxane in 7:3 acetone/water down a nitrate-loaded Amberlite® column, to afford **76·(NO$_3$)$_2$** and **77·(NO$_3$)$_2$**.

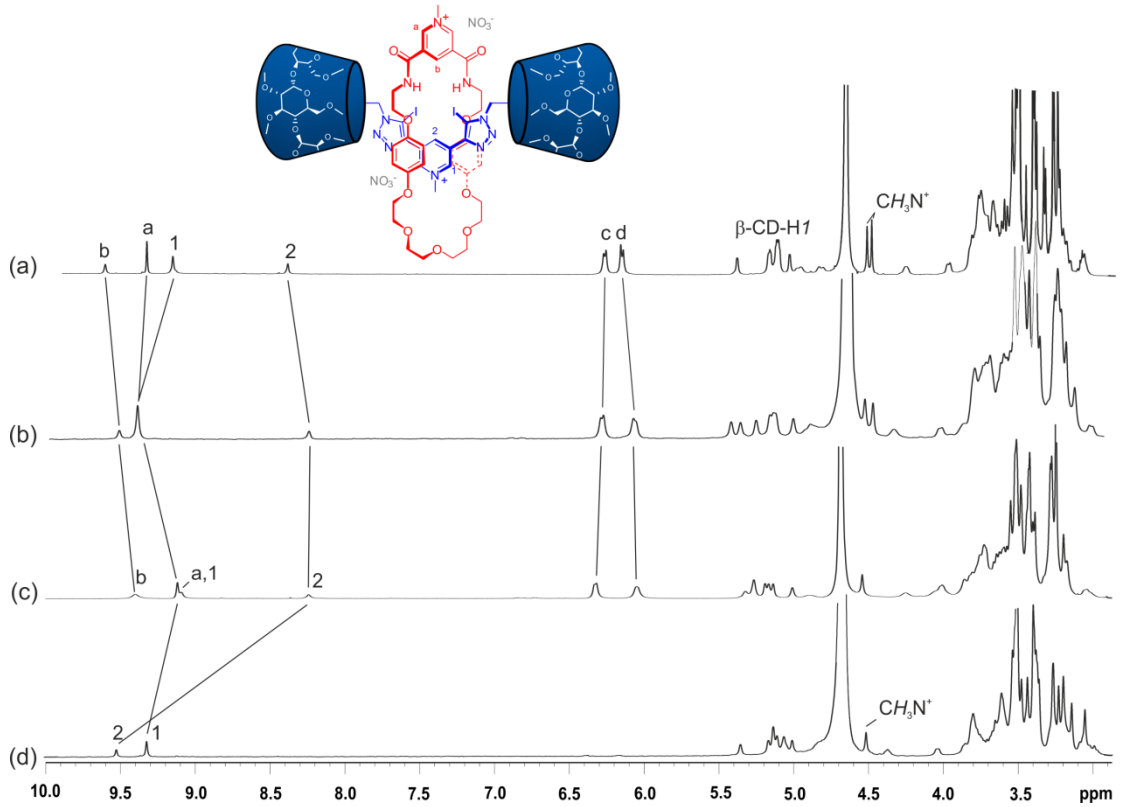

Figure 3.17 ^{1}H NMR spectra of XB rotaxane **76·(NO$_3$)$_2$** and precursors in D_2O (500 MHz, 298 K): (a) dicationic rotaxane **76·(NO$_3$)$_2$** and (b) **76·Cl·I**; (c) mono-cationic rotaxane **74·**Cl and (d) axle **72·Cl**.

The rotaxane structures were characterised by ^{1}H and ^{13}C NMR spectroscopy, and high-resolution electrospray mass spectrometry (HRMS). The ^{1}H NMR spectra of axle **72·NO$_3$**, monocationic XB rotaxane **74·Cl**, and both the mixed halide salt and nitrate salts of XB dicationic rotaxane **76^{2+}** in D_2O are compared in Figure 3.17. Of particular note is the significant upfield perturbation of internal pyridinium proton *2* upon formation of rotaxane **74·Cl** (Figure 3.17c), indicative of strong anion complexation in the rotaxane structure. Anion exchange to the nitrate salt resulted in the downfield perturbation of protons *2* and *b*, which are directed within the anion binding cavity and thus are sensitive to the presence of a bound anion guest. Additional evidence for the interlocked nature of both rotaxane **74·Cl** and **76·(NO$_3$)$_2$** was obtained in the ^{1}H ROESY NMR spectra (Figure 3.18), which reveal through space interactions between the macrocycle hydroquinone protons *c* and *d* and the axle pyridinium protons *1* and *2*.

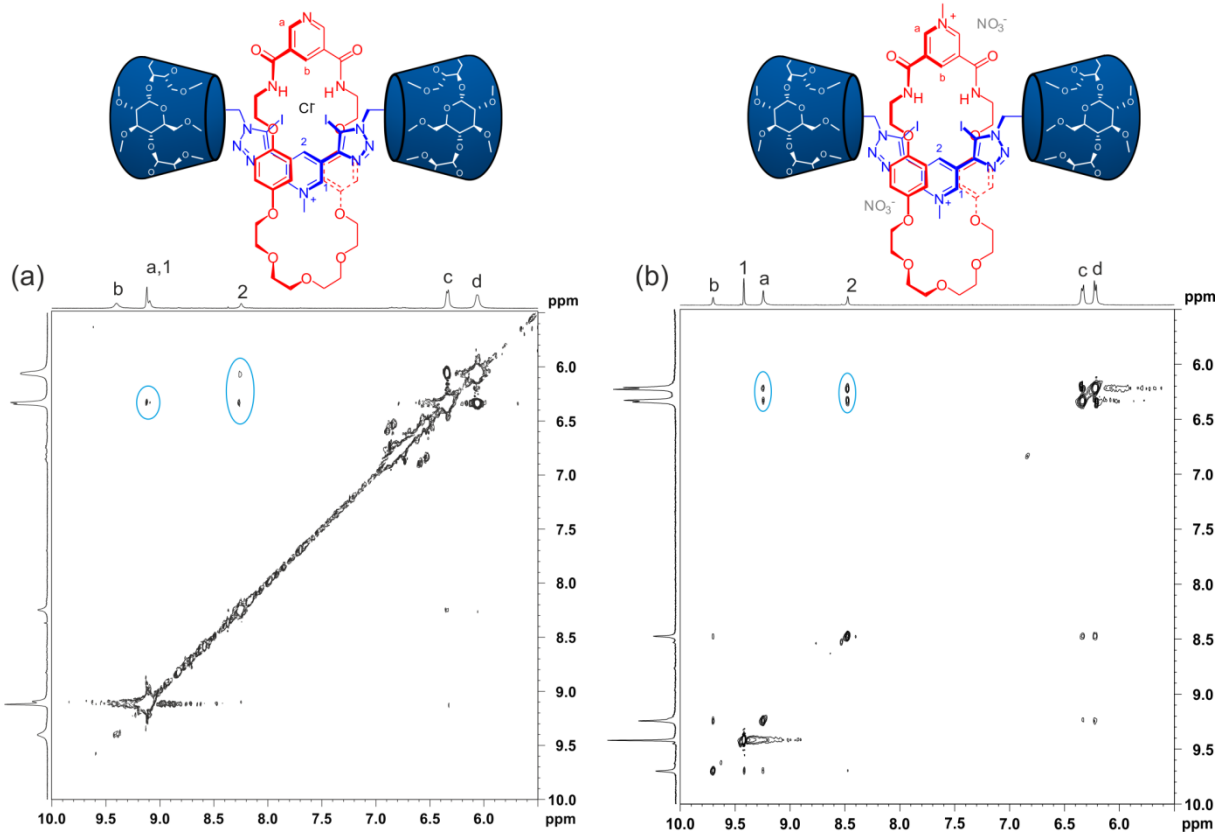

Figure 3.18 Section of the ^{1}H ROESY NMR spectrum in D_2O (500 MHz, 298 K) of: (a) mono-cationic rotaxane **74·Cl** and (b) dicationic rotaxane **76·(NO$_3$)$_2$**. Selected cross-peaks indicating through space interactions between the interlocked macrocycle and axle components are highlighted.

The ^{1}H NMR spectrum of the analogous dicationic, prototriazole rotaxane **77·(NO$_3$)$_2$** was similar to that of **76·(NO$_3$)$_2$**, with the expected addition of the triazole proton *3* (Figure 3.19), whilst inter-component through space interactions in the ^{1}H ROESY NMR spectrum confirmed the interlocked structure of the rotaxane.

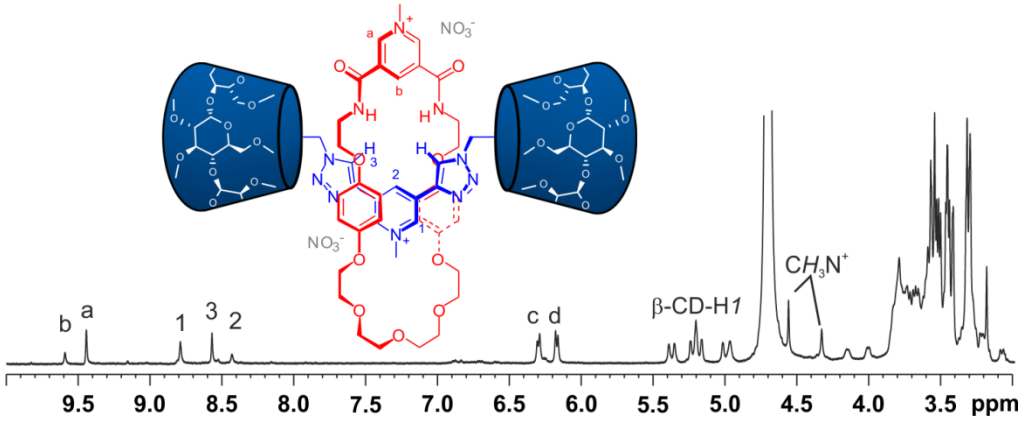

Figure 3.19 ^{1}H NMR spectra of HB prototriazole rotaxane **77·(NO$_3$)$_2$** in D_2O (500 MHz, 298 K).

3.3.3 Anion recognition studies in D_2O

The anion recognition studies of acyclic receptors **72·NO$_3$** and **73·NO$_3$**, and rotaxanes **76·(NO$_3$)$_2$** and **77·(NO$_3$)$_2$**, were investigated *via* ^{1}H NMR titration experiments, using the same procedure employed in Section 3.2.3. Addition of anions caused chemical shift perturbations of the protons that are directed into the anion binding cavity (protons *b*, *2*, and triazole proton *3*, where present). Representative spectra from the titration of XB rotaxane **76·(NO$_3$)$_2$** with NaI are shown in Figure 3.20

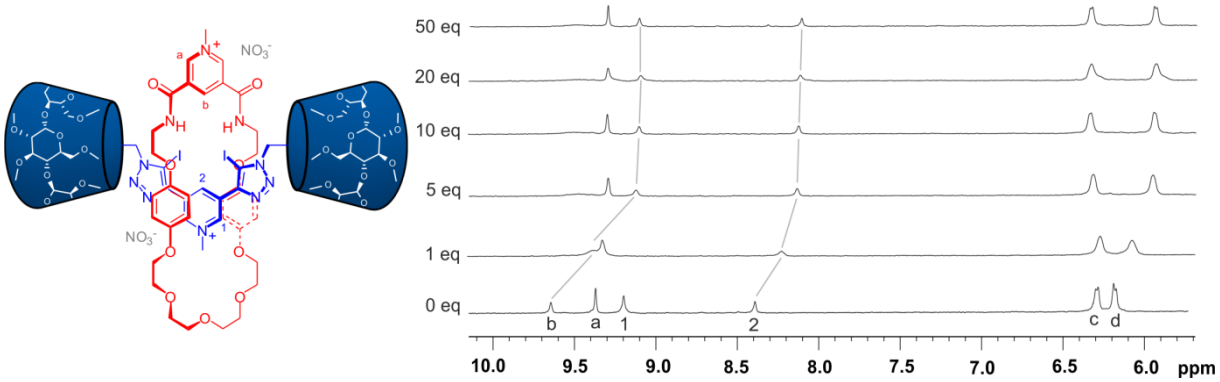

Figure 3.20 Changes in the ^{1}H NMR spectrum of rotaxane **77·(NO$_3$)$_2$** in D_2O (500 MHz, 298 K) upon addition of NaI.

In each case, the maximum chemical shift perturbation was observed with iodide, and the smallest with sulfate (Figure 3.21).

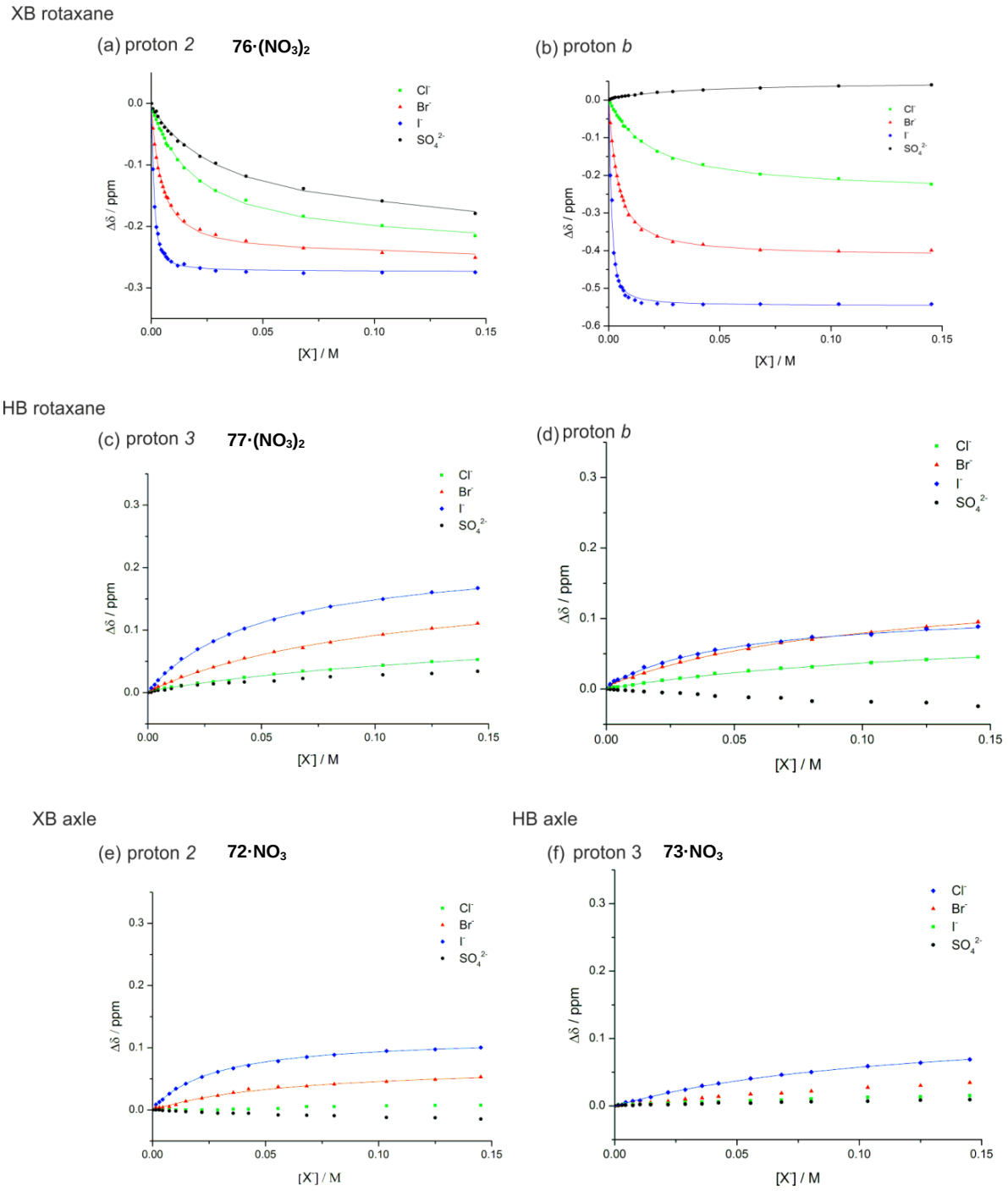

Figure 3.21 Plots of chemical shift change against anion concentration in D_2O for iodotriazole and prototriazole anion receptors (T = 298 K). Actual data represented by solid symbols, calculated 1:1 host–guest binding isotherm represented by solid lines. For atom labels see Figure 3.20.

Significant upfield perturbations of both the internal pyridinium proton *2* (Figure 3.21a) and macrocycle proton *b* (Figure 3.21b) were observed upon addition of anions to XB rotaxane **76·(NO$_3$)$_2$**. In contrast, upon addition of anions to acyclic XB axle **72·NO$_3$**, proton *2* perturbed in the downfield direction, and to a lesser extent (Figure 3.21e). In the case of the HB prototriazole rotaxane analogue **77·(NO$_3$)$_2$**, anion binding causes more modest downfield perturbations of triazole protons 3 (Figure 3.21c) and internal macrocycle proton *b* (Figure 3.21d), and small perturbations of the triazole protons *3* in the acyclic axle receptor **73·NO$_3$** (Figure 3.21f). No perturbation of the internal axle pyridinium proton *2* was observed in either of the HB prototriazole receptors.

The change in chemical shifts were monitored as a function of anion concentration, and WinEQNMR2 analysis of the titration data determined the 1:1 stoichiometric association constants shown in Table 3.2. Importantly, the association constants were determined for each of the cavity protons (*b*, *2* or *3*) that were perturbed upon anion binding, and the calculated values were found to be consistent and independent of the proton monitored. The K_a values reported in Table 3.2 are the average values of the association constants determined separately for each cavity proton. The association constant of iodide with rotaxane **76·(NO$_3$)$_2$** was repeated on two independently prepared samples, and the determined association constant values were found to be consistent across all three titration experiments.

Table 3.2 Anion association constants K_a (M^{-1}) in D_2O.

		K_a (M^{-1})[a]			
Triazole receptors		Cl^-	Br^-	I^-	SO_4^{2-}
XB	Axle **72·NO$_3$**	-[b]	15	40	-[b]
	Rotaxane **76·(NO$_3$)$_2$**	55	290	2200	30
HB	Axle **73·NO$_3$**	-[b]	-[b]	5	-[b]
	Rotaxane **77·(NO$_3$)$_2$**	-[b]	10	20	-[b]
Amide receptors (Section 3.2.3)					
HB	Rotaxane **65·(NO$_3$)$_2$**	15	35	50	-[b]
	Axle **62·NO$_3$**	-[b]	-[b]	-[b]	-[b]

T = 298 K, anions added as the sodium salt. [a] Calculated using chemical shift data of protons *b*, *2* and *3* where appropriate. Errors estimated to be <10%. [b] No binding.

With XB-donor rotaxane **76·(NO$_3$)$_2$** the larger halide anions are bound with remarkably strongly in water, in particular iodide which bound with an association constant of 2200 M^{-1} (Table 3.2). Binding of this magnitude in water is typically only observed in receptors bearing a much higher positive charge (see Section 3.1.1).[1] The sulfate anion is too large to penetrate the interlocked binding cavity, which combined with a large hydration energy, results in relatively weak binding.

The analogous HB-donor rotaxane **77·(NO$_3$)$_2$**, in which the iodotriazole XB donors are replaced by prototriazole HB donors, binds anions less favourably, to the extent that only weak association of bromide and iodide (K_a = 10 M^{-1} and 20 M^{-1} respectively), and no binding chloride or sulfate anions, was observed. The enhancement of iodide complexation by XB-donor rotaxane **76·(NO$_3$)$_2$** is particularly notable: over two orders of magnitude greater than for the HB-donor analogue **77·(NO$_3$)$_2$**. This impressive enhancement results from merely replacing two protons with two iodine atoms, thus interchanging HB-donors to XB-donors in the axle component, and suggests that halogen bonding is a superior intermolecular interaction for anion recognition in water.

This effect is further highlighted when the anion binding capability of the acyclic XB- and HB-donor axles **72·NO_3** and **73·NO_3** are considered. Acyclic XB-donor **72·NO_3** bound bromide and iodide with notable association constants (K_a = 15 M^{-1} and 40 M^{-1} respectively), and even more strongly than the dicationic HB-donor rotaxane host **77·$(NO_3)_2$**, despite the lower positive charge and simple acyclic nature of the receptor (Table 3.2). In contrast, the analogous HB-donor acyclic receptor **73·NO_3** formed only a very weak complex with iodide and no binding of the other anions was observed.

It is notable that the recognition properties of XB rotaxane **76·$(NO_3)_2$** are also vastly superior to that of the 3,5-bis-amide pyridinium HB rotaxane **65·$(NO_3)_2$** (*vide supra*). Similar amide-based N–H hydrogen bond donors incorporated within rotaxane host architectures have been shown to bind anions strongly in competitive organic–aqueous solvent mixtures,[6,32] and with higher affinity that the analogous 3,5-bis-prototriazole pyridinium analogues.[40] The observation that the anion association constants determined with the XB rotaxane **76·$(NO_3)_2$** are up to two orders of magnitude greater than even this potent amide-based receptor serves to demonstrate that the impressive anion binding affinities are a result of the strong XB interactions, and not merely that the bis-prototriazole pyridinium motif is a poorer anion receptor in general.

In all three rotaxanes studied in this chapter, namely HB rotaxanes **65·$(NO_3)_2$** and **77·$(NO_3)_2$**, and XB rotaxane **76·$(NO_3)_2$**, the association constants are considerably greater in magnitude than their acyclic counterparts. This is consistent with the effect observed with previously reported interlocked receptors in organic–aqueous solvent mixtures, such as those discussed in Chapter 2 and others reported elsewhere,[47] in which the three-dimensional binding cavity of the rotaxane encapsulates the anion and leads to an enhanced association strength relative to the parent axle component.

3.3.4 Quantification of the thermodynamic parameters of iodide binding in D_2O by HB- and XB-donor rotaxanes

To further investigate the origin of the strong iodide binding observed with rotaxane **76·(NO$_3$)$_2$**, the thermodynamic parameters for iodide complex formation were determined by Van't Hoff analysis of the titration data for both HB-donor rotaxanes **65·(NO$_3$)$_2$** and **77·(NO$_3$)$_2$**, and XB-donor rotaxane **76·(NO$_3$)$_2$** in D_2O. To this end the iodide association constants were determined at a range of additional temperatures by ^{1}H NMR anion binding titrations, and the 1:1 stoichiometric association constants determined as previously described. By plotting ln K_a as a function of reciprocal temperature (Figure 3.22), the enthalpic and entropic contributions to the free energy of iodide binding were determined, according to the Van't Hoff equation (Equation 3.1)

Equation 3.1 $$lnK = \frac{-\Delta H^{\circ}}{RT} + \frac{\Delta S^{\circ}}{R}$$

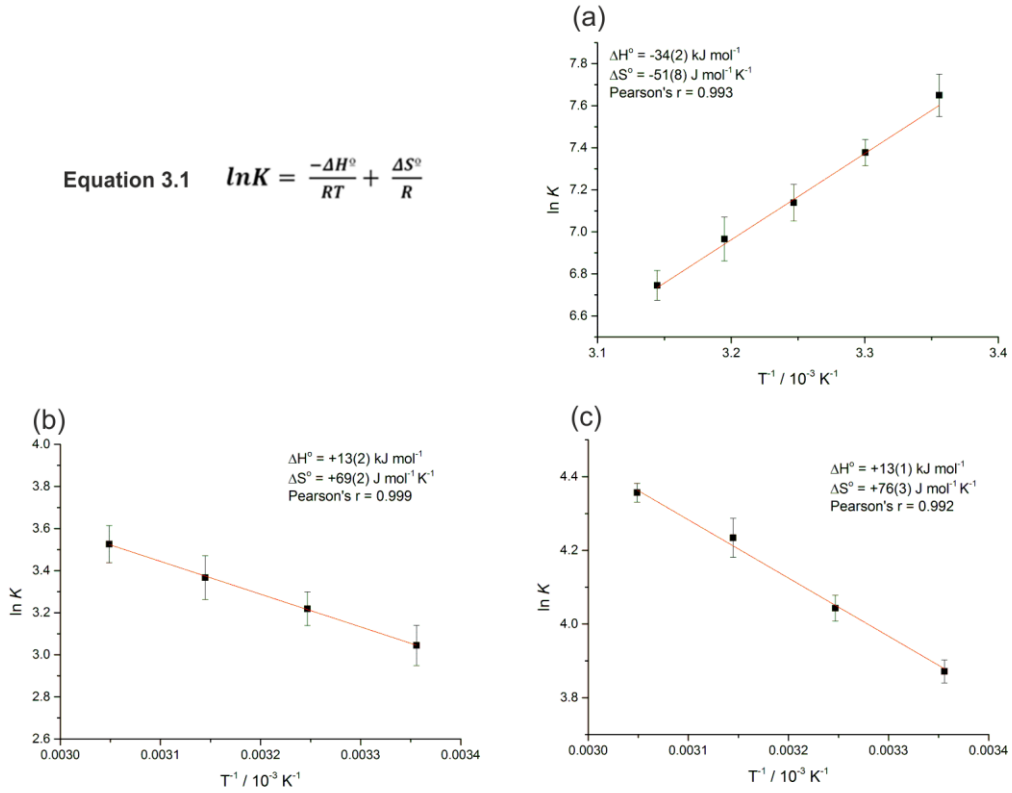

Figure 3.22 Van't Hoff analysis of iodide binding for (a) XB-rotaxane **76·(NO$_3$)$_2$**, (b) HB-triazole rotaxane **77·(NO$_3$)$_2$** and HB-amide rotaxane **65·(NO$_3$)$_2$** in D_2O. The determined enthalpy and entropy values, and the linear correlation coefficient are shown in each case.

This analysis revealed that iodide binding by the HB-donor receptors **65·(NO$_3$)$_2$** and **77·(NO$_3$)$_2$** is enthalpically unfavourable and driven entirely by a strong entropic contribution (Table 3.3). Indeed the few receptors capable of recognizing anions in water also exploit and utilise this hydrophobic effect, where in general the main driving force is the entropic gain resulting from the release of ordered water molecules from both host and guest species.[1]

Table 3.3 Thermodynamic parameters in kJ mol^{-1} for iodide binding by HB-rotaxanes **65·(NO$_3$)$_2$** and **77·(NO$_3$)$_2$**, and XB-rotaxane **76·(NO$_3$)$_2$** in D_2O at T = 298 K

		ΔG	**ΔH**	**TΔS**
HB rotaxanes	Triazole rotaxane **77·(NO$_3$)$_2$**	−7(1)	+13(2)	+21(1)
	Amide rotaxane **65·(NO$_3$)$_2$**	−10(1)	+13(1)	+23(1)
XB rotaxane	Iodotriazole rotaxane **76·(NO$_3$)$_2$**	−19(1)	−34(2)	−15(2)

Iodide added as the sodium salt. Errors in parentheses.

In stark contrast, iodide binding by the XB-donor rotaxane **76·(NO$_3$)$_2$** is driven by a strong favourable enthalpic (exothermic) contribution. This correlates with studies by Taylor[48] and Huber[16] on anion binding in organic solvents, and Brammer, Hunter and Perutz into the energetics of XBs from C_6F_5I to metal fluoride[49] and metal hydride[18] complexes in toluene, which all point to a dominant enthalpic contribution to binding of guest species mediated by halogen bonds. It is also notable that iodide binding by XB-rotaxane **76·(NO$_3$)$_2$** is entropically unfavourable, in contrast to the HB-donor analogues in which favourable entropy change is the dominant driving force for complexation.

The thermodynamic contribution from desolvation of the free iodide anion in solution, and from the 3,5-bis-amide pyridinium HB-donor recognition site of the macrocycle component of the respective rotaxanes, can reasonably be assumed to be similar for all three structurally similar rotaxane host systems. Hence the observed dramatic enhancement of iodide binding affinity exhibited by XB rotaxane **76·(NO$_3$)$_2$** may be ascribed to the presence of the iodine atoms within the anion binding domain.

The contrasting entropic contributions, being unfavourable with **76·(NO$_3$)$_2$**, and favourable with **65·(NO$_3$)$_2$** and **77·(NO$_3$)$_2$**, appear to suggest that the strong iodide binding by XB-donor **76·(NO$_3$)$_2$** does not result entirely from the iodine atoms merely providing a more lipophilic binding cavity. This would be expected to lead to an enhanced entropic contribution, arising from the hydrophobic effect, together with a possible enthalpic augmentation. With XB-donor **76·(NO$_3$)$_2$** however, enthalpy is exclusively favoured, which is consistent with a strong bonding interaction and suggests that halogen bonding is driving force for the increased recognition and binding strength.

3.3.5 Molecular dynamics simulations of the halide complexes of XB-rotaxane 76^{2+}

In order to obtain further insights into the unique halide binding properties of XB-rotaxane **76·(NO$_3$)$_2$**, molecular dynamics simulations were conducted by Igor Marques and Professor Vítor Félix, at the University of Aveiro, Portugal. Molecular mechanics (MM) and molecular dynamics (MD) calculations were conducted using the Amber 12 and the General Amber Force Field (GAFF),[50] in cubic periodic boxes of water.[51] The two XB interactions were described by the addition of a positively charged extra point (EP) to each C-I bond. DFT calculations (using the B3LYP functional) were conducted to ascertain I···X$^-$ distances in water solution, which were subsequently used to determine the optimal I-EP distance for each halide complex, facilitating the force field parameterisation of the XB interactions (see Appendix A1).

Throughout the MD simulations (see Appendix A2), the three halide complexes (**76·Cl**$^+$, **76·Br**$^+$ and **76·I**$^+$) exhibit an orthogonal arrangement of the axle and macrocycle components in the interlocked structure, as depicted in Figure 3.23 for **76·I**$^+$.

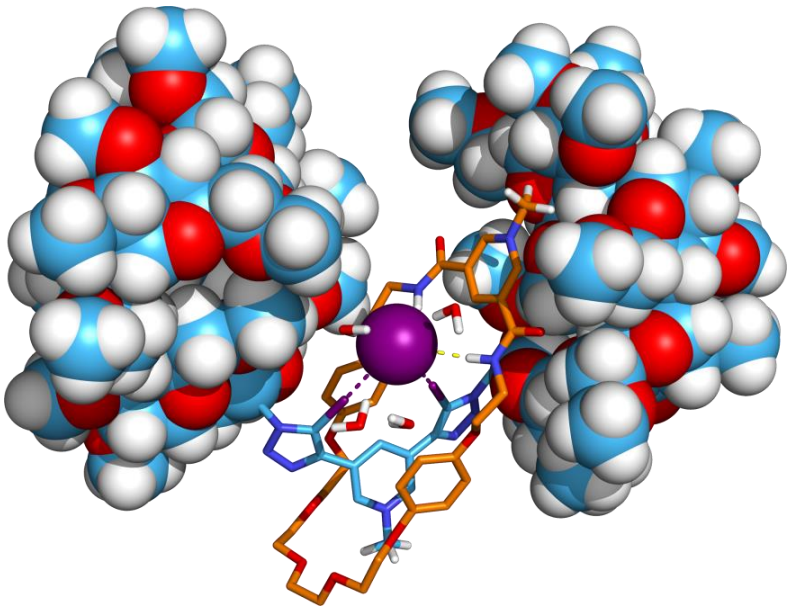

Figure 3.23 MD simulation of **76·(NO$_3$)$_2$** with I$^-$. Representative snapshot showing the iodide binding through two XB and HB interactions, surrounded by four water molecules. The N-H···I$^-$ and C-I···I$^-$ bonding interactions are drawn as purple and yellow dashed lines, respectively. The cyclodextrin stoppers are depicted by a space filling representation. Carbon atoms are shown in cyan in the axle and in orange in the macrocycle, while oxygen, nitrogen and iodine atoms are respectively shown in red, blue, and purple. Selected hydrogen atoms are shown in white.

The rotaxane tightly coordinates each halide anion *via* two independent linear XB interactions, assisted by two intermittent N–H···X$^-$ hydrogen bonds, as illustrated with the confined 3D histogram built with the positions occupied by the iodide for a single MD replicate of 50 ns (Figure 3.24).

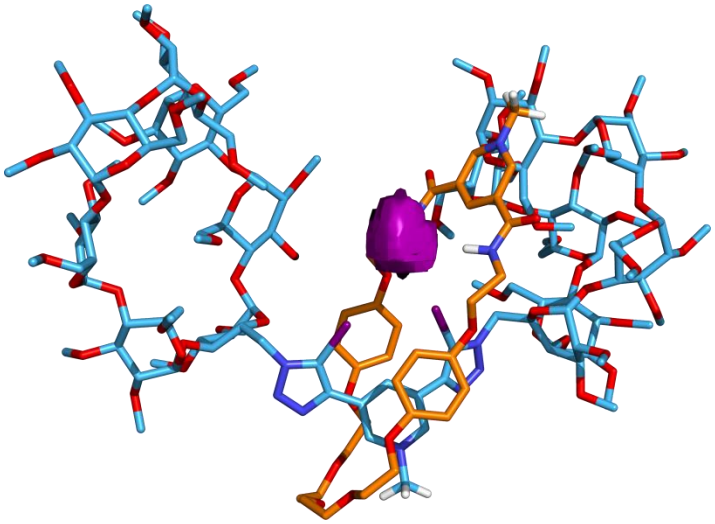

Figure 3.24 Histogram built with the positions occupied by the iodide along the 50 ns of MD simulation with **76(NO$_3$)$_2$**. Colour scheme as in Figure 3.23.

The anions are positioned slightly above the plane of the macrocycle with the N···X$^-$ and I···X$^-$ distances mirroring the increasing size of the halide anion (see Table 3.4).

Table 3.4 XB and HB distances (average ± standard deviations, Å), as well as the average number of water molecules within the first solvation shell of each bound halide anion (3.5 Å cut-off) for 100 ns of sampling of MD simulations of **76·(NO$_3$)$_2$** with halides.

X$^-$ [a]	I···X	N···X	Water molecules
Cl$^-$	3.50±0.14 ; 3.55±0.16	3.55±0.24 ; 3.76±0.38	3.58±0.73
Br$^-$	3.69±0.16 ; 3.74±0.19	3.96±0.65 ; 4.13±0.57	3.99±0.80
I$^-$	3.94±0.20 ; 4.06±0.24	4.21±0.55 ; 4.37±0.59	4.12±0.85

The selectivity of **76·(NO$_3$)$_2$** towards the halide anions was also studied by MD simulations within a cubic box of water. The relative binding free energies (ΔΔG) of a pair of halide anions were estimated *via* thermodynamic integration using the thermodynamic cycle depicted in Figure 3.25, where ΔΔG is given by Equation 3.2.

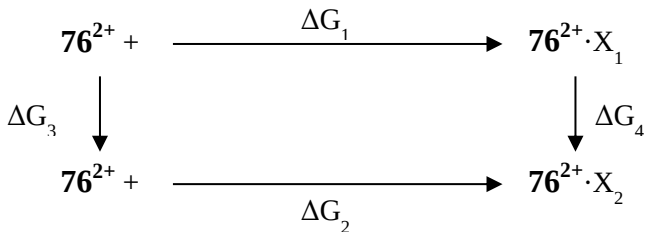

Figure 3.25 Thermodynamic cycle for the mutation of the halides, where halide X_1 is larger than halide X_2.

Equation 3.2 $$\Delta\Delta G = \Delta G_4 - \Delta G_3 = \Delta G_2 - \Delta G_1$$

The values of ΔG_3 and ΔG_4 were computationally assessed by mutating the larger halide anion X_1 into the smaller anion X_2 and calculating the free energy by the thermodynamic integration method (see Appendix A3 for further details). This mutation was performed independently for an isolated halide in water or halogen bonded to **76^{2+}**, to obtain the relative free energy values shown in Table 3.5.

Table 3.5 ΔΔG (kJ mol^{-1}) for halide complexes of **76·(NO$_3$)$_2$**

Mutation	ΔG **76^{2+}**·X$^-$	ΔG X$^-$	ΔΔG
I$^-$ → Br$^-$	−17.18	−35.61	18.39
Br$^-$ → Cl$^-$	−9.15	−27.13	17.97

The analysis revealed that the relative free energies of the halide complexes of **76^{2+}** are in agreement with the selectivity trend determined experimentally, albeit over-estimated by *ca.* 10 kJ mol^{-1}, with the complex stability increasing with the size of the halide anion. Importantly, this suggests that the selectivity for iodide arises from both the intrinsic geometric complementarity of the XB rotaxane's binding cavity for the anion and the Hofmeister series bias towards binding of the larger, less heavily solvated halides.

3.4 Conclusions and future work

In conclusion, the first examples of interlocked host architectures capable of the recognition of anions in pure water have been prepared, by the synthesis of permethylated *β*-cyclodextrin-stoppered rotaxanes.

It was established that incorporating halogen bond donors into such rotaxane-based anion receptors results in dramatic enhancement of anion binding in water compared to the equivalent hydrogen bonding analogues, with up to two orders of magnitude enhancement observed in the interlocked rotaxane host system. This XB-mediated enhancement of anion association is also observed in acyclic receptors, resulting in remarkable binding affinity despite the low charge and simplicity of the receptor.

Thermodynamic quantification of iodide binding by the rotaxane hosts reveals the strong binding by the XB-rotaxane is driven exclusively by favourable enthalpic contributions arising from the XB interactions, whereas weaker association with the HB-rotaxanes is entropically driven by hydrophobic effect. These observations demonstrate the unique nature of halogen bonding in water as a strong alternative interaction to the ubiquitous hydrogen bond in molecular recognition and assembly.

To expand on the work described in this chapter, an all-XB rotaxane host could be prepared, in which both the macrocycle and axle components interact with the anion purely through halogen bonds, potentially to achieve even greater anion binding affinities in water. Furthermore, it would be of interest to prepare neutral analogues of these receptors, by replacing the charged bis-triazole pyridinium motif with a neutral bis-triazole pyridine *N*-oxide moiety, to allow the study of halogen bonds in water that are not charge assisted.

3.5 References for Chapter 3

1. S. Kubik, *Chem. Soc. Rev.*, 2010, **39**, 3648–3663.
2. S. Kubik, R. Goddard, R. Kirchner, D. Nolting, and J. Seidel, *Angew. Chem. Int. Ed.*, 2001, **40**, 2648–2651.
3. S. Kubik and R. Goddard, *Proc. Natl. Acad. Sci.*, 2002, **99**, 5127–5132.
4. E. Graf and J. M. Lehn, *J. Am. Chem. Soc.*, 1976, **98**, 6403–6405.
5. J. Suk and K.-S. Jeong, *J. Am. Chem. Soc.*, 2008, **130**, 11868–11869.
6. L. M. Hancock, L. C. Gilday, S. Carvalho, P. J. Costa, V. Félix, C. J. Serpell, N. L. Kilah, and P. D. Beer, *Chem. - Eur. J.*, 2010, **16**, 13082–13094.
7. F. Zapata, A. Caballero, N. G. White, T. D. W. Claridge, P. J. Costa, V. Félix, and P. D. Beer, *J. Am. Chem. Soc.*, 2012, **134**, 11533–11541.
8. A. Caballero, F. Zapata, N. G. White, P. J. Costa, V. Félix, and P. D. Beer, *Angew. Chem. Int. Ed.*, 2012, **51**, 1876–1880.
9. N. L. Kilah, M. D. Wise, C. J. Serpell, A. L. Thompson, N. G. White, K. E. Christensen, and P. D. Beer, *J. Am. Chem. Soc.*, 2010, **132**, 11893–11895.
10. K. M. Mullen, J. Mercurio, C. J. Serpell, and P. D. Beer, *Angew. Chem.*, 2009, **121**, 4875–4878.
11. M. Cametti, K. Raatikainen, P. Metrangolo, T. Pilati, G. Terraneo, and G. Resnati, *Org. Biomol. Chem.*, 2012, **10**, 1329–1333.
12. M. G. Sarwar, B. Dragisic, S. Sagoo, and M. S. Taylor, *Angew. Chem. Int. Ed.*, 2010, **49**, 1674–1677.
13. R. Cabot and C. A. Hunter, *Chem. Commun.*, 2009, 2005–2007.
14. M. G. Sarwar, B. Dragisic, L. J. Salsberg, C. Gouliaras, and M. S. Taylor, *J. Am. Chem. Soc.*, 2010, **132**, 1646–1653.
15. C. Laurence, J. Graton, M. Berthelot, and M. J. El Ghomari, *Chem. – Eur. J.*, 2011, **17**, 10431–10444.
16. S. M. Walter, F. Kniep, L. Rout, F. P. Schmidtchen, E. Herdtweck, and S. M. Huber, *J. Am. Chem. Soc.*, 2012, **134**, 8507–8512.
17. T. M. Beale, M. G. Chudzinski, M. G. Sarwar, and M. S. Taylor, *Chem. Soc. Rev.*, 2013, **42**, 1667–1680.
18. D. A. Smith, L. Brammer, C. A. Hunter, and R. N. Perutz, *J. Am. Chem. Soc.*, 2014, **136**, 1288–1291.
19. G. Wenz, *Angew. Chem. Int. Ed. Engl.*, 1994, **33**, 803–822.
20. M. V. Rekharsky and Y. Inoue, *Chem Rev*, 1998, **98**, 1875–1918.
21. T. Loftsson and M. E. Brewster, *J. Pharm. Sci.*, 1996, **85**, 1017–1025.
22. T. Aree, H. Hoier, B. Schulz, G. Reck, and W. Saenger, *Carbohydr. Res.*, 2000, **328**, 399–407.
23. Z. Chen, J. S. Bradshaw, and M. L. Lee, *Tetrahedron Lett.*, 1996, **37**, 6831–6834.
24. S. Brown, J. Coates, D. Coghlan, C. Easton, S. Vaneyk, W. Janowski, A. Lepore, S. Lincoln, Y. Luo, B. May, D. Schiesser, P. Wang, and M. Williams, *Aust. J. Chem.*, 1993, **46**, 953–958.
25. S. A. Nepogodiev and J. F. Stoddart, *Chem Rev*, 1998, **98**, 1959–1976.
26. P. N. Taylor, M. J. O'Connell, L. A. McNeill, M. J. Hall, R. T. Aplin, and H. L. Anderson, *Angew. Chem. Int. Ed.*, 2000, **39**, 3456–3460.
27. K. Sakamoto, Y. Takashima, H. Yamaguchi, and A. Harada, *J Org Chem*, 2006, **72**, 459–465.
28. Y.-M. Zhang, Z. Wang, Y. Chen, H.-Z. Chen, F. Ding, and Y. Liu, *Org. Biomol. Chem.*, 2014, **12**, 2559–2567.

29. P. J. Skinner, A. Beeby, R. S. Dickins, D. Parker, S. Aime, and M. Botta, *J. Chem. Soc. Perkin Trans. 2*, 2000, 1329–1338.
30. B. du Roizel, J.-P. Baltaze, and P. Sinaÿ, *Tetrahedron Lett.*, 2002, **43**, 2371–2373.
31. S. Xiao, M. Yang, P. Sinaÿ, Y. Blériot, M. Sollogoub, and Y. Zhang, *Eur. J. Org. Chem.*, 2010, **2010**, 1510–1516.
32. L. M. Hancock and P. D. Beer, *Chem. – Eur. J.*, 2009, **15**, 42–44.
33. M. J. Hynes, *J. Chem. Soc. Dalton Trans.*, 1993, **2**, 311–312.
34. F. Hofmeister, *Arch. Exp. Pathol. Pharmacol.*, 1888, **24**, 247–260.
35. P. A. Evans, J. Qin, J. E. Robinson, and B. Bazin, *Angew. Chem. Int. Ed.*, 2007, **46**, 7417–7419.
36. V. V. Rostovtsev, L. G. Green, V. V. Fokin, and K. B. Sharpless, *Angew. Chem. Int. Ed.*, 2002, **41**, 2596–2599.
37. J. E. Hein and V. V. Fokin, *Chem. Soc. Rev.*, 2010, **39**, 1302–1315.
38. Y. Li and A. H. Flood, *Angew. Chem. Int. Ed.*, 2008, **47**, 2649–2652.
39. V. Haridas, S. Sahu, P. P. P. Kumar, and A. R. Sapala, *RSC Adv.*, 2012, **2**, 12594–12605.
40. N. G. White and P. D. Beer, *Chem. Commun.*, 2012, **48**, 8499–8501.
41. C. Spiteri and J. E. Moses, *Angew. Chem. Int. Ed.*, 2010, **49**, 31–33.
42. W. S. Brotherton, R. J. Clark, and L. Zhu, *J. Org. Chem.*, 2012, **77**, 6443–6455.
43. N. G. White, C. J. Serpell, and P. D. Beer, *Cryst. Growth Des.*, 2014.
44. K. Sonogashira, Y. Tohda, and N. Hagihara, *Tetrahedron Lett.*, 1975, **16**, 4467–4470.
45. H. Goto, J. M. Heemstra, D. J. Hill, and J. S. Moore, *Org. Lett.*, 2004, **6**, 889–892.
46. T. X. Neenan and G. M. Whitesides, *J. Org. Chem.*, 1988, **53**, 2489–2496.
47. G. T. Spence and P. D. Beer, *Acc. Chem. Res.*, 2013, **46**, 571–586.
48. M. G. Sarwar, B. Dragisić, E. Dimitrijević, and M. S. Taylor, *Chem. – Eur. J.*, 2013, **19**, 2050–2058.
49. S. Libri, N. A. Jasim, R. N. Perutz, and L. Brammer, *J. Am. Chem. Soc.*, 2008, **130**, 7842–7844.
50. J. Wang, R. M. Wolf, J. W. Caldwell, P. A. Kollman, and D. A. Case, *J. Comput. Chem.*, 2004, **25**, 1157–1174.
51. W. L. Jorgensen, J. Chandrasekhar, J. D. Madura, R. W. Impey, and M. L. Klein, *J. Chem. Phys.*, 1983, **79**, 926–935.

CHAPTER 4

Chapter 4 Lanthanide-containing rotaxanes for anion sensing

4.1 Introduction

4.1.1 Cation templation of interlocked molecules

The development of novel templating strategies for the construction of mechanically interlocked molecules has been an area of intense research in recent years, driven by proposed applications in molecular shuttles and machines. As was discussed in Chapter 1, following the seminal report of a Cu(I)-templated catenane synthesis by Sauvage in 1983, the use of metal cations as templates for mechanical bond formation has been extensively explored.[1–3] Transition metals, including Cu(I), Zn(II), Au(I) and Pd(II) have been imaginatively utilised to prepare a wide range of interlocked structures, and, to a lesser extent, the use of alkali and alkaline earth cations has also been demonstrated.[4–8] For example, Chiu and co-workers have recently demonstrated that sodium cations template the formation of a rotaxane consisting of a non-conjugated amide or urea axle component threaded through a bis-*para*-xylyl[26]crown-6 macrocycle (Scheme 4.1a).[7] Hancock and Beer have demonstrated that both sodium and barium cations, bound within a calix[4]diquinone macrocycle, template pseudorotaxane formation with a pyridine *N*-oxide threading component, facilitating rotaxane synthesis *via* a stoppering strategy (Scheme 4.1b).[9] Notably, removal of the cation template is concomitant with pirouetting of the macrocycle around the pyridine *N*-oxide axle component.

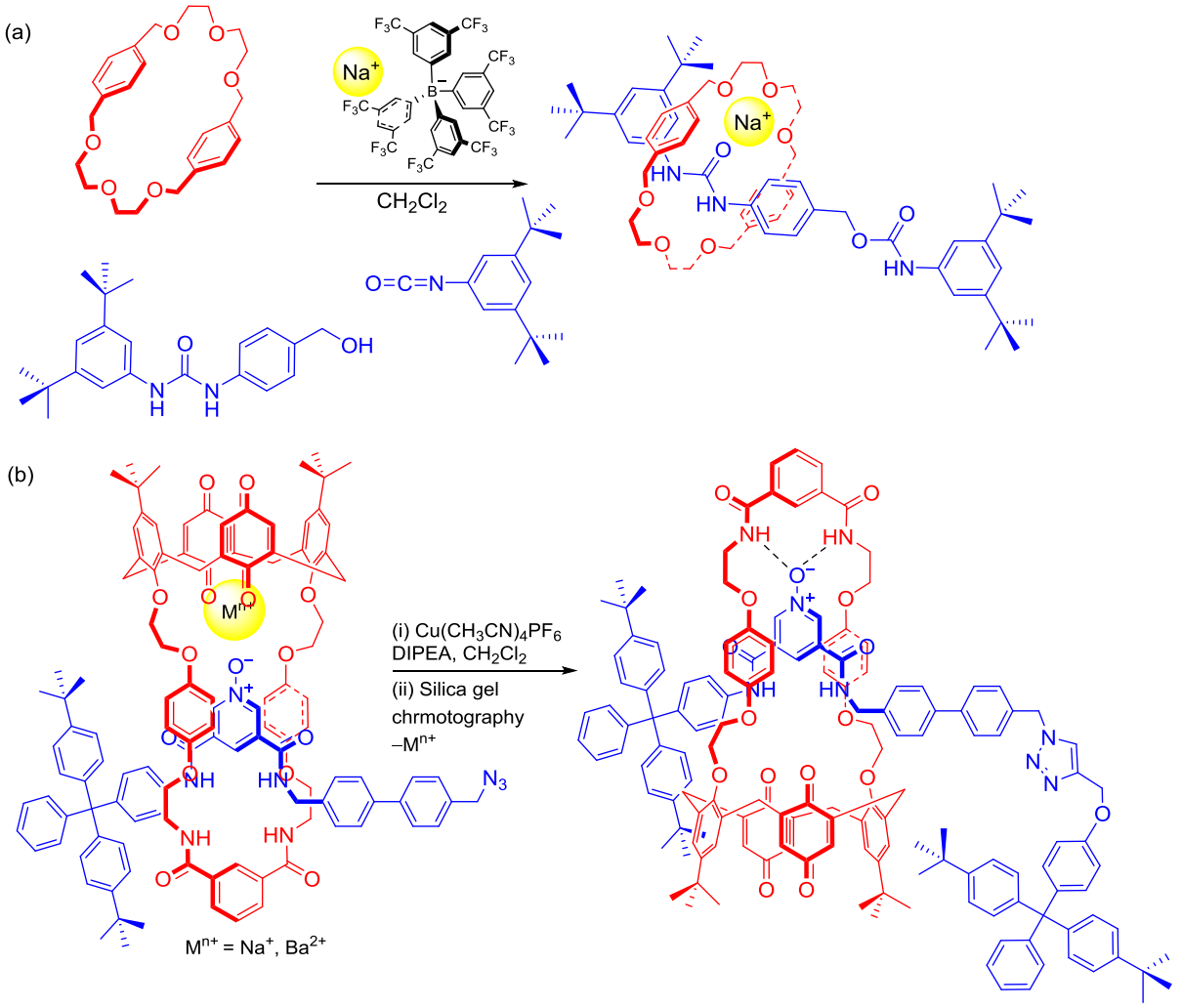

Scheme 4.1 Alkali and alkaline earth metal cation templated rotaxane syntheses: (a) Chiu's sodium templated rotaxane[7] and (b) Hancock and Beer's sodium and barium templation of a [2]rotaxane.[9]

4.1.2 Lanthanide-containing rotaxanes and catenanes

The long-lived luminescence from lanthanide centres has been used in concert with time-gating methods to afford imaging agents and sensors of high sensitivity, by eliminating the background fluorescence from organic chromophores and biological molecules.[10–14] However, given the usefulness of lanthanides in imaging and assay it is surprising that their incorporation into interlocked molecules, and indeed supramolecular assemblies in general,[15] remains relatively underdeveloped compared to their transition metal analogues. It follows that lanthanide complexes would be ideal reporter groups for incorporation into interlocked molecules for anion sensing (Chapter 1),[16] due to the aforementioned favourable properties.

Prior to the commencement of the work conducted in this chapter, the use of lanthanide cations as *templating* reagents for interlocked molecule assembly had not been demonstrated. The incorporation of lanthanides within interlocked structures, however, had previously been reported twice (*vide infra*), although the lanthanide cation played no role in the formation of the interlocked molecule. In 2004 Loeb reported the syntheses of metal organic rotaxane frameworks (MORFs) in which [2]pseudorotaxanes, comprising a bi-pyridinium axle and a dibenzo-[24]crown-8 macrocycle, form three-dimensional networks in the solid state, by coordination of terminal pyridine *N*-oxide motifs to the lanthanide cations (Figure 4.1).[17] The structures of the MORFs are dependent on the size of the cation: a square antiprismatic geometry is formed around the metal centre in the case of Sm(III), Eu(III), Gd(III) and Tb(III) cations, with the coordination sphere comprising six coordinating rotaxanes, one coordinated water molecule and a triflate counter anion. In the case of the smaller Yb(III) cation, a seven-coordinate pentagonal bipyramidal geometry is adopted with five rotaxanes occupying the equatorial sites and a further rotaxane and water molecule occupying the axial positions. The formation of the precursor pseudorotaxane itself, however, was templated by CH···O hydrogen bond interactions between the pyridinium thread and the crown ether macrocycle, whilst the lanthanide centres act as stoppers in the solid state rotaxane structure.

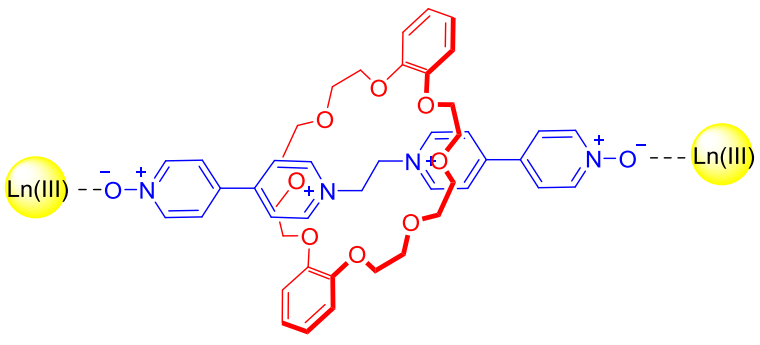

Figure 4.1 Loeb's metal organic rotaxane framework with lanthanide cation nodes and pseudorotaxane bridging ligands.

With the aim of exploring the time-gated luminescence detection of anions binding within a rotaxane host cavity, in 2012 Faulkner and Beer reported a lanthanide-appended rotaxane, prepared by the CuAAC-coupling of a propargyl-functionalised lanthanide complex with an azide-appended rotaxane (Scheme 4.2a).[18] Anion binding titrations in CH_2Cl_2 solution, conducted by monitoring the changes in the europium emission upon anion addition, revealed that the rotaxane is chloride-responsive, and possesses two independent anion binding sites. The first chloride anion binds strongly to the lanthanide cation at the vacant ninth coordination site, concomitant with dramatic quenching of the hypersensitive $\Delta J = 2$ transition (Scheme 4.2b). Further chloride binding within the rotaxane cavity leads to a gradual recovery of the lanthanide emission intensity. The rotaxane was demonstrated to be selective for Cl^- over both AcO^- and $H_2PO_4^-$.

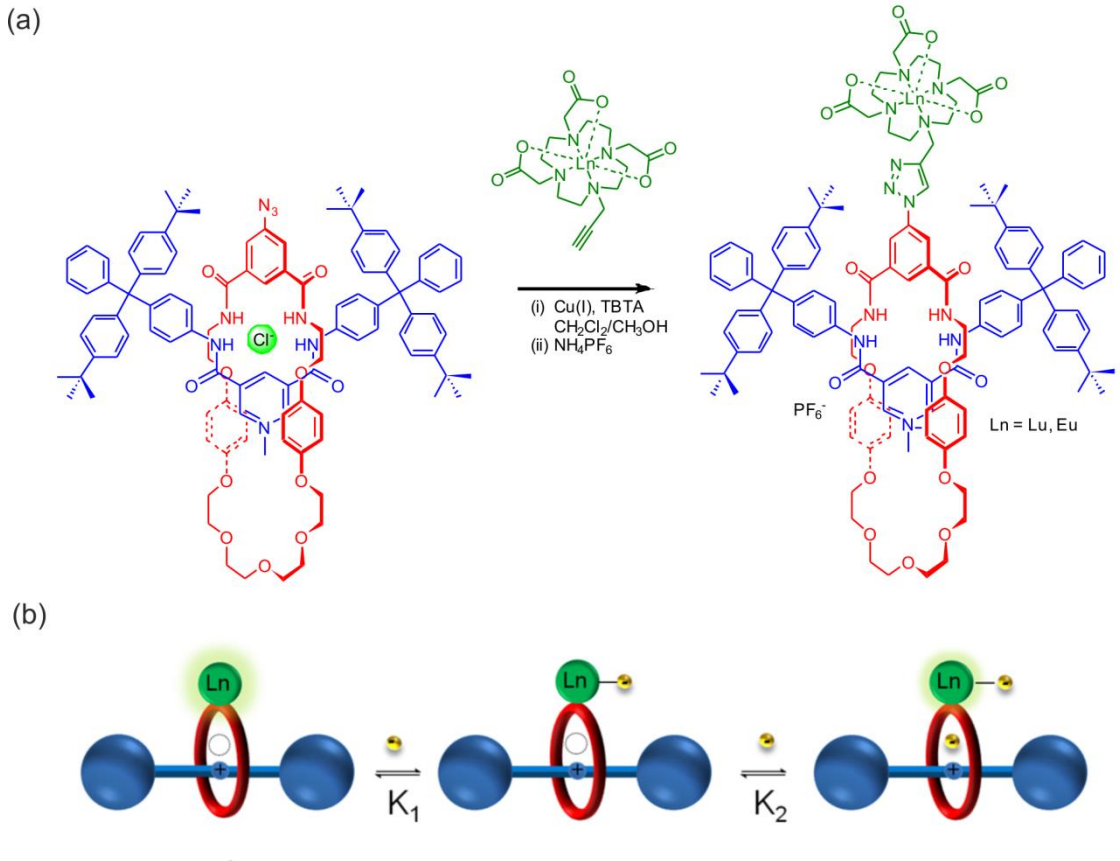

Scheme 4.2 (a) Preparation of a lanthanide-appended rotaxane and (b) schematic representation of successive chloride binding.[18]

In the wake of the publication of some of the work conducted in this chapter, Gunnlaugsson and co-workers reported the Eu(III)-templated synthesis of catenanes, using a Grubbs' II catalysed ring closing metathesis reaction to afford a mixture of [2]catenane and [3]catenane species (Scheme 4.3), as determined by mass spectrometry analysis.[19] The authors did not, however, attempt to separate or purify these two components and so the synthetic yield of these two interlocked species, and the nature of the other by-products, is not known.

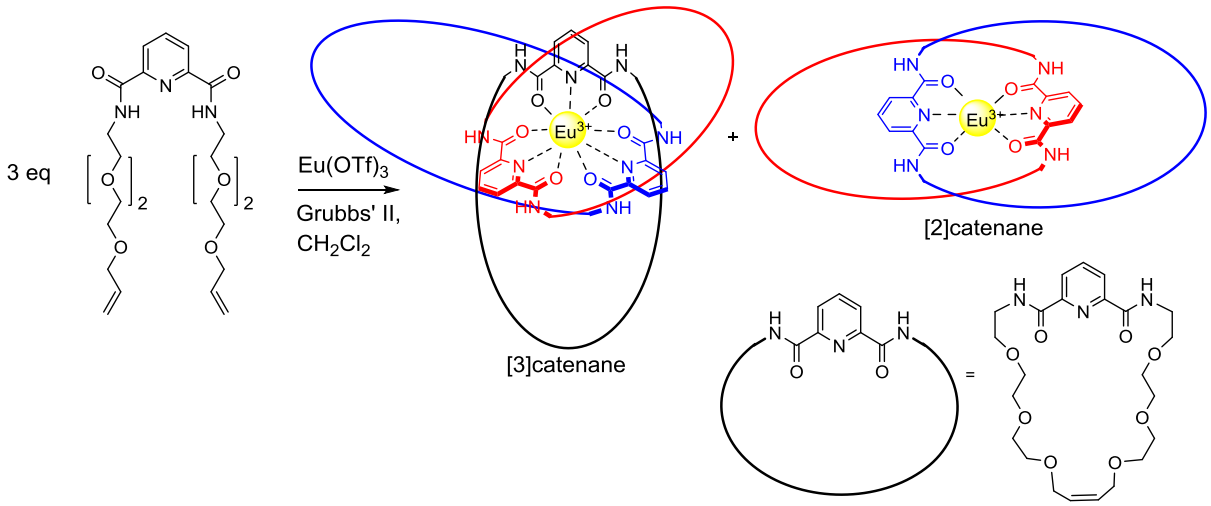

Scheme 4.3 Gunnlaugsson's assembly of europium catenanes.[19] The macrocycle components are depicted in different colours for clarity.

The chloride-responsive lanthanide-appended rotaxane shown in Scheme 4.2a does not fully exploit the unique selectivity of the interlocked host due to competing anion binding at the appended lanthanide centre. Ideally, the lanthanide cation forms an integral part of the binding domain such that the anion guest coordinates to the metal, whilst being bound simultaneously by hydrogen bonds from the organic rotaxane framework. It was expected that such a system should exhibit enhanced recognition by exploiting the selectivity of the three-dimensional binding cavity, while sensing the anion binding event by means of modulation of the lanthanide luminescence.

4.1.3 Chapter aims

The aim of the work described in this chapter was to investigate the use of lanthanide cations as templates for interlocked molecule formation, with the ultimate goal of preparing mechanically bonded anion host systems, in which the lanthanide cation forms an integral part of the anion binding cavity, and facilitating anion sensing by means of modulation of the lanthanide luminescence.

A novel lanthanide-cation templation methodology for rotaxane formation is demonstrated initially, through an interpenetrative pseudorotaxane assembly of a pyridine *N*-oxide threading component coordinating to a lanthanide cation, which itself is bound within a kinetically stable macrocycle. Stoppering of the pseudorotaxane assembly affords the [2]rotaxane. The structure and properties of the lutetium and europium rotaxane species are explored using NMR spectroscopy, mass spectrometry and luminescence spectroscopy techniques.

Secondly, the novel use of a nitrite anion template for the efficient synthesis of a lanthanide-containing rotaxane is discussed. The anion binding and sensing capability of the europium [2]rotaxane product is investigated by means of luminescence anion binding titrations.

4.2 Lanthanide-cation templated synthesis of rotaxanes[†]

The synthetic work conducted in Section 4.2 was carried out in collaboration with Dr Fabiola Zapata, whilst the majority of the lanthanide luminescence studies discussed in this chapter were undertaken by Dr Octavia Blackburn.

4.2.1 Synthetic strategy for rotaxane formation

Inspired by the use of sodium and barium cations for the template-directed synthesis of pyridine *N*-oxide rotaxanes (Scheme 4.1b), the synthetic strategy envisaged for the lanthanide cation templated synthesis of a rotaxane is shown in Scheme 4.4. A kinetically stable lanthanide complex is incorporated within a macrocycle derivative, such that a pseudorotaxane can be assembled with an appropriately functionalised pyridine *N*-oxide threading component, which satisfies the lanthanide cation's coordination sphere. Subsequent stoppering of the interpenetrative assembly affords the desired [2]rotaxane.

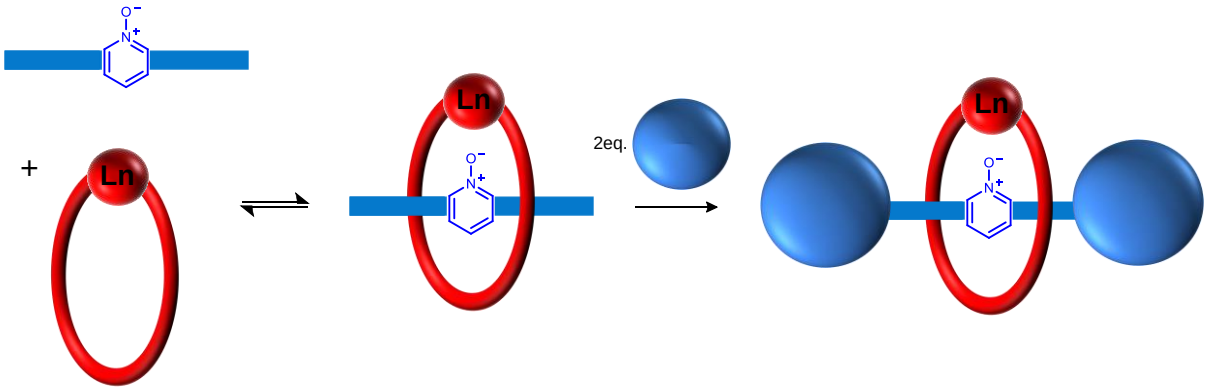

Scheme 4.4 Schematic representation of the preparation of a lanthanide [2]rotaxane, using Ln···*N*-oxide coordination.

[†]The work in the following section was published as a communication in the journal *Chemical Communications:* F. Zapata. O. Blackburn, M. J. Langton, S. Faulkner and P. D. Beer, *Chem Comm.*, 2013, **49**, 8157-8159.

4.2.2 Design and synthesis of the lanthanide-templated rotaxanes

In order to prepare a rotaxane in which the lanthanide cation forms an integral structural component of the anion binding domain, as opposed to providing a competing recognition site, a novel macrocycle was first conceived. The general design is shown schematically in Figure 4.2: the lanthanide cation is bound with high thermodynamic and kinetic stability within an eight-coordinate ligand, which itself is incorporated within the macrocycle. The structure is designed such that the vacant axial coordination site is directed into the internal void of the macrocycle, and is available to coordinate to a mono-dentate Lewis base, such as an anion or pyridine *N*-oxide motif.

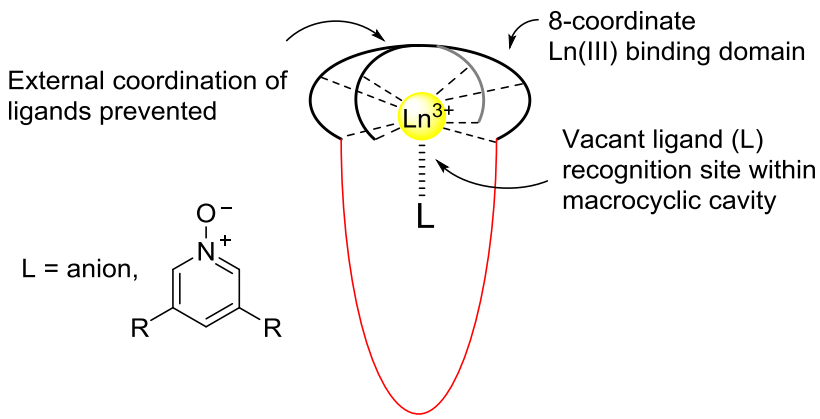

Figure 4.2 Schematic representation of the target lanthanide-integrated macrocyclic component.

An ideal class of hosts for recognising lanthanides in such a way are derivatives of the 1,4,7,10-tetraazacyclododecane (cyclen) motif (Figure 4.3a). Functionalisation of the nitrogen atoms with pendant carboxylate or amide groups results in a class of receptors that recognise lanthanide cations with high thermodynamic and kinetic stability. Cyclen appended with four carboxylates, namely 1,4,7,10-tetraazacyclododecane-1,4,7,10-tetraacetic acid, is generally referred to as DOTA (Figure 4.3b), while removal of one arm results in DO3A, and so on. Lanthanide complexes of such ligands have been used in a wide variety of applications, including magnetic resonance imaging,[20] radio-diagnostics and radio-therapy.[21]

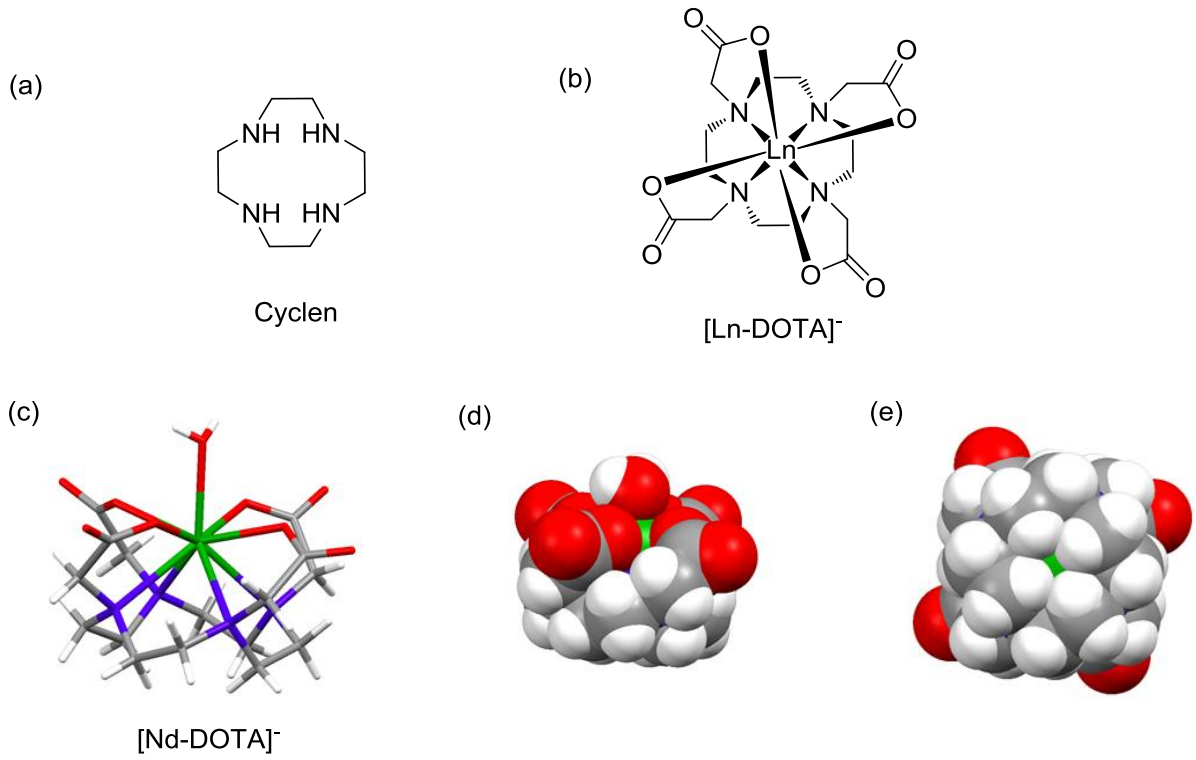

Figure 4.3 DOTA derivatives: (a) parent cyclen macrocycle and (b) Ln-DOTA complex. (c) Solid state structure of Nd(III)-DOTA square anti-prismatic complex with an axially coordinated water molecule, (d) space filling (side view) and (e) bottom view.

Analysis of crystal structures of lanthanide complexes of DOTA (the structure of the Nd(III) complex of DOTA is shown in Figure 4.3c–e for illustrative purposes[22]) reveals that DOTA is an ideal motif for incorporation into the target macrocycle. The four pendant carboxylates coordinate to the lanthanide cation from the top face, leaving one vacant coordination site in the axial position, which in this case is occupied by a ligating water molecule (Figure 4.3c,d). The nitrogen-donors of the cyclen motif coordinate from below the metal cation, whilst importantly; the bridging ethylene groups block access to the lanthanide from the bottom face of the complex (Figure 4.3e).

It was envisaged that replacing two of the pendant carboxylates with amides, which coordinate to the lanthanide cation through the carbonyl oxygen atoms, in a *N1*,*N*7 (*trans*) substitution pattern would provide a synthetic route towards incorporating the DOTA motif into a macrocycle. To this end the initial stage of the synthesis of the macrocycle involved the preparation of a trans-substituted cyclen derivative, using standard literature procedures

(Scheme 4.5).[23,24] Cyclen was first protected with carboxybenzyl (CBz) groups, which add in a regioselective *trans* substitution pattern, by adding benzylchloroformate to a solution of cyclen in chloroform at 0 ºC, to afford **78·(HCl)$_2$** which precipitated out of solution. The free base **78** was afforded by basifying with $NaOH_{(aq)}$. The *trans*-selectivity of the CBz-protection is believed to arise from the geometry of the cyclen, in which a *trans*-pair of nitrogen atoms each possess a lone pair of electrons that point outside of the macrocycle and facilitates rapid reaction with the benzylchloroformate, whilst precipitation of the hydrochloride salt prevents further substitution.[23] Reaction of **78** with two equivalents of *tert*-butyl bromoacetate in CH_3CN, in the presence of K_2CO_3, afforded compound **79** in 45% yield. Subsequent deprotection with H_2 in the presence of 10wt% Pd/C afforded the desired 1,7-DO2A diester derivative **80**.

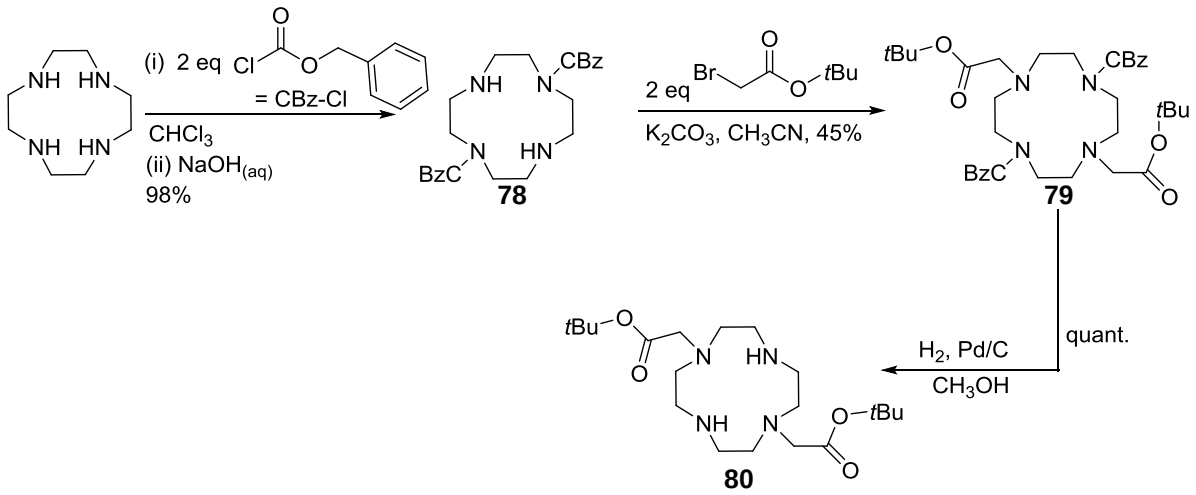

Scheme 4.5 Synthesis of *N*1,*N*7-disubstituted cyclen **80**.

The synthesis of the macrocycle incorporating the 1,7-DO2A diester motif is shown in Scheme 4.6. Macrocycle precursor **81** was prepared by condensing two equivalents of chloroacetylchloride with the corresponding bis-amine derivative **16**.[25] The synthesis of macrocycle **82** was then achieved by reacting equimolar quantities of 1,7-DO2A diester **80** with bis-amide macrocycle precursor **81** in the presence of K_2CO_3, under high dilution conditions (3 mM) in refluxing acetonitrile. The pure product was isolated in 70% yield after

recrystallisation. Presumably the macrocyclisation is templated by potassium cations, which are known to bind within DOTA derivatives, and may account for the remarkably high yield for this macrocyclisation reaction. Cleavage of the *tert*-butyl ester groups with TFA afforded the acid form **84**, which was followed by complexation with either lutetium or europium trifluoromethanesulfonate salts, affording the macrocyclic complexes **84·OTf** and **85·OTf**, respectively.

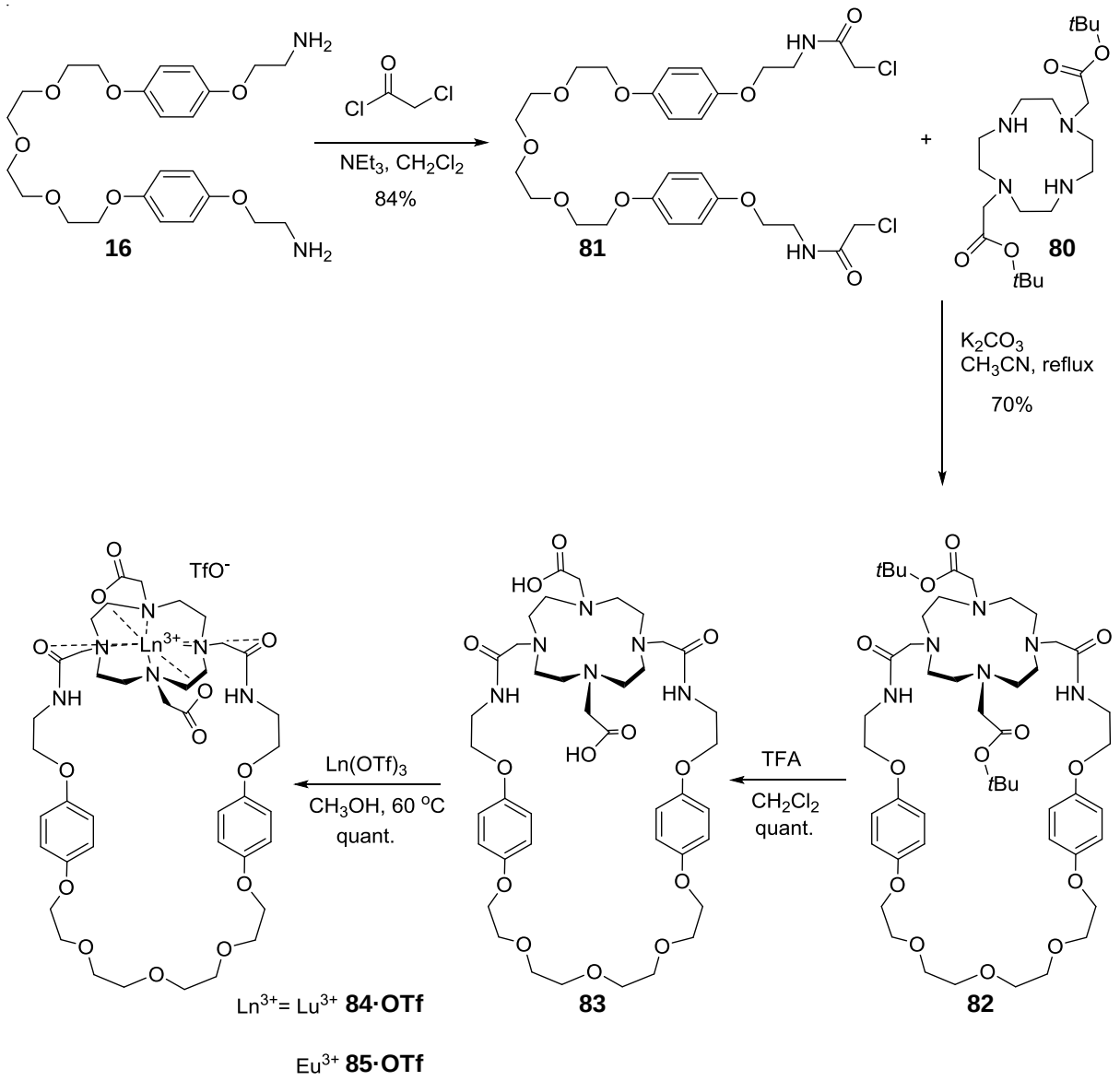

Scheme 4.6 Synthesis of macrocyclic lanthanide complexes **84·OTf** and **85·OTf**.

The choice of lanthanide cation was dictated by the analytical technique required: thus the diamagnetic Lu(III) complex facilitates characterisation by ^{1}H NMR analysis, whilst Eu(III) leads to paramagnetic shifts of the NMR spectrum but facilitates structural characterisation by analysis of its luminescence.

The pyridine *N*-oxide axle precursor component was prepared as shown in Scheme 4.7. The condensation reaction between 3,5-bis-chlorocarbonyl pyridine and two equivalents of 3-bromopropylamine hydrobromide afforded compound **86** in 50% yield. Azide nucleophilic substitution afforded the bis-azide compound **87**, which was oxidised to the corresponding pyridine *N*-oxide **88** using Oxone® in 1:1 H_2O/butanone.

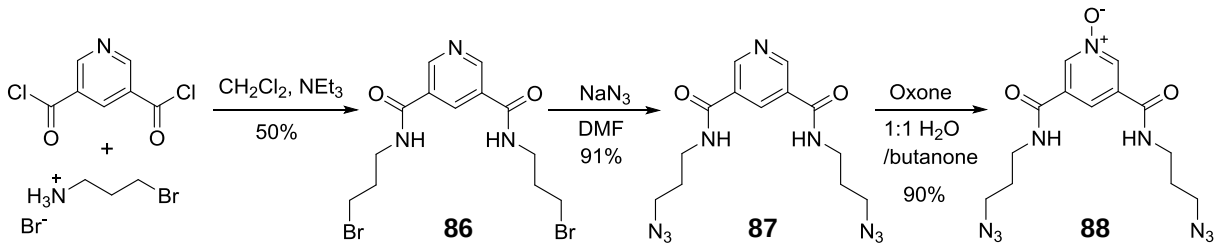

Scheme 4.7 Synthesis of pyridine *N*-oxide axle precursor component **88**.

Synthesis of the target lanthanide-templated [2]rotaxane was achieved using a copper(I)-catalysed azide–alkyne (CuAAC) stoppering methodology as shown in Scheme 4.8. The macrocycle complexes **84·OTf** and **85·OTf** were insoluble in CH_2Cl_2, and so a 3:2 CH_2Cl_2/CH_3CN mixture was employed to solubilise both the macrocycle and axle precursor starting materials. The appropriate macrocyclic complex (**84·OTf** and **85·OTf**), bis-azide pyridine *N*-oxide axle precursor **88** and two equivalents of alkyne-fuctionalised terphenyl stopper **40** in a 3:2 CH_2Cl_2/CH_3CN solution were stirred in the presence of catalytic $Cu(CH_3CN)_4PF_6$ and TBTA for 48 hours to afford the target lanthanide [2]rotaxanes **89·OTf** and **90·OTf** respectively. The interlocked products could not be purified by either silica gel or alumina column chromatography due to the presence of the charged lanthanide complex. Size exclusion chromatography, however, was able to separate the rotaxane product from the non-

interlocked axle and macrocycle by-products, to afford rotaxanes **89·OTf** and **90·OTf**, both in a 20% isolated yield.

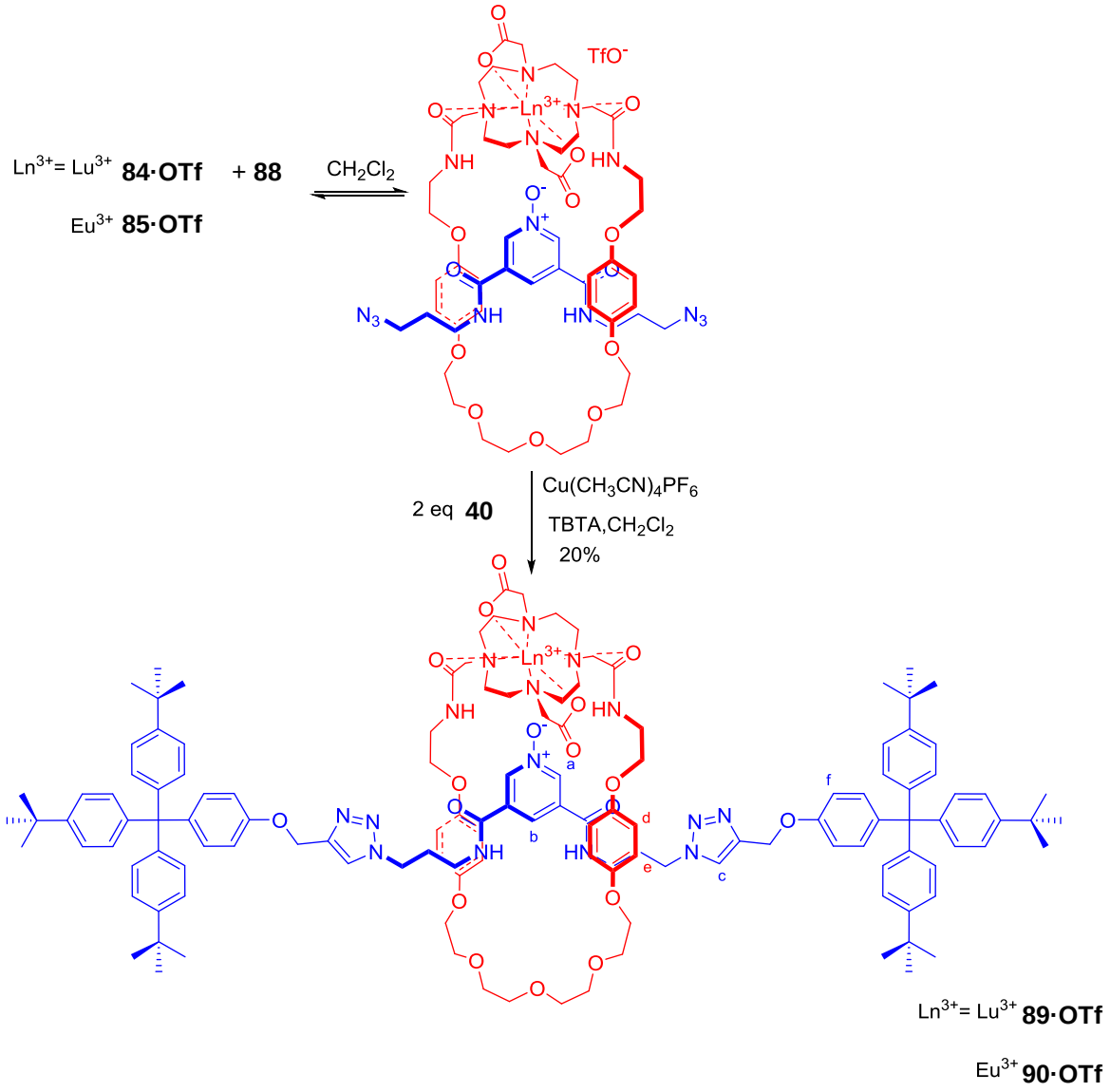

Scheme 4.8 Synthesis of lanthanide [2]rotaxanes **89·OTf** and **90·OTf**.

4.2.3 Characterisation of the lanthanide-[2]rotaxanes

4.2.3.1 NMR characterisation

The rotaxanes were characterised by NMR spectroscopy and high resolution mass spectrometry, as detailed below. The diamagnetic lutetium complexes could be fully characterised by ^{1}H and ^{13}C NMR analysis: a comparison of the ^{1}H NMR spectra of the Lu-[2]rotaxane **89·OTf**, Lu-macrocycle **84·OTf** and the non-interlocked axle by-product is shown in Figure 4.4.

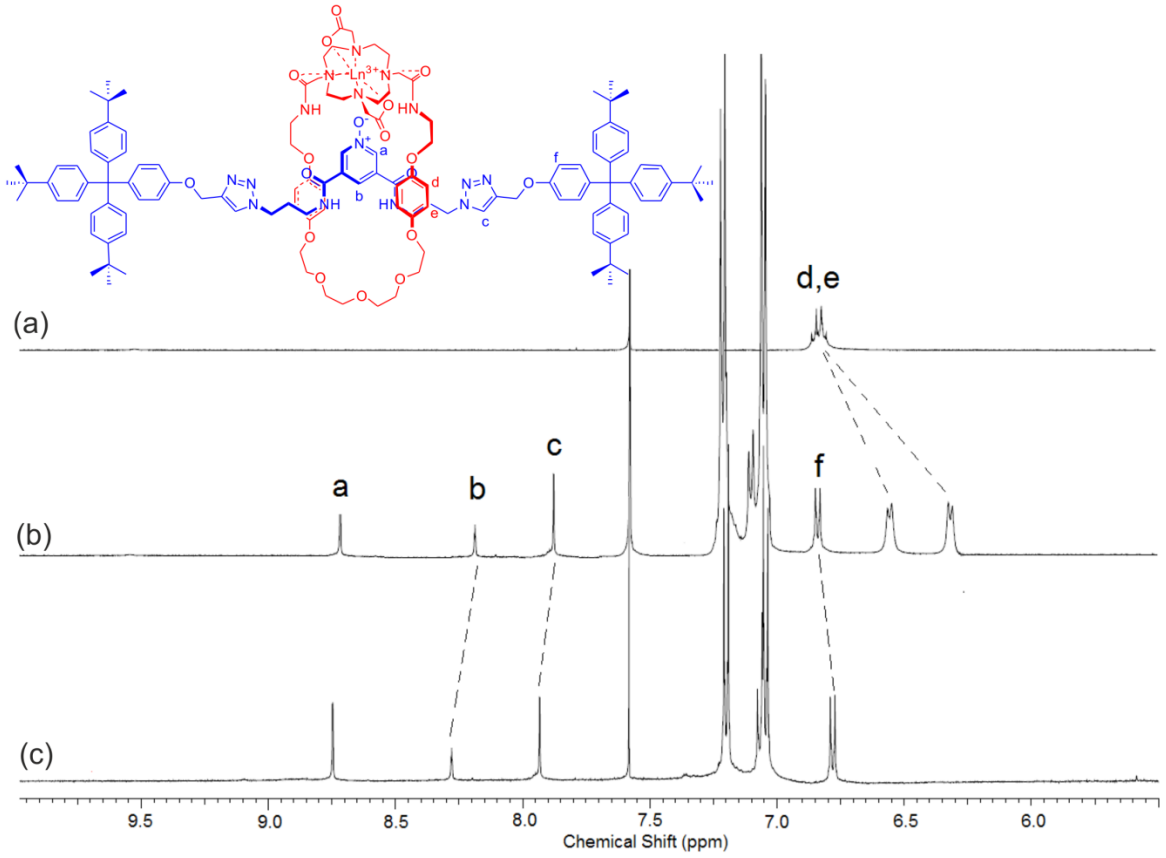

Figure 4.4 Partial ^{1}H NMR spectra in 1:1 $CDCl_3/CD_3OD$ (500 MHz, 298 K) of (a) Lu-macrocycle **84·OTf**, (b) Lu-rotaxane **89·OTf** and (c) non-interlocked axle.

Modest upfield shifts of protons *b* and *c* are observed, in addition to a small downfield perturbation of the stopper protons *f*. Importantly large upfield perturbations and splitting of the macrocycle hydroquinone protons *d* and *e* are also identified, which are diagnostic of the aromatic donor–acceptor interactions between the hydroquinones and the axle pyridine *N*-oxide motif in the interlocked structure. This provides convincing evidence as to the

mechanically bonded nature of the rotaxane, which is further confirmed by analysis of the ^{1}H ROESY NMR spectrum of **89·OTf** in which through-space correlations between the pyridine *N*-oxide protons *a* and *b* in the axle and hydroquinone protons *d* and *e* in the macrocycle component are identified (Figure 4.5).

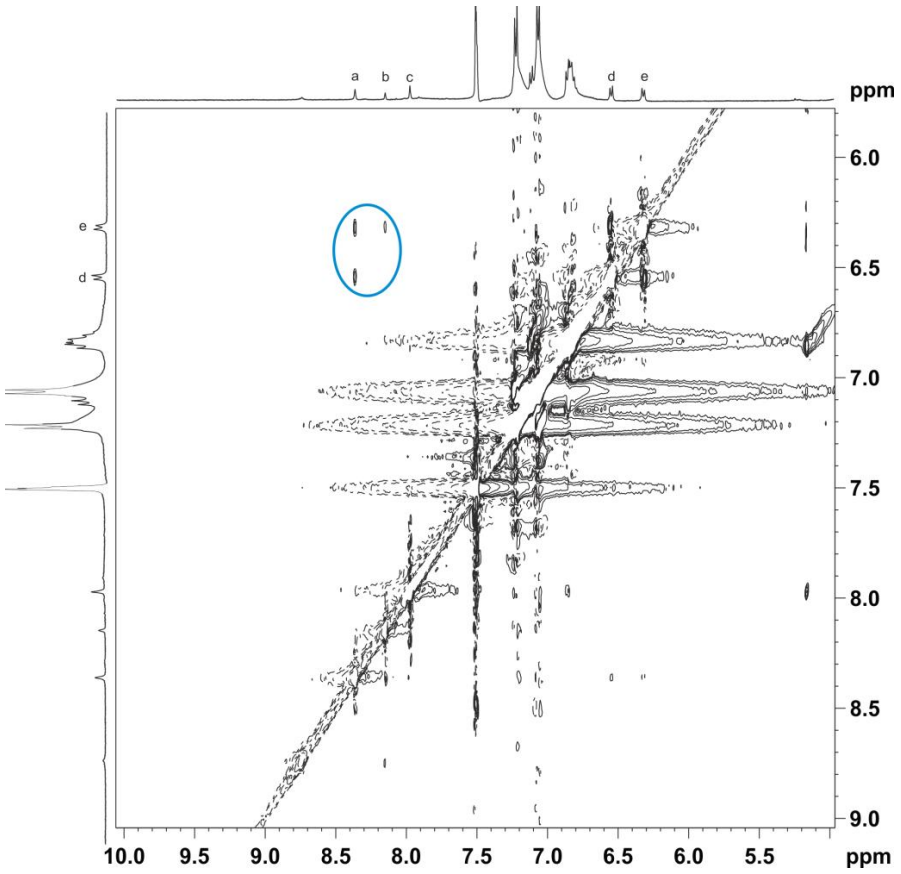

Figure 4.5 ^{1}H ROESY NMR spectrum of Lu rotaxane **89·OTf** in 1:1 $CDCl_3/CD_3OD$ (500 MHz, 298 K). For atom labels see Figure 4.4.

To further demonstrate that the pyridine *N*-oxide axle is indeed threaded through the macrocycle cavity, and not coordinated to the lanthanide in such a way that the system is not mechanically bonded, an equimolar solution of macrocycle **84·OTf** and the non-interlocked axle component in 3:2 CD_2Cl_2/CD_3CN was prepared, and the ^{1}H NMR spectrum compared to those of the separate species (Figure 4.6). Importantly, the hydroquinone protons are un-perturbed, in contrast to the ^{1}H NMR of rotaxane **89·OTf**, thus demonstrating that the axle component of the rotaxane is indeed threaded through the macrocycle. This experiment also

serves to prove that the stopper components are sufficiently large to prevent macrocycle threading or de-threading *via* a slippage mechanism.

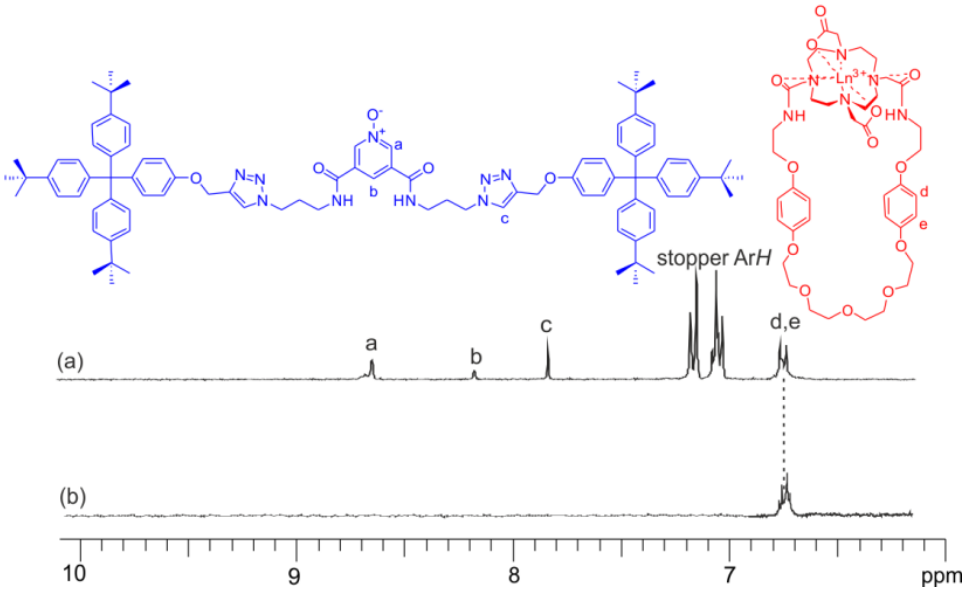

Figure 4.6 Partial ^{1}H NMR spectra in 3:2 CD_2Cl_2/CD_3CN (300 MHz, 298 K) of (a) 1:1 macrocycle **84·OTf** /axle and (b) macrocycle **84·OTf**.

An analogous titration experiment was conducted in the absence of the lanthanide cation, by adding one equivalent of pyridinie *N*-oxide threading component **88** to a solution of the non-complexed cyclen macrocycle **83** in 3:2 CD_2Cl_2/CD_3CN. The spectrum revealed no upfield perturbations of the macrocycle's hydroquinone protons which suggests that the contribution of aromatic donor–acceptor interactions to the overall mechanical bond formation process is minimal, and highlights the important templating role of the lanthanide cation. It should be noted that the copper(I) catalysed (CuAAC) stoppering rotaxane synthesis cannot be undertaken in the absence of the lanthanide cation template because of the propensity of the DOTA ligand to complex the copper(II) by-product.

The ^{1}H NMR spectrum of Eu-rotaxane **90·OTf** is complicated (Figure 4.7), but is consistent with the presence of the paramagnetic Eu(III) cation which causes perturbation of the proximal protons. The region between 10–0 ppm is significantly broadened compared to

that of the corresponding lutetium rotaxane (Figure 4.7, inset), however the signals corresponding to the pyridine *N*-oxide and stopper units can be clearly identified.

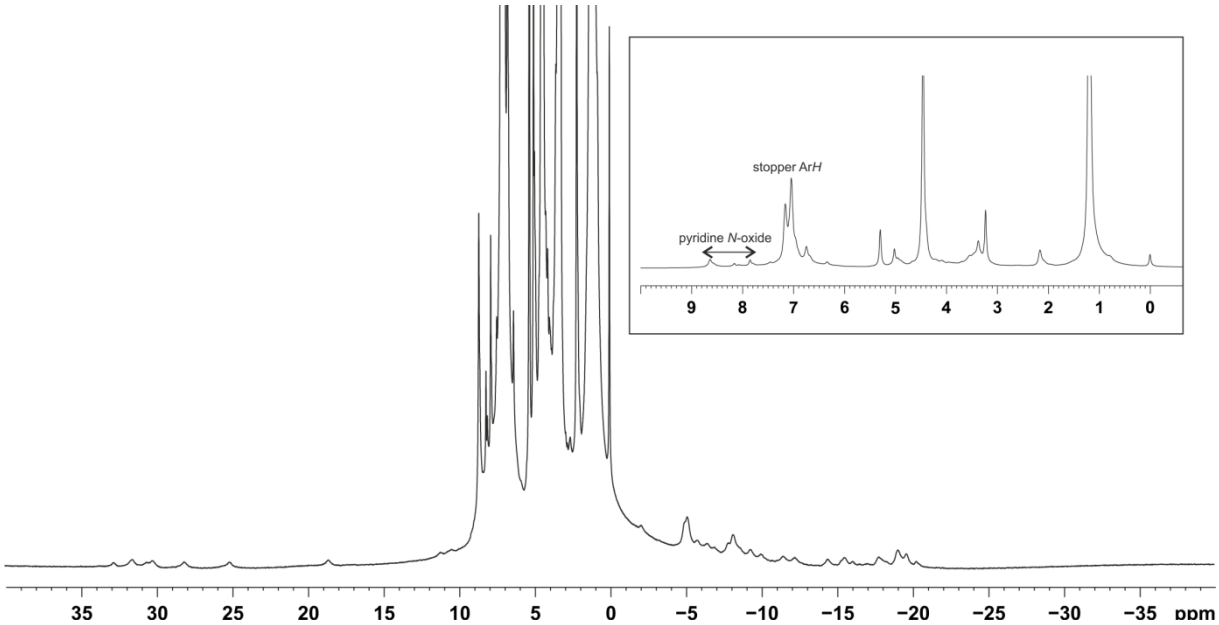

Figure 4.7 ^{1}H NMR spectrum of Eu-rotaxane **90·OTf** (1:1 $CDCl_3/CD_3OD$, 500 MHz, 298 K). Inset: expanded view of the region between 10–0 ppm.

High resolution mass spectrometry studies on both the lutetium and europium rotaxanes, **89·OTf** and **90·OTf** (Figure 4.7), provided further structural characterisation of the two interlocked species, with an excellent match between the measured spectra and the calculated isotope patterns obtained in each case.

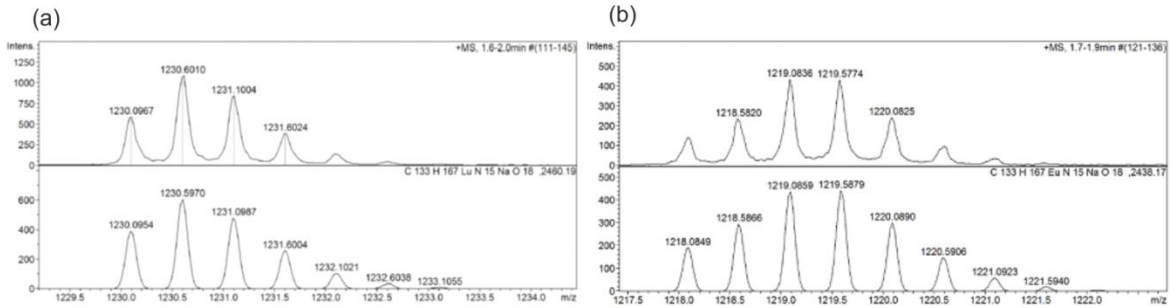

Figure 4.7 High resolution electrospray ionisation mass spectra of (a) lutetium rotaxane **89·OTf** and (b) europium rotaxane **90·OTf** (top), with theoretical isotope model for $[M-OTf+Na]^{2+}$ (bottom).

4.2.3.2 Structural characterisation of Eu-rotaxane 90·OTf using luminescence spectroscopy

Lifetime measurements of the europium excited state can be used to probe the number of inner sphere solvent molecules at the metal, from which the local structure can be deduced. The most efficient quenchers of lanthanide excited states are OH oscillators associated with a bound solvent molecule in the first coordination sphere, whilst quenching effects from the higher harmonics of NH, C–H and C=O contribute to a lesser extent.[26] In the case of europium, there is relatively efficient coupling of the Eu(III) excited state to the third vibrational overtone of proximate OH oscillators, due to favourable Franck–Condon overlap. The corresponding deuterated oscillators (X–D) exhibit lower stretching frequencies and thus energy matching is only achievable with the higher vibrational states, resulting in vibronic quenching that is at least 200 times less effective than the X–H analogues.

It should be noted that understanding the solvation of even straightforward lanthanide complexes in mixed solvent systems is challenging; however solubility limitations dictated the use of 1:1 CH_2Cl_2/CH_3OH for analysis of the lanthanide rotaxane and macrocycle systems in this case. It is reasonable to assume that given the residual charge on the lanthanide complex, any inner sphere solvent at the europium will comprise of methanol molecules rather than dichloromethane. Taking this approximation into account, it is possible to estimate q, the number of inner sphere methanol molecules bound to the lanthanide cation, from Equation 4.1, where x is the number of exchangeable amide N–H oscillators close to the metal centre.[12,27]

Equation 4.1 $$q = 2.4(\tau CH_3OH^{-1} - \tau CD_3OD^{-1} - 0.125 - 0.0375x)$$

In the protic solvent mixture of 1:1 CH_2Cl_2/CH_3OH, the observed luminescence lifetime for rotaxane **90·OTf** was found to be 0.94 ms, while in deuterated solvent (1:1 CD_2Cl_2/CD_3OD) the lifetime increased to 1.18 ms (Figure 4.8), equating to a calculated value of $q = 0$ if it is assumed that all four N–H oscillators contribute (two from the macrocycle and two from the axle component). This suggests that methanol is excluded from the inner coordination sphere of the europium centre in **90·OTf**, which is consistent with the pyridine *N*-oxide's oxygen atom acting as an axial donor to the lanthanide cation. The luminescence lifetime of macrocycle **85·OTf** in 1:1 CH_2Cl_2/CH_3OH is much shorter, and a bi-exponential fit affords lifetimes of 0.20 and 0.63 ms, which indicates solvation at the europium centre, in contrast to rotaxane **90·OTf**.

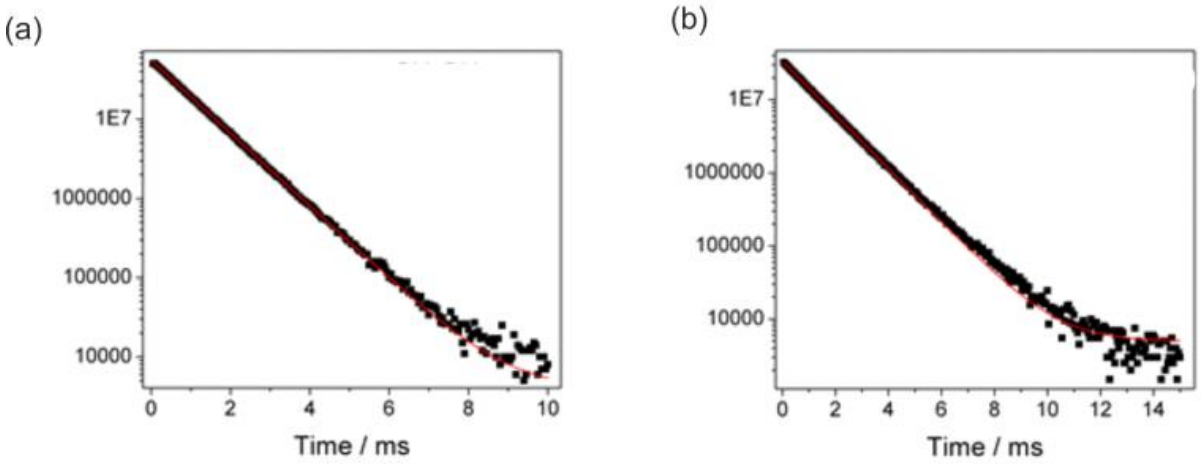

Figure 4.8 Lifetime data and fits (red lines) for rotaxane **90OTf** in (a) 1:1 CH_2Cl_2/CH_3OH and (b) 1:1 CD_2Cl_2/CD_3OD, exciting at 397 nm and observing at 616 nm.

4.2.4 Anion recognition properties

Preliminary experiments to investigate the possibility of using anions to displace the coordinating pyridine *N*-oxide ligand from the lanthanide centre were conducted initially by luminescence fluoride binding titrations. Addition of TBAF to a solution of europium rotaxane **90·OTf** in 1:1 CH_2Cl_2/CH_3OH (using a non-dilution protocol) caused significant quenching of the luminescence, following excitation at 350 nm (Figure 4.9a). The 1:1 stoichiometric association constant was calculated by modelling the changes in the emission spectrum using the DYNAFIT[28] program and determined to be 1900 M^{-1} (Figure 4.9b). The number of inner sphere solvent molecules *q* at the end of the titration was measured to be 0, which indicated that the *N*-oxide motif had been replaced with a bound fluoride anion, and not a solvent molecule.

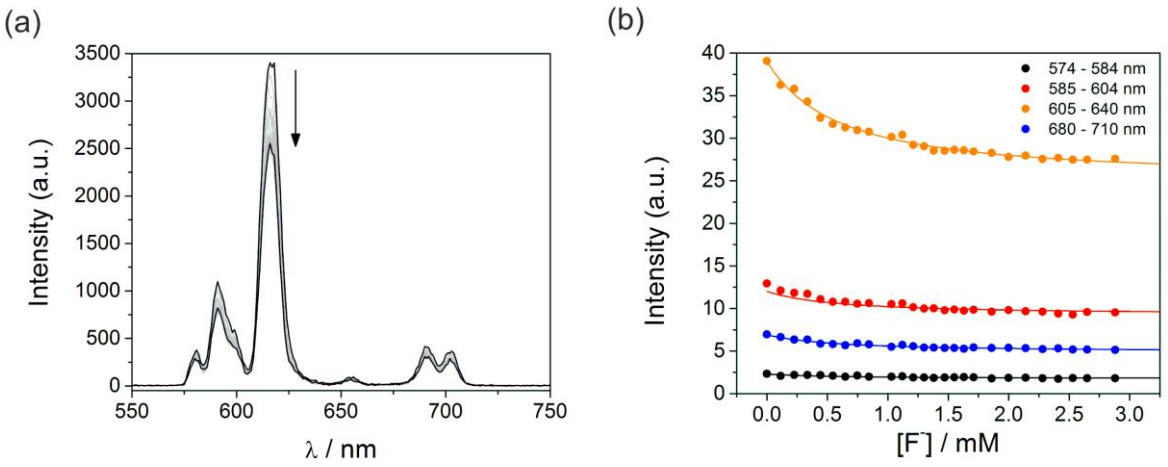

Figure 4.9 (a) Changes in the emission spectrum of a 10^{-4} M solution of europium rotaxane **90·OTf** upon addition of fluoride in 1:1 CH_2Cl_2/CH_3OH (350 nm excitation, 298 K); (b) plots of emission intensity change against fluoride concentration. Actual data represented by solid symbols for each europium emission bands, calculated 1:1 binding isotherms for the best global fit obtained represented by solid lines.

An analogous fluoride titration was conducted with the europium macrocycle **85·OTf** in the same solvent mixture. Addition of increasing amounts of TBAF resulted in an initial sharp enhancement of the europium emission intensity, followed by a shallower decrease in intensity, which was postulated to be due to a collisional quenching process (Figure 4.10).

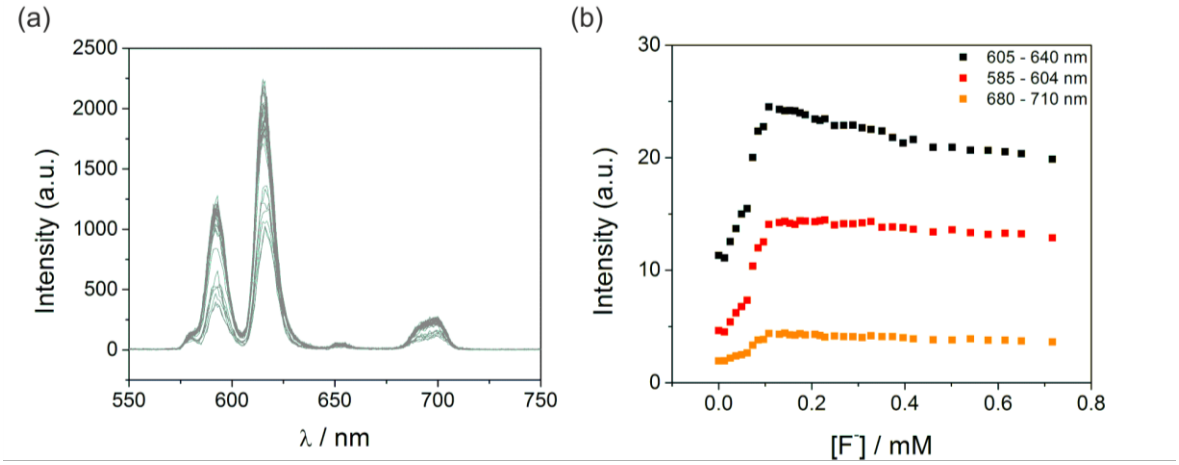

Figure 4.10 (a) Changes in the emission spectrum of a 10^{-4} M solution of europium macrocycle **85·OTf** upon addition of fluoride in 1:1 CH_2Cl_2/CH_3OH (350 nm excitation, 298 K); (b) plots of emission intensity change against fluoride concentration for the europium emission bands.

The complex behaviour of the emission profile upon addition of fluoride could not be modelled directly, however, but using the ratio of the hypersensitive $\Delta J = 2$ transition (605–640 nm) to the other europium centered transitions allowed the binding directly to the metal to be quantified. Using the ratio of $\Delta J = 2$ / $\Delta J = 1$, DYNAFIT analysis revealed a fluoride association constant of 76 000 M^{-1}, which equates to a 40-fold increase over that of the rotaxane (Figure 4.11).‡

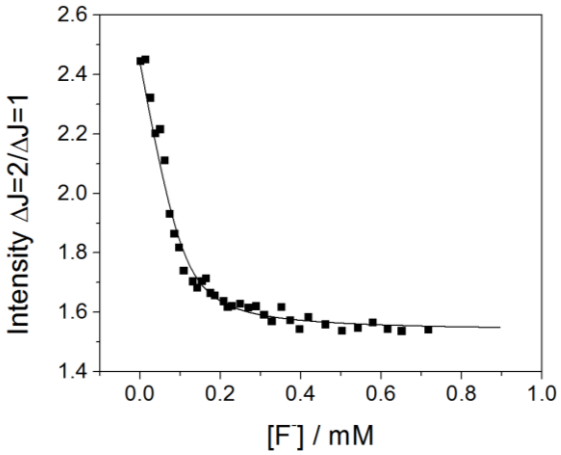

Figure 4.11 Plot of the ratio of the intensity of the $\Delta J = 2$ and $\Delta J = 1$ transitions against fluoride concentration. Actual data represented by solid symbols, calculated 1:1 binding isotherm represented by the solid line.

‡ Changes in the ratio $\Delta J = 2$ / $\Delta J = 1$ for rotaxane **90·OTf** were too small to model, presumably because F^- displacement of the pyridine *N*-oxide does not alter the number of directly ligated OH oscillators, and thus the contribution from vibronic quenching is relatively constant. A direct comparison between association constants determined by this ratiometric analysis, and those from global intensity changes, should in general be treated with caution. Nevertheless, the 40-fold difference in association constant between the macrocycle and the rotaxane can be reasonably assumed to be significant in this case.

The dramatic decrease in fluoride binding affinity by europium rotaxane **90·OTf** compared to the non-interlocked macrocycle **85·OTf** can be understood by considering the competition between the anion guest and axle pyridine *N*-oxide donor for the lanthanide centre in the rotaxane, which is absent in the case of the macrocycle (Figure 4.12).

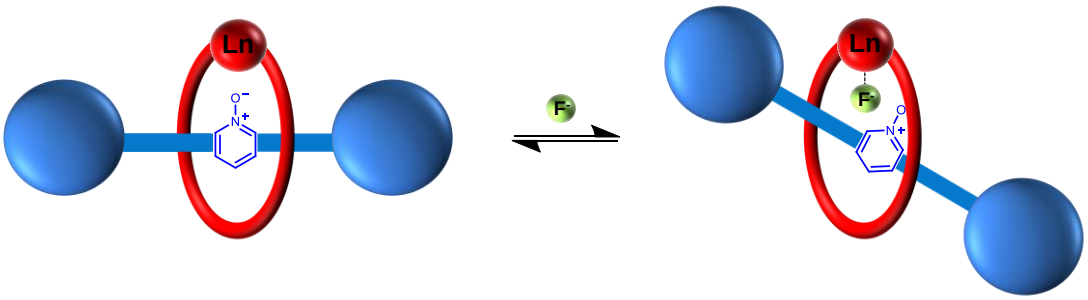

Figure 4.12 Schematic representation to illustrate the binding of fluoride to the lanthanide metal centre incorporated within the macrocycle component of rotaxane **90·OTf**, concomitant with displacement of the pyridine *N*-oxide ligand of the axle component.

The competitive ligation of the pyridine *N*-oxide motif to the metal centre diminishes the usefulness of this rotaxane as an anion sensor. Indeed, work to prepare alternative lanthanide-based rotaxanes in which the template can be removed prior to anion recognition studies is described in the remainder of this chapter. Whilst the association of anions to rotaxane **90·OTf** is considerably weaker than the corresponding non-interlocked macrocycle, analogous titrations with acetate revealed that the rotaxane displays enhanced selectivity for fluoride over acetate compared to macrocycle **85·OTf**. The association constants for AcO^- were found to be lower in both cases than for F^- ($K_a = 12\,000\ M^{-1}$ for the macrocycle, $K_a = 26\ M^{-1}$ for the rotaxane), whilst the degree of selectivity of the rotaxane for F^- over AcO^- [$K_{a(F-)} / K_{a(AcO-)}$] = 73) is over an order of magnitude greater for the rotaxane than with macrocycle **85·OTf** [$K_{a(F-)} / K_{a(AcO-)} = 6$]. These observations suggest that the three-dimensionally restrained nature of the rotaxane's interlocked binding cavity disfavours oxo-anion binding to the lanthanide centre to a greater extent than that of the smaller fluoride anion. The addition of chloride to both rotaxane **90·OTf** and macrocycle **85·OTf** caused no appreciable change in luminescence intensity and the binding, if any, could not be quantified.

4.3 Anion templated synthesis of lanthanide-containing rotaxanes[§]

4.3.1 Synthetic strategy for anion-templated lanthanide rotaxane synthesis

In the previous section the first example of a lanthanide cation templated synthesis of a rotaxane was presented, by incorporating a pyridine *N*-oxide motif within the axle component. The anion recognition and sensing capabilities of the rotaxane were modest however, due to the competition between the anionic guest species and the pyridine *N*-oxide template that remains incorporated within the axle component. In order to achieve strong recognition and sensing of anions an alternative templation approach was required. It was envisaged that a *discrete* anion could be used to template rotaxane formation: the anion is then subsequently removed from the binding domain by exchanging to a weakly coordinating counter-anion, facilitating anion recognition by eliminating the competing templating species.

The anion-templation concept for the preparation of a lanthanide-[2]rotaxane capable of anion sensing is shown in Scheme 4.9. An anion templates the formation of an initial pseudorotaxane assembly, by simultaneously coordinating to the lanthanide cation bound within a macrocycle component and to a hydrogen bonding motif incorporated within the axle precursor. Stoppering of this pseudorotaxane affords the [2]rotaxane product, from which the templating anion is removed to reveal a vacant anion-binding cavity formed between the interlocked macrocycle and axle components.

[§] The work in the following section describing the nitrite templated synthesis of Ln-rotaxanes and the anion sensing capability of the Eu-rotaxane product, was published as a communication in the journal *Angewandte Chemie:* M. J. Langton, O. A. Blackburn, T. Lang, S. Faulkner and P. D. Beer, *Angew. Chem. Int. Ed.,* 2014*,* **53***,* 11463–11466

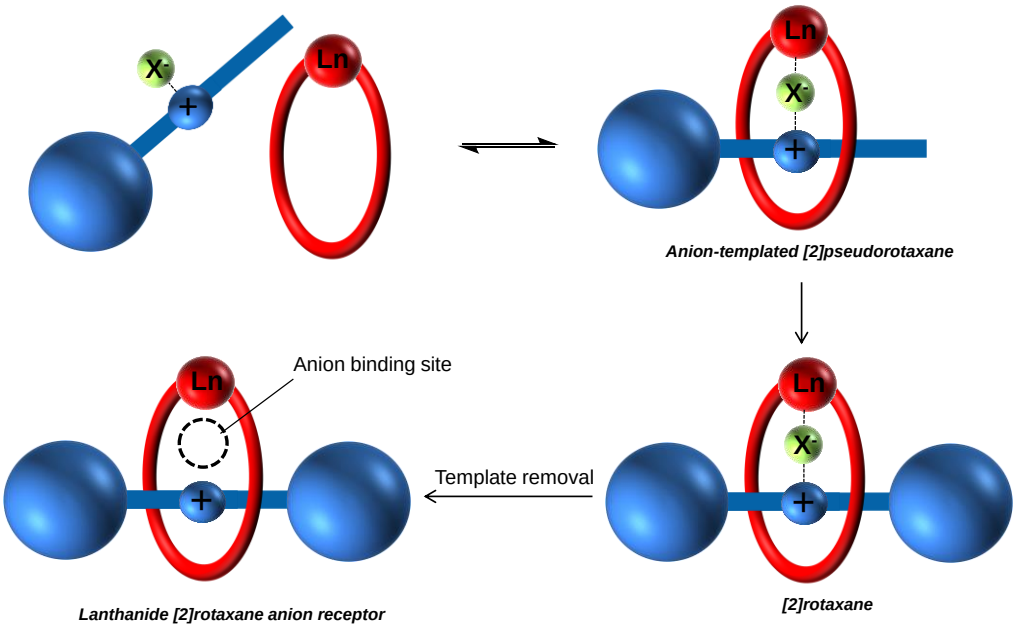

Scheme 4.9 Schematic representation of anion templation of a lanthanide-containing [2]rotaxane for anion recognition and sensing, *via* mono-stoppering of a [2]pseudorotaxane.

4.3.2 Anion templated lanthanide-[2]rotaxane synthesis

The mono-stoppered axle precursor used for this work **91·Cl** (Scheme 4.10) was prepared by Dr Thomas Lang, and was previously used in the chloride-templated synthesis of solution- and surface-assembled osmium(II) bipyridyl rotaxanes.[29] Of particular note is the 3,5-bis-amide pyridinium motif that strongly coordinates to anions by means of two hydrogen bonds, and a biphenyl spacer unit which has been shown to improve the efficiency of anion templated rotaxane synthesis compared to more flexible spacers.[29] The macrocycle components used in the synthesis are identical to those used in the preparation of the pyridine *N*-oxide lanthanide rotaxane (*vide supra*), namely lutetium macrocycle complex **84·OTf** and europium-complexed **85·OTf**.

In preliminary work chloride templated synthesis was investigated initially, by stirring one equivalent of **91·Cl** with 1.5 equivalent of lutetium macrocycle complex **84·OTf** and stopper alkyne **40** in dry 3:2 CH_2Cl_2/CH_3CN in the presence of catalytic $Cu(CH_3CN)_4PF_6$ and TBTA (Scheme 4.10). Mass spectrometry analysis of the crude reaction mixture revealed a small peak corresponding to the mass of the desired rotaxane product. Isolation and

purification of the rotaxane was attempted using size exclusion chromatography; however the interlocked product was formed in a yield too low to isolate.

The rotaxane formation was subsequently attempted using fluoride as the templating anion, as it has previously been demonstrated to bind strongly to the macrocycle's lanthanide centre (Section 4.2.4). One equivalent of TBAF was added to the hexafluorophosphate salt of axle precursor **91·PF$_6$** (prepared by washing a CH_2Cl_2 solution of the chloride salt **91·Cl** with aqueous NH_4PF_6) and rotaxane formation was carried out under otherwise identical conditions. Unfortunately however, mass spectrometry analysis of the reaction mixture revealed no evidence of the desired rotaxane product, with only peaks corresponding to the non-interlocked axle and macrocycle detected.

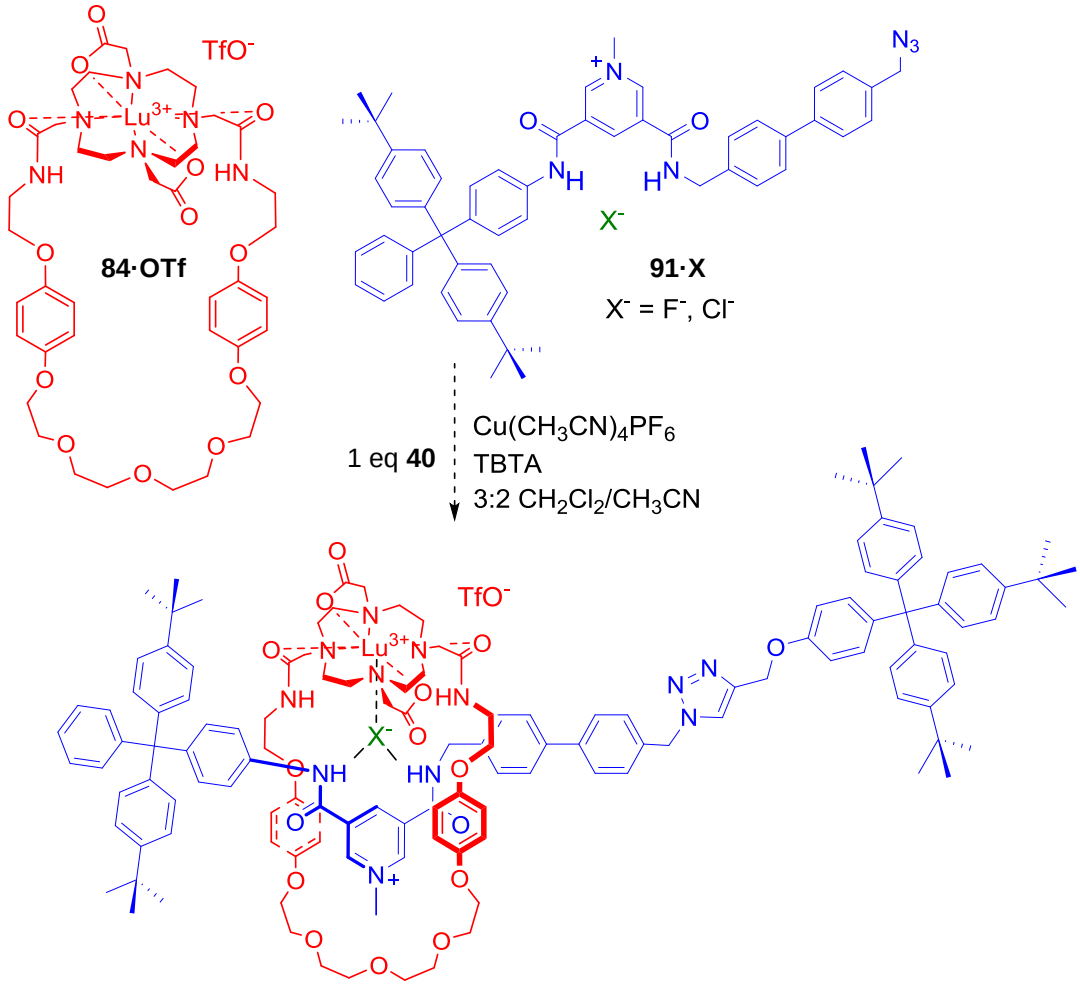

Scheme 4.10 Attempted chloride and fluoride templated synthesis of a lanthanide-containing rotaxane.

The simultaneous coordination of the template to both the macrocycle and axle precursor component is essential for rotaxane formation, and from the failure of the small, spherical halide anions to template the assembly of the interlocked product it was concluded that an anion of different size and geometry was required. Correspondingly, attention was turned to the *nitrite* anion, which possesses a bent geometry ($\alpha_{[O–N–O]} = 120^{o}$), and was anticipated to act as a bidentate templating anion, with one oxygen atom able to accept hydrogen bonds from the axle precursor, whilst the other coordinates to the lanthanide cation in the macrocycle.

Thus axle precursor **91·Cl** was converted to the corresponding nitrite salt **91·NO_2** by passing down a nitrite-loaded Amberlite® anion exchange resin, before rotaxane formation was attempted initially with Lu-macrocycle **84·OTf** using the same procedure as described above (Scheme 4.11). Mass spectrometry analysis of the crude mixture revealed in this case a dominant peak corresponding to the desired interlocked product. The copper catalyst was removed by washing a CH_2Cl_2 solution of the crude reaction mixture with EDTA solution, before purification using size exclusion chromatography afforded Lu-rotaxane **92·NO_2·OTf** in 51% yield. The rotaxane formation was repeated with the europium-containing macrocycle **85·OTf**, affording the corresponding Eu-[2]rotaxane **93·NO_2·OTf** in 45% yield. The [2]rotaxane products were characterised by NMR spectroscopy, mass spectrometry and HPLC analysis, as detailed in the following section.

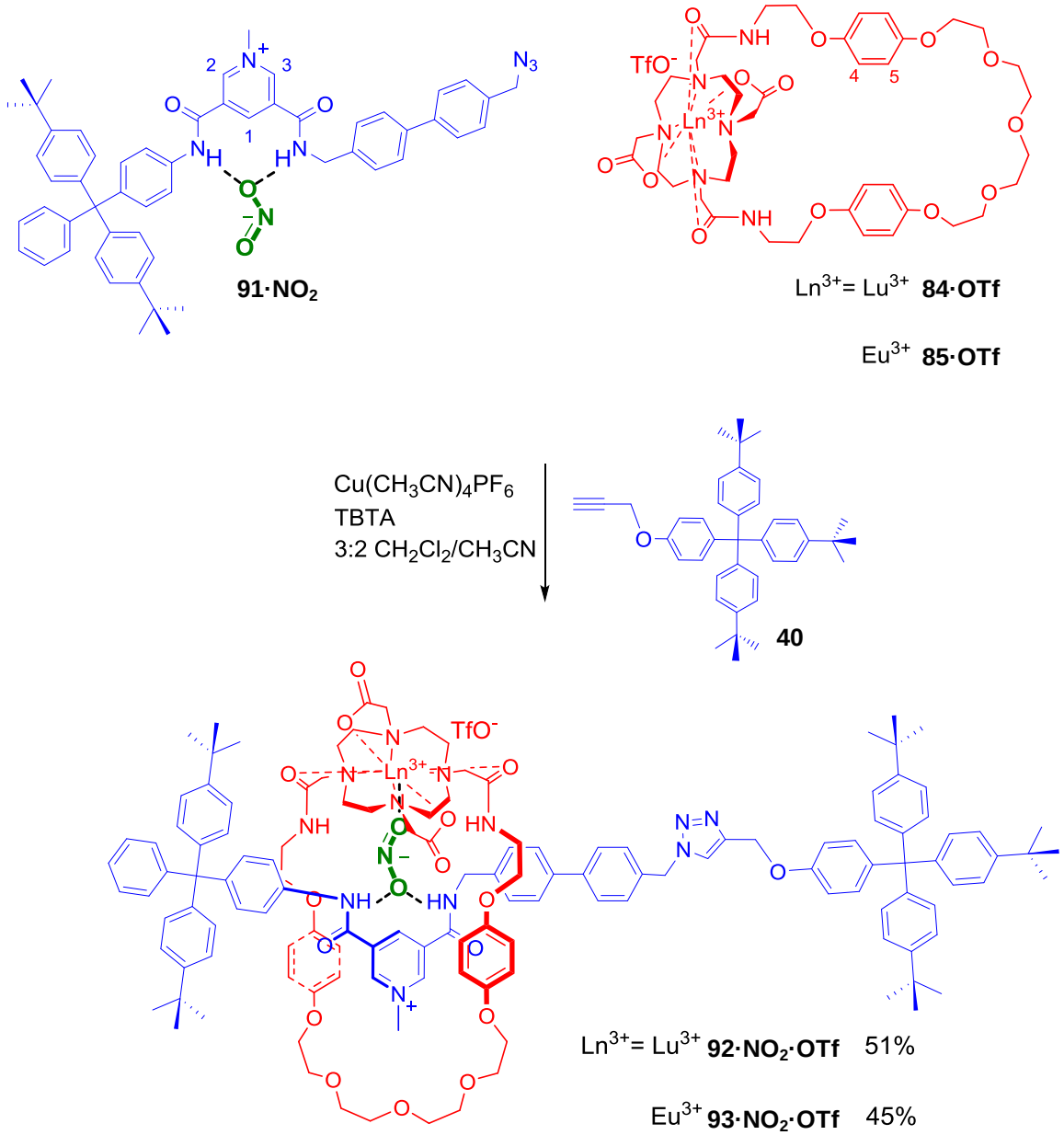

Scheme 4.11 Nitrite-templated synthesis of lanthanide-[2]rotaxanes **92·NO$_2$·OTf** and **93·NO$_2$·OTf**.

4.3.3 Characterisation of nitrite-templated rotaxanes

The ^{1}H NMR spectrum of Lu-[2]rotaxane **92·NO$_2$·OTf** is compared to the spectra of the non-interlocked axle (isolated as the major by-product from the reaction mixture) and macrocycle **84·OTf** in Figure 4.13. The spectrum of **92·NO$_2$·OTf** is broad and the aromatic protons are split into multiple signals, even when heated to 353 K in d_6-DMSO, which suggests that the rotaxane is in slow exchange between two or more conformers (Figure 4.13b,c).

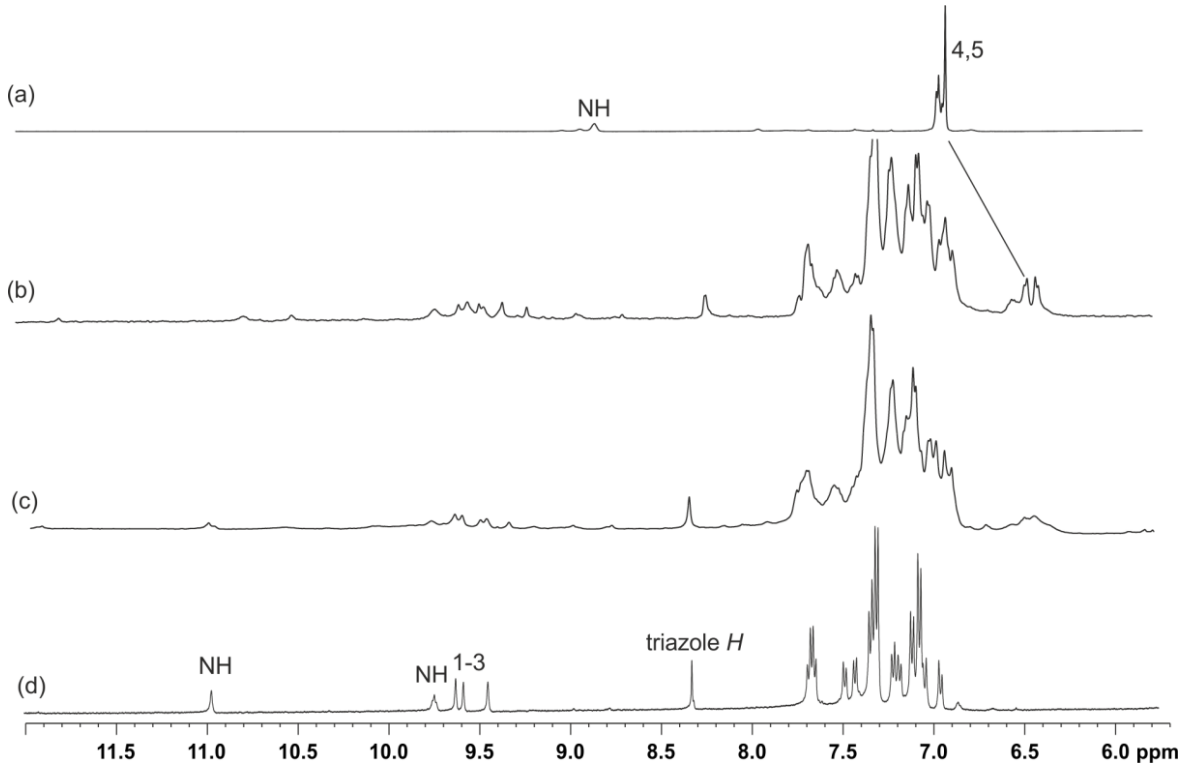

Figure 4.13 Partial ^{1}H NMR spectra in d_6-DMSO (500 MHz) of (a) Lu-macrocycle **84·OTf** (298 K), (b) Lu-rotaxane **92·NO$_2$·OTf** (353 K), (c) Lu-rotaxane **92·NO$_2$·OTf** (298 K) and (d) axle (298 K). For atom labels see Scheme 4.11.

The parent DOTA ligand is known to adopt either a square-antiprismatic or twisted square antiprismatic geometry in solution, which may interconvert through rotation of the acetate arms or the conformational inter-conversion of the ethylene groups of the cyclen macrocycle.[22,30] Whilst the structure of the DO2A motif of macrocycles **84**$^+$ and **85**$^+$ is undoubtedly more complicated than in this simple case, the broad features and peak splitting observed in the ^{1}H NMR spectrum indicate that the structure exists in two or more geometries that interconvert slowly on the NMR timescale. This contrasts with the pyridine *N*-oxide

rotaxane **89·OTf**, whose ^{1}H NMR is relatively sharp and only one set of aromatic protons is observed, which suggests that the presence of the axle's pyridine *N*-oxide donor rigidifies the system and locks the macrocycle's DO2A motif in one conformation. Nevertheless, the ^{1}H NMR spectrum of **92·NO_2·OTf** provides evidence as to the interlocked nature of the rotaxane, with upfield perturbation and splitting of the macrocycle hydroquinone protons being clearly observed, which is diagnostic of rotaxane formation (Figure 4.13b).

HPLC analysis was used to establish the purity of the rotaxanes **92·NO_2·OTf** (Figure 4.14) and **93·NO_2·OTf**, which exhibited marked differences in retention times to the non-interlocked axle and macrocycle components. This demonstrates that the species are not merely weakly associated, and provides further compelling evidence as to the interlocked nature of the rotaxane species.

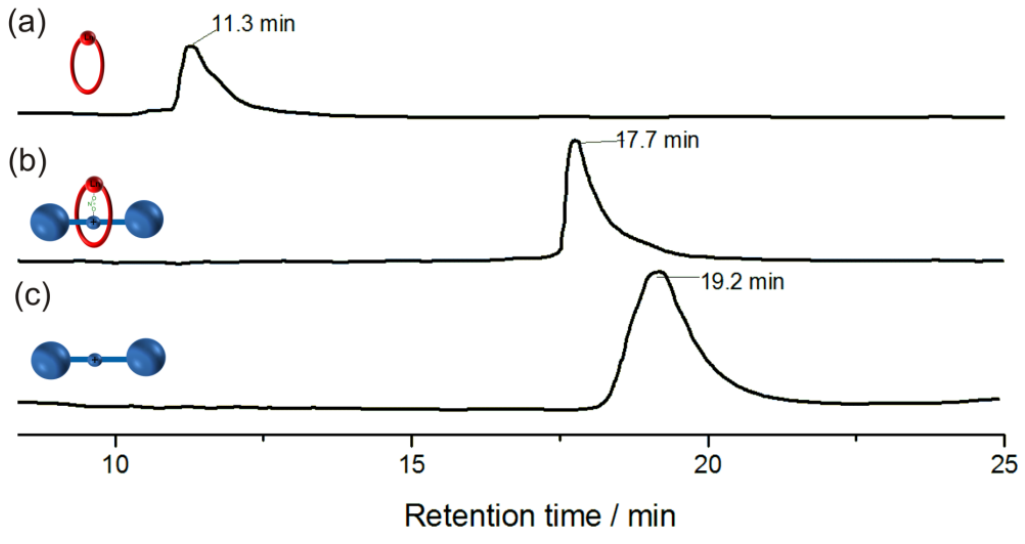

Figure 4.14 Comparison of HPLC chromatograms of (a) macrocycle **84·OTf**, (b) rotaxane **92·NO_2·OTf** and (c) non-interlocked axle by-product. Retention times indicated. Column: Discovery® Cyano, 5 μm particle size, 250 mm × 4.6 mm. Eluent: CH_3CN/H_2O gradient + 0.1% TFA, 1 mL/min. Detection: absorbance at 254 nm.

Mass spectrometry provided additional structural characterisation of the rotaxanes: an excellent match between the measured high resolution mass spectrum and the calculated isotope patterns was obtained for both rotaxane species (Figure 4.15 I and II). Furthermore, a comparison of the mass spectra of the Lu-rotaxane and a 1:1 mixture of macrocycle and axle components demonstrated that the two components do not associate under the conditions of the mass spectrometry experiment, and that the observed spectrum corresponds to the interlocked product (Figure 4.15 III).

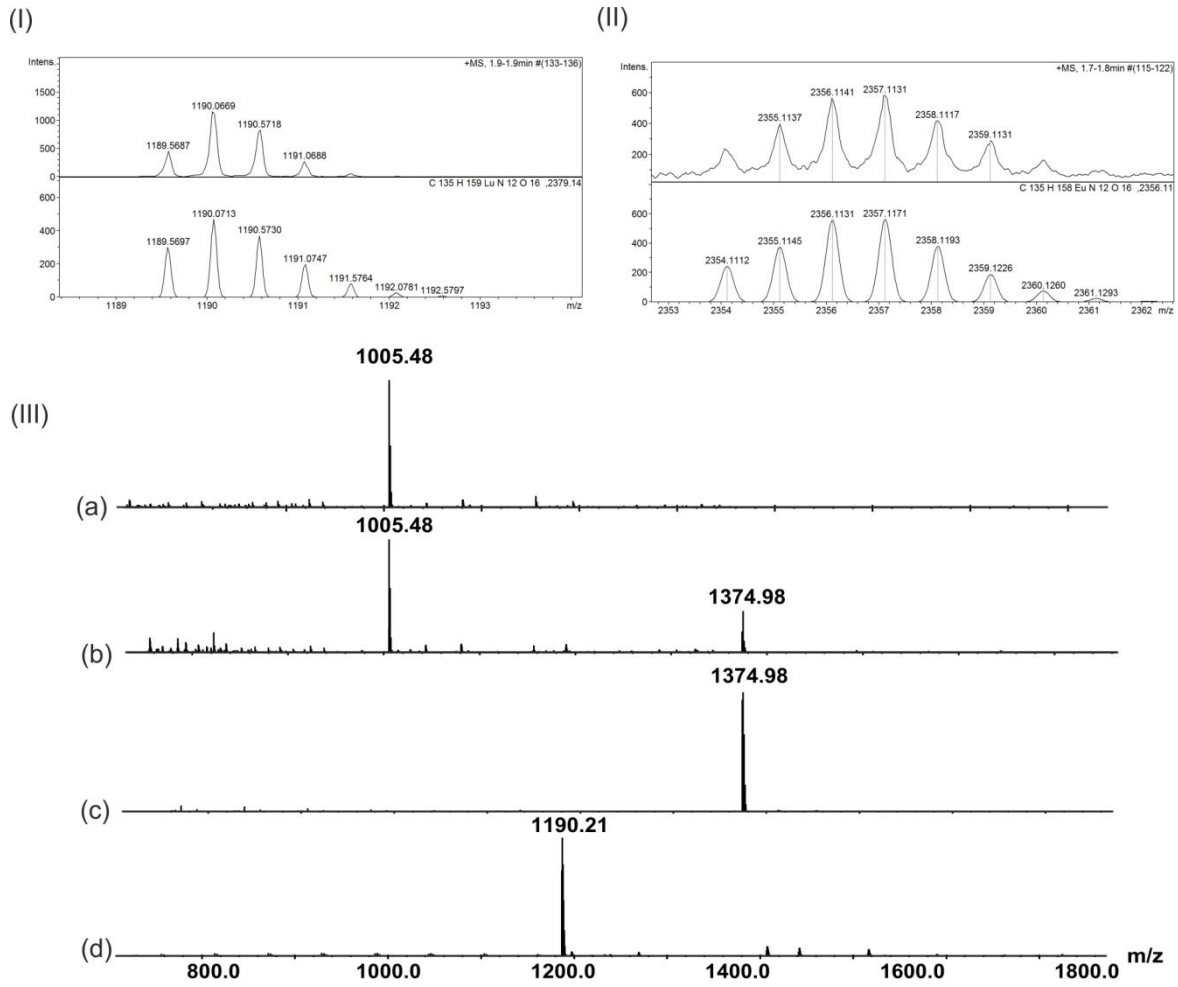

Figure 4.15 Mass spectrometry analysis: HRMS spectra (top) with theoretical isotope model for $[M-TfO-NO_2]^{2+}$ (bottom) for (I) Lu-rotaxane **92·NO₂·OTf** and (II) Eu-rotaxane **93·NO₂·OTf** (top). (III) Comparison of low resolution electrospray ionisation mass spectra, scanning between m/z = 750 to m/z = 2500 for samples of: (a) macrocycle **84·OTf**, (b) 1:1 mixture of macrocycle **84·OTf** and the non-interlocked axle by-product, (c) non-interlocked axle by-product and (d) Lu-rotaxane **92·NO₂·OTf**.

4.3.4 Anion recognition properties of the Eu-[2]rotaxane

In order to investigate the anion binding properties of Eu-[2]rotaxane **93**$^{2+}$, it was necessary to remove the nitrite anion template by converting to the weakly coordinating triflate salt. This was achieved by passing a solution of the rotaxane in 7:3 acetone/H_2O through a triflate-loaded Amberlite® anion exchange resin.

Luminescence anion binding titrations were conducted with both Eu-macrocycle **85·OTf** and Eu-rotaxane **93·(OTf)$_2$** in 99:1 acetone/H_2O using a non-dilution protocol, by adding aliquots of anions as their TBA salts and monitoring the changes in emission intensity from the europium centre (Figure 4.16). The aqueous–acetone solvent mixture was chosen to ensure that the axial 9th coordination site of the lanthanide cation incorporated within the macrocycle compound was occupied by a bound water molecule at the start of the titration. To avoid excitation of the acetone solvent, the compounds were excited into the tail of the organic chromophore absorption with 360 nm light.

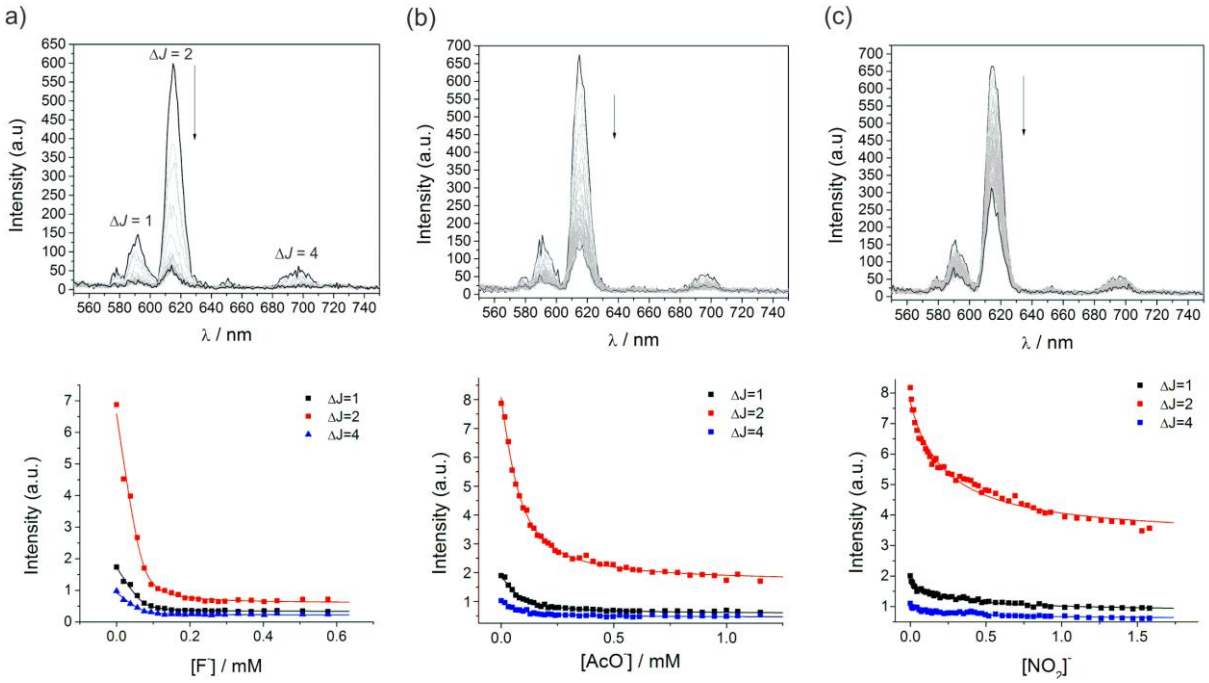

Figure 4.16 Top: Changes in the emission spectrum of a 5×10^{-5} M solution of Eu-rotaxane **93·(OTf)$_2$** upon addition of (a) F^-, (b) AcO^- and (c) NO_2^- in 99:1 acetone/H_2O (360 nm excitation, 298 K). Bottom: plots of emission intensity change against fluoride concentration. Actual data represented by solid symbols for each europium emission bands, calculated 1:1 binding isotherms for the best global fit obtained represented by solid lines.

Addition of fluoride to rotaxane **93·(OTf)$_2$** induced a dramatic quenching of the emission from the europium centre, with up to a 90% decrease from its original value at the end of the titration (Figure 4.16a). In contrast, addition of acetate and nitrite led to more modest quenching, with a 75% and 50% decrease in intensity, respectively, whilst no response was observed upon chloride addition. Likewise, addition of fluoride, acetate and nitrite to macrocycle **85·OTf** led to a similar quenching of the europium emission, and non-linear Stern-Volmer plots indicated that the decreasing luminescence is not due to collisional quenching.

The effect of fluoride on the emission was also evident in the lifetimes of the luminescence of the europium centre (Table 4.1). The lifetimes of both rotaxane **93·(OTf)$_2$** and macrocycle **85·OTf** are lengthened significantly upon addition of fluoride, which is indicative of displacement of water from the inner coordination sphere of the lanthanide cation, and is consistent with fluoride binding at the europium metal centre.

Table 4.1 Eu(III)-based luminescence lifetimes (ms) at 616 nm of **93·(OTf)$_2$** and **85·OTf** without anions, and at the end of the titrations.

Anion[a]	Eu-rotaxane **93·(OTf)$_2$**	Eu-macrocycle **85·OTf**
No anion	0.69, 0.16	0.51
F^-	1.12, 0.24	1.27
AcO^-	0.87, 0.16	0.91
NO_2^-	0.63, 0.11	0.46

Solvent: 99:1 acetone/water, 298 K. [a] Anions added as TBA salts. Errors <10%.

Further evidence for binding of fluoride at the metal centre can be gleaned from the marked change in the intensity of the hypersensitive $\Delta J = 2$ bands (605-630 nm) relative to the other bands observed in the emission spectrum (Figure 4.17a). In contrast, nitrite has comparatively little effect on the europium(III) luminescence lifetimes of either the rotaxane or macrocycle, and there is no significant change in the ratio of $\Delta J = 2$ band versus $\Delta J = 1$ and $\Delta J = 4$ over

the course of the titration (Figure 4.17c). This suggests that the quenching of the emission in this case may be assigned to association of the anion with the organic moieties of the rotaxane architecture, presumably at the positively charged pyridinium motif, which leads to diminished efficiency of the energy transfer from the chromophore to the lanthanide. In this case, the europium centre remains hydrated, as indicated by the invariant luminescence lifetime over the course of the titration.

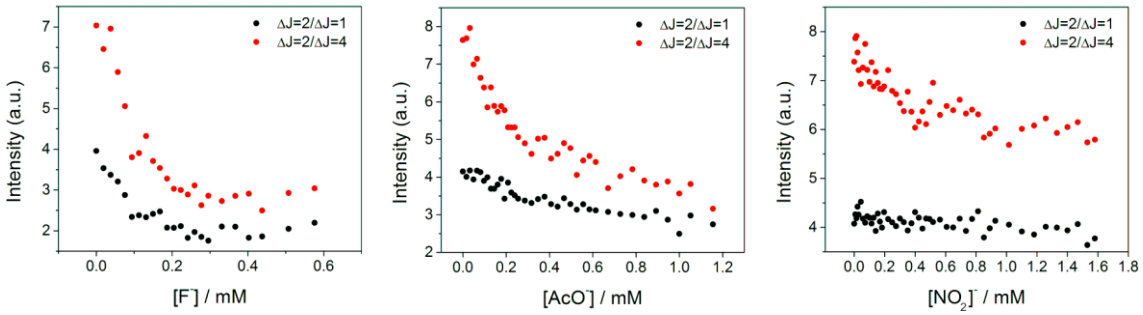

Figure 4.17 Ratio of the intensity of the hypersensitive $\Delta J = 2$ bands vs $\Delta J = 1$ and $\Delta J = 4$ for Eu-rotaxane **93·(OTf)$_2$** upon addition of (a) F^-, (b) AcO^- and (c) NO_2^-. (99:1 acetone/water, $T = 298$ K, 360 nm excitation).

Acetate presents an intermediate case, in which the lifetimes increased over the course of the titration but to a lesser degree than with fluoride, whilst the ratios of the intensity of the hypersensitive transition band to the other emission bands change to a lesser extent (Figure 4.17b). This suggests that a combination of effects are at play, arising from anion binding at the metal as well as association with the organic host framework.

Anion association constants for rotaxane **93·(OTf)$_2$** and macrocycle **85·OTf** were determined using the DYNAFIT[28] program, by fitting the intensity changes to a 1:1 stoichiometric binding model, and are reported in Table 4.2.

Table 4.2 Anion association constants (log K_a) for **93·(OTf)$_2$** and **85·OTf** in 99:1 acetone/water determined from luminescence data.

Anion[a]	Eu-rotaxane **93·(OTf)$_2$**	Eu-macrocycle **85·OTf**
F^-	5.4 [5.1–5.9]	4.9 [4.8–5.0]
AcO^-	4.4 [4.3–4.5]	3.2 [3.0–3.3]
NO_2^-	3.6 [3.5–3.7]	4.0 [3.8–4.2]
Cl^-	_[b]	_[b]

T = 298 K. Values in square brackets show 95% confidence intervals. [a] Anions added as TBA salts. [b] Addition of Cl^- caused no change in the luminescence intensity.

The anion association constants reveal a modest enhancement of fluoride binding by rotaxane **93·(OTf)$_2$** compared to the non-interlocked macrocycle **85·OTf**, with a greater binding enhancement observed for acetate. This indicates that the formation of the interlocked structure with additional hydrogen bond donor groups in the axle component augments anion binding at the lanthanide centre. The binding of the anion directly at the metal, however, appears to play the dominant role in the association, bearing in mind the above discussion. The nitrite anion is unable to displace the coordinated water molecule at the lanthanide centre, and the additional hydrogen bond donors confer no enhancement of the nitrite association in the rotaxane. Indeed, the association constant is somewhat lower than in the macrocycle alone, which is presumably due, in part, to steric constraints.

4.4 Towards anion sensing in water by a lanthanide-containing [2]rotaxane

4.4.1 Anion sensing in water using lanthanide complexes

In the previous sections it was shown that lanthanide-containing rotaxanes could be prepared *via* lanthanide cation templated synthesis, through the coordination of a pyridine *N*-oxide axle precursor component, or using a *nitrite* anion templation approach. In the latter case, the ability to remove the discrete anion template from the rotaxane allowed for the preparation of an interlocked anion sensor, which reported fluoride binding in an acetone–water solution by means of quenching of the europium-centred emission. As was discussed in Chapter 3, the design of molecular receptors capable of binding and sensing anions in pure water is of interest due to the need to operate in biological and environmentally relevant aqueous media. Indeed, Parker and co-workers have exploited the strong coordination of anions to the lanthanide metal in a range of complexes to detect and quantify anions such as bicarbonate, lactate, citrate and urate in a variety of biological fluids.[31] The detection of anions by Eu-[2]rotaxane **93·(OTf)$_2$** in water is hampered by poor solubility and therefore the remainder of this chapter discusses work conducted towards the preparation of analogous water-soluble lanthanide rotaxanes.

4.4.2 Nitrate templated synthesis

In Chapter 2 the utilisation of nitrate as a templating anion for rotaxane and catenane synthesis was presented, and in Chapter 3 it was shown that permethylated β-cyclodextrin derivatives could be employed as hydrophilic stopper components facilitating the preparation of water soluble rotaxane hosts.

It was envisaged that the chemistry developed in the previous chapters could be combined to offer a starting point for the development of water soluble, lanthanide rotaxane-

based anion sensors. Initially, the possibility of using a nitrate anion template to prepare lanthanide rotaxanes was explored using the same double-stoppering CuAAC methodology detailed in Chapter 2, in conjunction with lanthanide macrocycles **84·OTf** and **85·OTf**. As a test case, stoppering using propargyl-functionalised terphenyl stoppers was employed in the first instance, by stirring one equivalent of bis-azide axle precursor **36·NO$_3$** with 1.5 equivalents of the Lu-macrocycle **84·OTf** in the presence of two equivalents of stopper alkyne **40** and catalytic $Cu(CH_3CN)_4PF_6$ and TBTA (Scheme 4.12).

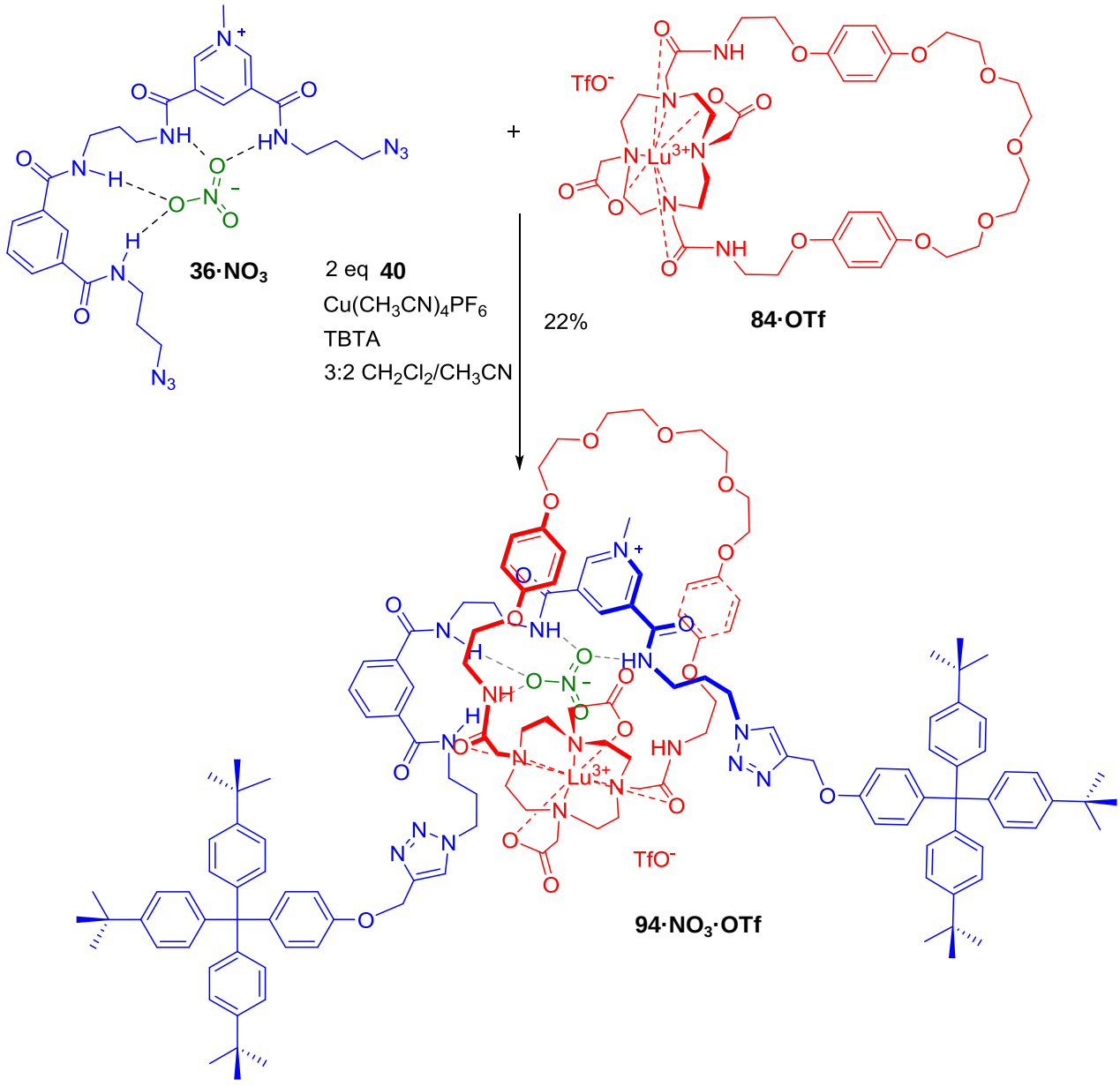

Scheme 4.12 Nitrate templated synthesis of Lu-[2]rotaxane **94·NO$_3$·OTf**.

Mass spectrometry analysis of the reaction mixture confirmed the presence of the desired rotaxane product, which was purified using size exclusion chromatography and isolated in 22% yield.

The ^{1}H NMR spectrum of rotaxane **94·NO$_3$·OTf** (Figure 4.18) is broad, although the upfield shift and splitting of the hydroquinone protons is clearly observed, indicative of successful rotaxane formation.

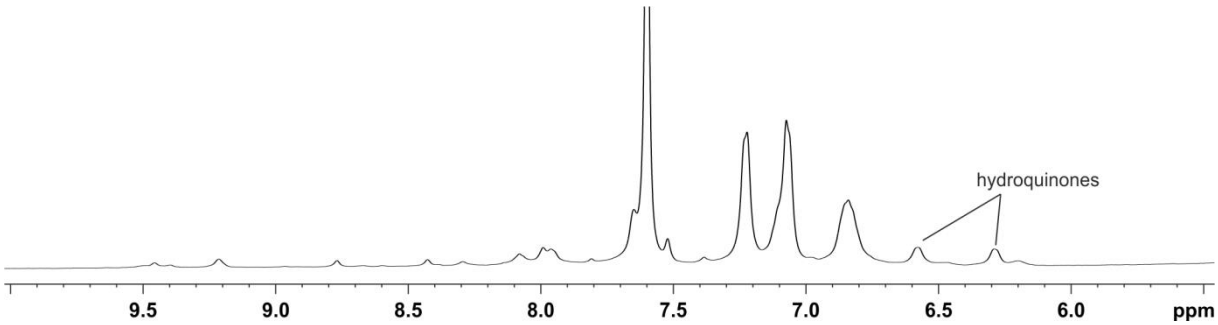

Figure 4.18 Partial ^{1}H NMR spectrum of rotaxane **94·NO$_3$·OTf** in 1:1 $CDCl_3/CD_3OD$ (500 MHz, 298 K).

The rotaxane was exchanged to the triflate salt by passing a solution of **94·NO$_3$·OTf** in 7:3 acetone/water through a triflate-loaded Amberlite® column, to afford **94·(OTf)$_2$**. The broad nature of the ^{1}H NMR spectrum of the rotaxane, however, hampered attempts to determine the anion recognition properties of the rotaxane by titration experiments. Indeed, whilst addition of $TBANO_3$ to **94·(OTf)$_2$** in 1:1 $CDCl_3/CD_3OD$ caused no apparent change in the spectrum, this may reflect the fact that the protons in the binding cavity are not easily identifiable. Nevertheless, the successful preparation of the terphenyl-stoppered rotaxane **94^{2+}** using nitrate anion templation suggested that the synthesis of a cyclodextrin-stoppered analogue would be possible using the same templation methodology. To this end 6^A-propargyl-permethylated-β-CD **95** was prepared initially, by the reaction of mono-alcohol **56** and propargyl bromide according to a literature procedure (Scheme 4.13).[32]

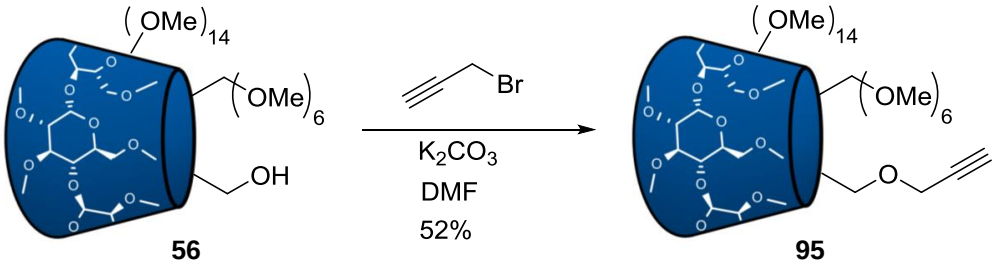

Scheme 4.13 Synthesis of 6^A-propargyl-permethylated-*β*-CD **95**.

The nitrate templated synthesis of the target water soluble cyclodextrin stoppered rotaxane was then undertaken by stirring **36·NO₃** and **84·OTf** in the presence of two equivalents of 6^A-propargyl-permethylated-*β*-CD **95** and the copper(I) catalyst in CH_2Cl_2/CH_3CN (Scheme 4.14).

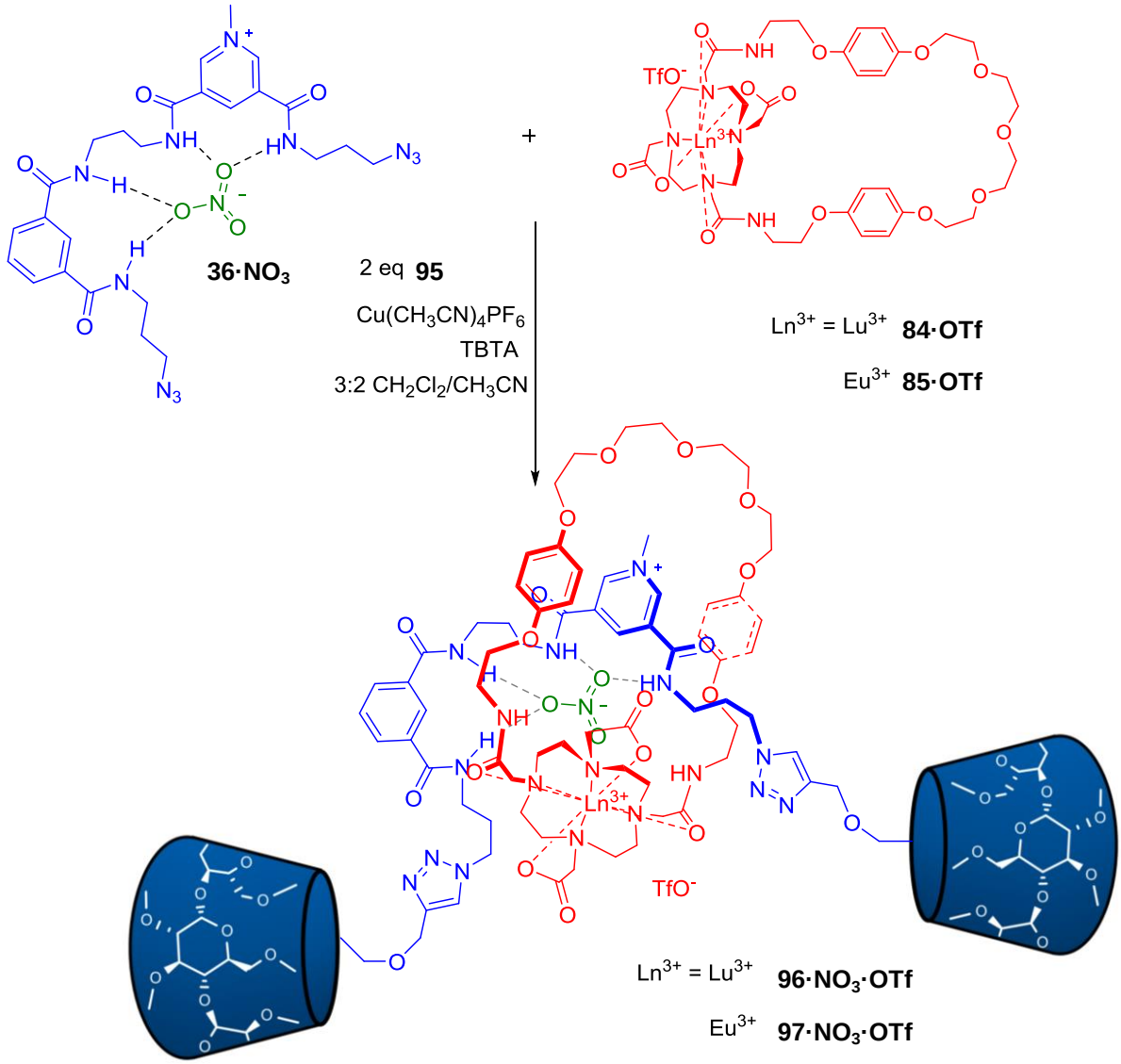

Scheme 4.14 Synthesis of cyclodextrin-stoppered rotaxanes **96·NO₃·OTf** and **97·NO₃·OTf**.

Mass spectrometry analysis of the reaction mixture revealed the presence of the target rotaxane **96·NO$_3$·OTf**, in addition to non-interlocked axle and macrocycle, which formed the major by-products of the reaction. In this case, size exclusion chromatography was employed to successfully remove the free macrocycle and cyclodextrin components, but the separation of the axle and rotaxane species was poor and only a small quantity of interlocked product (~1 mg) was isolated. The synthetic yield of the rotaxane, however, was estimated to be comparable to that of the terphenyl stoppered analogue **94**$^{2+}$ by analysis of the ^{1}H NMR spectrum of the crude reaction mixture (~20%). Characterisation of the rotaxane was hampered by the small quantity of the high molecular weight product, although the ^{1}H NMR spectrum in D_2O at 373 K clearly reveals the diagnostic upfield shifted and split hydroquinone protons of the rotaxane at 6.45 and 6.65 ppm (Figure 4.19), whilst the mass spectrum is also consistent with the presence of the mechanically bonded species.

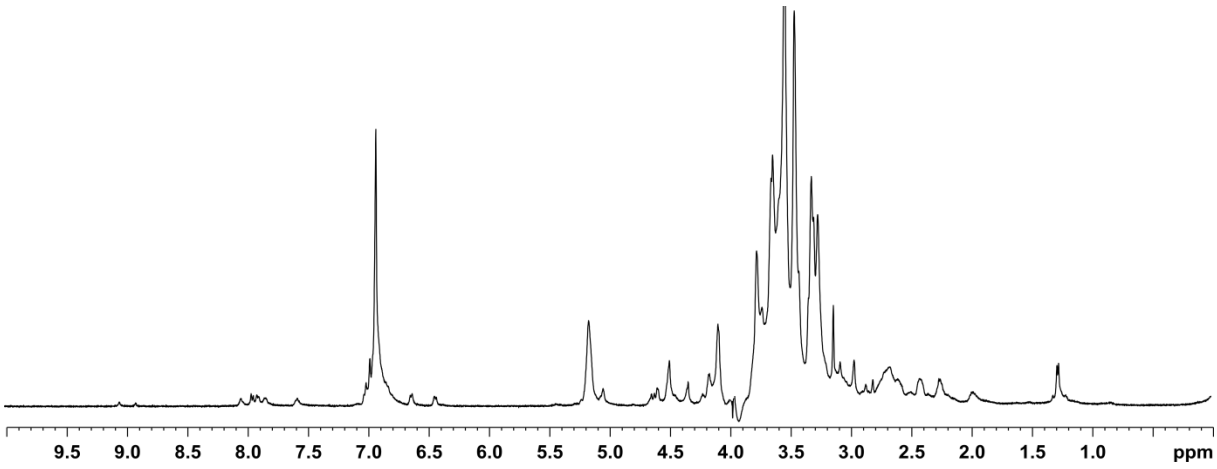

Figure 4.19 Partial ^{1}H NMR spectrum of rotaxane **96NO$_3$·OTf** in D_2O (373 K, 500 MHz).

The analogous Eu-rotaxane **97·NO$_3$·OTf** was synthesised in the same way as the lutetium analogue, but in this case it was not possible to separate the rotaxane from the axle by-product using size exclusion chromatography. As an alternative approach, purification using a Sephadex CM-25 cation exchange resin was attempted, by loading the resin with an aqueous solution of the rotaxane and axle mixture, before eluting with a 0.05 M $NaCl_{(aq)}$ solution. The dicationic rotaxane eluted behind the mono-cationic axle, although the resolution between the

two species was poor and the separation could only be conducted on a milligram scale per run. After repeated chromatography a small sample of rotaxane **97·(Cl)$_2$** was isolated as the chloride salt in 1.5 % yield.

Analysis of the anion binding properties of Eu-rotaxane **97·(OTf)$_2$**, prepared from the chloride salt using a triflate-loaded Amberlite® anion exchange resin, was attempted in buffered aqueous solution by monitoring the luminescence from the europium centre, exciting at 370 nm. Due to the limited material, the rotaxane was prepared as a 1×10^{-5} M solution at pH 7.4 (HEPES buffer). Whilst this level of dilution resulted in weak emission intensity and a high level of noise, the spectrum was of sufficient quality for preliminary anion binding investigations. Disappointingly, however, addition of sodium fluoride to the rotaxane resulted in no change in the emission spectrum (Figure 4.20), suggesting that the anion does not bind to the lanthanide in aqueous solution. This was further confirmed by analysis of the lifetime of the europium emission, which did not change upon addition of fluoride (t = 0.95 ms at the start and end of the titration), indicating that there is no change in the europium cation's hydration sphere and that fluoride does not displace the axially coordinated water molecule.

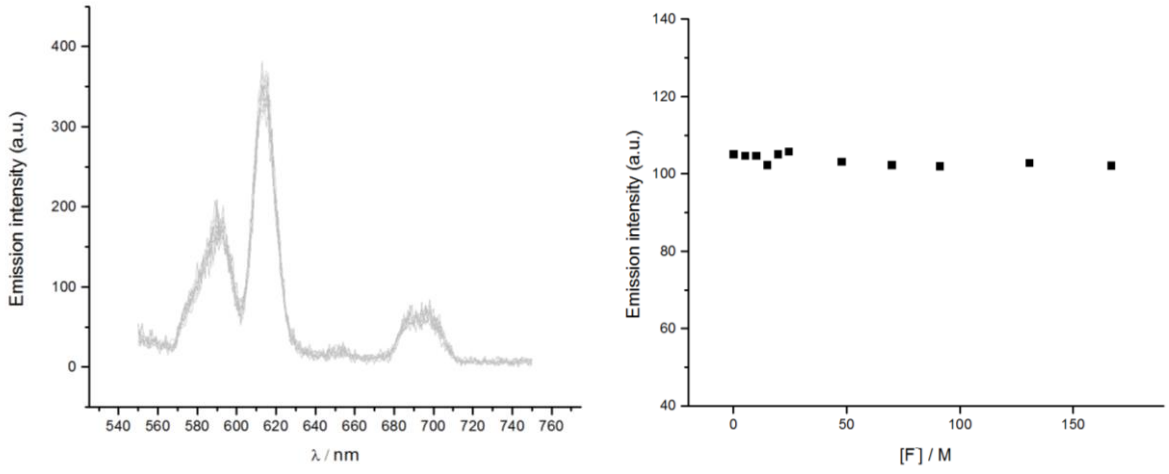

Figure 4.20 Titration of F^- into a 1×10^{-5} M solution of Eu-rotaxane **97·(OTf)$_2$**. Left: emission spectra and Right: plots of the emission intensity of the $\Delta J = 2$ transition at 620 nm against fluoride concentration.

Addition of sodium salts of NO_3^-, Cl^-, SO_4^{2-} or PO_4^{2-} also failed to induce a change in the emission spectrum, again suggesting that these anions are not bound by the receptor. Attempts to determine the anion recognition capability of the non-interlocked macrocycle **85·OTf** for comparison were hampered by a lack of aqueous solubility, even at low concentrations.

The inability of rotaxane **97·(OTf)$_2$** to recognise halides or oxoanions in water presumably results from the combination of electrostatics and hydrogen bonds of the host being of insufficient strength to overcome the hydration energy of the anions, in particular fluoride, in water. Whilst lanthanide complexes capable of recognising fluoride in water are known, such species are typically tri-cationic. This bestows a strong electrostatic component to the recognition, resulting in association constants of the order of log K_a = 1–5 in aqueous solution.[33–35] In the case of rotaxane **97·(OTf)$_2$**, the lanthanide macrocycle component bears an overall charge of one, whilst the axle component bears an additional positive charge. The potential enhancement of anion binding that results from the hydrogen bond donors of the axle component is presumably insufficient to compensate for the overall reduced electrostatic contribution to the binding.

4.5 Conclusions and future work

In conclusion, the novel utilisation of a lanthanide cation to template mechanical bond formation has been demonstrated. A pyridine *N*-oxide threading component coordinates to a lutetium or europium cation bound within a DOTA motif, which is itself incorporated within a macrocycle component. Stoppering of the pseudorotaxane assembly affords the lanthanide-containing [2]rotaxane. The anion recognition properties of the europium rotaxane were probed by analysing the luminescence from the emissive lanthanide centre. This revealed that the pyridine *N*-oxide motif, which coordinates to the lanthanide cation in the rotaxane, is displaced by fluoride. Whilst this competition for the metal centre resulted in an anion association constant of smaller magnitude compared to the non-interlocked macrocycle, the selectivity for fluoride over acetate was enhanced.

The anion templated synthesis of lanthanide-containing rotaxanes was also presented, using the bidentate coordination behaviour of the nitrite anion to template pseudorotaxane formation, by simultaneously coordinating to the lanthanide cation incorporated within the macrocycle component and the 3,5-bis-amide pyridinium hydrogen bond donor threading component. Stoppering of the pseudorotaxane assembly afforded the lutetium- and europium-containing [2]rotaxanes. Luminescence anion binding titrations with the europium host revealed that the rotaxane selectively recognises and senses fluoride anions over acetate, nitrite and chloride in an acetone/water mixture. To further explore the formation of lanthanide-based rotaxanes using anion templation, the synthesis of water-soluble, nitrate templated rotaxanes was also investigated.

To expand on the work described in this chapter, modification of the water-soluble lanthanide rotaxane host could be undertaken, with the aim of sensing anions in water. For instance, the overall charge of the interlocked host could be increased to facilitate enhanced anion binding, by substituting the pendant carboxylates of the macrocycle component with amide groups. Furthermore, modification of the axle component by varying the nature of the hydrogen bond donors, or replacement with halogen bond donors or metal cations, may further enhance the recognition and sensing capability of the system.

4.6 References for Chapter 4

1. J. P. Sauvage, *Acc. Chem. Res.*, 1990, **23**, 319–327.
2. J. D. Crowley, S. M. Goldup, A.-L. Lee, D. A. Leigh, and R. T. McBurney, *Chem. Soc. Rev.*, 2009, **38**, 1530–1541.
3. J. E. Beves, B. A. Blight, C. J. Campbell, D. A. Leigh, and R. T. McBurney, *Angew. Chem. Int. Ed.*, 2011, **50**, 9260–9327.
4. S. L. Castro, O. Just and W. S. Rees, *Angew. Chem. Int. Ed.*, 2000, **39**, 933–935.
5. G. Kaiser, T. Jarrosson, S. Otto, Y.-F. Ng, A. D. Bond, and J. K. M. Sanders, *Angew. Chem. Int. Ed.*, 2004, **43**, 1959–1962.
6. S.-Y. Hsueh, C.-C. Lai, Y.-H. Liu, S.-M. Peng, and S.-H. Chiu, *Angew. Chem. Int. Ed.*, 2007, **46**, 2013–2017.
7. Y.-H. Lin, C.-C. Lai, Y.-H. Liu, S.-M. Peng, and S.-H. Chiu, *Angew. Chem. Int. Ed.*, 2013, **52**, 10231–10236.
8. S.-T. Tung, C.-C. Lai, Y.-H. Liu, S.-M. Peng, and S.-H. Chiu, *Angew. Chem. Int. Ed.*, 2013, **52**, 13269–13272.
9. L. M. Hancock and P. D. Beer, *Chem. Commun.*, 2011, **47**, 6012.
10. A. Beeby, S. W. Botchway, I. M. Clarkson, S. Faulkner, A. W. Parker, D. Parker, and J. A. G. Williams, *J. Photochem. Photobiol. B*, 2000, **57**, 83–89.
11. D. Parker, R. S. Dickins, H. Puschmann, C. Crossland, and J. A. K. Howard, *Chem. Rev.*, 2002, **102**, 1977–2010.
12. S. Faulkner, S. J. A. Pope, and B. P. Burton-Pye, *Appl. Spectrosc. Rev.*, 2005, **40**, 1–31.
13. S. Faulkner, L. S. Natrajan, W. S. Perry, and D. Sykes, *Dalton Trans.*, 2009, 3890–3899.
14. C. Allain and S. Faulkner, *Future Med. Chem.*, 2010, **2**, 339–350.
15. C. M. G. dos Santos, A. J. Harte, S. J. Quinn, and T. Gunnlaugsson, *Coord. Chem. Rev.*, 2008, **252**, 2512–2527.
16. M. J. Langton and P. D. Beer, *Acc. Chem. Res.*, 2014, DOI:10.1021/ar500012a.
17. D. J. Hoffart and S. J. Loeb, *Angew. Chem. Int. Ed.*, 2005, **44**, 901–904.
18. C. Allain, P. D. Beer, S. Faulkner, M. W. Jones, A. M. Kenwright, N. L. Kilah, R. C. Knighton, T. J. Sørensen, and M. Tropiano, *Chem. Sci.*, 2012, **4**, 489–493.

19. C. Lincheneau, B. Jean-Denis, and T. Gunnlaugsson, *Chem. Commun.*, 2014, **50**, 2857–2860.
20. L. M. De León-Rodríguez, A. Ortiz, A. L. Weiner, S. Zhang, Z. Kovacs, T. Kodadek, and A. D. Sherry, *J. Am. Chem. Soc.*, 2002, **124**, 3514–3515.
21. X. Liang and P. J. Sadler, *Chem. Soc. Rev.*, 2004, **33**, 246–266.
22. F. Benetollo, G. Bombieri, L. Calabi, S. Aime, and M. Botta, *Inorg. Chem.*, 2003, **42**, 148–157.
23. L. M. De León-Rodríguez, Z. Kovacs, A. C. Esqueda-Oliva, and A. D. Miranda-Olvera, *Tetrahedron Lett.*, 2006, **47**, 6937–6940.
24. T. Hirayama, M. Taki, A. Kodan, H. Kato, and Y. Yamamoto, *Chem. Commun.*, 2009, 3196–3198.
25. L. M. Hancock and P. D. Beer, *Chem. – Eur. J.*, 2009, **15**, 42–44.
26. J. L. Kropp and M. W. Windsor, *J. Chem. Phys.*, 1965, **42**, 1599–1608.
27. A. Beeby, I. M. Clarkson, R. S. Dickins, S. Faulkner, D. Parker, L. Royle, A. S. de Sousa, J. A. G. Williams, and M. Woods, *J. Chem. Soc. Perkin Trans. 2*, 1999, 493–504.
28. P. Kuzmič, *Anal. Biochem.*, 1996, **237**, 260–273.
29. J. Lehr, T. Lang, O. A. Blackburn, T. A. Barendt, S. Faulkner, J. J. Davis, and P. D. Beer, *Chem. – Eur. J.*, 2013, **19**, 15898–15906.
30. S. Aime, M. Botta, and G. Ermondi, *Inorg. Chem.*, 1992, **31**, 4291–4299.
31. S. J. Butler and D. Parker, *Chem. Soc. Rev.*, 2013, **42**, 1652–1666.
32. J. A. Faiz, N. Spencer, and Z. Pikramenou, *Org. Biomol. Chem.*, 2005, **3**, 4239.
33. R. S. Dickins, S. Aime, A. S. Batsanov, A. Beeby, M. Botta, J. I. Bruce, J. A. K. Howard, C. S. Love, D. Parker, R. D. Peacock, and H. Puschmann, *J. Am. Chem. Soc.*, 2002, **124**, 12697–12705.
34. R. Tripier, C. Platas-Iglesias, A. Boos, J.-F. Morfin, and L. Charbonnière, *Eur. J. Inorg. Chem.*, 2010, **2010**, 2735–2745.
35. C. M. G. dos Santos and T. Gunnlaugsson, *Dalton Trans.*, 2009, 4712–4721.

CHAPTER 5

Chapter 5 Experimental

5.1 General remarks

5.1.1 Instrumental methods

NMR spectra were recorded on Varian Mercury 300, Bruker AVIII 400, Bruker AVII 500 (with cryoprobe), Bruker AVIII 500 and Bruker AVIII 700 (with cryoprobe) spectrometers. Mass spectra were carried out on Waters Micromass LCT and Bruker microTOF spectrometers. HPLC analysis was carried out using a Gilson 322-H2 HPLC instrument, with a UV-vis detector set to 254 nm, and a reverse phase cyano analytical column (Discovery® Cyano HPLC Column: 5 μm particle size, L × I.D: 25 cm × 4.6 mm). Analytical chromatography was conducted using CH_3CN/H_2O + 0.1% trifluoroacetic acid, using a gradient changing from 5:95 to 95:5 over 20 minutes, at a flow rate = 1 mL/min. Fluorescence spectra were recorded on a Varian Cary-Eclipse fluorescence spectrometer or Horiba Fluorolog 3. Europium luminescence spectra were collected in phosphoresecnce mode exciting at 360 nm using a flash delay of 0.05 ms.

5.1.2 ^{1}H NMR titration protocols

^{1}H NMR spectra were recorded on a Bruker AVIII 500 spectrometer at 298 K, unless otherwise stated. The initial sample volumes were 0.5 mL, at a concentration of 1.5 mM of host. A solution of the anion, as either the tetrabutylammonium (TBA) salt or sodium salt was added to the host solution and the chemical shift of the appropriate protons were monitored for 17 data points. The spectra were referenced to the residual solvent peak, or in the case of titrations conducted in D_2O, a trace amount of acetone was added as an internal reference, such that it made up less than 0.05% of the total volume, and all spectra were referenced its

resonance at 2.10 ppm. The values of the observed chemical shift and the guest concentration were entered into winEQNMR2[1] for every titration point and estimates for the binding constant and limiting chemical shifts were made. The parameters were refined using non-linear squares analysis to obtain the best fit between the observed and calculated chemical shifts for a 1:1 or 2:1 binding stoichiometry as appropriate. The input parameters were varied until the best-fit values of the stability constants, and their errors, converged. Van't Hoff analysis titrations were conducted using the same procedure, at a range of temperatures. The temperature of NMR sample was allowed to equilibrate for 15 minutes prior to the titration, and then for a further 2 minutes after each anion addition.

5.1.3 Luminescence anion binding titration protocols

Titrations were typically carried out by starting with 1.5 mL of a 5×10^{-5} M solution of the host and adding aliquots of a solution containing the same concentration of the host together with a known concentration of the anion under study. The titration data was fitted to a 1:1 stoichiometric binding model using the Dynafit program, using a global analysis.[2]

5.1.4 General procedure for acid chloride synthesis

To convert carboxylic acids to their acid chloride derivatives the following general procedure was used. To a suspension of acid (1 mmol) in dry CH_2Cl_2 (10 mL) was added oxalyl chloride (2 mmol) drop-wise under N_2. A drop of DMF (~0.01 mL, cat.) was added and the reaction refluxed at 40 °C under N_2 until the solution became homogeneous. The solvent was removed *in vacuo* to leave a yellow solid. This was immediately re-dissolved in dry CH_2Cl_2 and reacted on as desired. The yield was assumed to be quantitative.

5.1.5 Solvents, reactants and reagents

All reagents and solvents were purchased from commercial sources and used without further purification. Where necessary, solvents were dried by passing through a MBraun MPSP-800 column and degassed with nitrogen. Column chromatography was carried out on Merck® silica gel 60 under a positive pressure of nitrogen. Size exclusion chromatography was carried out using Biobeads SX-1, with $CHCl_3$ as the eluent. Where mixtures of solvents were used, ratios reported are by volume. Triethylamine was distilled from and stored over potassium hydroxide. Amberlite® columns were prepared by washing the resin with 10% $NaOH_{(aq)}$, H_2O, 1M NH_4X (where X is the anion required), H_2O and finally the solvent to be used in the anion exchange.

TBTA was prepared as previously described by Dr Lydia Gilday.[3] Compounds **40**[4] and **44**[5] were prepared by Dr Fabiola Zapata, compound **69**[6,7] by Sean Robinson and compound **91**[8] by Dr Thomas Lang.

5.2 Synthesis of novel compounds from Chapter 2

[3]rotaxane 1·(Cl)$_2$

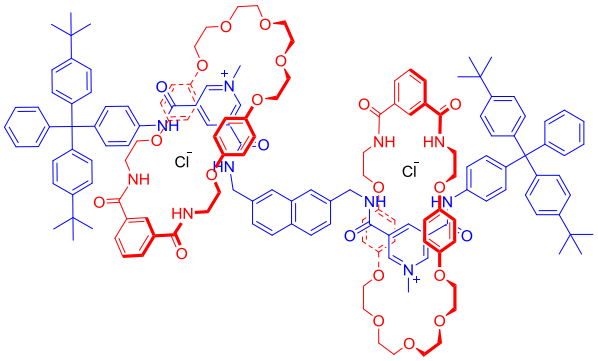

Axle **12·(Cl)$_2$** (110 mg, 0.0762 mmol) and bis-amine **16** (141 mg, 0.332 mmol) were dissolved in dry CH_2Cl_2 (10 mL) and stirred for 30 min at 0 °C under a N_2 atmosphere. NEt_3 (0.100 mL, 0.820 mol) was then added followed immediately by a drop-wise addition of isophthaloyl dichloride (46.0 mg, 0.332 mmol) dissolved in dry CH_2Cl_2 (5 mL). The reaction was allowed to reach rt and stirred for 3 hrs. The reaction mixture was then washed with 10% citric acid (2 × 20 mL) and H_2O (1 × 20 mL), the organic layer dried over $MgSO_4$, the solvent removed *in vacuo*. Purification was carried out first by preparative TLC (97:3 CH_2Cl_2/CH_3OH), and then size-exclusion chromatography ($CHCl_3$) to remove the free macrocycle by-product to give the product as a yellow solid (59 mg, 33%). ^{1}H NMR (700 MHz, d_6-DMSO) δ (ppm): 10.34 (s, 2H, pyridinium ArN*H*), 9.28 (s, 2H, pyridinium Ar*H*), 9.26 (s, 2H, pyridinium CH_2N*H*), 9.24 (s, 2H, pyridinium Ar*H*), 9.04 (s, 2H, pyridinium Ar*H*), 8.44 (s, 4H, isophthalamide N*H*), 8.41 (s, 2H, isophthalamide Ar*H*), 7.92 (d, ^3J = 7.7 Hz, 4H, isophthalamide Ar*H*), 7.86 (d, ^3J = 8.5 Hz, 2H, naphthalene Ar*H*), 7.74 (s, 2H, naphthalene Ar*H*), 7.56 (d, ^3J = 7.8 Hz, 4H, stopper Ar*H*), 7.47 (t, ^3J = 7.7 Hz, 2H, isophthalamide Ar*H*), 7.45 (d, ^3J = 8.5 Hz, 2H, naphthalene Ar*H*), 7.34–7.05 (m, 30H, stopper Ar*H*), 6.44 (d, ^3J = 8.4 Hz, 8H, hydroquinone Ar*H*), 6.30 (d, ^3J = 8.4 Hz, 8H, hydroquinone Ar*H*), 4.62 (s, 4H, C*H*$_2$NH), 4.33 (s, 6H, N$^+$C*H*$_3$), 4.04–3.49 (m, 56H, alkyl C*H*$_2$), 1.27 (s, 36H, C*H*$_3$).

^{13}C NMR (125 MHz, 1:1 $CDCl_3/CD_3OD$) δ (ppm): 169.1, 161.7, 160.4, 154.4, 153.3, 145.0, 148.3, 147.5, 147.0, 146.4, 144.9, 141.8, 137.0, 136.0, 135.8, 134.9, 134.9, 134.7, 134.4, 133.2, 132.5, 132.3, 132.0, 130.2, 129.6, 128.7, 127.9, 127.6, 127.2, 125.6, 121.8, 72.0, 71.9, 71.4, 71.1, 69.2, 68.3, 67.4, 65.2, 45.8, 41.5, 35.5, 32.4, 30.9. HRMS (ESI +ve) *m/z*: 1280.6579 ($[M-2Cl]^{2+}$, $C_{158}H_{172}N_{10}O_{22}$ requires 1280.6318).

[3]rotaxane 1·$(PF_6)_2$: A solution of **1·$(Cl)_2$** (25 mg, 0.011 mmol) dissolved in $CHCl_3$ (10 mL) was vigorously shaken with 0.1 M $NH_4PF_{6(aq)}$ (8 × 10 mL), then H_2O (2 × 10 mL). The organic layer was separated, dried over $MgSO_4$, and the solvent removed *in vacuo* to give the product as a yellow solid (25 mg, 97%). ^{1}H NMR (500 MHz, 1:1 $CDCl_3/CD_3OD$) δ (ppm): 9.11 (s, 2H, pyridinium Ar*H*), 9.07 (s, 2H, pyridinium Ar*H*), 8.85 (s, 2H, pyridinium Ar*H*), 8.43 (s, 2H, isophthalamide Ar*H*), 7.88 (d, ^3J = 7.7 Hz, 4H, isophthalamide Ar*H*), 7.83 (s, 2H, naphthalene Ar*H*), 7.75 (d, ^3J = 8.5 Hz, 2H, naphthalene Ar*H*), 7.65 (d, ^3J = 7.8 Hz, 4H, stopper Ar*H*), 7.38 (t, ^3J = 7.7 Hz, 2H, isophthalamide Ar*H*), 7.37 (d, ^3J = 8.5 Hz, 2H, naphthalene Ar*H*), 7.30–7.07 (m, 30H, stopper Ar*H*), 6.46 (d, ^3J = 9.1 Hz, 8H, hydroquinone Ar*H*), 6.27 (d, ^3J = 9.1 Hz, 8H, hydroquinone Ar*H*), 4.62 (s, 4H, CH_2NH), 4.41 (s, 6H, N^+CH_3), 3.99–3.51 (m, 56H, alkyl CH_2), 1.31 (s, 36H, CH_3). ^{13}C NMR (125 MHz, 1:1 $CDCl_3/CD_3OD$) δ (ppm): 169.3, 161.4, 160.3, 154.5, 153.3, 150.0, 148.3, 147.4, 146.5, 146.4, 144.9, 136.8, 136.1, 135.1, 134.8, 134.3, 133.6, 133.3, 132.4, 132.0, 130.3, 129.6, 128.7, 127.5, 127.2, 126.2, 125.7, 121.3, 116.4, 116.2, 71.9, 71.9, 71.4, 69.3, 67.4, 65.3, 54.8, 45.6, 41.5, 35.5, 32.4, 30.9, one missing presumed overlapped. ^{19}F NMR (75 MHz, 1:1 $CDCl_3/CD_3OD$) δ (ppm): −72.05 (d, ^2J = 710 Hz, PF_6^-).

Bis(4-(*tert*-butyl)phenyl)(phenyl)methanol 2[5]

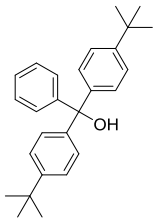

In a 3-necked 500 mL round bottom flask, Mg turnings (2.00 g) were heated to 120 °C under N_2 in a 3-necked flask for 16 hrs. Dry THF (10 mL) was added to cover the Mg, and cat. I_2 (~ 5mg) added, before 1-bromo-4-*tert*-butylbenzene (11.7 mL, 67.5 mmol) in dry THF (25 mL) was added drop-wise over 15 min and the reaction was heated until effervescence was observed, upon which heating was removed and the reaction allowed to stir for 2 hrs. Methyl benzoate (4.08 g, 32.9 mmol) dissolved in dry THF (10 mL) was then added over 15 min and the reaction stirred for 16 hrs at rt under a N_2 atmosphere. The reaction mixture was carefully neutralised with aqueous 10% $HCl_{(aq)}$, then extracted with *n*-hexane (3 × 100 mL). The combined organic layers were washed with H_2O (3 × 100 mL), dried over $MgSO_4$, and solvent removed *in vacuo* to give **2** as a brown oil. The product was re-crystallised from CH_3OH, to yield an off-white solid (10.1 g, 90%). ^{1}H NMR (300 MHz, $CDCl_3$) δ (ppm): 7.1–7.3 (m, 13H, Ar*H*), 3.05 (s, 1H, O*H*), 1.30 (s, 18H, CH_3). MS (ESI −ve) *m/z*: 371.2 ($[M-H]^-$, $C_{27}H_{31}O$ requires 371.2).

4-(bis(4-*tert*-butyl)phenyl)(phenyl)methyl)aniline 3[9]

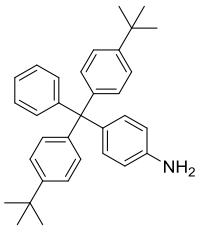

Bis(4-(*tert*-butyl)phenyl)(phenyl)methanol **2** (5.27 g, 14.1 mmol) was heated at reflux in acetyl chloride (28 mL) for 16 hrs (with the condenser fitted with a $CaCl_2$ drying tube). Excess acetyl chloride was removed *in vacuo* to give an pale yellow solid, which was heated in aniline (26 mL) at 105 °C for 48 hrs (colour change to dark purple). The solution was cooled to rt, poured onto aqueous 10% $HCl_{(aq)}$ (300 mL) and stirred for 20 mins. The precipitate was collected by vacuum filtration and then washed with sat. $K_2CO_{3(aq)}$ (50 mL) and H_2O (2 × 50 mL), then dissolved in CH_2Cl_2 (200 mL). The organic solution was dried over $MgSO_4$ and then filtered through a plug of silica to give a pale yellow solution. The solvent was removed to leave an orange oil which was recrystallised from toluene/hexane to give the product as a white solid (3.40 g, 52%). ^{1}H NMR (300 MHz, $CDCl_3$) δ (ppm): 7.1–7.3 (m, 13H, Ar*H*), 6.97 (d, ^3J = 8.5 Hz, 2H, aniline Ar*H*), 6.60 (d, ^3J = 8.5 Hz, 2H, aniline Ar*H*), 3.61(br s, 2H, NH_2), 1.31 (s, 18H, CH_3). MS (ESI +ve) *m/z*: 448.3 ($[M+H]^+$, $C_{33}H_{38}N$ requires 448.3).

Dimethyl pyridine-3,5-dicarboxylate 4[10]

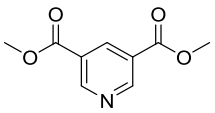

Pyridine-3,5-dicarboxylic acid (1.00 g, 5.98 mmol), dissolved in CH_3OH (3.6 mL) and conc. H_2SO_4 (3.4 mL), was irradiated with microwaves at 120 °C for 20 minutes. The solution was then cooled to rt and NH_4OH (10 mL) was added drop-wise. The product then was extracted with ether (3 × 20 mL). The organic layers were combined and dried over $MgSO_4$, before the

solvent was removed *in vacuo* to afford the product as a white solid (1.08 g, 93%). ^{1}H NMR (300 MHz, $CDCl_3$) δ (ppm): 9.37 (d, ^{4}J = 2.0 Hz, 2H, Ar*H*), 8.89 (t, ^{4}J = 2.0 Hz, 1H, Ar*H*), 3.98 (s, 6H, CH_3). MS (ESI +ve) *m/z*: 196.1 ($[M+H]^+$, $C_9H_{10}NO_4$ requires 196.1).

5-(Methoxycarbonyl)nicotinic acid 5[10]

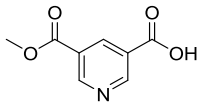

Dimethyl pyridine-3,5-dicarboxylate **4** (3.78 g, 19.4 mmol) dissolved in a solution of KOH (1.20 g, 21.3 mmol) in CH_3OH (225 mL), and stirred for 16 hrs under N_2. The solvent was removed *in vacuo* and the residue was dissolved in H_2O (60 mL). The product was extracted with ether in order to remove the bis-ester by-product (3 × 50 mL). The aqueous layer was adjusted to pH 7 by adding citric $acid_{(aq)}$, to form a white precipitate which was collected *via* vacuum filtration and dried under vacuum (3.00 g, 85%). ^{1}H NMR (300 MHz, d_6-DMSO) δ (ppm): 9.24 (d, ^{3}J = 2.2 Hz, 2H, Ar*H*), 8.63 (t, ^{3}J = 2.2 Hz, 1H, Ar*H*), 3.91 (s, 3H, CH_3). MS (ESI +ve) *m/z*: 182.1 ($[M+H]^+$, $C_8H_8NO_4$ requires 182.2).

Methyl 5-(4-(bis(4-*tert*-butylphenyl)(phenyl)methyl)phenyl)carbamoyl)nicotinate 6[10]

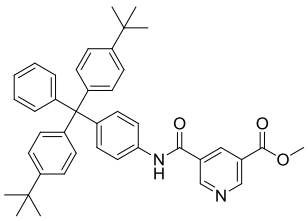

To the acid chloride of 5-(methoxycarbonyl)nicotinic acid **5** (0.744 g, 4.11 mmol) in CH_2Cl_2 (70 mL) was added a solution of 4-(bis(4-*tert*-butyl)phenyl)(phenyl)methyl)aniline **3** (2.02 g, 4.53 mmol) at 0 °C, and the reaction stirred at rt under a N_2 atmosphere for 16 hrs. The reaction mixture was washed with 10% $HCl_{(aq)}$ (100 mL) and 10% $NaOH_{(aq)}$ (2 × 100 mL), the organic layers dried over $MgSO_4$ and the solvent removed *in vacuo*, with the crude material being purified by silica gel chromatography (98:2 CH_2Cl_2/CH_3OH) to give the

product as an off-white solid (2.40 g, 92%). ^{1}H NMR (300 MHz, $CDCl_3$): δ (ppm): 9.37 (s, 1H, Ar*H*), 9.28 (s, 1H, Ar*H*), 8.74 (s, 1H, Ar*H*), 8.16 (br. s, 1H, N*H*), 7.54 (d, ^3J = 8.7 Hz, 2H, Ar*H*), 7.10–7.27 (m, 17H, Ar*H*), 3.98 (s, 3H, CH_3), 1.31 (s, 18H, CH_3). MS (ESI +ve) *m/z*: 633.3 ($[M+Na]^+$, $C_{41}H_{42}N_2NaO_3$ requires 633.3.

Methyl 5-(4-(bis(4-*tert*-butylphenyl)(phenyl)methyl)phenyl)carbamoyl)nicotinic acid 7[10]

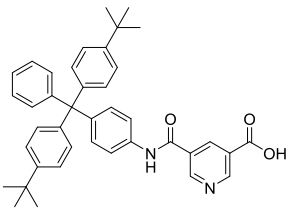

Ester **6** (2.36 g, 3.73 mmol) was dissolved in THF/H_2O (1:1, 70 mL). KOH (0.24 g, 4.10 mmol) was added and the solution stirred at rt for 16 hrs. 10% citric acid was added until pH 7, and the aqueous layer extracted with CH_2Cl_2 (3 x 100 mL) The combined organic layers were dried over $MgSO_4$, and the solvents removed *in vacuo*. The resulting brown solid was recrystallized from $CHCl_3$ to give **7** as a off-white solid (1.57 g, 70%). ^{1}H NMR (300 MHz, $CDCl_3$) δ (ppm): 10.59 (s, 1H, N*H),* 9.24 (d, ^3J = 2.0 Hz, 1H, Ar*H*), 9.19 (d, ^3J = 2.0 Hz, Ar*H*), 8.72 (t, ^3J = 2.0 Hz, 1H, Ar*H*), 8.28 (d, ^3J = 8.8 Hz, 2H, Ar*H*), 7.10–7.35 (m, 17H, Ar*H*), 1.26 (s, 18H, CH_3). MS (ESI +ve) *m/z*: 596.2 ($[M+H]^+$, $C_{40}H_{40}N_2O_3$ requires 596.3).

2,7-Bis(bromomethyl-napthalene) 8[11]

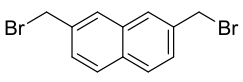

To a solution of 2,7-dimethyl-naphthalene (3.60 g, 23.0 mmol) in carbontetrachloride (180 mL), was added azobisisobutyronitrile (1.15 g, 7.00 mmol) and *N*-bromosuccinimide (8.00 g, 22.5 mmol) portion-wise over 30 min. The reaction was heated under reflux for 12 hrs, then allowed to cool to rt. $CHCl_3$ (100 mL) was added to cause the succinimide by-

product to precipitate, and the mixture was filtered through celite before the solvents were removed *in vacuo*. Recrystallisation from hot ethanol gave the title compound as a white solid (4.59 g, 64%). ^{1}H NMR (300 MHz, $CDCl_3$) δ (ppm): 7.83 (d, *J* = 8.9 Hz, 2H, Ar*H*), 7.82 (s, 2H, Ar*H*), 7.53 (d, *J* = 8.9 Hz, 2H, Ar*H*), 4.66 (s, 4H, Ar*H*).

2,7-bis(azidomethyl)-naphthalene 9[11]

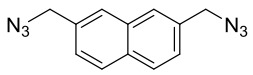

To a solution of 2,7-bis(bromomethyl-naphthalene) **8** (506 mg, 1.62 mmol) in DMSO (30 mL) was added sodium azide (215 mg, 3.30 mmol) and stirred at rt for 16 hrs. The solution was then poured into water (50 mL), and the white precipitate collected by vacuum filtration and dried under high vacuum to yield the product as a white solid (290 mg, 77%). ^{1}H NMR (300 MHz, $CDCl_3$) δ (ppm): 7.89 (d, ^{3}J = 8.2 Hz, 2H, Ar*H*), 7.78 (s, 2H, Ar*H*), 7.47 (d, ^{3}J = 8.2 Hz, 2H, Ar*H*), 4.52 (s, 4H, Ar*H*).

2,7-bis(aminomethyl)-naphthalene 10[11]

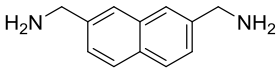

To a solution of 2,7-bis(azidomethyl)-naphthalene **9** (600 mg, 2.61 mmol) in CH_3OH was added Pd/C (5 wt%, 60 mg) and stirred vigorously under an atmosphere of H_2 (1 bar) for 48 hrs. The resulting mixture was filtered through celite and precipitated by addition of $CHCl_3$ to yield the product as an off-white solid (470 mg, 97%). ^{1}H NMR (300 MHz, $CDCl_3$) δ (ppm): 7.89 (d, ^{3}J = 8.2 Hz, 2H, Ar*H*), 7.78 (s, 2H, Ar*H*), 7.47 (d, ^{3}J = 8.2 Hz, 2H, Ar*H*), 4.52 (s, 4H, Ar*H*).

Bis-pyridyl naphthalene containing axle 11

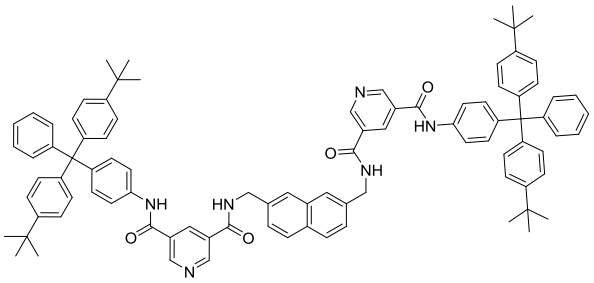

Stopper-acid **7**[10] (1.00 g, 1.68 mmol), EDC·HCl (357 mg, 1.68 mmol) and DMAP (cat.) were added to dry CH_2Cl_2 (20 mL) and stirred at 0 °C under a N_2 atmosphere until all the solids dissolved. At this point, a suspension of naphthalene bis-amine **10**[11] (75 mg, 0.42 mmol) in a solution of NEt_3 (0.2 mL, 1.68 mmol) in dry CH_2Cl_2 (10 mL) was added at 0 °C, and the reaction stirred at rt for 4 days under N_2. The reaction mixture was then washed with 10% citric acid (1 × 20 mL) and 10% $NaOH_{(aq)}$ (2 × 30 mL), the organic layer dried over $MgSO_4$, the solvent removed *in vacuo* and the crude material purified by silica gel chromatography (95:5 CH_2Cl_2/CH_3OH) to give the product as a yellow solid (290 mg, 51%). ^{1}H NMR (500 MHz, d_6-DMSO) δ (ppm): 10.58 (s, 2H, ArN*H*), 9.49 (t, ^3J = 5.8 Hz, 2H, CH_2N*H*), 9.23 (d, ^3J = 2.1 Hz, 2H, pyridinium Ar*H*), 9.20 (d, ^3J = 2.1 Hz, 2H, pyridinium Ar*H*), 8.73 (t, ^3J = 5.8 Hz, 2H, pyridinium Ar*H*), 7.88 (d, ^3J = 8.4 Hz, 2H, naphthalene Ar*H*), 7.84 (s, 2H, naphthalene Ar*H*), 7.67 (d, ^3J = 8.4 Hz, 4H, stopper Ar*H*), 7.50 (d, ^3J = 8.4 Hz, 2H, naphthalene Ar*H*), 7.27–7.10 (m, 30H, stopper Ar*H*), 4.27 (d, ^3J = 6.1 Hz, 4H, C*H*$_2$NH), 1.26 (s, 36H, C*H*$_3$). ^{13}C NMR (125 MHz, d_6-DMSO) δ (ppm): 164.3, 163.5, 150.8, 147.9, 146.8, 143.6, 142.4, 137.0, 136.4, 132.8, 131.3, 134.4, 130.7, 130.3, 130.0, 129.5, 127.8, 127.7, 125.8, 125.4, 124.5, 119.5, 63.3, 43.0, 40.1, 39.9, 34.1, 31.1, one peak missing, presumed overlapped. HRMS (ESI +ve) *m/z*: 1365.6916 ([M+Na]$^+$, $C_{92}H_{90}N_6O_4Na$ requires 1365.6916).

Dichloride salt of naphthalene containing axle 12·(Cl)$_2$

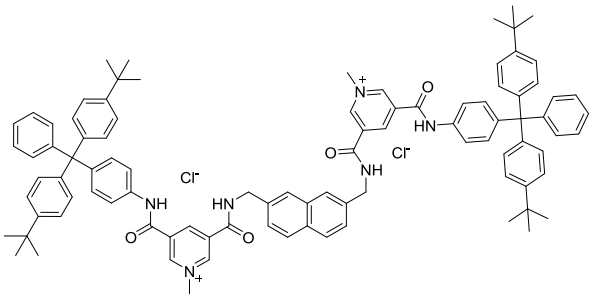

A solution of axle **11** (177 mg, 0.132 mmol) in CH_3I (4 mL), was heated under reflux for 16 hrs. The excess CH_3I was removed *in vacuo* to afford $\mathbf{12}^{2+}$ as the iodide salt. This was dissolved in $CHCl_3$ (10 mL) and washed with 1 M $NH_4Cl_{(aq)}$ (8 × 20 mL) and H_2O (2 × 20 mL). The organic layer was dried over $MgSO_4$ and the solvent removed *in vacuo* to give the chloride salt as a yellow solid (153 mg, 86%). ^{1}H NMR (300 MHz, 1:1 $CDCl_3/CD_3OD$) δ (ppm): 9.71 (s, 2H, pyridinium Ar*H*), 9.50 (s, 2H, pyridinium Ar*H*), 9.02 (s, 2H, pyridinium Ar*H*), 7.75−7.55 (m, 6H, naphthalene Ar*H*), 7.30 (d, ^3J = 8.4 Hz, 4H, stopper Ar*H*), 7.25−7.05 (m, 34H, stopper Ar*H*), 4.70 (s, 4H, CH_2NH), 4.07 (s, 6H, N^+CH_3), 1.26 (s, 36H, CH_3). ^{13}C NMR (125 MHz, 1:1 $CDCl_3/CD_3OD$) δ (ppm): 160.4, 157.4, 148.1, 146.5, 146.3, 146.0, 144.3, 143.1, 140.3, 135.7, 134.5, 132.8, 131.8, 131.4, 130.5, 130.2, 128.3, 126.9, 125.3, 124.9, 123.8, 121.5, 119.2, 119.1, 63.4, 52.9, 48.5, 47.3, 33.6, 30.6. HRMS (ESI +ve) *m/z*: 686.3732 ($[M-2Cl]^{2+}$, $C_{94}H_{96}N_6O_4$ requires 686.3741).

2-(4-hydroxyphenoxy)acetonitrile 13[12]

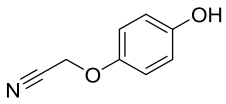

Hydroquinone (8.00 g, 72.7 mmol) and NaOH (5.82 g, 145 mmol) were dissolved in a 1:1 dioxane/water (300 mL) and degassed. A degassed solution of bromoacetonitrile (8.72 g, 72.7 mmol) in dioxane (50 mL) was added while stirring under N_2. The solution was stirred for 1 hr, and degassed throughout. The reaction was complete after 1 hr (TLC 98:2 CH_2Cl_2/CH_3OH). 1M $HCl_{(aq)}$ was added to acidify the reaction mixture, which was then extracted with CH_2Cl_2 (3 × 100 mL). The organics were dried over $MgSO_4$ and the solvent removed *in vacuo* to obtain a brown oil. Purification by silica gel chromatography (98:2 CH_2Cl_2/CH_3OH) afforded the product as pale yellow oil (6.83 g, 63%). ^{1}H NMR (300 MHz, $CDCl_3$) δ (ppm): 6.88 (d, ^3J = 2.88 Hz, 2H, Ar*H*), 6.81 (d, ^3J = 2.7 Hz, 2H, Ar*H*), 4.70 (s, 2H, CH_2).

Bis-mesylate tetra-ethylene glycol 14[12]

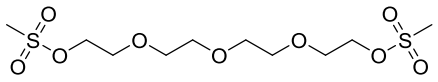

Tetraethyleneglycol was dissolved with dry triethylamine (12 mL) in CH_2Cl_2 (100 mL) at 0 °C. Mesyl chloride was added drop-wise over 30 mins and the reaction mixture warmed to rt. The reaction was stirred for 16 hrs before the solution was washed with 1M $HCl_{(aq)}$ (2 × 30 mL) and saturated $NaHCO_3$ (2 × 30 mL). The aqueous layer was extracted with CH_2Cl_2 (3 × 50 mL). The aqueous layers were combined, dried over $MgSO_4$ and the solvent removed *in vacuo* to give **14** as a yellow oil (7.97 g, 99%). ^{1}H NMR (300 MHz, $CDCl_3$) δ (ppm): 4.37 (m, 4H, CH_2), 3.76 (m, 4H, CH_2) , 3.65 (m, 8H, CH_2), 3.07 (s, 6H, CH_3).

Bis-nitrile 15[12]

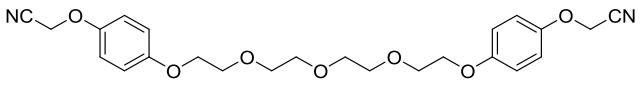

Bis-mesylate **14** (1.45 g, 4.56 mmol) and 2-(4-hydroxyphenoxy)acetonitrile **13** (1.36 g, 9.13 mmol) were dissolved in dry CH_3CN (90 mL) under N_2. Potassium carbonate (1.32 g, 9.58 mmol) was added and the reaction mixture refluxed at 80 °C under N_2 for 72 hrs. The reaction was cooled to rt and filtered, before the solvent was removed *in vacuo*. The residue was dissolved in $CHCl_3$ (20 mL) and filtered, before the solvent was removed *in vacuo* to give **15** a brown oil (1.69 g, 81 %). ^{1}H NMR (300 MHz, $CDCl_3$) δ (ppm): 6.94–6.76 (m, 8H, Ar*H*), 4.70 (br. s, 4H, C*H*$_2$CN), 4.07 (m, 4H, C*H*$_2$O), 3.84 (m, 4H, C*H*$_2$O), 3.71 (m, 8H, C*H*$_2$O). MS (ESI +ve) *m/z*: 479.2 ($[M+Na]^+$, $C_{24}H_{28}N_2O_7Na$ requires 479.5).

Bis amine macrocycle precursor 16[12]

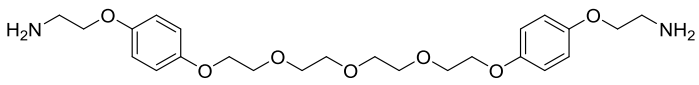

Bis-nitrile **15** (1.69 g, 3.64 mmol) was dissolved in dry THF (25 mL) under N_2. Borane in THF (25 mL) was added to the reaction mixture and refluxed at 70 °C for 4 hrs, before cooling to rt. CH_3OH (10 mL) was then added to quench the reaction followed by conc. $HCl_{(aq)}$ (10 mL). The solvent was removed *in vacuo* to form a white precipitate, which was collected and then re-dissolved in H_2O (10 mL). $KOH_{(aq)}$ (2 M, 20 mL) was added and stirred for 30 min to form a white precipitate. The precipitate was collected *via* vacuum filtration and dried in a desiccator to afford the amine product **16** (0.85 g, 51%). ^{1}H NMR (300 MHz, $CDCl_3$) δ (ppm): 6.82 (s, 8H, Ar*H*), 4.06 (t, ^3J = 4.58 Hz, 4H, C*H*$_2$), 3.92 (t, ^3J = 5.50 Hz, 4H, C*H*$_2$), 3.82 (m, 8H, C*H*$_2$), 3.70 (t,^3J = 4.9 Hz, 4H, C*H*$_2$), 3.04 (t, ^3J = 5.5 Hz, 4H, C*H*$_2$). MS (ESI +ve) *m/z*: 465.3 ($[M+H]^+$, $C_{24}H_{37}N_2O_7$ requires 465.6).

Tert-butyl macrocycle 19[13]

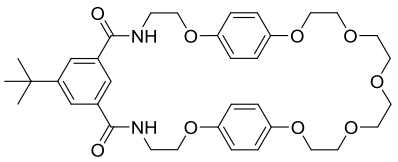

Bis amine macrocycle precursor **16** (0.85 g, 1.83 mmol), pyridinium chloride thread **18** (0.70 g, 1.83 mmol) and triethylamine (5.50 mL) were dissolved in dry CH_2Cl_2 by stirring under N_2 until all solid had dissolved. A solution of 5-(*tert*-butyl) isophthaloyl dichloride (0.48 g, 1.83 mmol) in dry CH_2Cl_2 (27 mL) was then added drop-wise at 0 °C. The reaction mixture was warmed to rt and stirred for 16 hrs under N_2. The solution was washed with 10% $HCl_{(aq)}$ (2 × 100 mL) and H_2O (2 × 100 mL). The organic phase was dried over $MgSO_4$ and solvent removed *in vacuo*. Purification by silica gel column chromatography (97:3 CH_2Cl_2/CH_3OH) yielded the product as pale yellow solid (384 mg, 32%). ^{1}H NMR (300 MHz, $CDCl_3$) δ (ppm): 8.08 (br. s, 2H, Ar*H*), 7.74 (br. s, 1H, Ar*H*), 6.77 (m, 8H, Ar*H*), 4.12–3.63 (m, 24H, CH_2), 1.36 (s, 9H, CH_3). MS (ESI +ve) *m/z*: 651.32 ($[M+H]^+$, $C_{36}H_{47}N_2O_9$ requires 651.32).

Asymmetric thread 20·PF_6

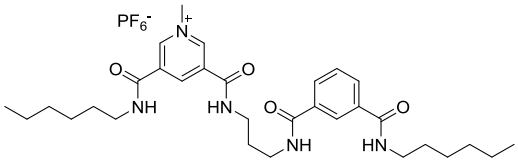

Methyl-iodide (2 mL) was added to a solution of **34** (70 mg, 0.130 mmol) in DMF (2 mL) and stirred under N_2 for 16 hrs. The solvent was removed *in vacuo* to give compound $\mathbf{20}^+$ as the iodide salt. Anion exchange to the PF_6^- salt was achieved by washing a solution of **20·I** in CH_2Cl_2 (20 mL) with a solution of with a 0.1 M $NH_4PF_{6(aq)}$ (8 × 12 mL) and water (2 × 10 mL). The organic layer was dried over $MgSO_4$ and the solvent removed *in vacuo* to give **20·PF_6** (70 mg, 77%). ^{1}H NMR (500 MHz, 1:1 $CDCl_3/CD_3OD$) δ (ppm): 9.48 (s, 1H, pyridinium Ar*H*), 9.43 (s, 1H, pyridine Ar*H*), 9.39 (s, 1H, pyridinium Ar*H*), 8.28 (t, ^4J = 1.7

Hz, 1H, Ar*H*), 7.97 (m, 2H, Ar*H*), 7.54 (t, ^3J = 7.7 Hz, 1H, Ar*H*), 4.53 (s, 3H, N^+CH_3), 3.58 (t, ^3J = 6.4 Hz, 2H, CH_2), 3.55 (t, ^3J = 6.4 Hz, 2H, CH_2), 3.46 (t, ^3J = 7.7 Hz, 2H, CH_2), 3.40 (t, ^3J = 7.2 Hz, 2H, CH_2), 1.99 (quintet, ^3J = 6.1 Hz, 2H, CH_2), 1.65 (m, 4H, CH_2), 1.33 (m, 12H, CH_2), 0.89 (t, ^3J = 7.2 Hz, 6H, CH_3). ^{13}C NMR (125 MHz, 1:1 $CDCl_3$ /CD_3OD) δ (ppm): 169.7, 169.1, 162.6, 162.3, 148.0, 147.8, 142.6, 136.3, 136.2, 136.0, 135.7, 131.6, 131.5, 130.2, 127.2, 42.1, 41.6, 38.9, 38.3, 32.9, 32.8, 30.6, 30.4, 29.7, 28.0, 28.0, 23.9, 23.8, 15.0, two peaks missing, presumed overlapped. ^{19}F NMR (282.5 MHz, 1:1 $CDCl_3$/CD_3OD) δ (ppm): −72.2 (d, ^1J = 717 Hz, PF_6^-). HRMS (ESI +ve) *m/z*: 552.3544 ($[M-PF_6]^+$, $C_{31}H_{46}N_5O_4$ requires 552.3544).

Methyl 5-(hexylcarbamoyl)nicotinate 22[13]

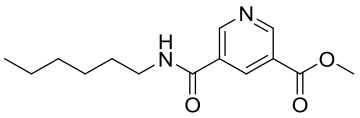

5-Methoxycarbonyl)nicotinic acid **5** (0.88 g, 4.86 mmol) was converted to the corresponding acid chloride using the general procedure, and dissolved in CH_2Cl_2 (50 mL), before a solution of hexylamine (0.704 mL, 5.35 mmol), triethylamine (1.02 mL, 7.29 mmol) in CH_2Cl_2 (40 mL) was added drop-wise at 0 °C. The reaction mixture was stirred at rt under N_2 for 16 hrs and then washed with 10% HCl (2 × 60 mL), 10% NaOH (60 mL) and brine (60 mL). The organic layer was dried over $MgSO_4$ and solvent removed *in vacuo*. Purification by silica gel chromatography (9:1 CH_2Cl_2/acetone) afforded the product as a pale yellow solid (801 mg, 62%). ^{1}H NMR (300 MHz, $CDCl_3$) δ (ppm): 9.31 (m, 2H, Ar*H*), 8.72 (s, 1H, Ar*H*), 6.48 (br. s, 1H, N*H*), 4.00 (s, 3H, CH_3O), 3.48 (m, 2H, CH_2), 1.72–1.25 (m, 10H, CH_2), 0.89 (t, ^3J = 7.0 Hz, 3H, CH_3). MS (ESI +ve) *m/z*: 287.1 ($[M+Na]^+$, $C_{14}H_{20}N_2O_3Na$ requires 287.3).

5-(Hexylcarbamoyl)nicotinic acid 23[13]

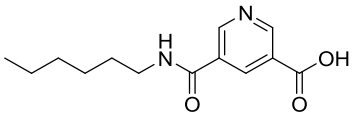

Methyl 5-(hexylcarbamoyl)nicotinate **22** (130 mg, 0.52 mmol) and KOH (43.0 mg, 0.78 mmol) were dissolved in H_2O (5 mL) and CH_3OH (4 mL) and stirred for 16 hrs under N_2. 10% citric acid was then added drop-wise, resulting in the formation of a white precipitate. The white solid was collected by filtration and washed with H_2O (2 × 20 mL) and CH_2Cl_2 (2 × 20 mL) before being dried *in vacuo* to afford **23** *(*72 mg, 59 %). ^{1}H NMR (300 MHz, d_6-DMSO) δ (ppm): 9.14 (s, 2H, Ar*H*), 8.83 (t, ^3J = 5.5 Hz, 1H, N*H*), 8.63 (s, 1H, Ar*H*), 3.25 (m, 2H, CH_2), 1.50 (m, 2H, CH_2), 1.25 (m, 6H, CH_2), 0.83 (t, ^3J = 6.2 Hz, 3H, CH_3) MS (ESI +ve) *m/z*: 251.2 ($[M+H]^+$ $C_{13}H_{19}N_2O_3$ requires 251.1).

3-(Methoxycarbonyl) benzoic acid 24[14]

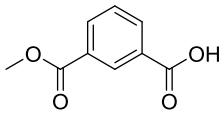

Dimethylisophthalate (5.00 g, 25.8 mmol) was dissolved with KOH (1.59 g, 28.4 mmol) in CH_3OH (150 mL), and the reaction mixture was stirred under N_2 for 16 hrs. The solvent removed *in vacuo* and re-dissolved in H_2O (50 mL). The solution was washed with CH_2Cl_2 (3 × 100 mL) and neutralised with 10% $HCl_{(aq)}$. The resulting precipitate was collected by vacuum filtration and washed with H_2O (2 ×10 mL) and dried to give **24** as a white solid (3.06 g, 66%). ^{1}H NMR (300 MHz, d_6-DMSO) δ (ppm): 8.46 (br. s, 1H, Ar*H*), 8.16 (m, 2H, Ar*H*), 7.64 (m, 1H, Ar*H*), 3.40 (s, 3H, CH_3). MS (ESI +ve) *m/z*: 181.1 ($[M+H]^+$ $C_9H_9O_4$ requires 181.2).

Methyl 3-(hexanoylcarbamoyl)benzoate 25

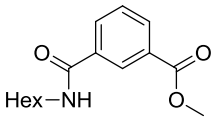

Acid **24**[14] (2.00 g, 11.1 mmol) was converted to its acid chloride using the general procedure. Assuming quantitative conversion, the crude acid chloride was immediately re-dissolved in CH_2Cl_2 (150 mL) and a solution of hexylamine (1.61 mL, 12.2 mmol), dry triethylamine (2.32 mL, 16.7 mmol) in CH_2Cl_2 (50 mL) was added drop-wise at 0 °C. The reaction mixture was stirred at rt under N_2 for 16 hrs and then washed with 10% citric acid (2 × 50 mL) and $NaHCO_3$ (2 × 50 mL). The organic layer was dried over $MgSO_4$ and solvent removed in vacuo. Purification by silica gel column chromatography (99:1 CH_2Cl_2/CH_3OH) to give **25** as a pale yellow oil (1.31 g, 45%). ^{1}H NMR (500 MHz, $CDCl_3$) δ (ppm): 8.35 (t, ^4J = 1.7 Hz, 1H, Ar*H*), 8.15 (m, 1H, Ar*H*), 8.04 (m, 1H, Ar*H*), 7.52 (t, ^3J = 7.8 Hz, 1H, Ar*H*), 6.30 (br. s, 1H, N*H*), 3.94 (s, 3H, CH_3), 3.46 (m, 2H, CH_2), 1.63 (quintet, ^3J = 6.9 Hz, 2H, CH_2), 1.38 (m, 2H, CH_2), 1.32 (m, 4H, CH_2), 0.89 (t, ^3J = 7.2 Hz, 3H, CH_3). ^{13}C NMR (125 MHz, $CDCl_3$) δ (ppm): 166.4, 135.1, 132.2, 131.8, 130.4, 128.9, 127.4, 52.3, 40.2, 31.5, 29.6, 26.6, 22.5, 14.0, one peak missing, presumed overlapped. HRMS (ESI +ve) m/z: 264.1601 ($[M+H]^+$, $C_{15}H_{22}NO_3$ requires 264.1594).

3-(hexanoylcarbamoyl)benzoic acid 26

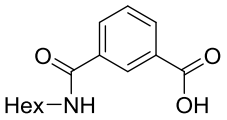

Methyl 3-(hexanoylcarbamoyl)benzoate **25** (610 mg, 2.31 mmol) was dissolved with KOH (140 mg, 2.54 mmol) in CH_3OH (35 mL). The reaction mixture was stirred under N_2 for 16 hrs. The solvent removed *in vacuo* and re-dissolved in H_2O (50 mL) and washed with CH_2Cl_2 (2 × 20 mL). The aqueous layer was neutralised with 10% citric acid and the resulting precipitate was collected by vacuum filtration and washed with H_2O (10 mL), CH_2Cl_2 (10 mL) and dried to give **26** as a white solid. (445 mg, 77%). ^{1}H NMR (500 MHz, d_6-DMSO) δ (ppm): 8.65 (t, ^3J = 5.3 Hz, 1H, CON*H*), 8.42 (s, 1H, Ar*H*), 8.07 (dd, ^3J = 7.7 Hz, ^4J = 1.8 Hz, 2H, Ar*H*), 7.59 (t, ^3J = 7.6 Hz, 1H, Ar*H*), 3.26 (m, 2H, CH_2), 1.53 (m, 2H, CH_2), 1.29 (m, 6H, CH_2), 0.88 (t, ^3J = 7.0 Hz, 3H, CH_3). ^{13}C NMR (125 MHz, d_6-DMSO) δ (ppm): 167.0, 165.3, 135.0, 131.6, 131.4, 131.0, 128.7, 128.0, 31.0, 30.0, 26.2, 22.1, 13.9, one peak missing, presumed overlapped. HRMS (ESI +ve) *m/z*: 272.1256 ($[M+Na]^+$, $C_{14}H_{19}NO_3Na$ requires 272.1257).

***Tert*-butyl (3-aminopropyl)carbamate 27[15]**

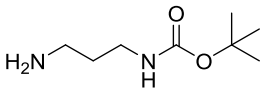

Di-*tert*-butyl bicarbonate (4.00 g, 0.018 mmol) was dissolved in $CHCl_3$ (100 mL) and the solution added drop-wise to a solution of 1,3-diaminopropane (35 mL) in $CHCl_3$ (200 mL) over 3 hrs stirring under N_2 at 0°C. The reaction mixture was warmed to rt and stirred under N_2 for 16 hrs. The mixture was washed with H_2O (8 × 250 mL) and the organic phase dried over $MgSO_4$. The solvent was removed *in vacuo* to give **27** as a pale yellow oil (1.35 g, 43%). ^{1}H NMR (300 MHz, $CDCl_3$) δ (ppm): 4.84 (br. s, 1H, N*H*), 3.13 (m, 2H, CH_2), 2.69 (t, ^3J = 6.6 Hz, 2H, CH_2), 1.54 (m, 2H, CH_2), 1.36 (s, 9H, CH_3).

Boc-protected amine 28

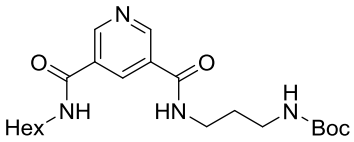

Acid **23**[13] (500 mg, 2.00 mmol) was converted to its corresponding acid chloride using the general procedure. Assuming quantitative conversion, the crude acid chloride was immediately re-dissolved in CH_2Cl_2 (40 mL). A solution of **27**[15] (380 mg, 2.20 mmol) and dry triethylamine (0.42 mL, 3.00 mmol) in CH_2Cl_2 (10 mL) was added drop-wise at 0 °C. The reaction mixture was stirred at rt under N_2 for 16 hrs and then washed with 10% citric acid (2 × 30 mL) and $NaHCO_3$ (2 × 30 mL). The organic layer was dried over $MgSO_4$ and solvent removed *in vacuo*. Purification by silica gel column chromatography (95:5 CH_2Cl_2/CH_3OH) afforded the product as a pale yellow solid (490 mg, 60%). ^{1}H NMR (500 MHz, $CDCl_3$) δ (ppm): 9.19 (br. s, 2H, pyridine Ar*H*), 8.57 (s, 1H, pyridine Ar*H*), 7.98 (br. s, 1H, N*H*), 6.78 (br. s, 1H, N*H*), 4.96 (br. s, 1H, CON*H*), 3.53 (m, 2H, CH_2), 3.47 (m, 2H, CH_2), 3.26 (m, 2H, CH_2), 1.74 (m, 2H, CH_2), 1.63 (m, 2H, CH_2), 1.45 (s, 9H, CH_3), 1.38 (m, 2H, CH_2), 1.31 (m, 4H, CH_2), 0.89 (t, ^3J = 6.6 Hz, 3H, CH_3). ^{13}C NMR (125 MHz, $CDCl_3$) δ (ppm): 164.7, 164.6, 157.2, 150.7, 150.1, 133.5, 130.1, 129.9, 80.0, 40.3, 37.0, 36.1, 31.4, 29.8, 29.5, 28.4, 26.6, 22.5, 14.0. HRMS (ESI +ve) *m/z*: 429.2476 ($[M+Na]^+$, $C_{21}H_{34}N_4O_4Na$ requires 429.2472).

Thread precursor 29·CF_3CO_2

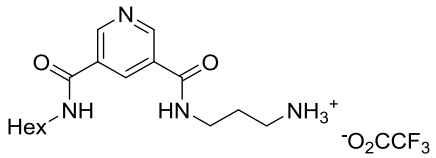

To a solution of **28** (490 mg, 1.21 mmol) in CH_2Cl_2 (30 mL) at 0 °C was added trifluoroacetic acid (5 mL) drop-wise. The reaction mixture was allowed to warm to rt and stirred under N_2. The reaction was monitored using TLC (9:1 CH_2Cl_2/CH_3OH) until all the amine had been

de-protected. The solvent was removed *in vacuo* and re-dissolved in CH_3OH which was subsequently again removed *in vacuo*. This was repeated until all the excess TFA had been removed to give the trifluoroacetate salt of the product (420 mg, 83%) ^{1}H NMR (500 MHz, CD_3OD) δ (ppm): 9.16 (br. s, 2H, pyridine Ar*H*), 8.70 (s, 1H, pyridine Ar*H*), 3.57 (t, ^3J = 6.2 Hz, 2H, CH_2), 3.45 (t, ^3J = 6.8 Hz, 2H, CH_2), 3.06 (t, ^3J = 7.5 Hz, 2H, CH_2NH), 2.01 (quintet, ^3J = 7.0 Hz, 2H, CH_2), 1.66 (quintet, ^3J = 7.7 Hz, 2H, CH_2), 1.43 (m, 2H, CH_2), 1.37 (m, 4H, CH_2), 0.94 (t, ^3J = 6.9 Hz, 3H, CH_3). ^{13}C NMR (125 MHz, CD_3OD) δ (ppm): 167.8, 166.9, 161.4, 159.0 (quartet, ^1J = 41.9 Hz, *C*F_3), 151.2, 151.1, 136.1, 117.2, 115.0, 41.4, 38.4, 37.8, 32.8, 30.5, 28.9, 28.0, 23.9, 14.6. HRMS (ESI +ve) m/z: 307.2126 ($[M–CF_3CO_2]^+$, $C_{16}H_{27}N_4O_2$ requires 307.2129).

Thread precursor 30

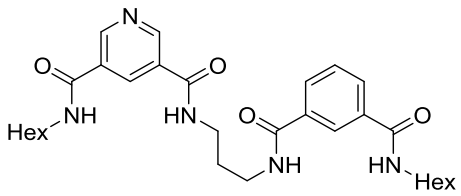

To a suspension of acid **26** (68 mg, 0.272 mmol) in CH_2Cl_2 (10 mL) was added EDC·HCl (63 mg, 0.327 mmol), HOBt (50 mg, 0.327 mmol) and DMAP (cat. ~1 mg). This was stirred for 16 hrs under N_2 until the solution became homogeneous. To this was added dry triethylamine (0.19 mL, 1.36 mmol) and a solution of amine salt **29·CF_3CO_2** (100 mg, 0.327 mmol) in DMF (3 mL). The reaction mixture was stirred for 2 days under N_2 and washed with 10 % citric acid (2 × 5 mL) and $NaHCO_3$ (2 × 5 mL). The organic layer was dried over $MgSO_4$ and the solvent removed *in vacuo*. The product was purified using silica gel column chromatography (95:5 CH_2Cl_2/CH_3OH) to afford a yellow solid (79 mg, 54%). ^{1}H NMR (500 MHz, 1:1 $CDCl_3/CD_3OD$) δ (ppm): 9.12 (s, 1H, pyridine Ar*H*), 9.10 (s, 1H, pyridine Ar*H*), 8.64 (s, 1H, pyridine Ar*H*), 7.98 (m, 2H, Ar*H*), 7.54 (t, ^3J = 7.73, 1H, Ar*H*), 3.52 (m, 4H, CH_2), 3.41 (m, 4H, CH_2), 1.94 (m, 2H, CH_2), 1.64 (m, 4H, CH_2), 1.39 (m, 4H, hexyl CH_2), 1.33 (m, 8H, CH_2), 0.90 (m, 6H, CH_3). ^{13}C NMR (125 MHz, 1:1 $CDCl_3/CD_3OD$) δ (ppm): 169.6, 169.3, 167.3, 166.9, 151.7, 151.5, 136.4, 135.8, 135.8, 131.7, 131.3, 130.1, 127.1, 118.1, 41.6, 41.6, 38.5, 38.4, 32.8,32.8, 30.6, 30.5, 28.0, 28.0, 23.8, 15.0, four peaks missing, presumed overlapped. HRMS (ESI +ve) *m/z*: 560.3211 ($[M+Na]^+$, $C_{30}H_{43}N_5O_4Na$ requires 560.3207).

Axle precursor 32·NO_3

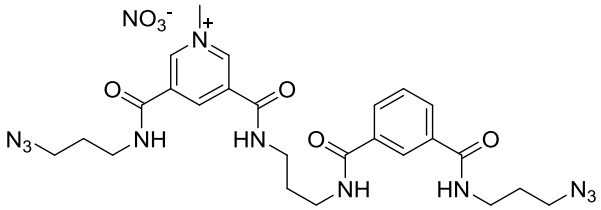

Methyl-iodide (2 mL) was added to a solution of **39** (48 mg, 0.089 mmol) in DMF (2 mL) and stirred under N_2 for 16 hrs. The solvent was removed *in vacuo*. Ion exchange to the nitrate salt was achieved by passing down a nitrate loaded Amberlite® column in 9:1 acetone/water. The solvent was removed *in vacuo* to leave a pale yellow oil (52 mg, 94%). ^{1}H NMR (500 MHz, 1:1 $CDCl_3$/d_6-acetone) δ (ppm): 9.79 (br. s, 1H, pyridinium Ar*H*), 9.65 (br. s, 1H, pyridinium Ar*H*), 9.57 (br. s, 1H, pyridinium Ar*H*), 9.19 (t, ^3J = 5.4 Hz, 1H, N*H*), 9.04 (t, ^3J = 5.3 Hz, 1H, N*H*), 8.47 (br. s, 1H, Ar*H*), 8.37 (t, ^3J = 5.9 Hz, 1H, N*H*), 8.20 (t, ^3J = 5.3 Hz, 1H, N*H*), 8.05 (d, ^3J = 7.8 Hz, 1H, Ar*H*), 8.02 (d, ^3J = 7.8 Hz, 1H, Ar*H*), 7.49 (t, ^3J = 7.8 Hz, 1H, Ar*H*), 4.75 (s, 3H, N^+CH_3), 3.56 (m, 4H, CH_2), 3.52 (m, 4H, CH_2), 3.46 (m, 4H, CH_2), 1.94 (m, 6H, CH_2).^{13}C NMR (125 MHz, 1:1 $CDCl_3$/d_6-acetone) δ (ppm): 167.3, 167.3, 161.6, 161.5, 148.2, 147.9, 141.6, 135.6, 135.1, 135.1, 135.1, 131.4, 131.2, 129.4, 126.1, 50.3, 50.0, 49.9, 49.8, 38.5, 38.1, 37.4, 29.7, 29.3, 28.7. HRMS (ESI +ve) *m/z*: 550.2613 ($[M-NO_3]^+$, $C_{25}H_{32}N_{11}O_4$ requires 550.2633).

32·PF_6: Anion exchange of a further sample of **32·NO_3** to the PF_6^- salt was achieved by passing down a PF_6^- loaded Amberlite® column in 9:1 acetone/water, to afford **32·PF_6** in a quantitative yield. ^{1}H NMR (500 MHz, 1:1 $CDCl_3$/CD_3OD) δ (ppm): 9.61 (s, 1H, pyridinium Ar*H*), 9.56 (s, 1H, pyridinium Ar*H*), 9.49 (s, pyridinium Ar*H*), 8.38 (s, 1H, Ar*H*), 8.05 (d, ^3J = 7.8 Hz, 1H, Ar*H*), 8.00 (d, ^3J = 7.8 Hz, 1H, Ar*H*), 7.61 (t, ^3J = 7.8 Hz, 1H, Ar*H*), 4.56 (s, 3H, N^+CH_3), 3.56 (m, 4H, CH_2), 3.52 (m, 4H, CH_2), 3.46 (m, 4H, CH_2), 1.94 (m, 6H, CH_2). ^{19}F NMR (282.5 MHz, 1:1 $CDCl_3$/CD_3OD) δ (ppm): −73.5 (d, ^1J = 712 Hz, PF_6^-).

Methyl 3-[(3-azidopropyl)carbamoyl]benzoate 33

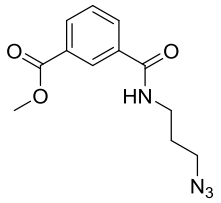

Mono-acid **24**[14] (1.50 g, 8.33 mmol) was converted to its respective acid chloride *via* the general procedure. Assuming quantitative yield the acid chloride was re-dissolved in dry CH_2Cl_2 (150 mL) and cooled to 0 °C. To this was added dry triethylamine (5.80 mL, 41.7 mmol) drop-wise before adding 3-bromopropylamine hydrobromide (3.64 g, 16.7 mmol). The reaction mixture was allowed to warm to rt and stirred under N_2 for 16 hrs. The solution was washed with 10 % citric acid (2 × 30 mL) and $NaHCO_3$ (2 × 30 mL) and the organic layer dried over $MgSO_4$ before removing the solvent *in vacuo* to give a pale yellow oil. This was dissolved in DMF (50 mL) before adding sodium azide (1.08 g, 16.7 mmol) to the solution. The reaction mixture was stirred under N_2 and refluxed at 70 °C for 16 hrs. The solution was allowed to cool to rt before pouring into H_2O (100 mL). The product was extracted into CH_2Cl_2 (3 × 40 mL) and the combined organic layers dried over $MgSO_4$. The solvent was removed *in vacuo* and the resulting oil purified by silica gel column chromatography (98:2 CH_2Cl_2/CH_3OH) to afford a colourless oil (1.89 g, 87%). ^{1}H NMR (500 MHz, $CDCl_3$) δ (ppm): 8.37 (t, ^4J = 1.7 Hz, 1H, Ar*H*), 8.18 (m, 1H, Ar*H*), 8.04 (m, 1H, Ar*H*), 7.55 (t, ^3J = 7.8 Hz, 1H, Ar*H*), 6.51 (br. s, 1H, N*H*), 3.95 (s, 3H, CH_3), 3.59 (app. quartet, ^3J = 6.5 Hz, 2H, CH_2), 3.47 (t, ^3J = 6.5 Hz, 2H, CH_2) 1.94 (quintet, ^3J = 6.7 Hz, CH_2).^{13}C NMR (125 MHz, $CDCl_3$) δ (ppm): 166.5. 166.3, 134.7, 132.5, 131.8, 130.5, 129.0, 127.4, 52.4, 49.5, 37.9, 28.7. HRMS (ESI +ve) *m/z*: 285.0960 ($[M+Na]^+$, $C_{12}H_{14}N_4O_3Na$ requires 285.0958).

Methyl 3-[(3-azidopropyl)carbamoyl]nicotinate 34

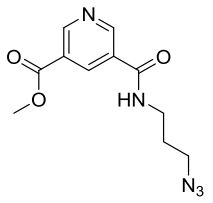

Acid **5**[10] (1.41 g, 7.79 mmol) was converted to its respective acid chloride by the general method. Assuming quantitative yield, the acid chloride was immediately re-dissolved in dry CH_2Cl_2 (150 mL) and cooled to 0 °C. To this was added dry triethylamine (5.43 mL, 39.0 mmol) drop-wise before adding 3-bromopropylamine hydrobromide (3.42 g, 15.6 mmol). The reaction mixture was allowed to warm to room temperature and stirred under N_2 for 16 hrs. The solution was washed with 10 % citric acid (2 × 50 mL) and $NaHCO_3$ (2 × 50 mL) and the organic layer dried over $MgSO_4$ before removing the solvent *in vacuo* to give a pale yellow oil. This was dissolved in DMF (50 mL) before adding sodium azide (1.01 g, 15.6 mmol) to the solution. The reaction mixture was stirred under N_2 and refluxed at 70 °C for 16 hrs. The solution was allowed to cool to rt before pouring into H_2O (100 mL). The product was extracted into CH_2Cl_2 (3 × 40 mL) and the combined layers dried over $MgSO_4$. The solvent was removed *in vacuo* and the resulting oil purified by silica gel column chromatography (98:2 CH_2Cl_2/CH_3OH) to afford a colourless oil (0.85 g, 41%). ^{1}H NMR (500 MHz, d_6-DMSO) δ (ppm): 9.22 (d, ^4J = 2.2 Hz, 1H, pyridine Ar*H*), 9.21 (d, ^4J = 2.1 Hz, 1H, pyridine Ar*H*), 8.94 (br. s, 1H, CON*H*), 8.69 (t, ^4J = 2.2 Hz, 1H, pyridine Ar*H*), 3.94 (s, 3H, OCH_3), 3.44 (t, ^3J = 6.6 Hz, 2H, CH_2), 3.38 (m, 2H, CH_2), 1.81 (quintet, ^3J = 6.8 Hz, 2H, CH_2). ^{13}C NMR (125 MHz, d_6-DMSO) δ (ppm): 164.8, 163.8, 152.3, 151.9, 135.4, 129.8, 125.3, 52.7, 48.5, 36.8, 28.1. HRMS (ESI +ve) *m/z*: 286.0902 ($[M+Na]^+$, $C_{11}H_{13}N_5O_3Na$ requires 286.0911).

3-[(3-azidopropyl)carbamoyl]benzoic acid 35

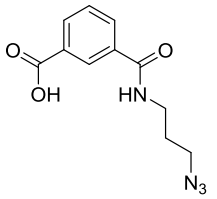

Ester **33** (1.04 g, 3.97 mmol) and KOH (0.24 g, 4.37 mmol) were dissolved in CH_3OH (55 mL) was stirred for 16 hrs under N_2. The solvent was removed *in vacuo* and the residue was dissolved in H_2O (100 mL) and washed with CH_2Cl_2 (3 × 50 mL) The aqueous layer was neutralised by addition of 10% citric acid drop-wise and the white precipitate was collected through vacuum filtration and washed with H_2O (10 mL) and CH_2Cl_2 (10 mL). The product was dried under vacuum to afford a white solid (536 g, 54%). ^{1}H NMR (500 MHz, d_6-DMSO) δ (ppm): 8.73 (app t, ^3J = 5.4 Hz, 1H, N*H*), 8.43 (t, ^4J = 1.6 Hz, 1H, Ar*H*), 8.08 (m, 2H, Ar*H*), 7.16 (t, ^3J = 7.9 Hz, 1H, Ar*H*), 3.43 (t, ^3J = 6.9 Hz, 2H, CH_2), 3.36 (t, ^3J = 6.7 Hz, 2H, CH_2), 1.80 (quintet, ^3J = 6.5 Hz, 2H, CH_2). ^{13}C NMR (125 MHz, d_6-DMSO) δ (ppm): 166.9, 165.5, 134.8, 131.8, 131.5, 131.0, 128.7, 128.0, 48.5, 36.7, 28.3. HRMS (ESI +ve) *m/z*: 271.0810 ($[M+Na]^+$, $C_{11}H_{12}N_4O_3Na$ requires 271.0802).

5-[(3-azidopropyl)carbamoyl]nicotinic acid 36

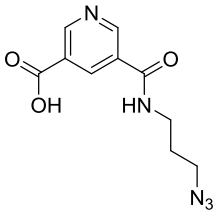

Ester **34** (850 mg, 3.23 mmol) and KOH (200 mg, 3.55 mmol) were dissolved in CH_3OH (48 mL) and stirred for 16 hrs under N_2. The solvent was removed *in vacuo* and the resulting solid re-dissolved in H_2O (75 mL). This solution was washed with CH_2Cl_2 (3 × 30 mL) and the aqueous layer neutralised by addition of 10 % citric acid drop-wise. The resulting white precipitate was collected through vacuum filtration, washed with H_2O (10 mL) and

CH_2Cl_2 (10 mL), and dried under vacuum to afford a white solid (550 mg, 68%). ^{1}H NMR (500 MHz, d_6-DMSO) δ (ppm): 9.19 (d, ^4J = 2.2 Hz, 1H, pyridine Ar*H*), 9.17 (d, ^4J = 2.2 Hz, 1H, pyridine Ar*H*), 8.92 (t, ^3J = 2.2 Hz, 1H, N*H*), 8.68 (t, ^4J = 2.2 Hz, 1H, pyridine Ar*H*), 3.44 (t, ^3J = 6.7 Hz, 2H, CH_2), 3.36 (m, 2H, CH_2), 1.81 (quintet, ^3J = 6.7 Hz, 2H, CH_2). ^{13}C NMR (125 MHz, d_6-DMSO) δ (ppm): 165.8, 164.0, 152.2, 151.0, 135.5, 129.7, 126.5, 48.5, 36.7, 28.2. HRMS (ESI +ve) *m/z*: 272.0750 ($[M+Na]^+$, $C_{10}H_{11}N_5O_3Na$ requires 272.0754).

Boc-protected amine 37

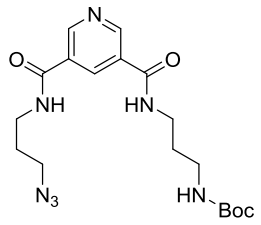

Mono-acid **34** (200 mg, 0.803 mmol) was converted to an acid chloride *via* the general method**.** Assuming quantitative yield the acid chloride was immediately re-dissolved in CH_2Cl_2 (25 mL) and a solution of protected amine **27**[15] (210 mg, 1.21 mmol), dry triethylamine (0.168 mL, 1.21 mmol) in CH_2Cl_2 (5 mL) was added drop-wise at 0 °C. The reaction mixture was stirred at room temperature under N_2 for 16 hrs and then washed with 10% citric acid (2 ×10 mL) and $NaHCO_3$ (2 × 10 mL). The organic layer was dried over $MgSO_4$ and solvent removed *in vacuo*. Silica gel chromatography (98:2 CH_2Cl_2/CH_3OH then 96:4) was used to purify giving a pale yellow solid (224 mg, 69%). ^{1}H NMR (500 MHz, $CDCl_3$) δ (ppm): 9.16 (br. s, 2H, pyridine Ar*H*), 8.55 (br. s, 1H, pyridine Ar*H*), 8.04 (br. s, 1H, N*H*), 7.44 (br. s, 1H, N*H*), 5.02 (br. s, 1H N*H*), 3.56 (m, 2H, CH_2), 3.50 (m, 2H, CH_2), 3.44 (t, ^3J = 6.6 Hz, 2H, CH_2), 3.23 (m, 2H, CH_2), 1.92 (quintet, ^3J = 6.6 Hz, 2H, CH_2), 1.72 (m, 2H, CH_2), 1.44 (s, 9H, CH_3). ^{13}C NMR (125 MHz, $CDCl_3$) δ (ppm): 165.2, 164.8, 157.2, 150.8,

150.4, 133.5, 129.9, 129.8, 79.9, 53.4, 37.8, 37.1, 36.3, 30.9, 29.8, 28.7. HRMS (ESI +ve) *m/z*: 428.2019 ($[M+Na]^+$, $C_{18}H_{27}N_7O_4Na$ requires 428.2017).

Amine 38·CF_3CO_2

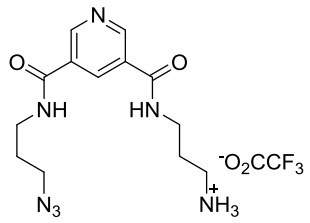

To a solution of **37** (220 mg, 0.543 mmol) in CH_2Cl_2 (10 mL) at 0 °C, was added trifluoroacetic acid (2 mL) drop-wise. The reaction mixture was allowed to warm to room temperature and stirred under N_2. The reaction was monitored using thin layer chromatography (9:1 CH_2Cl_2/CH_3OH) until all the amine had been deprotected. The solvent was removed *in vacuo* and re-dissolved in CH_3OH. The CH_3OH was removed *in vacuo* and this was repeated until all the excess TFA had been removed to give the trifluoroacetate salt of the product in a quantitative yield (228 mg). ^{1}H NMR (500 MHz, CD_3OD) δ (ppm): 9.13 (br. s, 2H pyridine Ar*H*), 8.67 (t, ^4J = 1.9 Hz, 1H, pyridine Ar*H*), 8.00 (br. s, 1H, CON*H*), 3.56 (t, ^3J = 6.7 Hz, 2H, CH_2), 3.52 (t, ^3J = 6.9 Hz, 2H, CH_2), 3.45 (t, ^3J = 6.6 Hz, 2H, CH_2), 3.06 (t, ^3J = 7.5 Hz, 2H, CH_2), 2.02 (quintet, ^3J = 7.2 Hz, 2H, CH_2), 1.92 (quintet, ^3J = 6.7 Hz, 2H, CH_2). ^{13}C NMR (125 MHz, CD_3OD) δ (ppm): 167.7, 167.2, 164.9 (quartet, ^1J = 34.7 Hz, *C*F_3), 162.9, 151.5, 151.4, 135.9, 131.8, 131.4, 50.2, 38.6, 38.4, 37.7, 29.7, 28.8. HRMS (ESI +ve) *m/z*: 306.1662 ($[M+H]^+$, $C_{13}H_{20}N_7O_2$ requires 306.1673).

3,5-bisamide pyridine–isophthalamide precursor 39

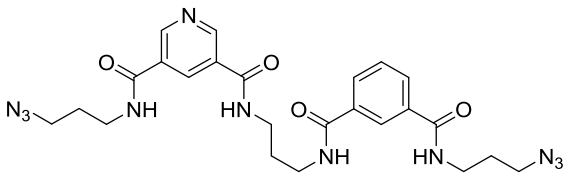

To a suspension of acid **33** (64 mg, 0.257 mmol) in CH_2Cl_2 (10 mL) was added EDC·HCl (59 mg, 0.308 mmol), HOBt (47 mg, 0.308 mmol) and DMAP (cat. ~1 mg). This was stirred for 2 hrs under N_2 until the solution became homogeneous. To this was added dry triethylamine (0.18 mL, 1.29 mmol) and a solution of amine **38·CF_3CO_2** (140 mg, 0.344 mmol) in DMF (3 mL). The reaction mixture was stirred for 4 days under N_2 and then the solvent removed *in vacuo*. The solution was washed with 10% citric acid (2 × 5 mL) and $NaHCO_{3(aq)}$ (2 × 5 mL). The organic layer was dried with $MgSO_4$ and the solvent removed *in vacuo.* The product was purified using silica gel chromatography (96:4 CH_2Cl_2/CH_3OH) to afford **39** as a white solid (52 mg, 38%).^{1}H NMR (500 MHz, 1:1 $CDCl_3$/CD_3OD) δ (ppm): 9.14 (br. s, 1H, pyridine Ar*H*), 9.11 (br. s, 1H, pyridine Ar*H*), 8.67 (t, ^4J = 2.0 Hz, 1H, pyridine Ar*H*), 8.28 (t, ^4J = 1.7 Hz, 1H, Ar*H*), 7.98 (m, 2H, Ar*H*), 7.55 (t, ^3J = 7.7 Hz, 1H, Ar*H*), 3.52 (m, 8H, N*H*), 3.43 (m, 4H, CH_2), 1.92 (m, 6H, CH_2). ^{13}C NMR (125 MHz, 1:1 $CDCl_3$/CD_3OD) δ (ppm): 169.6,169.5, 167.1, 167.0, 151.5, 151.4, 136.1, 135.9, 131.6, 131.4, 130.2, 127.2, 50.4, 50.3, 38.8, 38.7, 38.5, 38.4, 30.2, 29.9, 29.8, three peaks missing, presumed overlapped. HRMS (ESI +ve) *m/z*: 558.2287, ($[M+Na]^+$, $C_{24}H_{29}N_{11}O_4Na$ requires 558.2296).

Terphenyl-stoppered alkyne 41[4]

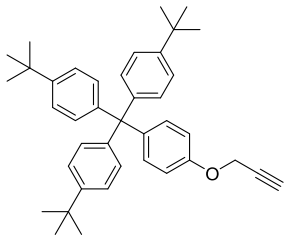

Compound **40**[4] (2.50 g, 4.95 mmol) and propargyl bromide (80% solution in toluene, 0.80 mL, 7.43 mmol) were dissolved in DMF (40 mL). K_2CO_3 (411 mg, 2.97 mmol) was then added to the solution before heating at 80°C for 18 hrs under N_2. The reaction mixture was allowed to cool to rt, filtered and concentrated. H_2O (10 mL) was added and the resulting solution extracted with EtOAc (3 × 20 mL). The combined organic fractions were dried over $MgSO_4$, filtered, and the solvent removed *in vacuo* to give the crude product as a pale brown residue. This was suspended in boiling CH_3CN (150 mL), and hot $CHCl_3$ (15 mL) added to dissolve the solid. The solution was concentrated to ~100 mL and cooled. The resulting precipitate was filtered, washed with cold CH_3CN and dried to afford the product (1.38 g, 51%). ^{1}H NMR (300 MHz, $CDCl_3$) δ (ppm): 7.25–7.18 (m, 6H, Ar*H*), 7.15–7.05 (m, 8H, Ar*H*), 6.89–6.80 (m, 2H, Ar*H*), 4.62 (s, 2H, C*H*$_2$), 2.3 (s, 1H, C≡C*H*), 1.31 (s, 27H, C*H*$_3$). MS (ESI +ve) *m/z* 565.39 ($[M+Na]^+$, $C_{40}H_{46}NaO$ requires 565.34).

Rotaxane 42·NO_3

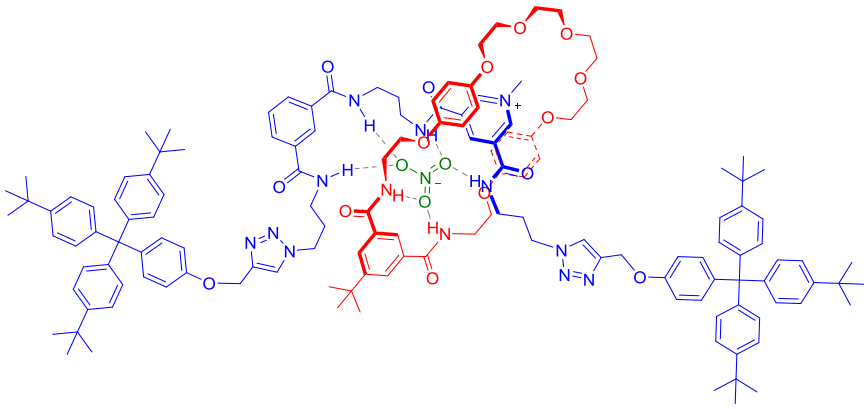

A solution of **32·NO_3** (26 mg, 0.043 mmol) and macrocycle **19** (25 mg, 0.038 mmol) was stirred for 30 mins under N_2 in dry 4:1 CH_2Cl_2/acetone (2 mL). A solution of stopper alkyne **4**[4] (46 mg, 0.085 mmol) in dry 4:1 CH_2Cl_2/acetone (0.5 mL) was prepared. Half of this solution, $Cu(CH_3CN)_4PF_6$ (4.8 mg, 0.0155 mmol) and TBTA (5.2 mg, 0.0155 mmol) was added to reaction mixture and allowed to stir for a further 30 mins. The remaining stopper alkyne **4** solution was added and the reaction mixture stirred under N_2 for 3 days. The reaction was then washed with 0.1 M $ETDA_{(aq)}$ solution (3 mL), H_2O (3 mL) and the organic layer dried over $MgSO_4$. The solvent was removed *in vacuo*. Size exclusion chromatography ($CHCl_3$) was used to remove any remaining macrocycle followed by silica gel chromatography (97:3 CH_2Cl_2/CH_3OH). A final preparative thin layer chromatography (acetone) was used to afford rotaxane **42·NO_3** as a yellow solid (22 mg, 24%). ^{1}H NMR (500 MHz, $CDCl_3$) δ (ppm): 9.53 (br. s, 1H, pyridinium Ar*H*), 9.08 (br. s, 1H, isophthalamide macrocycle Ar*H*), 8.84 (br. s, 2H, pyridinium Ar*H*), 8.76 (br. s, 1H, CON*H*), 8.63 (br. s, 1H, CON*H*), 8.50 (br. s, 1H, CON*H*), 8.39 (br. s, 1H, CON*H*), 8.31 (s, 2H, isophthalamide macrocycle Ar*H*), 8.22 (br. s, 1H, isophthalamide Ar*H*), 8.12 (m, 2H, isophthalamide Ar*H*), 7.82 (s, 1H, triazole C*H*), 7.80 (s, 1H, triazole C*H*), 7.51 (t, 1H, ^3J = 7.7 Hz, isophthalamide Ar*H*), 7.23 (m, 12H, stopper Ar*H*), 7.09 (m, 4H, stopper Ar*H*), 7.07 (m, 12H, stopper Ar*H*), 6.87 (d, ^3J = 8.8 Hz, 2H, stopper Ar*H*), 6.82 (d, ^3J = 9.0 Hz, 2H, stopper Ar*H*), 6.37 (d, ^3J =

8.7 Hz, 4H, hydroquinone Ar*H*), 6.10 (d, ^{3}J = 7.7 Hz, 4H, hydroquinone Ar*H*), 5.19 (s, 2H, CH_2-C triazole), 5.11 (s, 2H, CH_2-C triazole), 4.66 (s, 3H, $N^{+}CH_3$), 4.52 (br. m, 2H, CH_2-N triazole), 4.45 (br. m, 2H, CH_2-N triazole) 4.09 (br. m, 2H, CH_2NH macrocycle), 4.01 (br. m, 2H, CH_2NH macrocycle), 3.82–3.64 (br. m, 20H, CH_2O macrocycle), 3.63–2.97 (br. m, 8H, CH_2NH), 2.04–1.41 (br. m, 6H, CH_2). ^{13}C NMR (125 MHz, $CDCl_3$) δ (ppm): 167.1, 166.9, 166.2, 160.1, 159.4, 156.2, 153.6, 153.0, 151.8, 148.3, 144.7, 144.4, 144.2, 144.0, 140.2, 140.1, 132.3, 132.3, 130.7, 129.2, 129.1, 124.0, 123.4, 122.9, 121.5, 114.7, 114.3, 113.2, 70.6, 70.6, 70.0, 68.4, 65.2, 63.0, 62.0, 61.8, 58.4, 50.9, 49.9, 48.3, 47.9, 41.1, 37.6, 37.4, 37.2, 37.1, 36.9, 35.1, 34.4, 34.3, 31.0, 30.3, 30.0, 29.7, 29.5, 29.3, thirteen peaks missing, presumed overlapped due to apparent symmetry.

Rotaxane 42·PF_6: Anion exchange to the hexafluorophosphate salt was achieved by passing **42·NO_3** down a hexafluorophosphate loaded Amberlite® column (9:1 acetone/H_2O). The solvent was removed *in vacuo* to afford **42·PF_6** in quantitative yield. ^{1}H NMR (500 MHz, 1:1 $CDCl_3$/CD_3OD) δ (ppm): 8.98 (s, 1H, pyridinium Ar*H*), 8.93 (s, 1H, pyridinium Ar*H*), 8.82 (s, 1H, pyridinium Ar*H*), 8.42 (app s, 1H, isophthalamide macrocycle Ar*H*), 8.32 (t, ^{4}J = 1.4 Hz, 1H, isophthalamide Ar*H*), 8.12 (d, ^{4}J = 1.6 Hz, 2H isophthalamide macrocycle Ar*H*), 7.97 (s, 1H, C*H* triazole), 7.96 (m, 2H, isophthalamide Ar*H*), 7.94 (s, 1H, C*H* triazole), 7.53 (t, ^{3}J = 7.9 Hz, 1H, isophthalamide Ar*H*), 7.22 (m, 12H, stopper Ar*H*), 7.11–7.07 (m, 4H, stopper Ar*H*), 7.06 (m, 12H, stopper Ar*H*), 6.85 (d, ^{3}J = 9.1 Hz, 2H, stopper Ar*H*), 6.82 (d, ^{3}J = 9.1 Hz, 2H, stopper Ar*H*), 6.47 (d, ^{3}J = 9.0 Hz, 4H, hydroquinone Ar*H*), 6.25 (d, ^{3}J = 9.1 Hz, 4H, hydroquinone Ar*H*), 5.14 (s, 2H, CH_2-C triazole), 5.09 (s, 2H, CH_2-C triazole), 4.50 (s, 3H, $N^{+}CH_3$), 4.49 (t, ^{3}J = 7.0 Hz, 2H, CH_2-N triazole), 4.30 (t, ^{3}J = 7.0 Hz, 2H, CH_2-N triazole), 4.14 – 4.02 (m, 4H, CH_2NH macrocycle), 3.81 – 3.65 (m, 20H, CH_2O macrocycle), 3.49–3.34 (m, 8H, CH_2NH), 2.25 (quintet, ^{3}J = 6.5 Hz, 2H, CH_2CH_2NH), 2.12 (quintet, ^{3}J = 6.5 Hz, 2H, CH_2CH_2NH), 1.86 (quintet, ^{3}J = 6.5 Hz, 2H, CH_2CH_2NH). ^{13}C NMR

(125 MHz, 1:1 $CDCl_3/CD_3OD$) δ (ppm): 169.9, 169.4, 169.4, 161.9, 161.7, 157.4, 157.5, 157.5, 154.5, 154.2, 153.4, 149.7, 145.5, 141.7, 135.9, 135.5, 133.6, 132.0, 131.7, 130.2, 129.7, 127.3, 125.4, 125.2, 123.7, 116.2, 116.1, 114.5, 72.0, 71.9, 71.4, 69.4, 67.4, 64.4, 62.7, 62.7, 41.6, 39.1, 38.7, 38.5, 38.4, 36.4, 35.5, 33.2, 32.4, 32.1, 31.3, 30.9, 30.6, twenty peaks missing, presumed overlapped due to apparent symmetry. ^{19}F NMR (282.5 MHz, 1:1 $CDCl_3/CD_3OD$) δ (ppm): −73.2 (d, ^1J = 710 Hz, PF_6^-). HRMS (ESI +ve) m/z: 2286.2915 ($[M-NO_3]^+$, $C_{141}H_{170}N_{13}O_{15}$ requires 2286.2966).

Macrocycle precursor 43·NO_3

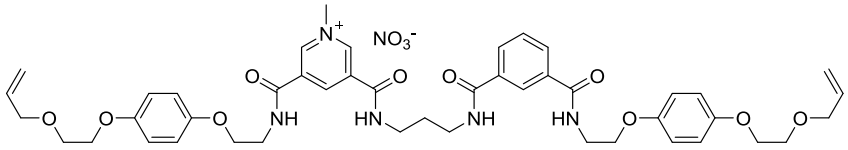

Methyl-iodide (2 mL) was added to a solution of **51** (70 mg, 0.086 mmol) in DMF (2 mL) and stirred under N_2 for 16 hrs. The solvent was removed *in vacuo* to give compound **43**$^+$ as the iodide salt. Ion exchange to the nitrate salt was achieved passing down a nitrate loaded Amberlite® column in 9:1 acteone/water. The solvent was subsequently removed *in vacuo* to give **43·NO_3** (71 mg, 92%). ^1H NMR (500 MHz, 1:1 $CDCl_3/CD_3OD$) δ (ppm): 9.17 (app. s, 3H, Ar*H*), 8.38 (s, 1H, N*H*), 8.10 (s, 1H, N*H*), 7.85 (m, 3H, Ar*H*), 7.40 (t, ^3J = 7.0 Hz, 1H, Ar*H*), 6.72 (m, 8H, hydroquinone Ar*H*), 5.83 (m, 2H, *H*C=CH_2), 5.23–5.10 (m, 4H, HC=CH_2), 4.34 (s, 3H, CH_3), 3.98 (m, 12H, CH_2), 3.69 (m, 8H, CH_2), 3.39 (m, 4H, CH_2), 1.80 (app. t, ^3J = 6.1 Hz, 2H, CH_2). ^{13}C NMR (101 MHz, $CDCl_3$) δ (ppm): 168.5, 168.3, 161.9, 161.8, 161.7, 161.7, 153.8, 153.7, 153.5, 153.3, 146.8, 146.7, 141.9, 135.2, 135.1, 135.0, 134.8, 130.9, 130.8, 129.5, 126.0, 118.0, 116.2, 116.1, 72.8, 69.1, 68.6, 68.5, 67.5, 67.0, 40.8, 40.2, 38.2, 7 peaks missing, presumed overlapped due to apparent symmetry. HRMS (ESI +ve) *m/z*: 824.3848 ($[M-NO_3]^+$, $C_{45}H_{54}N_5O_{10}$ requires 824.3865).

Vinyl-appended methyl-benzoate 45

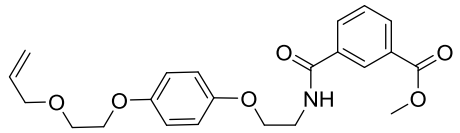

To a suspension of **24** (320 mg, 1.77 mmol) in CH_2Cl_2 (20 mL) was added EDC·HCl (372 mg, 1.95 mmol), HOBt (50 mg, 0.327 mmol) and DMAP (cat. ~1 mg). This was stirred for 1 hr under N_2 until the solution became homogeneous. To this was added dry triethylamine (0.26 mL, 1.95 mmol) and a solution of amine **44**[5] (420 mg, 1.77 mmol). The reaction mixture was stirred for 2 days under N_2, and then washed with 10% citric acid (2 × 5 mL) and $NaHCO_{3(aq)}$ (2 × 5 mL). The organic layer was dried over $MgSO_4$ and the solvent removed *in vacuo*. The product was purified using silica gel column chromatography (75:20:5 CH_2Cl_2/acetone/CH_3OH) to afford a white solid (450 mg, 60%). ^{1}H NMR (400 MHz, $CDCl_3$) δ (ppm): 8.40 (s, 1H, Ar*H*), 8.14 (d, ^3J = 8.6 Hz, 1H, Ar*H*), 8.02 (t, ^3J = 8.6 Hz, 1H, Ar*H*), 7.49 (t, ^3J = 8.6 Hz, 1H, Ar*H*), 6.84 (m, 4H, hydroquinone Ar*H*), 5.93 (m, 1H, *H*C=CH_2), 5.31–5.18 (m, 2H, HC=CH_2), 4.07 (m, 6H, CH_2), 3.91 (s, 3H, CH_3), 3.84 (m, 2H, CH_2), 3.76 (m, 2H, CH_2).^{13}C NMR (101 MHz, $CDCl_3$) δ (ppm):166.8, 166.4, 153.4, 152.8, 134.6, 132.5, 131.9, 130.5, 128.9, 127.8, 117.3, 115.7, 115.5, 72.4, 68.6, 68.1, 67.3, 52.4, 39.8. HRMS (ESI +ve) *m/z*: 422.1578 ($[M+Na]^+$, $C_{22}H_{25}NO_6Na$ requires 422.1574).

Vinyl-appended methyl nicotinate 46

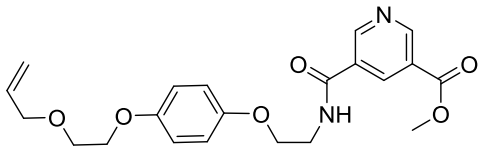

To a suspension of acid **5**[10] (300 mg, 1.66 mmol) in CH_2Cl_2 (20 mL) was added EDC·HCl (348 mg, 1.82 mmol), HOBt (50 mg, 0.327 mmol) and DMAP (cat. ~1 mg). This was stirred for 1 hr under N_2 until the solution became homogeneous. To this was added dry triethylamine (0.25 mL, 1.82 mmol) and a solution of amine (390 mg, 1.66 mmol). The reaction mixture was stirred for 2 days under N_2 and washed then with 10% citric acid (2 × 5 mL) and $NaHCO_{3(aq)}$ (2 × 5 mL). The organic layer was dried over $MgSO_4$ and the solvent removed *in vacuo*. The product was purified using silica gel column chromatography (75:20:5 CH_2Cl_2/acetone/CH_3OH) to afford a white solid (290 mg, 45%). ^{1}H NMR (400 MHz, $CDCl_3$) δ (ppm): 9.26 (d, ^3J = 2.2 Hz, 1H, pyridine Ar*H*), 9.19 (d, ^3J = 2.2 Hz, 1H, pyridine Ar*H*), 8.65 (t, ^3J = 2.2 Hz, 1H, pyridine Ar*H*), 6.80 (m, 4H, hydroquinone Ar*H*), 5.96 (m, 1H, *H*C=CH_2), 5.30–5.22 (m, 2H, HC=CH_2), 4.10–4.04 (m, 6H, CH_2), 3.94 (s, 3H, CH_3), 3.85 (q, ^3J = 4.8 Hz, 2H, CH_2), 3.75 (t, ^3J = 4.8 Hz, 2H, CH_2). ^{13}C NMR (101 MHz, $CDCl_3$) δ (ppm): 165.0, 165.0, 153.4, 152.9, 152.7 152.1, 135.8, 134.6, 129.9, 125.8, 117.3, 115.7, 72.4, 68.6, 68.0, 67.1, 52.6, 39.9. HRMS (ESI +ve) *m/z*: 423.1530 ($[M+Na]^+$, $C_{21}H_{24}N_2O_6Na$ requires 423.1527).

Vinyl-appended benzoic acid 47

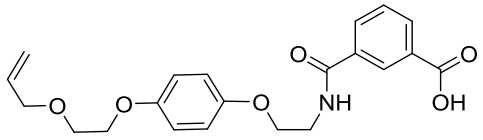

Ester **45** (450 mg, 1.13 mmol) was dissolved with KOH (95 mg, 1.70 mmol) in CH_3OH (15 mL). The reaction mixture was stirred under N_2 for 16 hrs. The solvent removed *in vacuo*

and re-dissolved in H_2O (50 mL) and washed with CH_2Cl_2 (2 × 10 mL). The aqueous layer was neutralised with 10% citric acid and the resulting precipitate was collected by vacuum filtration and washed with H_2O (10 mL), CH_2Cl_2 (10 mL) and dried to give a white solid. (380 mg, 87%). ^{1}H NMR (500 MHz, d_6-DMSO) δ (ppm): 8.89 (t, ^3J = 5.5, 1H, Ar*H*), 8.45 (s, 1H, Ar*H*), 8.09 (d, ^3J = 7.9 Hz, 2H, Ar*H*), 7.60 (t, ^3J = 7.9 Hz, 1H, Ar*H*), 6.87 (m, 4H, hydroquinone Ar*H*), 5.89 (m, 1H, *H*C=CH$_2$), 5.31–5.19 (m, 2H, HC=C*H*$_2$), 4.08 (m, 6H, C*H*$_2$), 3.66 (m, 4H, C*H*$_2$). ^{13}C NMR (101 MHz, $CDCl_3$) δ (ppm): 167.4, 166.3, 153.1, 153.0, 135.7, 135.1, 132.4, 132.0, 131.7, 129.3, 128.6, 117.0, 115.9, 71.6, 68.7, 68.0, 66.9. HRMS (ESI +ve) *m/z*: 408.1415 ([M+Na]$^+$, $C_{21}H_{23}NO_6Na$ requires 408.1418).

Vinyl-appended nicotinic acid 48

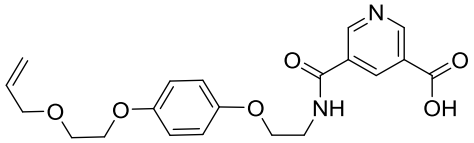

Ester **46** (180 mg, 0.45 mmol) was dissolved with KOH (40 mg, 0.68 mmol) in CH_3OH (10 mL). The reaction mixture was stirred under N_2 for 16 hrs. The solvent removed *in vacuo* and re-dissolved in H_2O (50 mL) and washed with CH_2Cl_2 (2 × 10 mL). The aqueous layer was neutralised with 10% citric acid and the resulting precipitate was collected by vacuum filtration and washed with H_2O (10 mL), CH_2Cl_2 (10 mL) and dried to give a white solid (150 mg, 85%). ^{1}H NMR (500 MHz, d_6-DMSO) δ (ppm): 13.54 (br. s, 1H, COO*H*), 9.21 (s, 1H, pyridine Ar*H*), 9.18 (s, 1H, pyridine Ar*H*), 9.11 (s, 1H, N*H*), 8.70 (s, 1H, pyridine Ar*H*), 6.89 (m, 4H, hydroquinone Ar*H*), 5.90 (m, 1H, *H*C=CH$_2$), 5.30–5.14 (m, 2H, HC=C*H*$_2$), 4.08 (t, ^3J = 5.7 Hz 2H, C*H*$_2$), 4.01 (m, 4H, C*H*$_2$), 3.67 (m, 4H, C*H*$_2$). ^{13}C NMR (101 MHz, $CDCl_3$) δ (ppm): 166.4, 164.7, 153.1, 153.0, 152.8, 152.5, 136.0, 135.7, 130.0, 117.0, 116.0, 115.8, 71.6, 68.7, 67.9, 66.8. HRMS (ESI −ve) *m/z*: 385.1416 [M−H]$^-$, $C_{20}H_{21}N_2O_6$ requires 385.1405).

Boc-protected amine 49

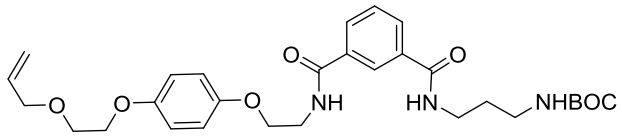

To a suspension of acid **47** (370 mg, 0.96 mmol) in CH_2Cl_2 (20 mL) was added EDC·HCl (200 mg, 1.06 mmol) and DMAP (cat. ~1 mg). This was stirred for 1 hr under N_2 until the solution became homogeneous. To this was added dry triethylamine (0.26 mL, 1.95 mmol) and a solution of **27**[15] (170 mg, 0.96 mmol). The reaction mixture was stirred for 2 days under N_2 and washed with $NaHCO_3$ (2 × 5 mL). The organic layer was dried over $MgSO_4$ and the solvent removed *in vacuo*. The product was purified using silica gel column chromatography (75:20:5 CH_2Cl_2/acetone/CH_3OH) to afford an off-white oil (230 mg, 45%). ^{1}H NMR (400 MHz, $CDCl_3$) δ (ppm): 8.26 (s, 1H, Ar*H*), 7.96 (d, ^3J = 8.3 Hz, 2H, Ar*H*), 7.53 (br. s, 1H, N*H*), 7.48 (t, ^3J = 8.3 Hz, 1H, Ar*H*), 7.05 (br. s, 1H, N*H*), 6.82 (m, 4H, hydroquinone Ar*H*), 5.93 (m, 1H, *H*C=CH_2), 5.30–5.20 (m, 2H, HC=CH_2), 4.07 (m, 6H, CH_2), 3.81 (t, ^3J = 5.0 Hz, 2H, CH_2), 3.76 (t, ^3J = 5.0 Hz, 2H, CH_2), 3.47 (q, ^3J = 5.9 Hz, 2H, CH_2), 3.20 (br. s, 2H, NH_2), 1.68 (quintet, ^3J = 5.9 Hz, 2H, CH_2), 1.43 (s, 3H, CH_3). ^{13}C NMR (101 MHz, $CDCl_3$) δ (ppm): 167.0, 166.8, 157.0, 153.3, 152.8, 134.8, 134.5, 130.4, 130.1, 129.0, 125.3, 117.4, 115.7, 115.5, 79.7, 72.4, 68.6, 68.1, 67.2, 39.8, 30.0, 28.4. HRMS (ESI +ve) *m/z*: 564.2686 ($[M+Na]^+$, $C_{29}H_{39}N_3O_7Na$ requires 564.2680).

Amine 50·CF_3CO_2

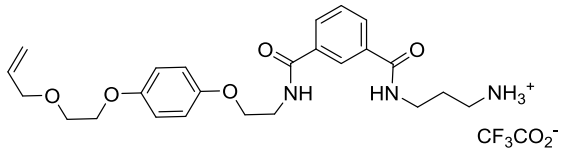

To a solution of **49** (130 mg, 0.24 mmol) in CH_2Cl_2 (5 mL) at 0 °C was added trifluoroacetic acid (1 mL) drop-wise. The reaction mixture was allowed to warm to room temperature and stirred under N_2. The reaction was monitored using thin layer chromatography (9:1 CH_2Cl_2/CH_3OH) until all the amine had been deprotected. The solvent was removed *in vacuo* and re-dissolved in CH_3OH which was again removed *in vacuo*. This was repeated until all the excess TFA had been removed to give the trifluoroacetate salt of the product (136 mg, 99%). ^{1}H NMR (400 MHz, 1:1 $CDCl_3$/CD_3OD) δ (ppm): 8.21 (s, 1H, Ar*H*), 7.92 (d, ^3J = 8.5 Hz, 2H, Ar*H*), 7.46 (t, ^3J = 8.5 Hz, 1H, Ar*H*), 6.78 (m, 4H, hydroquinone Ar*H*), 5.85 (m, 1H, *H*C=CH_2), 5.26–5.12 (m, 2H, HC=CH_2), 4.01 (m, 6H, CH_2), 3.71 (t, ^3J = 7.2 Hz, 2H, CH_2), 3.43 (t, ^3J = 7.2 Hz, 2H, CH_2), 1.89 (quintet, ^3J = 7.2 Hz, 2H, CH_2). ^{13}C NMR (101 MHz, $CDCl_3$) δ (ppm): 168.7, 167.7, 153.2, 153.0, 134.4, 134.3, 133.7, 130.7, 130.5, 129.0, 125.6, 117.5, 72.3, 68.6, 68.0, 67.0, 39.7, 36.7, 36.2, 27.1. HRMS (ESI +ve) *m/z*: 442.2335 ([M−CF_3CO_2]$^+$, $C_{24}H_{32}N_3O_5$ requires 442.2336).

3,5-bisamide pyridine–isophthalamide precursor 51

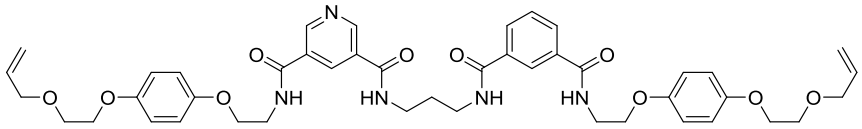

To a suspension of **48** (95 mg, 0.246 mmol) in CH_2Cl_2 (10 mL) was added EDC·HCl (52 mg, 0.271 mmol), HOBt (25 mg, 0.160 mmol) and DMAP (cat. ~1 mg). This was stirred for 1 hr under N_2 until the solution became homogeneous. To this was added dry triethylamine (0.1 mL, 0.780 mmol) and a solution of **50·CF_3CO_2** (136 mg, 0.246 mmol) in dry DMF (3 mL). The reaction mixture was stirred for 7 days under N_2 and washed with 10% citric acid, before

the solvent was removed *in vacuo*. The product was purified using silica gel column chromatography (75:20:5 CH_2Cl_2/acetone/CH_3OH) to afford a white solid (70 mg, 35%). ^{1}H NMR (500 MHz, 1:1 $CDCl_3$/CD_3OD) δ (ppm): 9.05 (br. s, 1H, Ar*H*), 8.57 (s, 1H, Ar*H*), 8.21 (s, 1H, Ar*H*), 7.91 (t, ^3J = 7.6 Hz, 2H, Ar*H*), 7.46 (m, 2H, Ar*H*), 6.77 (m, 8H, hydroquinone Ar*H*), 5.82 (m, 2H, *H*C=CH_2), 5.24-5.11 (m, 4H, HC=CH_2), 4.02 (m, 12H, CH_2), 3.71 (m, 8H, CH_2), 3.43 (q, ^3J = 6.4 Hz, 4H, CH_2), 1.84 (quintet, ^3J = 6.4 Hz, 2H, CH_2). ^{13}C NMR (125 MHz, $CDCl_3$) δ (ppm): 168.7, 166.4, 153.8, 153.6, 151.2, 151.0, 135.1, 135.0, 134.8, 131.0, 130.9, 129.5, 126.3, 118.0, 116.3, 116.0, 72.9, 69.1, 68.6, 67.6, 67.4, 40.5, 40.3, 37.6, 30.2, 29.4, 14 peaks missing, presumed overlapped due to apparent symmetry. HRMS (ESI +ve) *m/z*: 832.3524 ($[M + Na]^+$, $C_{44}H_{51}N_5O_{10}Na$ requires 832.3528).

Catenane 52·NO_3

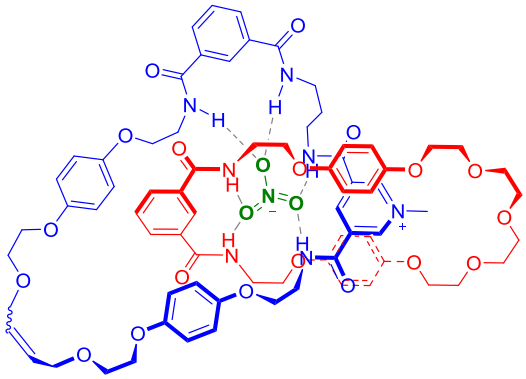

43·NO_3 (26 mg, 0.029 mmol) and macrocycle **17** (26 mg, 0.044 mmol) were dissolved in CH_2Cl_2 (3 mL) under N_2. Grubbs' 2nd generation catalyst (3 mg) was added and the reaction stirred for 48 hrs. The solvent was removed *in vacuo*, and the crude purified by preparative thin layer chromatography (95:5 CH_2Cl_2/CH_3OH) to afford catenane **52·NO_3** (7.5 mg, 20%). ^{1}H NMR (500 MHz, 1:1 $CDCl_3$/CD_3OD) δ (ppm): 9.22 (s, 1H, pyridinium Ar*H*), 9.16 (s, 1H, pyridinium Ar*H*), 9.10 (s, 1H, pyridinium Ar*H*), 9.00 (s, 1H, isophthalamide Ar*H*), 8.79 (s, 1H, N*H*), 8.16 (s, 1H, N*H*), 8.49 (s, 1H, isophthalamide Ar*H*), 8.05 (m, 2H, isophthalamide Ar*H*), 8.17 (d, ^3J = 7.9 Hz, 1H, isophthalamide Ar*H*), 8.12 (d, ^3J = 7.9 Hz, 1H, isophthalamide

Ar*H*), 7.67 (m, 2H, isophthalamide Ar*H*), 7.04 (d, ^{3}J = 9.0 Hz, 2H, hydroquinone Ar*H*), 7.00 (d, ^{3}J = 9.0 Hz, 2H, hydroquinone Ar*H*), 6.95 (d, ^{3}J = 9.0 Hz, 2H, hydroquinone Ar*H*), 6.91 (d, ^{3}J = 9.0 Hz, 2H, hydroquinone Ar*H*), 6.55 (d, ^{3}J = 9.0 Hz, 4H, hydroquinone Ar*H*), 6.32 (d, ^{3}J = 9.0 Hz, 4H, hydroquinone Ar*H*), 5.97 (s, 2H, *H*C=C*H*), 4.71 (s, 3H, CH_3), 4.40 (br. m, 2H, CH_2), 4.33 (br. m, 2H, CH_2), 4.28 (br. m, 2H, CH_2), 4.20 (br. m, 4H, CH_2), 4.20 (m, 2H, CH_2), 4.05–3.73 (br. m, 28H, CH_2), 1.88 (quintet, ^{3}J = 6.6 Hz, 2H, CH_2). ^{13}C NMR (125 MHz, 1:1 $CDCl_3$/CD_3OD) 168.3, 168.0, 161.1, 161.1, 160.3, 160.2, 153.9, 153.5, 153.5, 153.3, 152.4, 145.8, 145.4, 134.8, 134.7, 133.9, 133.5, 133.3, 132.3, 131.6, 131.4, 129.9, 129.8, 129.6, 125.3, 124.9, 116.4, 116.2, 115.9, 115.8, 115.2, 114.9, 71.5, 71.4, 71.1, 70.5, 68.9, 68.9, 68.7, 68.6, 67.5, 67.1, 65.6, 58.1, 50.1, 41.4, 40.8, 40.5, 38.2, 37.9, 32.4, 4 peaks missing presumed overlapped due to apparent symmetry. HRMS (ESI +ve) *m/z*: 706.8010 ($[M-NO_3+Na]^{2+}$, $C_{75}H_{88}N_7O_{10}Na$ requires 706.8011).

Catenane 52·PF$_6$: Anion exchange to the hexafluorophosphate salt was achieved by washing a solution of **52·NO$_3$** (7.5 mg, 0.005 mmol) in 10 mL CH_2Cl_2 with 8 × 10 mL of a 0.1 M solution of aqueous ammonium hexafluorophosphate, followed by 2 × 10 mL H_2O. The organic layer was dried over $MgSO_4$, filtered and the solvent removed *in vacuo* to afford **52·PF$_6$** in quantitative yield (8 mg). ^{1}H NMR (500 MHz, 1:1 $CDCl_3$/CD_3OD) δ (ppm): 9.11 (s, 1H, pyridinium Ar*H*), 9.00 (s, 1H, pyridinium Ar*H*), 8.98 (s, 1H, pyridinium Ar*H*), 8.74 (s, 1H, N*H*), 8.60 (s, 1H, isophthalamide Ar*H*), 8.53 (s, 1H, N*H*), 8.46 (s, 1H, isophthalamide Ar*H*), 8.12 (m, 4H, isophthalamide Ar*H*), 7.67 (m, 2H, isophthalamide Ar*H*), 6.99 (app s 4H, hydroquinone Ar*H*), 6.92 (m, 4H, hydroquinone Ar*H*), 6.95 (d, ^{3}J = 9.0 Hz, 2H, hydroquinone Ar*H*), 6.91 (d, ^{3}J = 9.0 Hz, 2H, hydroquinone Ar*H*), 6.59 (d, ^{3}J = 9.0 Hz, 4H, hydroquinone Ar*H*), 6.39 (d, ^{3}J = 9.0 Hz, 4H, hydroquinone Ar*H*), 5.95 (s, 2H, *H*C=C*H*), 4.55 (s, 3H, CH_3), 4.26–4.04 (br. m, 14H, CH_2), 4.26–4.04 (br. m, 40H, CH_2), 1.93 (quintet, ^{3}J = 6.6 Hz, 2H, CH_2).

5.3 Synthesis of novel compounds from Chapter 3

6^{A}-azido-permethylated-β-cyclodextrin 55[16]

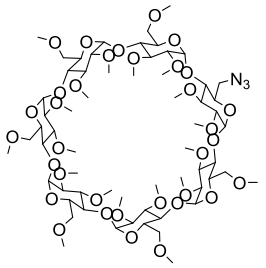

6^{A}-hydroxy-permethylated-β-cyclodextrin **57** (0.60 g, 0.424 mmol) was dissolved in THF (10 mL) and triethylamine (0.1 mL) added. The reaction was cooled to 0 °C and mesyl chloride (150 mg, 1.27 mmol) was added. After 3 hrs the solvent was removed under vacuum, and the residue dissolved in water (10 mL). The product was extracted into $CHCl_3$ (3 × 25 mL), dried over $MgSO_4$ and the solvent removed *in vacuo* to yield the corresponding mesylate **60**. The product was immediately dissolved in DMF (30 mL) and sodium azide (0.33 g, 15.2 mmol) added, and the solution stirred at 40 °C for 16 hrs. The reaction mixture was poured into water (30 mL), extracted with $CHCl_3$ (3 × 50 mL), dried over $MgSO_4$ and the solvent removed *in vacuo* to yield the product as a white solid (0.44 g, 88%). R_f = 0.70 (10:1 $CHCl_3$/CH_3OH). ^{1}H NMR (500 MHz, CD_3OD) δ (ppm): 5.17 (m, 7H), 4.00–3.75 (m, 14H), 3.70–3.10 (m, 88H). MS (ESI +ve): *m/z*: 1462.7 ($[M+Na]^+$, $C_{62}H_{109}O_{34}N_3Na$ requires 1462.7).

6^{A}-amino-permethylated-β-cyclodextrin 56[16]

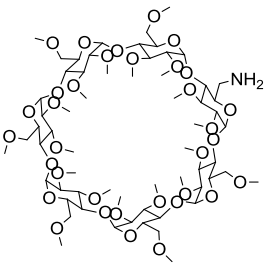

This known compound[16] was prepared through a novel reduction procedure: To a solution of 6^{A}-azido-permethylated-β-cyclodextrin[17] **55** (120 mg, 0.083 mmol) in CH_3OH (2 mL) was

added a suspension of Pd/C (10 wt%, 20 mg) in H_2O (1 mL), followed by hydrazine monohydrate (25 μL, 0.416 mmol). The reaction mixture was refluxed for 1 hrs, before cooling to rt. The catalysts were filtered off by passing through celite and the solvents removed *in vacuo.* The residue was dissolved in CH_2Cl_2 (10 mL) and washed with H_2O (2 × 2 mL), dried over $MgSO_4$, filtered and the solvents removed *in vacuo* to afford the product as a white solid (118 mg, 97%). R_f = 0.2 (10:1 $CHCl_3$/CH_3OH). ^{1}H NMR (300 MHz, $CDCl_3$) δ (ppm): 5.15 (7H, m, *β*-CD H_1), 4.00–3.70 (14H, m), 3.65–3.10 (88H, m). MS (ESI +ve): *m/z*: 1414.6 ($[M+H]^+$, $C_{62}H_{112}O_{34}$ requires 1414.5).

6^A-hydroxy-permethylated-*β*-cyclodextrin 57

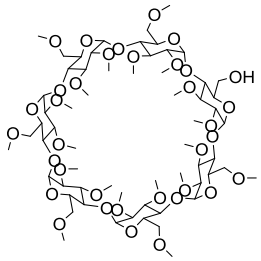

This known compound was prepared according to two methods, adapted from literature procedures: **Method 1**:[18] *β*-Cyclodextrin (4.54 g, 4.0 mmol) (dried for 2 weeks under vacuum) and imidazole (1.22 g, 18.0 mmol) were dissolved in dry DMF (200 mL) under nitrogen. *Tert*-butyldimethylsilyl chloride (2.85 mL, 50% in toluene, 8.2 mmol) was added and stirred for 16 hrs. The solution was cooled to 0 ^{o}C and sodium hydride (10.6 g, 60% dispersion in mineral oil, 260 mmol) was added portion-wise over 5 minutes. The mixture was allowed to warm to room temperature and stirred for 3 hrs. The reaction was cooled to 0 ^{o}C and 30 mL CH_3I added portion wise over 4 hrs and allowed to warm to rt. The reaction was stirred for 48 hrs, before quenching methanol (10 mL) at 0 ^{o}C, and poured into 400 mL of iced water. The solution was extracted into $CHCl_3$ (4 × 100 mL), the combined organic extracts were washed with aqueous sodium thiosulfate solution (100 mL, 3% w/v) and water (2 × 100 mL), and dried over $MgSO_4$. The solvent was removed *in vacuo* to yield the crude

silyl ether as a yellow oil. The residue was dissolved in methanol (300 mL) and ammonium fluoride (2.15 g, 58.1 mmol) added, and stirred at reflux for 30 hrs. The solvent was removed *in vacuo* and the residue re-dissolved in ethyl acetate (200 mL), filtered to remove the ammonium salts and the solvent removed to yield a yellow solid. Purification by silica gel chromatography (99:1 $CHCl_3/CH_3OH$) gave the product (1.40 g, 20%). (TLC 10:1 $CHCl_3/CH_3OH$ $R_f = 0.52$, permethylated cyclodextrin by-product at 0.7).

Method 2:[19] Permethylated-*β*-cyclodextrin **58** (6.93 g, 4.85 mmol) was dissolved in toluene (200 mL), to which was added diisobutylammonium hydride (25 wt% in toluene, 7.27 mL, 7.27 mmol) and heated at 50 ºC for 4 hrs. The reaction mixture was then cooled to 0 ºC, before 1M $HCl_{(aq)}$ (2 mL) was added and the mixture stirred vigorously for 15 min. The reaction mixture was filtered through celite, which was washed thoroughly with CH_2Cl_2 (2 × 100 mL). The combined organics were washed with brine (2 × 50 mL), dried over $MgSO_4$, filtered and the solvents removed *in vacuo.* Purification by silica gel chromatography (99:1 $CHCl_3/CH_3OH$) gave the product **57** (1.40 g, 20%) and diol **59** (3.00 g, 43%). ^{1}H NMR (300 MHz, D_2O) δ (ppm): 5.17 (m, 7H, *β*-CD H_1), 3.80–3.70 (m, 14H), 3.70–3.10 (m, 88H). MS (ESI +ve): *m/z*: 1437.7 ($[M+Na]^+$, $C_{62}H_{110}O_{35}Na$ requires 1437.7).

Bis-amide pyridine axle precursor 61

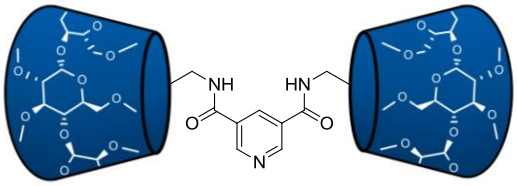

To a solution of 3,5-pyridine dicarboxylic acid (30 mg, 0.18 mmol), EDC·HCl (67 mg, 0.59 mmol), DMAP (cat.) and 1-hydroxy-benzotriazole (60 mg, 0.36 mmol) in CH_2Cl_2 (30 mL) was added a solution of 6^A-amino-permethylated-*β*-cyclodextrin **56** (510 mg, 0.36 mmol) and NEt_3 (0.1 mL) and stirred at rt for 72 hrs. Purification by silica gel

chromatography ($CHCl_3/CH_3OH$ 97:3) gave **61** as a white solid (385 mg, 70%). ^{1}H NMR (500 MHz, CD_3OD) δ (ppm): 9.16 (d, ^4J = 2.1 Hz, 2H, pyridine Ar*H*), 8.68 (t, ^4J = 2.1 Hz, 1H, pyridine Ar*H*), 5.36–5.15 (m, 14H, *β*-CD H_1), 4.05–3.11 (m, 206H, *β*-CD $H_{2–6}$, CH_3O). ^{13}C NMR (125 MHz, CD_3OD) δ (ppm): (167.0; amide *C*), (151.6, 136.0, 131.9; pyridine *C*). *β*-CD signals consistent with loss of C_7 symmetry: (99.7–99.2; *β*-CD C_1), 83.7–82.7, 81.1–79.4, 72.9–72.2, 61.9–61.5, 59.8–58.9. HRMS (ESI +ve) *m/z*: 1502.6870 ($[M+2Na]^{2+}$, $C_{131}H_{223}N_3Na_2O_{70}$ requires 1502.6900).

Bis-amide pyridinium axle precursor 62·Cl

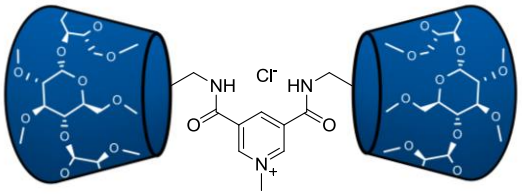

Pyridine axle **61** (135 mg, 0.046 mmol) was dissolved in CH_3I (5 mL) and stirred at 35 ˚C for 4 hrs, after which the volatiles were removed under vacuum. Anion exchange to the chloride salt was achieved by passing through an Amberlite® (chloride) column. The solvent was removed *in vacuo* and the product dried under high vacuum to yield **62·Cl** as the chloride salt (117 mg, 90%). To exchange to the nitrate salt, **62·Cl** (20 mg, 0.007 mmol) was passed down a nitrate loaded Amberlite® column, and the solvents removed *in vacuo*, quantitatively yielding **62·NO_3**. ^{1}H NMR (500 MHz, CD_3OD) δ (ppm): 9.52 (d, ^4J = 1.3 Hz, 2H, pyridinium Ar*H*), 9.32 (t, ^4J = 1.3 Hz, 1H, pyridinium Ar*H*), 7.97 (s, 2H, N*H*), 5.45–5.10 (m, 14H, *β*-CD H_1), 4.58 (s, 3H, N^+-CH_3), 4.05–3.10 (m, 206H, *β*-CD $H_{2–6}$, CH_3O). ^{13}C NMR (125 MHz, CD_3OD) δ (ppm): (163.2, amide *C*), (148.2, 143.0, 135.8; pyridinium *C*), *β*-CD signals consistent with loss of C_7 symmetry: (99.7–98.7; *β*-CD C_1), 84.0–82.0, 81.1–78.9, 73.2–72.0, (71.4, N^+-*C*), 61.9–61.6, 60.0–58.7. HRMS (ESI +ve) *m/z*: 1498.7098 ($[M–Cl+Na]^{2+}$, $C_{132}H_{226}N_3NaO_{70}$ requires 1498.7069).

Rotaxane 63·Cl

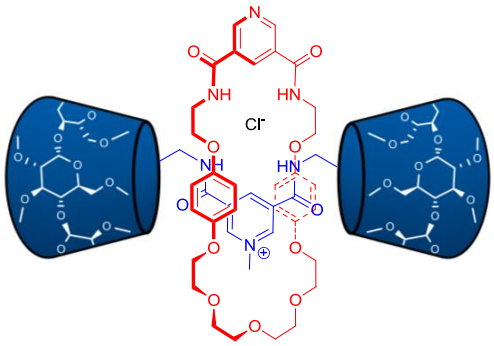

62·Cl (90 mg, 0.029 mmol) and bis-amine **16**[12] (138 mg, 0.290 mmol) were dissolved in dry CH_2Cl_2 (70 mL) and stirred for 30 min at 0°C under a N_2 atmosphere. NEt_3 (0.1 mL, 0.820 mmol) was then added followed immediately by a drop-wise addition of 3,5-bis-chlorocarbonyl pyridine (59 mg, 0.290 mmol) dissolved in dry CH_2Cl_2 (5 mL). The reaction was allowed to reach rt and was then stirred for 3 hrs. The solvent was removed *in vacuo*, and purified first by silica gel prep TLC (9:1 CH_2Cl_2/CH_3OH), and then size-exclusion chromatography to remove the free macrocycle by-product, to yield the mono-cationic rotaxane **63·Cl** as the chloride salt (28 mg, 33%). ^{1}H NMR (500 MHz, CD_3OD) δ (ppm): 9.58 (s, 2H, overlapped pyridinium and pyridine Ar*H*), 9.32 (d, ^4J = 1.9 Hz, 2H, pyridine Ar*H*), 9.11 (app. s, 2H, pyridinium Ar*H*), 6.64 (d, ^3J = 8.9 Hz, 4H, hydroquinone Ar*H*), 6.34 (d, ^3J = 8.9 Hz, 4H, hydroquinone Ar*H*), 5.40–5.03 (m, 14H, *β*-CD H_1), 4.53 (s, 3H, N^+-CH_3, 4.27–2.83 (m, 228H, *β*-CD H_{2-6}, CH_3O, polyether CH_2). ^{13}C NMR (125 MHz, CD_3OD) δ (ppm): (166.5, 162.3; amide *C*), (154.5, 153.7, hydroquinone *C*), (152.4, 147.3, 136.3, 134.6, 132.4, 131.0, 129.9; pyridinium and pyridine *C*), (116.3, 116.0; hydroquinone *C*), *β*-CD signals consistent with loss of C_7 symmetry: (99.7–98.4; *β*-CD C_1), 84.0–79.3, (77.8; N^+-*C*), 73.4–67.3, 62.2–58.5. HRMS (ESI +ve) *m/z*: 1796.3348 ($[M–Cl+Na]^{2+}$, $C_{163}H_{263}N_6NaO_{79}$ requires 1796.3333).

Rotaxane 65·$(NO_3)_2$

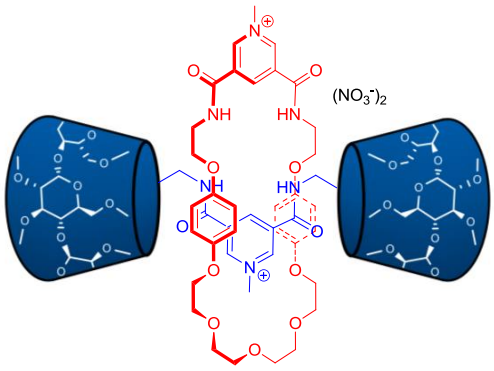

Dicationic rotaxane **65·$(NO_3)_2$** was prepared by dissolving rotaxane **63·Cl** (28 mg, 0.008 mmol) in 2 mL of neat CH_3I, and stirred at 35 ˚C for 4 hrs, after which the volatiles were removed under vacuum. Anion exchange to the nitrate salt was achieved by passing through an Amberlite® (nitrate) column. The solvent was removed *in vacuo* and the product dried under high vacuum to yield rotaxane **65·$(NO_3)_2$** as the nitrate salt (27 mg, 95%). ^{1}H NMR (500 MHz, CD_3OD) δ (ppm): 9.79 (s, 1H, macrocycle pyridinium Ar*H*), 9.61 (s, 2H, macrocycle pyridinium Ar*H*), 9.17 (s, 1H, axle pyridinium Ar*H*), 9.01 (s, 2H, axle pyridinium Ar*H*), 6.69 (d, ^3J = 8.5 Hz, 4H, hydroquinone Ar*H*), 6.41 (d, ^3J = 8.5 Hz, 4H, hydroquinone Ar*H*), 5.49–5.09 (m, 14H, *β*-CD H_1), 4.64 (s, 6H, N^+-CH_3, 4.25–3.06 (m, 228H, *β*-CD $H_{2–6}$, CH_3O, polyether CH_2). ^{13}C NMR (125 MHz, CD_3OD) δ (ppm): (163.0, 162.7; amide *C*), (154.4, 153.6; hydroquinone *C*), (148.8, 147.5, 135.7, 134.8, 132.4, 129.9; pyridinium *C*), (116.4, 116.1 hydroquinone *C*). *β*-CD signals consistent with loss of C_7 symmetry: (100.0–98.2; *β*-CD C_1), 84.6–79.1, 77.0 (N^+-*C*), 73.5–67.3, 62.2–58.4. HRMS (ESI +ve) *m/z*: 1803.8410 ($[M –2NO_3–H+Na]^{2+}$, $C_{163}H_{265}N_6NaO_{79}$ requires 1803.8428).

Bis-guanidinium biphenyl compound 68·$(NO_3)_2$

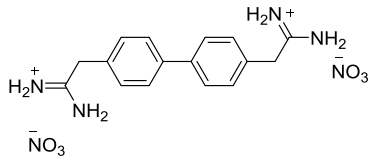

To a solution of 1,1'-biphenyl-4,4'-methylamine[8] (132 mg, 0.623 mmol) in DMF (1 mL) was added diisopropylethylamine and 1H-pyrazole-1-carboxamidine hydrochloride (184 mg, 1.24 mmol) and stirred at rt for 16 hrs. Diethyl ether (5 mL) was added to precipitate the product, which was collected and washed with diethyl ether (2 × 10 mL). Following recrystallization from methanol, the product was isolated as the chloride salt, which was subsequently converted to the nitrate salt by passing through a nitrate-loaded Amberlite® column to afford **68·$(NO_3)_2$** in 50% yield. ^{1}H NMR (500 MHz, 1:1 $CDCl_3$/CD_3OD) 7.55 (d, ^3J = 8.5 Hz, 4H, Ar*H*), 7.35 (d, ^3J = 8.5 Hz, 4H, Ar*H*), 3.90 (s, 4H, CH_2). ^{13}C NMR (125 MHz, CD_3OD) δ (ppm): 166.2, 163.2, 129.8, 117.9, 115.8. HRMS (ESI +ve) *m/z*: 297.1813 ($[M-2NO_3]^{2+}$, $C_{16}H_{21}N_6$ requires 297.1822).

Bis-iodotriazole pyridine 70

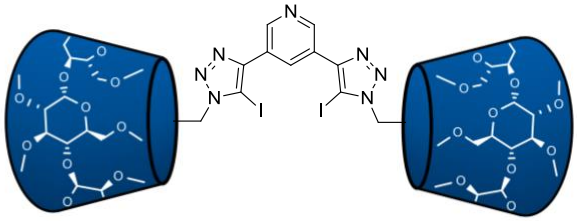

Bis-iodotriazole pyridine **70** was prepared using an adapted literature procedure for one-pot iodotriazole synthesis.[20] To a solution of 6^A-azido-permethylated-*β*-cyclodextrin **55** (50 mg, 0.035 mmol) in a 1:1 mixture of dry, degassed THF/CH_3CN was added sodium iodide (19 mg, 0.126 mmol), copper(II) perchlorate hexahydrate (23 mg, 0.063 mmol) and stirred for 5 minutes. TBTA (0.17 mg, 0.0003 mmol), 1,8-Diazabicyclo[5.4.0]undec-7-ene (DBU) (4.8 mg, 0.032 mmol, in 0.2 mL 1:1 THF/CH_3CN) and 3,5-diethynylpyridine **69**[6,11] (2.0 mg,

0.016 mmol) were then added and stirred under N_2 atmosphere for 3 days. The reaction mixture was diluted with CH_2Cl_2 (5 mL) and washed with 1 M $NH_4OH_{(aq)}$ (1 mL), brine (2 × 1 mL) and dried over $MgSO_4$. Purification by preparative silica gel thin-layer chromatography (9:1 EtOAc/CH_3OH) afforded **70** (34 mg, 65%). ^{1}H NMR (500 MHz, $CDCl_3$) δ (ppm): 9.16 (s, 2H, pyridine Ar*H*), 9.02 (s, 1H, pyridine Ar*H*), 5.38–4.84 (m, 14H, *β*-CD H_1), 4.37–3.12 (m, 206H, *β*-CD $H_{2–6}$, CH_3O). ^{13}C NMR (125 MHz, $CDCl_3$) δ (ppm): (146.4, 144.9; pyridine *C),* (125.9; iodotriazole *C*), *β*-CD signals consistent with loss of C_7 symmetry: (98.7–97.2; *β*-CD C_1), 83.0–78.4, 70.4–69.5, 60.9–60.4, 58.0–57.5, 50.6. HRMS (ESI +ve) *m/z*: 1652.5981 ($[M + 2Na]^{2+}$, $C_{133}H_{221}I_2N_7Na_2O_{68}$ requires 1652.5979).

Bis-prototriazole pyridine 71

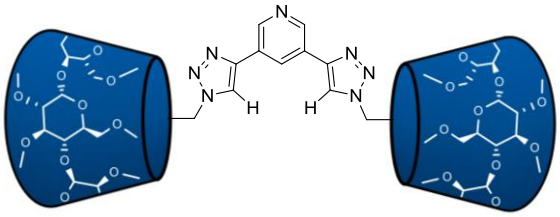

To a solution of 6^A-azido-permethylated-*β*-cyclodextrin **55** (100 mg, 0.071 mmol) and 3,5-diethynylpyridine **69**[6,11] (4.0 mg, 0.032 mmol) in dry CH_2Cl_2 (10 mL) was added $Cu(CH_3CN)_4PF_6$ (5.0 mg, 0.016 mmol), TBTA (9.0 mg, 0.016 mmol) and DIPEA (2.0 mg, 0.016 mmol) and stirred under an N_2 atmosphere for 2 days. The reaction mixture was washed with NH_4OH (1 mL), brine (2 × 1 mL) and dried over $MgSO_4$. Purification by preparative silica gel thin-layer chromatography (9:1 EtOAc/CH_3OH) gave **71** (50 mg, 52%). ^{1}H NMR (500 MHz, $CDCl_3$) δ (ppm): 8.95 (s, 2H, pyridine Ar*H*), 8.57 (s, 1H, pyridine Ar*H*), 8.00 (s, 2H, prototriazole *H*), 5.30–4.89 (m, 14H, *β*-CD H_1)), 4.07–2.98 (m, 206H, *β*-CD $H_{2–6}$, CH_3O). ^{13}C NMR (125 MHz, $CDCl_3$) δ (ppm): (144.6, 142.6; pyridine *C),* (126.2, 121.9 prototriazole C), *β*-CD signals consistent with loss of C_7 symmetry: (98.2–97.2; *β*-CD C_1), 81.5–77.8,

70.6–69.1, 60.8–60.4, 60.0–57.5, 50.6. HRMS (ESI +ve) *m/z*: 1526.2020 ($[M + 2Na]^{2+}$, $C_{133}H_{223}N_7Na_2O_{68}$ requires 1526.1996).

Bis-iodotriazole pyridinium 72·Cl

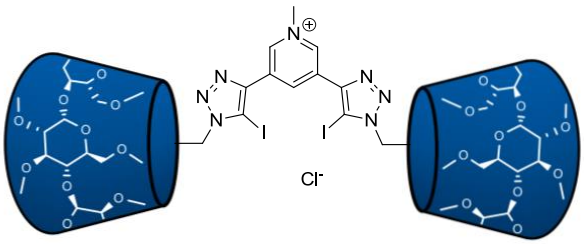

Bis-iodotriazole pyridine **70** (35 mg, 0.012 mmol) was dissolved in CH_3I (2 mL) and stirred at 35 ˚C for 4 hrs, after which the volatiles were removed under vacuum. Anion exchange to the chloride salt was achieved by passing through an Amberlite® (chloride) column. The solvent was removed *in vacuo* and the product dried under high vacuum to yield $\mathbf{72}^+$ as the chloride salt (38 mg, 98%). To exchange to the nitrate salt, **72·Cl** was passed down a nitrate loaded Amberlite® column, and the solvents removed *in vacuo* to afford $\mathbf{72{\cdot}NO_3}$ in a quantitative yield. ^{1}H NMR (500 MHz, $CDCl_3$) δ (ppm): 10.11 (s, 1H, pyridinium Ar*H*), 9.32 (s, 2H, pyridinium Ar*H*), 5.48 (app. s, 2H, *β*-CD H_1), 5.27 (app. s, 2H, *β*-CD H_1), 5.14–4.96 (m, 10H, *β*-CD H_1), 4.53 (s, 3H, N^+-CH_3), 4.37–3.10 (m, 206H, *β*-CD $H_{2–6}$, CH_3O). ^{13}C NMR (125 MHz, $CDCl_3$) δ (ppm): (140.6, 139.1; pyridinium *C),* (134.4, 133.9; iodotriazole *C*), *β*-CD signals consistent with loss of C_7 symmetry: (98.4–97.9; *β*-CD C_1), 82.9–79.4, 71.0–70.8, (70.5; N^+-*C*), 62.0–61.1, 59.9–58.1. HRMS (ESI +ve) *m/z*: 1648.6129 ($[M-Cl+Na]^{2+}$, $C_{134}H_{224}I_2N_7NaO_{68}$ requires 1648.6147).

Bis-prototriazole pyridinium 73·Cl

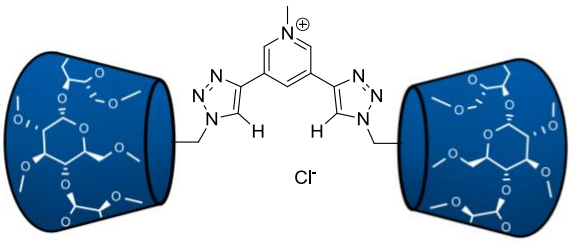

Bis-prototriazole pyridine **71** (50 mg, 0.017 mmol) was dissolved in 2 mL of CH_3I and stirred at 35 ˚C for 4 hrs. The CH_3I was removed under vacuum, the residue re-dissolved in 1:1 acetone/H_2O and passed through an Amberlite® (chloride) column. The solvent was removed *in vacuo* and the product dried under high vacuum to yield $\mathbf{73}^+$ as the chloride salt (50 mg, 99%). To exchange to the nitrate salt, **73·Cl** was passed down a nitrate loaded Amberlite® column three times, and the solvents removed *in vacuo* to afford **73·NO_3** in a quantitative yield. ^{1}H NMR (500 MHz, $CDCl_3$) δ (ppm): 9.75 (s, 2H, pyridinium Ar*H*), 9.36 (s, 1H, pyridinium Ar*H*), 8.96 (s, 2H, prototriazole *H*), 5.45–5.11 (m, 14H, *β*-CD H_1), 4.75 (s, 3H, N^+-CH_3), 4.13–3.02 (m, 206H, *β*-CD $H_{2–6}$, CH_3O). ^{13}C NMR (125 MHz, $CDCl_3$) δ (ppm): (138.7, 135.0, 131.8; pyridinium *C),* (126.1, 124.1; prototriazole *C*), *β*-CD signals consistent with loss of C_7 symmetry: (98.2–97.1; *β*-CD C_1), 81.0–77.5, 70.7–69.8, (68.6; N^+-*C*), 60.7–57.3. HRMS (ESI +ve) *m/z*: 1522.2143 ($[M-Cl+Na]^{2+}$, $C_{134}H_{226}N_7NaO_{68}$ requires 1522.2164).

Bis-iodotriazole rotaxane 74·Cl

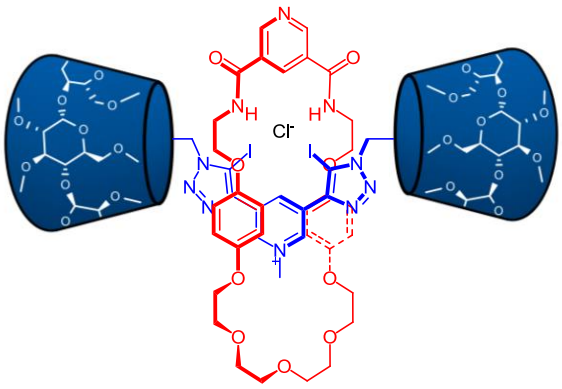

Bis-iodotriazole pyridinium **72·Cl** (46 mg, 0.014 mmol) and bis-amine **16**[12] (66 mg, 0.139 mmol) were dissolved in dry CH_2Cl_2 (40 mL) and stirred for 30 min at 0 °C under a N_2 atmosphere. NEt_3 (0.05 mL, 0.410 mmol) was then added followed immediately by a drop-wise addition of 3,5-bis-chlorocarbonyl pyridine (28 mg, 0.139 mmol) dissolved in dry CH_2Cl_2 (5 mL). The reaction was allowed to reach rt and was then stirred for 3 hrs. The solvent was removed *in vacuo*, and purified by preparative silica gel thin-layer chromatography (9:1 $CHCl_3/CH_3OH$), to yield the mono-cationic rotaxane **74·Cl** (20 mg, 37%). ^{1}H NMR (500 MHz, D_2O) δ (ppm): 9.41 (s, 1H, pyridine Ar*H*), 9.13 (s, 2H, pyridine Ar*H*), 9.10 (s, 2H, pyridinium Ar*H*), 8.26 (s, 1H, pyridinium Ar*H*), 6.34 (d, ^3J = 7.9 Hz, 4H, hydroquinone Ar*H*), 6.06 (br. app. s, 4H, hydroquinone Ar*H*), 5.34–4.90 (m, 14H, *β*-CD H_1), 4.56 (s, 3H, N^+-CH_3), 4.28 (app. s, 2H, *β*-CD H_6), 4.04 (app. s, 2H, *β*-CD H_6), 3.88–3.07 (m, 224H, *β*-CD H_{2-6}, CH_3O, polyether CH_2). ^{13}C NMR (125 MHz, D_2O) δ (ppm): (166.6; amide *C*), (157.0, 156.8, hydroquinone *C*), (152.4, 151.8, 151.6, 142.1, 141.6; pyridinium, pyridine, triazole *C*), (115.2, 114.4; hydroquinone *C*), *β*-CD signals consistent with loss of C_7 symmetry: (97.3–97.0; *β*-CD C_1), 81.9–81.0, (79.8; N^+-*C*), 71.4–67.5, 60.1–57.8. HRMS (ESI +ve) *m/z*: 1945.7426 ($[M–Cl+Na]^{2+}$, $C_{165}H_{261}I_2N_{10}NaO_{77}$ requires 1945.7396).

Bis-iodotriazole rotaxane 76·$(NO_3)_2$

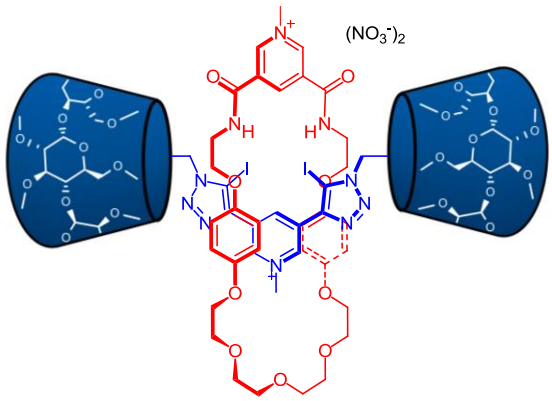

Dicationic rotaxane **76·$(NO_3)_2$** was prepared as the nitrate salt by dissolving **74·Cl** (20 mg, 0.005 mmol) in 2 mL of neat CH_3I, and stirred at 35 ˚C for 4 hrs, after which the volatiles were removed under vacuum. Anion exchange to the nitrate salt was achieved by passing through an Amberlite® (nitrate) column. The solvent was removed *in vacuo* and the product dried under high vacuum to yield rotaxane **76·$(NO_3)_2$** (20 mg, 96%). ^{1}H NMR (500 MHz, D_2O) δ (ppm): 9.70 (s, 1H, macrocycle pyridine Ar*H*), 9.45 (s, 2H, macrocycle pyridine Ar*H*), 9.24 (s, 2H, axle pyridinium Ar*H*), 8.47 (s, 1H, axle pyridinium Ar*H*), 6.33 (d, ^3J = 8.2 Hz, 4H, hydroquinone Ar*H*), 6.21 (d, ^3J = 8.2 Hz, 4H, hydroquinone Ar*H*), 5.44 (app. s, 2H, *β*-CD H_1), 5.22 (m, 4H, *β*-CD H_1), 5.16 (m, 2H, *β*-CD H_1), 5.08 (m, 2H, *β*-CD H_1), 4.87 (m, 2H, *β*-CD H_1), 4.56 (s, 3H, N^+-CH_3), 4.53 (s, 3H, N^+-CH_3), 4.30 (m, 2H, *β*-CD H_6), 4.01 (m, 2H, *β*-CD H_6), 3.86–3.09 (m, 224H, *β*-CD H_{2-6}, CH_3O, polyether CH_2). ^{13}C NMR (125 MHz, D_2O) δ (ppm): (163.0, amide *C*), (152.3, 152.0; hydroquinone *C*), (146.9, 142.4, 141.6, 141.6; pyridinium *C*), (134.6, 130.4 iodotriazole *C*), (114.9 hydroquinone *C*), *β*-CD signals consistent with loss of C_7 symmetry: (97.8–96.6; *β*-CD C_1), 81.6–76.6, 70.7–69.4, (67.5, 66.6 N^+-*C*), 60.5–59.9, 58.8–57.8. HRMS (ESI +ve) *m/z*: 1941.7617 ($[M–2NO_3]^{2+}$, $C_{166}H_{264}I_2N_{10}O_{77}$ requires 1941.7564).

Bis-prototriazole rotaxane 77·$(NO_3)_2$

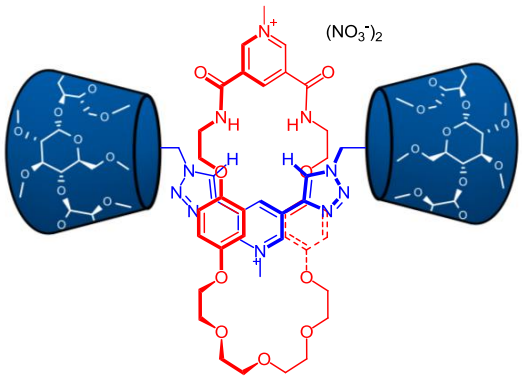

Bis-prototriazole pyridinium axle **73·Cl** (22 mg, 0.007 mmol) and bis-amine **16**[12] (51 mg, 0.110 mmol) were dissolved in dry CH_2Cl_2 (20 mL) and stirred for 30 min at 0 °C under a N_2 atmosphere. NEt_3 (0.025 mL, 0.200 mmol) was then added followed immediately by a drop-wise addition of 3,5-bis-chlorocarbonyl pyridine (18 mg, 0.109 mmol) dissolved in dry CH_2Cl_2 (2 mL). The reaction was allowed to reach rt and was stirred for 3 hrs. The solvent was then removed *in vacuo*, and initially purified by preparative silica gel thin-layer chromatography (9:1 EtOAc/CH_3OH), to yield a mixture of the mono-cationic rotaxane **75Cl·I** and macrocycle by-product which could not be separated at this stage. The mixture was then subjected to methylation conditions (dissolve in 2 mL CH_3I) and stirred at 35 ˚C for 4 hrs, after which the volatiles were removed under vacuum. Anion exchange to the nitrate salt was achieved by passing through an Amberlite® (nitrate) column. The solvent was removed *in vacuo* and the product dried under high vacuum to yield rotaxane **77$(NO_3)_2$** (7 mg, 25%). ^{1}H NMR (500 MHz, D_2O) δ (ppm): 9.59 (s, 1H, macrocycle pyridinium Ar*H*), 9.44 (s, 2H, macrocycle pyridinium Ar*H*), 8.79 (s, 2H, axle pyridinium Ar*H*), 8.57 (s, 2H, triazole *H*), 8.43 (s, 1H, axle pyridinium Ar*H*), 6.30 (d, ^3J = 8.3 Hz, 4H, hydroquinone Ar*H*), 6.17 (d, ^3J = 8.3 Hz, 4H, hydroquinone Ar*H*), 5.37 (m, 4H, *β*-CD H_1), 5.21 (m, 6H, *β*-CD H_1), 4.99 (m, 4H, *β*-CD H_1), 4.56 (s, 3H, N^+-CH_3), 4.33 (s, 3H, N^+-CH_3), 4.16 (m, 2H, *β*-CD H_6), 4.00 (m, 2H, *β*-CD H_6), 3.80–2.93 (m, 224H, *β*-CD H_{2-6}, CH_3O, polyether CH_2). ^{13}C NMR (125 MHz, D_2O) δ (ppm): (163.1, amide *C*), (152.3, 152.0; hydroquinone *C*), (147.5, 140.2,

140.1; pyridinium *C*), (134.6, 130.4 prototriazole *C*), (114.9, 114.5, hydroquinone *C*), *β*-CD signals consistent with loss of C_7 symmetry: (97.4–96.2; *β*-CD C_1), 82.2–79.7, 78.7–76.7, 70.9–69.4, (67.7, 66.4 N^+-*C*), 60.4–59.6, 58.8–57.7. HRMS (ESI +ve) *m/z*: 1815.8610 ([M–$2NO_3$]$^{2+}$, $C_{166}H_{266}N_{10}O_{77}$ requires 1815.8598).

5.4 Synthesis of novel compounds from Chapter 4

CBz-protected cyclen 78[21]

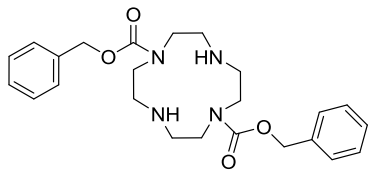

1,4,7,10-Tetraazacyclododecane (2.00g, 11.6 mmol) was dissolved in $CHCl_3$ (100 mL). Benzyl chloroformate (3.97 g, 23.2 mmol) was added drop-wise at 0 °C, before the reaction was allowed to warm to room temperature and stirred for 16 hrs. The solvent was removed *in vacuo,* before diethylether (100 mL) was added. The solid was collected by filtration, washed with diethylether (2 × 50 mL) and dried under vacuum to afford the product as the hydrochloride salt. NaOH (3 M, 100 mL) was added to the solid, and the aqueous phase was extracted with $CHCl_3$ (3 × 100 mL), dried over $MgSO_4$, filtered and the solvents removed *in vacuo* to afford **78** as a colourless oil (5.55 g, 98%). ^{1}H NMR (300 MHz, $CDCl_3$) δ (ppm): 7.35 (m, 6H, Ar*H*), 7.22 (m, 4H, Ar*H*), 5.20 (s, 4H, CH_2), 3.60–3.40 (m, 8H, CH_2), 3.05–2.70 (m, 8H, CH_2). MS (ESI +ve): *m/z*: 441.3 ($[M+H]^+$, $C_{22}H_{35}N_4O_4$ requires 441.2).

CBz-protected cyclen diester 79[22]

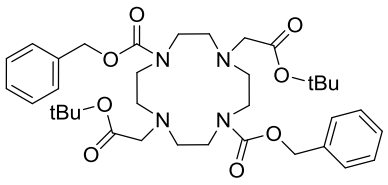

To a solution of **78** (5.19 g, 11.7 mmol) in CH_3CN (60 mL) was added *tert*-butyl bromoacetate (4.46 g, 23.2 mmol) and K_2CO_3 (4.40 g, 31.9 mmol). After refluxing overnight, the mixture was filtered through celite, and the solvents removed *in vacuo.* The residue was purified by silica gel chromatography (98:2 CH_2Cl_2/CH_3OH) to afford **79** as a colourless waxy solid (2.35 g, 45%). ^{1}H NMR (300 MHz, $CDCl_3$) δ (ppm): 7.37–7.20 (m, 10H, Ar*H*), 5.20 (s, 4H, CH_2), 3.45–3.20 (m, 12H, CH_2), 2.80 (br. s, 8H, CH_2), 1.44 (s, 18H, CH_3). MS (ESI +ve): *m/z*: 669.4 ($[M+H]^+$, $C_{36}H_{53}N_4O_4$ requires 669.4).

Cyclen diester 80[22]

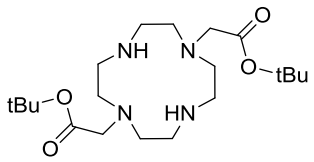

To a solution of **79** (2.35 g, 3.67 mmol) in CH_3OH (40 mL) was added 10% Pd/C (100 mg), and the mixture stirred under a hydrogen atmosphere (1 atm) for 16 hrs. Following filtration through celite, removal of the solvents *in vacuo* afforded **80** as a white solid (1.46 g, quant.). ^{1}H NMR (300 MHz, CD_3OD) δ (ppm): 3.45–3.30 (m, 8H, CH_2), 3.20–2.80 (br. s, 8H, CH_2), 1.44 (s, 18H, CH_3). MS (ESI +ve): *m/z*: 401.3 ($[M+H]^+$, $C_{20}H_{41}N_4O_4$ requires 401.3).

Macrocycle precursor 81

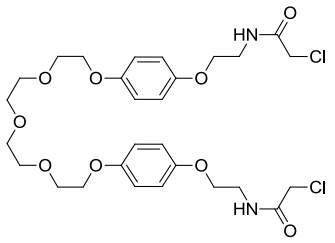

Bis-amine **16**[12] (2.00 g, 4.31 mmol) and NEt_3 (4 ml) were dissolved in dry CH_2Cl_2 (100 ml). A solution of 2-chloroacetylchloride (0.8 ml, 9.48 mmol) in dry CH_2Cl_2 (20 ml) was added drop-wise and the mixture was stirred for 6 hrs. The mixture was allowed to room temperature and washed with HCl 10% (3 × 30 ml) and then with $NaHCO_3$ (2 × 50 ml) and water (1 × 100 ml). The organic phase was dried over $MgSO_4$, filtered and the solvent removed. Finally the residue was recrystallized from diethyl ether to afford **81** (2.23 g, 84%). ^{1}H NMR (300 MHz, $CDCl_3$) δ (ppm): 6.97 (br. s, 2H, N*H*), 6.78 (d, ^3J = 9.0 Hz, 4H, Ar*H*), 6.74 (d, ^3J = 9.0 Hz, 4H, Ar*H*), 4.03–3.98 (8H, m), 3.94 (t, ^3J = 6.0 Hz, 4H, CH_2), 3.76 (t, ^3J = 6.0 Hz, 4H, CH_2), 3.64–3.62 (m, 12H, CH_2). ^{13}C NMR (75 MHz, $CDCl_3$) δ (ppm): 163.8, 145.2, 119.9, 71.4, 69.9, 68.3, 42.4, 37.2. HRMS (ESI +ve) *m/z*: 639.1839 ([M+Na]$^+$, $C_{28}H_{38}Cl_2N_2O_9Na$ requires 639.1847).

***Tert*-butyl ester macrocycle 82**

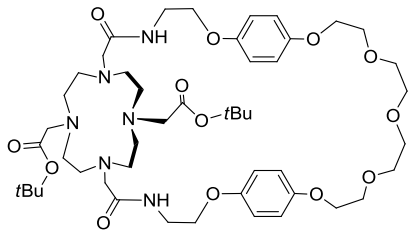

Bis-chloro compound **81** (500 mg, 1.24 mmol) was dissolved in dry CH_3CN (415 ml) and *trans*-substituted cyclen **80**[22] (767 mg, 1.24 mmol) and K_2CO_3 (2.40 g) were added, the mixture was heated at 70 ^{o}C for 3 days under N_2. The reaction mixture was then filtered, and the solvent was removed from the filtrate in *vacuo*. The solid residue was recrystallized from

diethyl ether and dried under vacuum to afford **82** as orange solid (0.82 g, 70%). ^{1}H NMR (300 MHz, $CDCl_3$) δ (ppm): 8.41 (br. s, 2H, N*H*), 6.83–6.74 (m, 8H, Ar*H*), 4.05–3.93 (m, 8H, CH_2), 3.83–3.80 (m, 4H, CH_2), 3.70–3.59 (m, 12H, CH_2), 3.19–2.51 (m, 24H, CH_2), 1.41 (s, 18H, CH_3); ^{13}C NMR (125 MHz, $CDCl_3$/CD_3OD) δ (ppm): 172.2, 170.3, 153.0, 152.8, 81.2, 70.8, 7.07, 69.8, 69.7, 68.2, 68.0, 66.8, 65.8, 64.3, 62.2, 59.4, 56.6, 54.3, 52.7, 39.7, 39.3, 39.0, 38.5, 28.2. HRMS (ESI +ve) *m/z*: 945.5579 ($[M+H]^+$, $C_{48}H_{77}N_6O_{13}$ requires 945.5543).

Free-base macrocycle 83

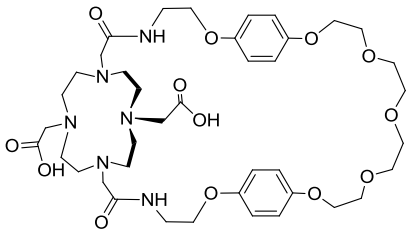

Macrocycle **82** (250 mg, 0.249 mmol) was dissolved in CH_2Cl_2 (5 mL) and trifluoroacetic acid (5 mL) was added drop-wise. This was left to stir at room temperature for 48 hours, after which all volatiles were evaporated under reduced pressure yielding an orange oil. Trituration with diethyl ether afforded macrocycle **83** (220 mg, quant.) ^{1}H NMR (300 MHz, CD_3OD) δ (ppm): 6.84–6.72 (m, 8H, Ar*H*), 4.05–3.95 (m, 12H, CH_2), 3.86–3.76 (m, 4H, CH_2), 3.69–3.64 (m, 16H, CH_2), 3.52–3.44 (m, 16H, CH_2). ^{13}C NMR (125 MHz, $CDCl_3$/CD_3OD) δ (ppm): 175.5, 174.5, 173.9, 172.3, 158.3, 158.0, 121.3, 118.9, 71.6, 71.5, 71.0, 69.5, 69.4, 69.3, 68.4, 68.1, 68.0, 67.7, 65.6, 62.6, 62.0, 55.9, 54.9, 54.0, 53.3, 52.6, 52.2, 50.6, 43.4, 41.7, 40.6, 40.3, 40.1, 39.6. HRMS (ESI +ve) *m/z*: 833.4308 ($[M + H]^+$, $C_{40}H_{61}N_6O_{13}$ requires 833.4291).

Lanthanide macrocycle complexes 84·OTf (Ln = Lu) and 85·OTf (Ln = Eu)

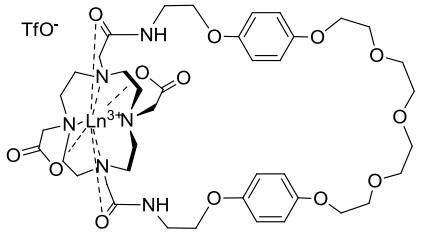

General procedure: Macrocycle **83** (1 equiv, 0.05 M) and the corresponding lanthanide triflate (1 equiv.) were dissolved in methanol (3 mL); the mixture was stirred for 48 hrs at 60 °C. The solvent was removed under reduced pressure and diethyl ether was added until a solid was obtained, affording the lanthanide complexes **84·OTf** and **85·OTf** in a quantitative yield. **Lu-macrocycle 84·OTf**: ^{1}H NMR (500 MHz, CD_3OD) δ (ppm): 6.86–6.80 (m, 8H, Ar*H*), 4.04–4.0 (m, 10H, CH_2), 3.82–3.78 (m, 8H, CH_2), 3.69–3.65 (m, 12H, CH_2), 3.49–3.40 (m, 10H, CH_2), 2.79–2.73 (m, 4H, CH_2), 2.57–2.38 (m, 4H, CH_2). ^{13}C NMR (125 MHz, CD_3OD δ (ppm): 177.9, 172.9, 154.9, 154.6, 154.5, 154.1, 154.0, 125.6, 123.1, 120.5, 71.7, 71.6, 70.9, 70.8, 69.4, 69.3, 69.2, 68.4, 67.4, 67.1, 66.9, 65.6, 62.1, 57.6, 57.2, 56.7, 56.3, 41.7, 41.5, 41.3, 41.0, 40.6. HRMS (ESI +ve) *m/z*: 1005.3453 ($[M-CF_3CO_2]^+$, $C_{40}H_{58}LuN_6O_{13}$ requires 1005.3464). **Eu-macrocycle 85·OTf**: ^{1}H NMR (500 MHz, CD_3OD) δ (ppm, excluding region between 0 and 10 ppm): 31.61, 30.81, −0.43, −0.93, −2.28, −4.07, −6.24, −8.03, −9.63, −14.38, −15.25, −18.9. HRMS (ESI +ve) *m/z*: 981.3260 ($[M-CF_3CO_2]^+$, $C_{40}H_{58}EuN_6O_{13}$ requires 981.3255).

Bis-bromo precursor 86

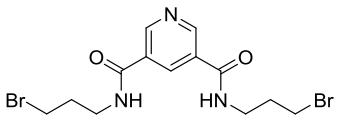

A solution of pyridine-3,5-dicarbonyl dichloride (2.30 g, 11.3 mmol) was dissolved in CH_2Cl_2 (40 mL). This was added drop-wise to a cooled suspension of bromopropylamine hydrobromide (4.94 g, 22.6 mmol) in CH_2Cl_2 (100 mL) and NEt_3 (9.4 mL, 60 mmol). The reaction mixture was left to stir for 2 hrs before washing with 10% $HCl_{(aq)}$ (2 × 50 mL) and the aqueous phase was neutralized with saturated $NaHCO_{3(aq)}$ to give a white precipitate, which was filtered and washed with H_2O (5 × 20 mL). The solid was then dried under high vacuum affording compound **86** as a pale yellow solid (2.29 g, 50%). ^{1}H NMR (300 MHz, d_6-DMSO) δ (ppm): 9.10 (d, ^4J = 3.7 Hz, 2H, Ar*H*), 8.87 (t, ^3J = 5.3 Hz, 2H, N*H*), 8.59 (t, ^4J = 2.1 Hz, 1H, Ar*H*), 3.60, (t, ^3J = 6.5 Hz, 4H, CH_2Br), 3.42, (m, 4H, CH_2), 2.09 (quint, ^3J = 6.6 Hz, 4H, CH_2); ^{13}C NMR (75 MHz, d_6-DMSO) δ (ppm): 164.5, 150.4, 134.0, 129.6, 37.9, 32.5, 32.1. HRMS (ESI +ve) *m/z*: 405.9754 ($[M+H]^+$, $C_{13}H_{18}N_3Br_2O_2$ requires 405.9760).

Bis-azide precursor 87

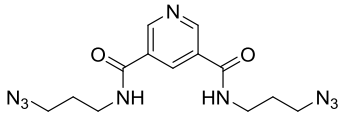

Compound **86** (1.00 g, 2.45 mmol) was dissolved in dry degassed DMF (50 mL) and sodium azide (0.48 g, 7.37 mmol) was added at rt before being left to stir for 24 hours at 80 ^{o}C under N_2. H_2O (50 ml) was then added and the product extracted into CH_2Cl_2 (6 × 20 mL). The organic layer was then dried over $MgSO_4$, filtered and the solvent removed in *vacuo*. The crude product was recrystallised from chloroform/hexane to afford **87** as an off-white solid (740 mg, 91%). ^{1}H NMR (300 MHz, $CDCl_3$) δ (ppm): 9.10 (s, 2H, Ar*H*), 8.50 (t, ^4J = 2.1 Hz,

1H, Ar*H*), 7.33 (t, ^{3}J = 5.9 Hz, 2H), 3.59 (m, 4H, CH_2), 3.47 (t, ^{3}J = 6.5 Hz, 4H, CH_2), 1.93 (quint, ^{3}J = 6.6 Hz, 4H, CH_2); ^{13}C NMR (75 MHz, $CDCl_3$) δ (ppm): 165.1, 150.5, 143.7, 133.6, 49.4, 38.0, 28.6. HRMS (ESI +ve) *m/z*: 332.1572 ($[M+H]^+$, $C_{13}H_{18}N_9O_2$ requires 332.1578).

Bis-azide *N*-oxide 88

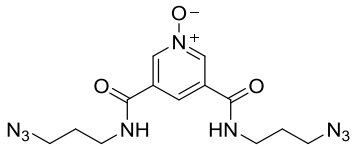

A saturated solution of Oxone® (2.22 g, 3.61 mmol) in H_2O (11 mL) was added drop-wise to a vigorously stirred mixture of **87** (0.40 g, 1.20 mmol) and $NaHCO_3$ (3.00 g, 3.61 mmol) in 1:1 H_2O/butanone at rt. After stirring for 2 hrs, NaCl (12.45 g, 222 mmol) was added prior to the product being extracted into $CHCl_3$ (3 × 50 mL). The organic phase was then dried over $MgSO_4$, filtered, and solvent removed *in vacuo* to give **88** as a yellow solid (0.38 g, 90%). ^{1}H NMR (300 MHz, $CDCl_3$) δ (ppm): 8.98 (s, 2H, Ar*H*), 8.37 (s, 1H, Ar*H*), 8.15 (t, ^{3}J = 5.3 Hz, 2H, N*H*), 3.70 (m, 4H, CH_2), 3.46 (t, ^{3}J = 6.5 Hz, 4H, CH_2), 1.95 (quint, ^{3}J = 6.6 Hz, 4H, CH_2). ^{13}C NMR (75 MHz, $CDCl_3$) δ (ppm): 162.4, 148.5, 140.3, 133.9, 49.1, 38.1, 28.4. HRMS (ESI +ve) *m/z:* 348.1523 $[M+H]^+$, $C_{13}H_{18}N_9O_3$ requires 348.1527).

Lanthanide *N*-oxide rotaxanes 89·OTf (Ln = Lu) and 90·OTf (Ln = Eu)

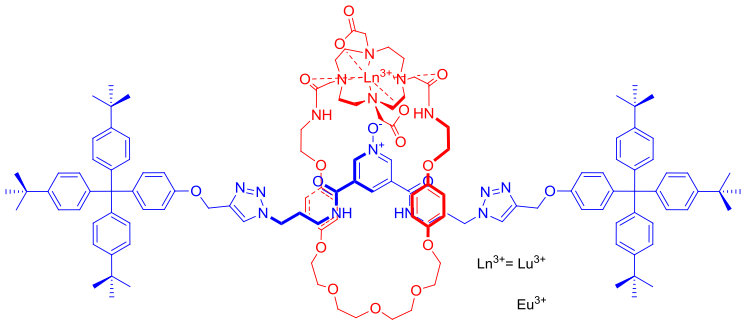

To a solution of the corresponding lanthanide macrocycle **84·OTf** or **85·OTf** (1 equiv. 0.3 M) in a dry mixture of 3:2 CH_2Cl_2/CH_3CN, *N*-oxide axle precursor **88** (1.2 equiv. 0.3 M) was then added. The reaction mixture was stirred for 30 min, followed by the addition of stopper alkyne **40**[4] (2.2 equiv.), $Cu(CH_3CN)_4PF_6$ (0.4 equiv.), TBTA (0.4 equiv.), and DIPEA (3 equiv.). The reaction was stirred for 3 days at RT under N_2. After this time the solvent was evaporated under reduced pressure, the crude was dissolved in CH_2Cl_2, and washed with aqueous EDTA (2 × 5 mL) and then with water (10 mL). The organic phase was dried over $MgSO_4$ and solvent removed in *vacuo*. The resulting solid wash purified by using size exclusion chromatography with chloroform to give the corresponding rotaxane in 20% yield. The synthesis was generally conducted on a scale of 10 mg of **88**.

Lu-rotaxane 89OTf: ^{1}H NMR (500 MHz, 1:1 $CDCl_3/CD_3OD$) δ (ppm): 8.85 (s, 2H, pyridine Ar*H*), 8.27 (s, 1H, pyridine Ar*H*), 7.59 (s, 2H, triazole *H*), 7.23–7.04 (m, 28H, stopper Ar*H*), 6.87–6.79 (m, 4H, stopper Ar*H*), 6.56 (d, ^3J = 10 Hz, 4H, hydroquinone Ar*H*), 6.31 (d, ^3J = 10 Hz, 4H, hydroquinone Ar*H*), 4.02–3.36 (m, 48H, C*H*$_2$), 2.80–2.17 (m, 16H, C*H*$_2$), 1.24 (s, 54H, C*H*$_3$). ^{13}C NMR (125 MHz, 1:1 $CDCl_3/CD_3OD$) δ (ppm): 157.5, 153.9, 153.8, 153.4, 149.8, 145.5, 133.7, 132.0, 125.4, 117.1, 117.0, 116.8, 116.1, 116.0, 114.5, 72.2, 72.2, 72.0, 71.9, 71.4, 71.1, 71.1, 69.5, 69.4, 69.0, 67.9, 67.7, 66.9, 66.6, 65.8, 65.1, 64.8, 64.5, 62.9, 57.8, 57.6, 56.9, 56.4, 56.3, 56.0, 35.6, 33.2, 31.0, 30.7. HRMS (ESI +ve) *m/z*: 1230.0967 ($[M+Na-CF_3SO_3^-]^{2+}$, $C_{133}H_{167}LuN_{15}O_{18}$ requires 1230.0954).

Eu-rotaxane 90·OTf: ^{1}H NMR (500 MHz, 1 :1 CD_2Cl_2/CD_3OD) δ (ppm, excluding region between 0 and 10 ppm): 34.95, 33.70, 32.74, 32.39, 30.27, 27.28, 20.72, 13.26, 12.52, −0.04, −3.04, −3.69, −4.35, −4.82, −5.79, −6.09, −7.24, −7.92, −9.39, −10.16, −12.36, −13.45, −14.00, −15.73, −17.00, −17.55, −18.20. HRMS (ESI +ve) *m/z*: 1219.0836 $[M+Na-CF_3SO_3]^{2+}$, $C_{133}H_{167}EuN_{15}O_{18}$ requires 1219.0859).

Nitrite template Ln-rotaxane 92·NO_2·OTf (Ln = Lu) and 93·NO_2·OTf (Ln = Eu)

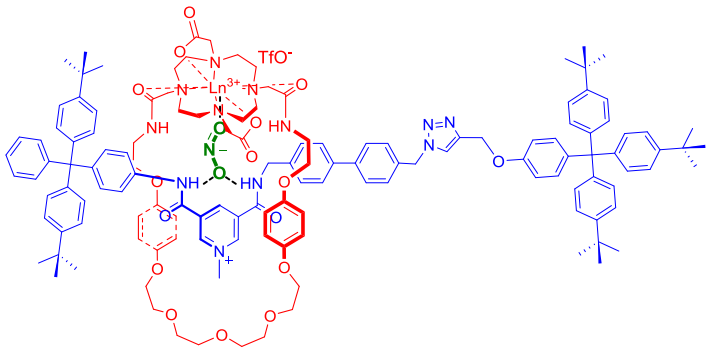

General procedure: To a solution of the corresponding macrocyclic lanthanide complex **84·OTf** or **85·OTf** (1.5 equiv. 0.024 M) in a 3:2 mixture of anhydrous CH_2Cl_2/CH_3CN compound **91·NO_2** (1.0 equiv.) was added. The reaction mixture was stirred for 30 min and then stopper alkyne **40**[4] (1 equiv.), $Cu(CH_3CN)_4PF_6$ (0.5 equiv.), TBTA (0.5 equiv.), and DIPEA (2 equiv.) were added. The reaction was stirred for 48 hrs at rt under N_2. After this time the solvent was evaporated under reduced pressure, the crude was dissolved in $CHCl_3$, and washed with aqueous EDTA (2 × 5 mL) and then with water (5 mL). The organic phase was dried over $MgSO_4$ and solvent removed in *vacuo*. The resulting solid was purified by using size exclusion chromatography with chloroform to afford the rotaxane product: (**92·NO_2·OTf** in 51% yield, **93·NO_2·OTf** in 45% yield). Eu-rotaxane **93·NO_2·OTf** was exchanged to the triflate salt by passing down a triflate-loaded Amberlite® column three times as a solution in 9:1 acetone/water to afford **93·$(OTf)_2$** in quantitative yield. The synthesis was generally conducted on a 10 mg of **91·NO_2** scale.

Lu-rotaxane 92·NO_2·OTf: ^{1}H NMR (500 MHz, d_6-DMSO, 353 K) δ (ppm): 11.76, 10.75, 10.49, 9.77, 9.58, 9.53, 9.45, 9.34, 9.21, 8.84, 8.68, 8.22, 7.67, 7.51, 7.40, 7.31, 7.21, 7.11, 7.06, 7.01, 6.91, 6.54, 6.46, 6.41, 5.62, 5.10, 4.50, 4.43, 4.19, 4.04, 3.81, 3.72, 3.59, 2.65, 2.60, 2.37, 1.32. HRMS (ESI +ve) *m/z:* 1189.5687, ($[M-NO_2-CF_3SO_3]^{2+}$ $C_{135}H_{159}LuN_{12}O_{16}$ requires 1189.5697).

Eu-rotaxane 93·NO_2·OTf: ^{1}H NMR (500 MHz, 1:1 $CDCl_3/CD_3OD$, 298 K) δ (ppm, excluding region between 0 and 10 ppm): 32.90, 30.68, −5.10, −8.26, −15.18, −16.00, −18.91, −20.22. HRMS (ESI +ve) *m/z:* 2355.1137, ($[M-NO_2-CF_3SO_3-H]^+$, $C_{135}H_{158}EuN_{12}O_{16}$ requires 2355.1145).

Terphenyl-stoppered rotaxane 94·NO_3·OTf

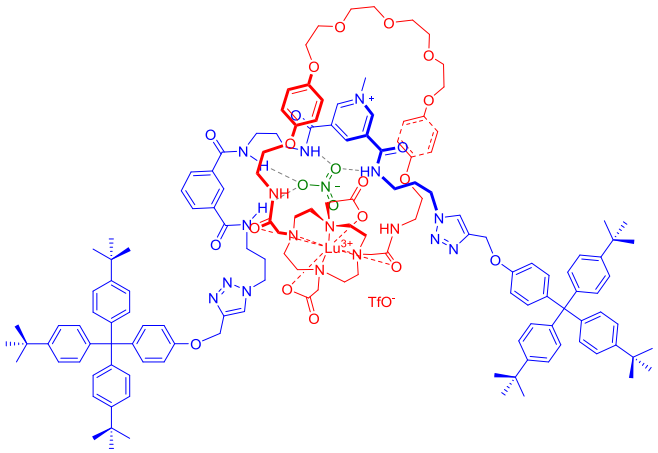

To a solution of Lu-macrocycle **84·OTf** (24 mg, 0.024 mmol) in anhydrous 3:2 CH_2Cl_2/CH_3CN solution was added axle precursor **36·NO_3** (10.0 mg, 0.016 mmol) and stirred for 30 min under N_2. Stopper alkyne **40**[4] (18.0 mg, 0.033 mmol), $Cu(CH_3CN)_4PF_6$ (2.6 mg, 0.008 mmol), TBTA (4.3 mg, 0.008 mmol), and DIPEA (1.2 mg, 0.008 mmol) were then added and the reaction stirred for 48 hrs. After this time the solvent was evaporated under reduced pressure, the crude was dissolved in $CHCl_3$, and washed with aqueous EDTA (2 × 5 mL) and then with water (5 mL). The organic phase was dried over $MgSO_4$ and solvent removed in *vacuo*. The resulting solid was purified by using size exclusion chromatography

with chloroform to afford the rotaxane product **94·NO_3·OTf** (10 mg, 22%). ^{1}H NMR (500 MHz, 1 :1 $CDCl_3$/CD_3OD) δ (ppm): 9.50, 9.46, 9.39, 9.22, 8.77, 8.43, 8.29, 8.09, 7.99, 7.96, 7.82, 7.65, 7.53, 7.38, 7.23, 7.07, 6.85, 6.29, 5.33, 5.15, 5.09, 4.26, 4.06, 3.83, 3.71, 3.65, 3.48, 3.19, 2.27, 2.03, 1.68, 1.62, 1.29, 0.88. MS (ESI +ve) 1320.73, ($[M-NO_3-CF_3SO_3]^{2+}$, $C_{145}H_{182}LuN_{17}O_{19}$ requires 1320.66).

6^A-propargyl-permethylated-*β*-cyclodextrin CD 95[23]

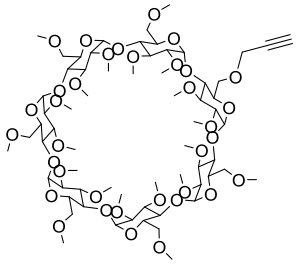

To a solution of 6^A-hydroxy-permethylated-*β*-cyclodextrin **56** (286 mg, 0.202 mmol) in DMF (10 mL) was added sodium hydride (60 wt% in mineral oil, 160 mg, 4.04 mmol) at 0 ºC and the solution stirred for 30 mins, before propargyl bromide (80% solution in toluene, 0.80 mL, 8.08 mmol) was added and the reaction allowed to stir for 48 hrs at rt under N_2. After this time the reaction was quenched with methanol (1 mL), before H_2O (10 mL) was added, and the solution washed with $CHCl_3$ (3 × 30 mL). The organics were dried over $MgSO_4$, filtered and the solvent removed *in vacuo.* Purification by silica gel chromatography (99:1 EtOAc/CH_3OH) afforded compound **95** (150 mg, 52%). ^{1}H NMR (300 MHz, $CDCl_3$) δ (ppm): 5.17 (m, 7H), 3.80–3.70 (m, 14H), 3.70–3.10 (m, 88H), 1.9 (s, 1H, C≡C*H*). MS (ESI +ve): *m/z*: 1476.8 ($[M+Na]^+$, $C_{65}H_{112}O_{35}Na$ requires 1476.7).

Cyclodextrin-stoppered Ln-rotaxanes 96·NO_3·OTf (Ln = Lu) and 97·NO_3·OTf (Ln = Eu)

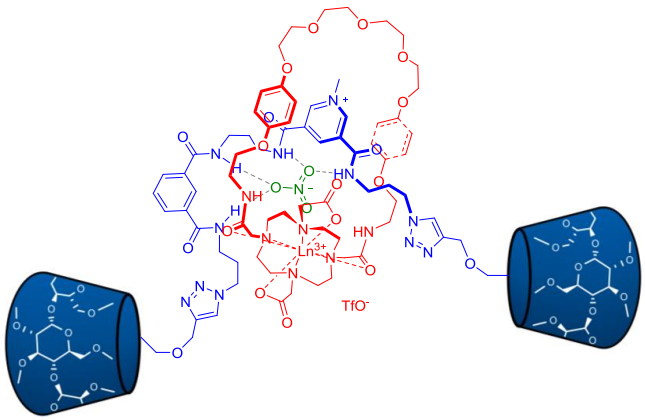

General procedure: To a solution of the corresponding macrocyclic lanthanide complex **84·OTf** or **85·OTf** (1.5 equiv, 0.024 M) in a 3:2 mixture of anhydrous CH_2Cl_2/CH_3CN, bis-azide axle precursor **36·NO_3** (1.0 equiv.) was added. The reaction mixture was stirred for 30 min and then stopper propargyl-functionalised CD **95**[23] (2 equiv.), $Cu(CH_3CN)_4PF_6$ (0.5 equiv.), TBTA (0.5 equiv.), and DIPEA (2 equiv.) were added. The reaction was stirred for 48 hrs at rt under N_2. After this time the solvent was evaporated under reduced pressure, the crude was dissolved in $CHCl_3$, and washed with aqueous EDTA (2 × 5 mL) and then with water (5 mL). The organic phase was dried over $MgSO_4$ and solvent removed *in vacuo*. Analysis of the ^{1}H NMR revealed that the rotaxane yield ~20%. Purification: size exclusion chromatography with chloroform, before Sephadex CM-25 cation exchange chromatography (eluting with a 0.05 M $NaCl_{(aq)}$ solution). The rotaxanes were obtained in an isolated yield of 1.5% in both cases. The synthesis was generally conducted on a 5 mg of **36·NO_3** scale. **Lu-rotaxane 96·NO_3·OTf**: ^{1}H NMR (500 MHz, D_2O, 373 K) δ (ppm): 9.05, 8.93, 8.04, 7.97, 7.92, 7.85, 7.59, 6.98, 6.63, 6.43, 5.17, 5.05, 4.62, 4.50, 4.35, 4.16, 4.08, 3.77–2.97, 2.69, 2.41, 2.26, 1.99, 1.27. MS (ESI +ve) 1488.84, $([M\text{-}NO_3+H]^{3+}$, $C_{195}H_{315}LuN_{17}O_{87}$ requires 1488.67). **Eu-rotaxane 97·NO_3·OTf**: MS (ESI +ve) 1488.00, $([M-NO_3+H]^{3+}$, $C_{195}H_{315}EuN_{17}O_{87}$ requires 1487.99).

5.5 References for Chapter 5

1. M. J. Hynes, *J. Chem. Soc. Dalton Trans.*, 1993, **2**, 311–312.
2. P. Kuzmič, *Anal. Biochem.*, 1996, **237**, 260–273.
3. B.-Y. Lee, S. R. Park, H. B. Jeon, and K. S. Kim, *Tetrahedron Lett.*, 2006, **47**, 5105–5109.
4. V. Aucagne, K. D. Hänni, D. A. Leigh, P. J. Lusby, and D. B. Walker, *J. Am. Chem. Soc.*, 2006, **128**, 2186–2187.
5. J. A. Wisner, P. D. Beer, M. G. B. Drew, and M. R. Sambrook, *J Am Chem Soc*, 2002, **124**, 12469–12476.
6. H. Goto, J. M. Heemstra, D. J. Hill, and J. S. Moore, *Org. Lett.*, 2004, **6**, 889–892.
7. T. X. Neenan and G. M. Whitesides, *J. Org. Chem.*, 1988, **53**, 2489–2496.
8. J. Lehr, T. Lang, O. A. Blackburn, T. A. Barendt, S. Faulkner, J. J. Davis, and P. D. Beer, *Chem. – Eur. J.*, 2013, **19**, 15898–15906.
9. H. W. Gibson, S. H. Lee, P. T. Engen, P. Lecavalier, J. Sze, Y. X. Shen, and M. Bheda, *J. Org. Chem.*, 1993, **58**, 3748–3756.
10. L. M. Hancock and P. D. Beer, *Chem. Commun.*, 2011, **47**, 6012.
11. I. S. Choi, X. Li, E. E. Simanek, R. Akaba, and G. M. Whitesides, *Chem. Mater.*, 1999, **11**, 684–690.
12. L. M. Hancock and P. D. Beer, *Chem. – Eur. J.*, 2009, **15**, 42–44.
13. G. T. Spence, C. Chan, F. Szemes, and P. D. Beer, *Dalton Trans.*, 2012, **41**, 13474–13485.
14. S. Umbreen, M. Brockhaus, H. Ehrenberg, and B. Schmidt, *Eur. J. Org. Chem.*, 2006, **2006**, 4585–4595.
15. D. Muller, I. Zeltser, G. Bitan, and C. Gilon, *J. Org. Chem.*, 1997, **62**, 411–416.
16. P. J. Skinner, A. Beeby, R. S. Dickins, D. Parker, S. Aime, and M. Botta, *J. Chem. Soc. Perkin Trans. 2*, 2000, 1329–1338.
17. P. J. Skinner, S. Blair, R. Kataky, and D. Parker, *New J Chem*, 2000, **24**, 265–268.
18. Z. Chen, J. S. Bradshaw, and M. L. Lee, *Tetrahedron Lett.*, 1996, **37**, 6831–6834.
19. B. du Roizel, J.-P. Baltaze, and P. Sinaÿ, *Tetrahedron Lett.*, 2002, **43**, 2371–2373.
20. W. S. Brotherton, R. J. Clark, and L. Zhu, *J. Org. Chem.*, 2012, **77**, 6443–6455.
21. L. M. De León-Rodríguez, Z. Kovacs, A. C. Esqueda-Oliva, and A. D. Miranda-Olvera, *Tetrahedron Lett.*, 2006, **47**, 6937–6940.
22. T. Hirayama, M. Taki, A. Kodan, H. Kato, and Y. Yamamoto, *Chem. Commun.*, 2009, 3196–3198.
23. J. A. Faiz, N. Spencer, and Z. Pikramenou, *Org. Biomol. Chem.*, 2005, **3**, 4239.

CHAPTER 6

Chapter 6 Conclusions

The work described in this thesis underscores the superiority of interlocked molecules as anion hosts, capable of their selective recognition and sensing in competitive aqueous solvent mixtures. The potential and utility of halogen bonding over hydrogen bonding as an intermolecular interaction for the strong binding of anions in water has been established, demonstrating the unique nature of halogen bonding and exemplifying the interaction as a strong alternative to the ubiquitous hydrogen bond for molecular recognition and assembly in aqueous environments.

Chapter 2 emphasised the importance of host–guest complementarity in designing interlocked anion host systems. Using a novel nitrate templation methodology both rotaxane and catenane hydrogen bonding hosts were prepared, which exhibited unprecedented affinity and selectivity for the templating nitrate anion even in highly competitive aqueous solvent media. Furthermore, the ability of interlocked molecules to dramatically change their co-conformation was exploited in the preparation of a [3]rotaxane, which was able to sense sulfate anions selectively by means of modulated emission of an integrated naphthalene reporter group.

In Chapter 3 it was demonstrated that water soluble rotaxane hosts could be prepared using hydrophilic mono-functionalised permethylated β-cyclodextrin stopper derivatives. It was established that incorporating halogen bond (XB) donors into such receptors resulted in dramatic enhancement of halide anion binding in water compared to the equivalent hydrogen bonding analogues, with up to two orders of magnitude enhancement observed in the interlocked rotaxane host system with iodide. Furthermore, this XB-mediated enhancement of anion association was also observed in an acyclic receptor, resulting in remarkable binding affinity despite the low charge and simplicity of the receptor. Strong iodide binding by the XB-rotaxane was demonstrated to be driven exclusively by favourable enthalpic contributions arising from the XB interactions, whereas weaker association with the hydrogen bonding rotaxanes was entropically driven.

Chapter 4 continues with the theme of anion sensing first presented in Chapter 2, by investigating the incorporation of luminescent lanthanide cations into rotaxane hosts designed for the optical sensing of anions. The first lanthanide cation templated synthesis of an interlocked molecule was described, through the initial formation of a pseudorotaxane consisting of a pyridine *N*-oxide threading component coordinating to a lanthanide cation incorporated within a macrocycle. Stoppering of the interpenetrative assembly afforded the [2]rotaxanes. A novel nitrite templation strategy for the synthesis of lanthanide-containing rotaxanes was also presented, and the anion sensing properties of the interlocked hosts determined by means of luminescence anion binding titrations.

In summary, the results described herein demonstrate that rotaxane and catenane hosts, prepared by novel anion and lanthanide-cation templation methodologies, exhibit enhanced anion recognition and sensing capabilities, facilitating recognition even in highly competitive aqueous solvent mixtures. Furthermore, halogen bonding has been exemplified as a superior and unique intermolecular interaction for anion binding in pure water.

APPENDICES

Appendices – Molecular dynamics computational methods

Molecular dynamics simulations were conducted by Igor Marques and Professor Vítor Félix, at the University of Aveiro, Portugal.

A1 Computational methods

Starting structures

The starting models were generated through appropriate atomic manipulation of suitable crystal structures deposited with CCDC:[1] LEVKII refcode for the axle binding moiety and macrocycle, and BIFGIH refcode for the permethylated cyclodextrin stoppers.

Quantum calculations

All quantum calculations were performed with Gaussian09.[2] The DFT geometry optimizations were carried out using the B3LYP functional, with H, C, N, O and Cl treated with the 6-311+G** basis set. Br and I were described with the aug-cc-pVDZ-PP basis set,[3,4] obtained from the EMSL website.[5,6] The water solvent effects were introduced *via* the Polarizable Continuum Model (PCM), using the integral equation formalism variant (IEFPCM).[7] The RESP charges used in Molecular Mechanics (MM) and Molecular Dynamics (MD) simulations were obtained using the Gaussian IOp: 6/33=2, 6/41=4, 6/42=6 from the structures previously optimised at HF/6-31G* level. The iodine atoms were also treated with the aug-cc-pVDZ-PP basis set.

Classical force field calculations

All MM and MD simulations were carried out with Amber12.[8] The rotaxane components (axle and macrocycle), as well as the nitrate counteranion, were described with parameters taken from the Generalized Amber Force Field (GAFF)[9,10] and RESP charges.[11] The solvent

molecules were described with the TIP3P water model.[12] The halides were described with a −1 discrete charge and the appropriate settings for the selected water model.[13] The analysis of MD simulations were performed with *cpptraj*.[14]

The preliminary MM calculations on the axle and macrocycle of **76·(NO$_3$)$_2$** showed that the use of X-*ca*-*na*-X default torsion angles for the pyridinium moiety lead to the bending of *N*-methyl group relatively to the aromatic ring. Therefore, the atom type of the carbon atoms adjacent to the nitrogen in the pyridinium ring were changed from *ca* to *cd* and used with the X-*cd*-*na*-X torsion angle parameters (4 6.8 180.0 2), where *cd* is a sp^2 carbon in a non-aromatic system. This simple modification prevented the bending of *N*-methyl group in subsequent MM and MD simulations.

Parameterization of halogen bond (XB) interactions

The force field parameterisation of XB interactions was preceded by DFT optimisations (*vide supra*) of the complexes composed only by the axle binding core **72**$^+$ and each halide. In this model receptor the bulky stoppers were replaced by methyl groups affording **72$_{methyl}$**$^+$. These optimised structures allowed the I···X distances in gas-phase and water continuum solvent medium to be ascertained. Their values are gathered in Table A1 and were subsequently used to determine the I-EP optimal distance for each halide complex.

Table A1. I···X distances (Å) in DFT calculations of **72$_{methyl}$**$^+$ halide complexes

Optimisation conditions	I···Cl$^-$		I···Br$^-$		I···I$^-$	
Gas-phase	2.962	2.962	3.091	3.091	3.302	3.301
Water model continuum	3.224	3.223	3.342	3.341	3.561	3.562

Subsequently, following Félix and Beer's previous work on halide recognition mediated by macrocyclic halo-imidazolium receptors,[15,16] the XB interactions were described with resort to an extra-point (EP) of charge added to the GAFF.[23] Furthermore, the EP has van der Waals parameter and mass set to zero, a C-I-EP angle of 180° with a 150 kcal mol^{-1} rad^{-2} angle bending force constant and an I-EP optimal distance for each halide, with a

600 kcal mol^{-1} Å^{-2} bond stretching force constant. A range of I-EP distances was systematically tested, with the distribution of the electrostatic potential calculated independently for each I-EP distance, in order to derive appropriate RESP charges for the XB interactions with Cl^-, Br^- or I^-. The RESP charges for each $\mathbf{72_{methyl}}^+$ structure with EP positioned at different I-EP distances were determined from a previously HF/6-31G* optimised structure. After the calculation of RESP charges, the $\mathbf{72_{methyl}}\cdot\mathbf{X}$ complexes were optimised by means of MM.

For each $\mathbf{72_{methyl}}\cdot\mathbf{X}$ complex it was possible to define an I-EP distance that reproduced the I···X distance obtained from the DFT calculations with the water PCM solvent model: 2.48, 2.69 and 2.92 Å for chloride, bromide and iodide complexes, respectively. However, the subsequent use of such I-EP distances in solvated systems was shown to be instable, therefore it was necessary to test other values. The final I-EP optimal distances that were used in the test and production simulations of $\mathbf{72_{methyl}}\cdot\mathbf{X}$ and $\mathbf{76}^{2+}\cdot$X were: 2.44 Å for systems with Cl^-; 2.61 Å for systems with Br^-; and 2.83 Å for systems with I^-. Table A2 shows the average I···X distances calculated for 10 ns of MD simulation of $\mathbf{72_{methyl}}\cdot\mathbf{X}$ complexes, which compares well with I···X DFT distances obtained in solvent continuum medium (the simulation methods are given below).

Table A2. XB distances (average ± standard deviation, Å) for 10 ns MD simulation with halide complexes of $\mathbf{72_{methyl}}^+\cdot$

X	Cl^-	Br^-	I^-
I···X	3.43±0.14 ; 3.44±0.14	3.60±0.15 ; 3.59±0.15	3.86±0.18 ; 3.86±0.18

Calculation of RESP charges

An initial set of RESP charges was calculated for the macrocycle optimised structure (*vide supra*). However, to obtain RESP atomic charges less dependent on the conformation, the optimised structure was submitted to a MD quenched run of 1 ns in gas-phase at 1000 K, using a 1 fs time step. 10000 structures were saved and further full energy minimised by means of MM until the convergence criterion of 0.0001 kcal mol^{-1} was achieved. Four

different and representative conformations with both binding sites in an *anti-anti* configuration were selected for new geometry optimizations at the HF/6-31G* level of theory. The final atomic charges of the macrocycle used in the ensuing MD simulations (*vide infra*) were computed through a multi-conformation RESP fitting, based on five different conformations.

The charges for the axle had to be derived using a fragment-based approach due to its large size (over 400 atoms). The permethylated cyclodextrin stopper was optimised at the HF/6-31G* level and its charges were derived based on the single conformation observed in the crystal structure (*vide supra*). One of the narrower rim methoxymethyl units was removed, leaving a free atomic position, which was used to bind the stopper to the axle binding core.

The charges for the core fragment of the axle were derived independently for each I-EP distance determined above. Following a fragment based-approach, the axle cyclodextrin stoppers were replaced with glucose capping units and optimised at the HF/6-31G* theory level. Afterwards, during the charge derivation procedure, two restrains were imposed: a) the methylene groups linking the core and each glucose must have the same net charge as the methoxymethyl unit removed in the cyclodextrin stopper; b) the sum of the net charge of the glucose plus the methylene linkers must amount to 0, while the net charge of the binding core (including the two extra-points) was set to 1. After charge derivation, the glucose capping groups were removed. Finally, after having derived the charges for all the fragments, the axle was rebuilt, linking the two permethylated cyclodextrins (at the free atomic positions) to the methylene linkers in the axle core.

A2 MD simulation methods

The starting structures for the MD simulations with the $\mathbf{72}_{\mathbf{methyl}}\cdot\mathbf{X}$ complexes were obtained from previous DFT optimizations. Subsequently these structures were solvated in cubic boxes (number of water molecules ranging between 2481 and 2484). The starting structures for the simulations with the halide complexes of $\mathbf{76}^{2+}$ were obtained attaching the optimised structures of the permethylated stoppers to a previously DFT optimised structure of the anion

complex of the pseudo-rotaxane model composed of axle $\mathbf{72}_{\mathbf{methyl}}^{+}$ and the macrocycle. This structure was subsequently submitted to a gas-phase simulated annealing run, consisting of a quick heating to 300 K, followed by a slow cooling until 0 K. This structure, as well as the corresponding iodide and chloride analogous, were energy minimized *via* MM in the gas-phase. The final minimised structures were then solvated in cubic boxes (number of water molecules ranging between 5867 and 6641) and a nitrate anion was added to neutralise the system net charge.

The following methods apply to the simulations with $\mathbf{72}_{\mathbf{methyl}}^{+}$ and $\mathbf{76}^{2+}$. Each solvated system was equilibrated under periodic boundary conditions using the following multi-stage protocol. The system was relaxed by MM minimisation of solvent molecules and by keeping the anion rotaxane association and the counter-ion fixed with a positional restraint of 500 kcal mol^{-1} $Å^{-2}$. The restraint was then removed and the entire system was allowed to relax. The equilibration stage proceeded with heating up of the system at 300 K for 50 ps using a NVT ensemble and a weak positional restraint (10 kcal mol^{-1} $Å^{-2}$) on the solutes. Each system was allowed to equilibrate in a NPT ensemble at 300 K and 1 atm for 1 ns. Finally, NPT data collection runs were carried out for 50 ns (for systems with $\mathbf{76}^{2+}$) or 10 ns (for systems with $\mathbf{72}_{\mathbf{methyl}}^{+}$), with the trajectory frames being saved every 1 ps. During the MD stages of the simulations with $\mathbf{76}^{2+}$ a weak distance restraint of 5 kcal mol^{-1} $Å^{-2}$ was applied between the halide anion and both nitrogen amide binding sites. Two independent replicates were performed for each system with halide complexes of $\mathbf{76}^{2+}$. These simulations were carried out with the CUDA version of the PMEMD executable for the production runs.[18–20] The bond lengths involving all bonds to hydrogen atoms were constrained with the SHAKE algorithm allowing the usage of 2 fs time step.[21] The Particle Mesh Ewald (PME) method[22] was used to treat the long-range electrostatic interactions and the non-bonded van der Waals interactions were truncated with a 10 Å cut-off.

A3 Thermodynamic integration

The relative binding free energies of the halide complexes of $\mathbf{76}^{2+}$ ($\Delta\Delta G$ binding) were estimated by MD simulations *via* thermodynamic integration using the thermodynamic cycle depicted in Chapter 3. The values of ΔG_3 and ΔG_4 were computationally assessed as follows: a halide (X_1) was alchemically mutated into another halide (X_2), by coupling its Hamiltonian to a mutation variable (λ), which spanned from 0 to 1 along the mutation $X_1 \rightarrow X_2$. The corresponding free energy calculated by the thermodynamic integration is given by the integral:

Equation A1 $$\Delta G = G(\lambda = 1) - G(\lambda = 0) = \int_{\lambda=0}^{\lambda=1} \langle \frac{\partial V}{\partial \lambda} \rangle_\lambda \, d\lambda$$

where G and V represents the free and potential energies, respectively.

This mutation was performed independently for an isolated halide in water or halogen bonded to $\mathbf{76}^{2+}$, using a dual topology in a single step mutation. For the "free" state, only the vdW parameters of the anions were mutated. In the bonded state, both the vdW parameters of the anions were mutated together with charges and I-EP distances of the axle core, given the different distribution of charges and I-EP distances for each halide's complex.

The mutation was divided in nine windows with λ assuming the discrete values of 0.01592, 0.08198, 0.19331, 0.33787, 0.50000, 0.66213, 0.80669, 0.91802 and 0.98408. Each window consisted of a constrained molecular dynamics simulation preceded by an initial two step minimization stage, followed by an equilibration stage equivalent to the described above for the MD simulations performed in water solution, but using shorter simulation times for the initial NVT (50 ps) and NPT (200 ps) runs, followed by a NPT data collection run of 500 ps. The remaining simulation settings are the same as those used in the MD simulations carried out in the water solution. The starting frames were selected from the end of the equilibration stages of the above MD simulations ($\mathbf{76}^{2+}\cdot\mathbf{X}$) or from previously equilibrated cubic simulation boxes for each anion (solvated with 999 TIP3P water molecules and charge neutralized with a sodium cation). The free energy given by Equation A1 was estimated through the Gaussian quadrature method, as defined in the Amber12 manual, using selected λ values and the corresponding weights. Finally the relative free energies ($\Delta\Delta G = \Delta G_3 - \Delta G_4$) were computed.

A4 References

1. F. H. Allen, *Acta Crystallogr. B*. 2002, **58**, 380-388.
2. M. J. Frisch. *et al.* 2009, Gaussian 09, Revision A.01, Gaussian, Inc., Wallingford CT.
3. K. A. Peterson, D. Figgen, E. Goll, H. Stoll and M. J. Dolg, *Chem. Phys*. 2003, **119**, 11113-11123.
4. K. A. Peterson, B. C. Shepler, D. Figgen and H. J. Stoll, *Phys. Chem. A,* 2006, **110**, 13877-13883.
5. D. J. Feller *Comput. Chem*., 1996, **6**, 1571-1586.
6. K. L. Schuchardt *et al*. *J. Chem. Inf. Model*., 2007, **47**, 1045-1052.
7. S. Miertuš, E. Scrocco, and J. Tomasi, *J. Chem. Phys.* 1981, **55**, 117-129.
8. D. A. Case *et al.* (2012), AMBER 12, University of California, San Francisco.
9. J. Wang, R. M. Wolf, J. W. Caldwell, P. A. Kollman and D. A. Case, *J. Comput. Chem*., 2004, **25**, 1157-1174 (2004).
10. J. Wang, R. M. Wolf, J. W. Caldwell, P. A. Kollman and D. A. Case, J. *Comput. Chem*., 2005, **26**, 114-114 (2005).
11. C. I. Bayly, P. Cieplak, W. Cornell and P. A. Kollman, *J. Phys.Chem*., 1993, **97**, 10269-10280.
12. W. L. Jorgensen, J. Chandrasekhar, J. D. Madura, R. W, Impey and M. L. Klein, *J. Chem. Phys.* 1983, **79**, 926.
13. I. S. Joung and T. E. Cheatham, *J. Phys. Chem. B*. 2008, **112**, 9020-9041.
14. D. R. Roe and T. E. Cheatham, *J. Chem. Theory Comput*. 2013, **9**, 3084-3095.
15. F. Zapata *et al*., *J. Am. Chem. Soc*. 2012, **134**, 11533-11541.
16. A. Caballero *et al*., *Angew. Chem. Int. Ed.,* 2012, **51**, 1876-1880.
17. M. A. Ibrahim, *J. Comput. Chem*. 2011, **32**, 2564-2574.
18. R. Salomon-Ferrer, A. W. Gotz, D. P. Poole, S. Le Grand and R. C. Walker, *J. Chem. Theory Comput.,* 2013, **9**, 3878-3888.
19. A. W. Gotz *et al., J. Chem. Theory Comput*., 2012, **8**, 1542-1555.
20. S. Le Grand, A. W. Götz and R. C. Walker, *Comput. Phys. Commun*., 2013, **184**, 374-380.
21. J. P. Ryckaert, G. Ciccotti and H. J. C. Berendsen, *J. Comput. Phys.* 1977, **23**, 327-341.
22. T. Darden, D. York and L. J. Pedersen, *J. Chem. Phys.*, 1993, **98**, 10089-10092.